On the control of virtual violins - Physical modelling and control of bowed string instruments

Matthias Demoucron

KTH Computer Science
and Communication

On the control of virtual violins

Physical modelling and control of bowed string instruments

MATTHIAS DEMOUCRON

Doctoral Thesis
Stockholm, Sweden 2008

TRITA-CSC-A 2008:17
ISSN-1653 5723
ISRN KTH/CSC/A–08/17-SE
ISBN 978-91-7415-163-3

KTH
School of Computer Science and Communication
SE-100 44 Stockholm
SWEDEN

Akademisk avhandling som med tillstånd av Kungl Tekniska högskolan och Université Pierre et Marie Curie (Paris VI) framlägges för avläggande av teknologie doktorsexamen inom ramen för gemensam forskarutbildning måndagen den 24 november 2008 klockan 10.30 i Salle Stravinsky, IRCAM-Centre Pompidou, 1 Place Igor Stravinsky, 75004 Paris, Frankrike. Avhandlingen försvaras på engelska.

Dépôt de thèse académique pour l'obtention du titre de docteur dans le cadre de la convention de cotutelle de thèse internationale entre Kungl Tekniska högskolan et l'Université Pierre et Marie Curie (Paris VI). Soutenance le lundi 24 Novembre 2008 à 10:30, salle Stravinsky, IRCAM-Centre Pompidou, 1 Place Igor Stravinsky, 75004 Paris, France. La thèse sera soutenue en anglais.

Tryck: Universitetsservice US-AB

KTH Computer Science
and Communication

THESE DE DOCTORAT DE
L'UNIVERSITE PIERRE ET MARIE CURIE (PARIS)
et du
ROYAL INSTITUTE OF TECHNOLOGY (KTH, STOCKHOLM)

Spécialité

Acoustique, Traitement du signal et Informatique appliqués à la Musique

(Sciences Mécaniques, Acoustique et Electronique de Paris, SMAE, E.D. no 391)

Présentée par

M. DEMOUCRON Matthias

Pour obtenir le grade de

DOCTEUR de l'UNIVERSITÉ PIERRE ET MARIE CURIE
et de
DOCTOR OF TECHNOLOGY OF THE ROYAL INSTITUTE OF TECHNOLOGY

Sujet de la thèse :

On the control of virtual violins : Physical modelling and control of bowed strings instruments

soutenue le 24 novembre 2008

Directeurs de thèse : M. CAUSSE René / ASKENFELT Anders / FABRE Benoît

devant le jury composé de :

M. WANDERLEY Marcelo (Opponent)

M. ROCCHESSO Davide (Examinateur)

M. CARTLING Bo (Rapporteur)

M. HAYWARD Vincent (Rapporteur)

Université Pierre & Marie Curie - Paris 6
Bureau d'accueil, inscription des doctorants et base de données
Esc G, 2ème étage
15 rue de l'école de médecine
75270-PARIS CEDEX 06

Tél. Secrétariat : 01 42 34 68 35
Fax : 01 42 34 68 40
Tél. pour les étudiants de A à EL : 01 42 34 69 54
Tél. pour les étudiants de EM à ME : 01 42 34 68 41
Tél. pour les étudiants de MF à Z : 01 42 34 68 51
E-mail : scolarite.doctorat@upmc.fr

Institut de Recherche et de Coordination Acoustique Musique
IRCAM Centre Pompidou
1 place Igor Stravinsky
75004 Paris, France

Université Pierre et Marie Curie (Paris 6)
Institut Jean le Rond d'Alembert
Équipe Lutherie Acoustique Musique
11 rue Lourmel
75015 Paris, France

KTH-Computer Science and Communication
Dept. of Speech, Music and Hearing
Lindstedtsvägen 24
100 44 Stockholm, Sweden

Abstract

This thesis treats the control of sound synthesis of bowed string instruments based on physical modelling. The work followed two approaches: (a) a systematic exploration of the influence of control parameters (bow force, bow velocity, and bow-bridge distance) on the output of a physical model of the violin, and (b) measurements and analyses of the bowing parameters in real violin playing in order to model and parameterize basic classes of bowing patterns for synthesis control.

First a bowed-string model based on modal solutions of the string equation is described and implemented for synthesis of violin sounds. The behaviour of the model is examined through simulations focusing on playability, i.e. the control parameter space in which a periodic Helmholtz motion is obtained, and the variations of the properties of the simulated sound (sound level and spectral centroid) within this parameter space. The response of the model corresponded well with theoretical predictions and empirical expectations based on observations of real performances. The exploration of the model allowed to define optimal parameter regions for the synthesis, and to map sound properties on the control parameters.

A second part covers the development of a sensor for measuring the bow force in real violin performance. The force sensor was later combined with an optical motion capture system for measurement of complete sets of bowing parameters in violin performance.

In a last part, measurements of the control parameters for basic classes of bowing patterns (*sautillé, spiccato, martelé*, *tremolo*) are analyzed in order to propose a realistic control of the sound synthesis. The time evolution of the bowing parameters were modelled by analytical functions, which allowed to describe and control simulated bowing patterns by a limited set of control parameters. For sustained bowing patterns such as *détaché*, control strategies for basic elements in playing (variations in dynamic level, bow changes) were extracted from exemplary measurements, and simple rules deduced, which allowed extrapolation of parameters to modified bow strokes with other durations and at different dynamic levels.

Keywords: Bowed string, physical modelling, sound synthesis, performance control, violin playing.

Sammanfattning

Denna avhandling behandlar styrning av syntes av stråkinstrument med tillämpningar inom fysikalisk modellering av musikinstrument. Problemet har angripits i två steg, först genom en systematisk undersökning av inflytandet av styrparametrarna i violinspel (stråkkraft, stråkhastighet, och avstånd stråke-stall) på utsignalen från en fysikalisk modell, följt av mätningar och analyser av stråkningsparametrarna i normalt violinspel med syfte att modellera och parameterisera grundläggande klasser av stråkarter för styrning av syntesen.

En modell av interaktionen mellan stråke-sträng har utvecklats baserad på modal syntes och modellen har implementerats för syntes av violintoner. Modellen har utforskats genom simuleringar inriktade dels på spelbarheten, dvs. gränserna för den parameterrymd inom vilken en periodisk Helmholtz-rörelse erhålls, och dels på variationerna hos det syntetiserade ljudets egenskaper (ljudnivå och spektral centroid) inom detta parameterområde. Modellens egenskaper motsvarade väl de teoretiska prediktionerna och förväntade resultat från observationer av violinster. Utforskningen av modellen gjorde det möjligt att definiera optimala parameterområden för styrning av syntesen, och även avbilda ljudens egenskaper på styrparametrarna.

En sensor för mätning av stråkkraften utvecklades för att kunna genomföra mätningar under normalt spel. Sensorn kombinerades senare med ett optiskt system för rörelseanalys vilket gjorde det möjligt att mäta kompletta uppsättningar av stråkparametrar under spel. Uppmätta styrparametrar för grundläggande klasser av stråkarter (*sautillé, spiccato, martelé*, *tremolo*) analyserades för att ge tillgång till realistiska styrförlopp av syntesen. Stråkningsparametrarna modellerades med analytiska funktioner, för att kunna beskriva och styra simulerade stråkningsförlopp med ett begränsat antal modellparametrar. För stråkarter med uthållna toner som *détaché* utvecklades styrstrategier för grundläggande element i spelet, som ändringar i styrkegrad och stråkväxlingar, utifrån mätningar på typfall. Enkla regler formulerades för att kunna extrapolera parametrarna till modifierade stråk med andra durationer och styrkegrader.

Sökord: Struken sträng, fysikalisk modellering, ljudsyntes, musikutförande, violinspel.

Résumé

Cette thèse porte sur le contrôle de la synthèse sonore par modélisation physique des instruments à corde frottée. Il se base, d'une part, sur l'exploration systématique de l'influence des paramètres de contrôle (pression d'archet, vitesse de l'archet et distance au chevalet) sur le comportement du modèle, et d'autre part, sur la mesure et l'analyse du contrôle effectif qu'exerce l'instrumentiste afin de modéliser et paramétriser des modes de jeu typiques pour le contrôle de la synthèse.

Un modèle de corde frottée basé sur la résolution modale de l'équation de la corde est d'abord présenté et implémenté pour la synthèse sonore du violon. Le comportement du modèle physique est ensuite examiné en effectuant un grand nombre de simulations et se concentre sur deux aspects : la "jouabilité", c'est-à-dire l'espace des paramètres de contrôle dans lequel un mouvement de Helmholtz périodique est obtenu, et les variations des propriétés du son synthétisé (niveau sonore et centroïde spectral) à l'intérieur de cet espace de paramètres. Un très bon accord a été trouvé entre, d'une part, le résultat des simulations et, d'autre part, les prédictions théoriques ou empiriques basées sur l'expérience des instrumentistes. Cette exploration systématique a permis de définir des régions optimales pour le jeu dans l'espace des paramètres de contrôle et de décrire quantitativement la correspondance entre les propriétés sonores pertinentes et les paramètres de contrôle.

La deuxième partie de ce travail concerne la mise au point d'un capteur pour mesurer la force d'appui de l'archet sur la corde dans un contexte de jeu réel. Le capteur est ensuite combiné avec un système optique de capture du mouvement afin de mesurer les paramètres de jeu du violoniste.

La dernière partie présente l'analyse des mesures de ces paramètres de contrôle pour des modes de jeu typiques (*sautillé, spiccato, martelé*, *tremolo*), afin de proposer un contrôle réaliste de la synthèse sonore. L'évolution temporelle des paramètres de jeu est modélisée par des fonctions analytiques, ce qui permet de décrire et de simuler différents modes de jeu par un nombre limité de paramètres. Pour les modes de jeu soutenus tels que le *détaché*, les mesures permettent de décrire des stratégies de contrôle pour des tâches typiques (variation de niveau sonore, changement de direction d'archet), et des procédures simples ont été déduites, permettant d'extrapoler les paramètres de contrôle afin de changer le niveau sonore ou la durée des coups d'archet.

Mots-clés : Corde frottée, modélisation physique, synthèse sonore, contrôle gestuel, violon

Acknowledgements

First of all I would to thank my three advisers for their confidence, support and constant availability. They accepted this project at a step when it was just an idea not very well defined and it took a long time before a clear picture developed. However, they spared me from pressure, they let me free to a certain extent and they made the conditions for this work close to ideal.

I spent most of the time at IRCAM, Paris, and consequently, my first acknowledgements go to René Caussé, who has been my adviser there. Among other things, I would like to thank him for his availability, his enthusiasm that drove me constantly further and for conversations that went far outside this work.

As I was planning to develop Anders Askenfelt's work on measurements of bowing gestures, it seemed natural to ask him for a collaboration which gave rise to a joint doctoral program between KTH and the Université Pierre et Marie Curie. Consequently, I am extremely grateful to Anders Askenfelt for having accepted this collaboration and for having spent so much time with administrative things in order to make the cooperation possible. Thanks to him, I had the opportunity of working in a different scientific environment, which was inestimable for this work. Most of all, he gave invaluable scientific comments on this work, and this manuscript would not be as it is without his constant corrections and suggestions for rewritings and clarifying comments.

Finally, Benoît Fabre was the "mother-in-law" of this project, according to his own words. However, he went beyond this administrative role and provided me valuable comments on my manuscripts and advices for organizing my work. In particular, through observations of the deficiencies of the present manuscript at an early stage, he gave me the outline of the introduction while I was stopped in the writing.

I would really like to thank them again because I suppose many PhD students don't have the advantage of working so freely and being at the same time supervised by such a combination of expertise, knowledge, generosity, good mood and availability. It was the perfect combination for me and I am extremely grateful for that.

In the course of this work, several people showed interest for this project and worked more or less closely with me. I learned a lot through these collaborations and they all contributed in a way or another to the present work. First, I would

like to thank my closest scientific partners, Nicolas Rasamimanana at IRCAM and Erwin Schoonderwaldt at KTH-TMH, without whom these four years would have been an ocean of loneliness. Thanks to them, I always had an understanding interlocutor for talking about ideas, violin and bowed strings, and other much more interesting things. I also want to thank Alain Terrier for his invaluable know-how and for having let me play with his drills, milling machines, cutting machines when I was tired of computers. I also learned a lot from Emmanuel Fléty who made the miniature electronic boards of the bow force sensor, and Remy Müller who made the first real-time implementation of the bowed-string model. Marcelo Wanderley hosted me at IDMIL-McGill University for a few weeks and an essential part of this work would lack without the measurements that were carried out in his laboratory. In addition, numerous people provided me useful comments or support during these years and I would like to thank Knut Guettler, Christophe Vergez, Frédéric Bevillacqua, Norbert Schnell, Erik Jansson, Jim Woodhouse, partners from the CONSONNES project and in particular Jean Kergomard.

I am particularly grateful for the financial supports received during this work and fundings from the Université Pierre and Marie Curie, the Swedish Institute, the Cost 287-ConGas action, the project CONSONNES funded by the Agence Nationale pour la Recherche, and the French Acoustical Society.

At Ircam, there would be many people to thank for their good mood, for long chats beside the coffee machine or on the “passerelle”, for all the things that I discovered thanks to them and for their availability when it was about solving troubles. However, very very special thanks go the people with whom the story began one year before, when attending the same courses : Damien Tardieu, Nicolas Rasamimanana, Arshia Cont and Grégoire Carpentier, to whom should be added Julien Bloit. At TMH, I would like to thank the music group in general and the “innebandy” team in particular.

Elika Hedayat had to bear bad temper in the morning and geographic separations, among other things, during a long part of this work. Thanks to her exasperating capacity for making fun of them, many sad feelings became suddenly insignificant. I am infinitely grateful to her for that, for making such a moving work and for all the things that she brings in my life everyday.

To conclude, this work would not have been possible without the support and confidence of my family and parents. I especially appreciated my grandfather’s efforts to understand what I was doing and I would have been very glad to give him a copy of this manuscript. I hope he would have appreciated it.

Contents

List of Figures

List of Tables

Declaration

The contents of this dissertation is my own original work except for commonly understood and accepted ideas or where explicit reference is made. The dissertation is written as a monograph including six chapters, of which Ch. 4 is composed of an introduction and two manuscripts submitted for publication.

Paper I

Demoucron M. & Caussé R. "Measuring bow force in bowed string performance: Theory and implementation of a bow force sensor"
Submitted for publication in *Acta Acustica*, September 2008.

Paper I represents my own work.

Paper II

Schoonderwaldt E. & Demoucron M. "Extraction of bowing parameters from violin performance combining motion capture and sensors"
Submitted for publication in *Journal of Acoustical Society of America*, July 2008.

In Paper II, the sections related to the motion capture method and calculation of bowing parameters based on motion capture data represents the work of Schoonderwaldt. My own work concerned the measurement of bow force and writing of the corresponding parts of the manuscript (Sect. IV-V, Appendix B and C).

Introduction

The violin and the other bowed string instruments offer a musical expressivity comparable to the singing voice. The key to the expression in performance is the bowing gestures by which the sound properties are shaped continuously during a stroke. The seemingly simple bow constituates a sensitive control device with unexpected possibilities, by which the perceptual properties of the sound can be controlled in detail. Physically, the sound of the bowed string instruments is produced by drawing the bow across the string. As the bow moves, the string is forced to oscillate due to the bow-string interaction, which is governed by the frictional force between the bow hair and string, and a dynamical triggering mechanism defined by repeated reflections of the travelling waves on the string. The string vibrations are transmitted via the bridge to the violin body, which in turn radiates the sound.

The violinist's control of the bow-string interaction is described by three main bowing parameters:

- *Bow-bridge distance.* The distance from the bridge to the position of the contact point between the bow hair and the string ("contact point" or "sounding point"). In normal playing the contact point is located between the bridge and the termination of the fingerboard, so the variation in bow-bridge distance is limited to one fifth of the string length.

- *Bow force.* The force with which the bow is pressed against the string (called "bow pressure" by musicians). In playing, the bow is held at the frog (the handle) in a pivoting grip between the thumb and the middle and ring fingers. The bow force depends on the actions of the index and little fingers, pressing on top of the bow stick on either side of the pivoting point. In this way the bow is balanced and a suitable strength of the force couple can be applied. Playing at the tip requires a very strong action of the index finger. A high bow force at the tip of about 1 N requires about 10 N at the index finger. In contrast, when playing with low bow force near the frog, the action of the little finger is required to compensate for the contribution from gravity to the bow force. Consequently, parts of the bow strokes requiring high bow force are preferably played close to the frog, and parts with low force close to the tip, if possible.

- *Bow velocity.* The velocity of the bow motion in the bowing direction.

In addition, the *tilting* of the bow around the axis of the bow stick changes the amount of bow hair in contact with the string and offers a subtle control of the bow force. For example, the bow is usually tilted when approaching the frog in order to avoid strong variations in bow force.

The training of the budding violinist has two main goals. First, it aims at developing a motoric skill to perform gestures with the arm and hand, which allows a precise control of the bowing parameters. The violinist's bowing gestures are far from natural and require long-term practicing in order to obtain the necessary suppleness of the arm, hand, and fingers. From the shoulder to the bowing position, the physiological and mechanical system controlling the bowing parameters measures between 70 and 130 cm, and is composed of six body parts which require perfect coordination to perform a well-controlled bowing gesture. For instance, drawing a straight line with the hand in the bowing direction over a distance of 65 cm (corresponding to the length of the bow) is not elementary, especially as the bow should be kept parallel to the bridge during the entire gesture.

The second goal of the string player's training is implicit and consists in exploring the bowing parameter space and building an intuitive mapping between the bowing gestures and the resulting sound. In performance, such a well-established mapping between bow control and sound is needed in order to continuously adapt the bowing parameters to a combination which gives the intended tonal properties. This is a difficult task as such, which is made even more demanding by the large set of musical and technical constraints given by the score.

This work will not deal with the first of these goals, i.e. the acquisition of a specific bowing technique and the correspondence between the gesture and bowing parameters. Instead, we will focus on the relation between the bowing parameters and the sound, and more precisely, on the control of the parameters for a specific musical purpose. During the years of training, the violin student progressively learns subtle differences in the control of the instrument. At the beginning, the focus is on obtaining the right type of string vibration and making the violin "speak well". A too high bow force will make the violin's voice creaky, and a too low will make the violin whistling. The violinist-to-be successively discovers the "good" force range which can be used in adequate combination with the other bowing parameters. Once it works, she tries to increase the sound level by pressing harder, but the sound becomes creaky once more. The exploration starts again. She makes different tries, bows closer to the bridge because it sounds better, and maybe increases the bow velocity. Her hearing is refined and subtle effects appear: softer tones are easy to obtain when bowing above the fingerboard, very brilliant notes are possible to produce close to the bridge. From now on, the entire sound palette of the violin is open to her, and she can play with different sound levels from *pianissimo* to *fortissimo* and use different sound nuances according to the musical context by coordinating the bowing parameters adequately.

However, music is time, and the violin technique cannot be reduced to the production of specific sounds. An essential part of the musical expression depends on the timing of the notes, and variations in the sound during the notes. The

global shape of a note is obtained through bowing gestures producing the desired time evolution of the bowing parameters. The most usual way of bowing is to draw the bow back and forth with the hair in continuous contact with the string. The strokes are separated by very short stops at the changes in bowing direction ("bow changes"). This basic bowing pattern is called *détaché* ("separated"). If the strokes are heavily accentuated at the beginning and clearly separated, the bowing pattern is termed *martelé*. The string can also be set in vibration by letting the bow bounce on the string, like in *sautillé* and *spiccato* playing. Détaché, spiccato and martelé constitute the core components of the violinist's bowing vocabulary, with infinite possible variations. They are very different in terms of the controlling bowing gestures, and require years of dedicated practicing in order to be mastered in performance.

The previous description has illustrated the fundamentals of the sound control in violin playing. We will now touch upon problems related to sound synthesis for imitating the sound of the violin. The most basic approach is a straightforward reproduction from recordings of the sound, which is the principle of sampling-based synthesis. Another method consists in modeling some of the perceptually most important properties of the sound, like the spectrum. The information about the frequencies of the partials, their amplitude, and their time evolution are used to resynthesize a signal which shares many properties of the original sound.

Leaving aside the question of realism or naturalness, the problems related to sound synthesis are of two types. First, a synthesis method should be able to reproduce the main part of the expressive capabilities of the instrument, in particular the usual sounds that can be produced. Secondly, the control of the synthezised sounds becomes more and more central as the quality and complexity of the synthesis methods increase. This evolution brings the problem of control parameters to the foreground. A method for synthesizing sounds needs a small number of parameters by which the user can control the sound. The control parameters can be more or less intuitive, or related to a given purpose. For example, spectral synthesis is based on the description of low-level properties of the sound, which is adequate from a perceptual point of view. Specific mappings to the bowing parameters have to be found, however, if a control of the synthesis based on violinists' gestures is demanded [60].

From these two points of view, sound synthesis based on physical modelling is a promising method. Provided that an adequate physical description of the instrument can be formulated, the method offers the same sound possibilities as the real instrument, and also the same control parameters which relate the action of the player to the sound. In the case of a virtual violin, the control parameters are the bow-bridge distance, the bow force, and the bow velocity, and some models include a control of the bow tilt as well. However, the drawback of the method is that the effects of the control parameters and their time evolution are not obvious for non-violinists. Even when violinists "play" violin synthesis based on physical modelling, the quantification of the bowing parameters is far from easy and repeated

tries with changed parameter envelopes and ranges of values are required in order to obtain an acceptable sound, exactly like when learning to play the real instrument. The physical interface to the model is of particular importance in order to take advantage of the motoric capability of a human player. A stick of about the same length as a sweeping motion by the arm, combined with sensors for the motion, suggests itself as an interesting control device with a large potential of musical expression by gesture control.

Putting aside the question of the physical interface, three general problems in the control of synthesis of musical instruments can be identified:

- The playability, i.e. the ranges and combination of parameters that can be used in order to obtain an appropriate motion of the string.
- The mapping between the perceptual properties of the sound and the control parameters. The question is, for example: "I have no experience of violin playing and I want to produce a louder sound, or a more brilliant sound, or a progressive increase in dynamics (crescendo). What do I have to do with my control parameters?"
- The realism of the control and the production of typical bowing patterns, i.e. the time evolution of the control parameters in typical performance situations related to the technique of violin playing.

The starting point of this thesis lies in the last point. Whereas the modelling of musical instruments and the implementation for sound synthesis purposes have been widely investigated in the past, very few works have tackled the problem of realistic control. In the eighties, Chafe [15] and Jaffe [42] worked on a score-and-rule-based generation of control parameters. More recently, the possibility of real-time implementations of the models has driven the question of control interfaces [85], and since a few years different devices for measurement of gesture parameters have been presented [68, 51, 92]. There is now a need for studies on how the control of physical models based on realistic bowing parameters influences the realism of the synthesis. In particular, examination of different bowing patterns could be used to propose adequate control methods according to the musical intentions.

The work has been divided into three phases, reflected in the outline of the thesis. First it was necessary to develop the basic tools to work with: (1) A physical model of the violin, and (2) devices for measurement of bowing parameters in real violin performance. Concerning the development of the physical model, the guideline was to implement a reliable model using modal formalism. For the measurement of bowing parameters, the central point was to design a sensor enabling measurements of bow force in real performance. In a second step, the physical model and the measurements and observations on the bowing parameters had to be brought together for sound synthesis, in order to propose adequate ways of controlling the model.

The dissertation is structured as follows:

- In Chapter 1, we will present basic observations on the motion of the bowed string together with studies related to the modelling of the bow-string system and different implementations for simulation purposes.
- In Chapter 2, the physical model that was developed and used during this work will be presented in detail. We will describe the modal formulation on which the model is based, the numerical implementation, and an empirical procedure used to synthesize violin sound from the simulations. The influence of computation parameters will be examined, and some possible developments discussed.
- In Chapter 3, systematic simulations will be performed in order to observe the behaviour of the model with a given set of control parameters. The playability of the model during attacks and during the steady part of the simulations will be compared with theoretical results. Further, an examination of the sound properties (spectral centroid and sound level) within the playable parameter space will be used to describe the mapping between perceptual properties of the sound and the control parameters.
- Chapter 4 is dedicated to a description of the devices used for measuring bowing parameters. The chapter consists of two submitted manuscripts reporting the design and implementation of a bow force sensor (Paper I), and a complete setup combining an optical motion capture system with the force sensor (Paper II). In an introductory part a background is given together with some information on the use of the bow force sensor in the performance of contempory music.
- In Chapter 5, gesture-based control of the model will be covered. For that purpose, measurements of rather fast and dynamic bowing patterns, including sautillé, martelé and tremolo, will be presented. We will show how these bowing patterns can be modelled in order to produce the time evolution of the bowing parameters from a limited set of intuitive high-level parameters. Measurements will be fitted to the models, and used to extract typical parameter sets, reflecting the musical intentions of the performance.
- Finally, in Chapter 6, we will observe measurements of sustained bowing patterns such as détaché, in order to characterize the time evolution of the bowing parameters, and extract some simple rules describing the player's control strategies for performing changes in dynamic level. The basic task of changing the direction of the bow motion ("bow change") is examined closely by observations of performance habits, modelling, and evaluation of simulated modifications.

Before closing this introduction, a few remaining points should be discussed. First, we have frequently used the word "violin" and will continue to do so in the following. Very often this word can be replaced by "bowed string instruments" as we will consider the violin as an exemplary case that can be easily extended to other instruments of the same family.

Further, in this work we will often question the realism of synthesized sounds. The reader will, however, not find any systematic and scientifically based evaluations of the realism in the thesis. Formal listening tests were not possible to do within the given time of this work. They were left for future studies to complete the empirical evaluations reported here. When it will be written that "the resulting sound is realistic", it will be according to the judgement of the author, and sometimes also according to the judgement by other listeners. The author has played the violin since more than 20 years, has a strong musical background and can be considered as a subject with an experienced musical hearing, able to identify subtle differences in violin sound. It is important to mention that the experience as a string player involves a specific sensitivity for judging the realism, which seems to be based mainly on some kind of intuitive recognition of the control gestures.

To conclude, the present work would not have been possible to perform without my musical background. The following pages originate from the meeting between a young advanced amateur violinist and a former little boy who always wanted to check how his parent's video recorder worked inside but never could put the parts together. It was sometimes difficult to keep the violinist silent when the little child was digressing to deeply into the technical and scientific aspects. As a result, sometimes the violinist will speak to the reader, sometimes the little child will speak, sometimes the potential user of a future advanced virtual violin will speak, and sometimes they will speak all together. I hope the reader will forgive this blending of genres, and appreciate the different views they give on the fascinating topic of bowed string instruments.

Chapter 1

Mechanics of the bowed string and simulation methods

This chapter presents some basic results of studies on bowed strings and the coupling to the instrument. Since Pythagoras and other early works on vibrating strings, the understanding of the dynamics of the bowed string has increased successively due to pioneering works by Helmholtz, Rayleigh, and Raman, who gave the basis of the modern view on the problem. By first introducing the basic knowledge obtained in the historical works, and then adding the most important results of contemporary studies, some landmarks will be given which allow a comparison between simulations, idealized theory and experimental results.

After the presentation of these important landmarks, we will give an overview of the phenomena that should be taken into account for obtaining a complete physical description of the bowed string and violin. The bowed-string model that will be used in the experiments and analyses in the following chapters uses only a limited set of these ingredients. It is therefore important to show why it can be called a "minimal" model, compared to all the elements that could be included in a more extensive description of the bowed string and instrument.

Finally, different techniques for simulation of the motion of the bowed string will be presented. Recent developments of computers and improved efficiency of algorithms make it possible to run even rather sophisticated simulation models in real time. These simulation methods form the basis of contemporary sound synthesis based on physical modelling.

1.1 Kinematics of the bowed string

From a radical point of view, the description of the violin in physical terms can be reduced to the study of the bowed string. Questions related to the the coupling between the different elements of the violin (string, bridge, body), the radiation into the air, and the classical issues related to tone quality and violin making, can all be

regarded as auxiliary compared to the main characteristics of the instrument, which is the excitation through friction by a bow drawn across the string. Whereas an analytical description of the string vibration in the case of free oscillations has been available since D'Alembert and Bernoulli (18th century), the motion of the bowed string remained unknown until the second half of the 19th century and Helmholtz's pioneering work [40].

By observing the actual motion of the string, he concluded that the string motion consisted in a sharp corner travelling around a parabolic trajectory. From this idealized motion he predicted the influence of the bow velocity and bow-bridge distance on the vibration amplitude of the string. By considering that real strings cannot show a perfectly sharp corner, Cremer and Lazarus [19] introduced a smoothing of the Helmholtz corner which enabled to describe the influence of the bow force on the vibrations. It is interesting to notice that all these results were obtained without any precise measurements on the string motion, but entirely based on kinematic considerations and very strong approximations in the dynamics of the bowed string. Actually, before the access to computers, a detailed description of the vibrations of the bowed string was almost impossible to approach. Raman [65] was the first trying to deal with the problem at the very beginning of the 20th century. In order to be able to solve the problem by hand, he had to simplify the problem by considering a flexible string with purely resistive terminations, bowed at an integer fraction of the string length. In addition to Helmholtz motion, he discovered a great variety of possible periodical motions of the string.

The string equation

The dynamical behaviour of the string depends on the boundary conditions at the terminations and a set of mechanical string properties including the tension, mass and length. If the string is represented by a one-dimensional continuum in the x direction, with tension T_0 and linear density ρ_L, the equation describing the displacement $y(x,t)$ of the string can be written as (see for example [24])

$$\rho_L \frac{\partial^2 y(x,t)}{\partial t^2} = T_0 \frac{\partial^2 y(x,t)}{\partial x^2} \tag{1.1}$$

This is a classical equation of wave propagation and D'Alembert (1717-1783) gave a general solution consisting in the sum of two waves travelling in opposite directions

$$y(x,t) = y_+(x-ct) + y_-(x+ct) \qquad \text{with} \quad c = \sqrt{\frac{T_0}{\rho_L}} \tag{1.2}$$

In this solution, y_+ represents a wave propagating in the +x direction with a velocity c while y_- propagates in the -x direction. The finite length L can be taken into account by considering the boundary conditions. The simplest conditions are obtained by assuming that the displacement is zero at the bridge and the nut (fixed

ends), giving a total reflection of the incoming waves with opposite polarity. The state of the vibration is identical once the travelling waves have made a round trip on the string, and the fundamental frequency of the oscillation is given by

$$f_0 = \frac{1}{2L}\sqrt{\frac{T_0}{\rho_L}}$$

Another formulation of the solution has been given by Bernoulli, also considering fixed terminations of the string. The solution can then be written as a superposition of particular solutions with separate variables x and t

$$y(x,t) = \sum_{n=1}^{\infty} a_n \sin\frac{n\pi x}{L}\sin n\omega t \qquad \omega = \frac{\pi}{L}\sqrt{\frac{T_0}{\rho_L}} \tag{1.3}$$

The string equation can be solved analytically for free oscillations produced by struck and plucked excitations, but sustained excitations produced by drawing a bow across the string are substantially more difficult to examine. As mentioned by Helmholtz (1862):

> "No complete mechanical theory can yet be given for the motion of strings excited by the violin bow, because the mode in which the bow affects the motion of the string is unknown" ([40], cited in [91]).

A better understanding of the bow-string interaction was necessary for approaching an analytical description of sustained oscillations. It turned out, however, that even with simple models such as the ones used by Raman (1918) [65], or later, Friedlander (1953) [26], and Keller (1953) [44], a number of approximations were necessary for obtaining a solution. Direct observations of the motion of the bowed string gave an invaluable starting point for improving the dynamical description of the vibrations.

Helmholtz and the idealized motion of the bowed string

Using a vibration microscope, Helmholtz observed a surprisingly simple motion of the string when played by a bow. At any position the displacement followed a triangular pattern, and the velocity consequently alternated between two values with opposite polarity. This motion is illustrated in Fig. 1.1, right.

When observing the motion at a given point x_1, the oscillation is made up of two successive phases whose total duration corresponds to the period of the vibration of the free string T. During a time T_+, the string moves in the same direction as the bow, with velocity v_+. Then, during the time T_-, the string moves in the opposite direction with velocity v_-. The duration of the two phases depends on the position x_1 where the motion is observed. If the string is observed between the bridge and the midpoint, T_+ is greater than T_- and vice versa on the other half toward the nut. At the middle, the two phases have exactly the same duration.

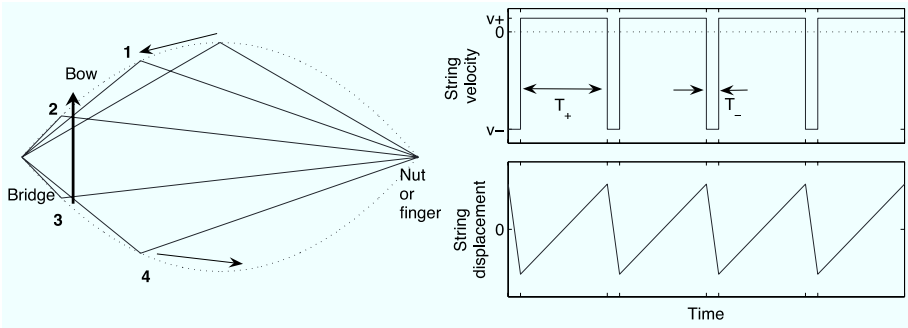

Figure 1.1: Illustration of the idealized Helmholtz motion. Left: At any time, the string is composed of two straight segments connected at a sharp corner (the "Helmholtz corner"). When bowing the string, the corner travels around a parabolic trajectory, the capture and release of the string corresponding to the moment when the corner passes under the bow. Right: The resulting string velocity (top) at any point of the string shows an alternation between two phases with opposite sign, giving a sawtooth pattern for the displacement (bottom).

At the bowing position x_0, the interpretation of these two phases is straightforward, showing an alternation between two states of the bow-string interaction: slip and stick. During the time T_+, the string sticks to the bow hair and consequently moves with the same velocity ($v_+ = v_b$), and during the time T_-, the string slips under the bow with a velocity whose sign is opposite to v_b.

Using these observations and the basic model of the string described in the previous section, it was possible for Helmholtz to quantify the motion. As a first approximation, he used the general solution for the free oscillation (Bernoulli's solution, Eq. 1.3) and deduced the Fourier coefficients a_n for the triangular patterns that he observed experimentally. This gave proportional relations between the time intervals T_+, T_-, T, the length L, and the observation position x_1

$$T_+ = \frac{2(L - x_1)}{c}, \qquad T_- = \frac{2x_1}{c}, \qquad T = \frac{2L}{c}$$

The velocity at any point x_1 along the string can be written as a function of the bow velocity v_b at the bowing position x_0

$$v_- = -\frac{(L - x_1)}{x_0} v_b, \qquad v_+ = \frac{x_1}{x_0} v_b$$

Finally, the maximum displacement of the string at a position x_1 can be written as

$$y_m(x_1) = \frac{v_b T}{2} \frac{(L - x_1)x_1}{Lx_0} \tag{1.4}$$

The displacement envelope is seen to be composed of two parabolas passing through zero at the string terminations. The corresponding overall motion of the string is illustrated in Fig. 1.1, left. At any moment, the string configuration is made up of two straight-line segments whose corner lies on the parabola, the so-called Helmholtz motion (dotted line, Eq. 1.4). When the string is bowed, the corner travels around the parabolic trajectory in one period. As the eye cannot follow this quick motion of the string, the observer sees only the parabolic envelope which gives the impression of a uniform vibration, as if the whole string was vibrating back and forth.

The successive phases of the vibration can be followed in Fig. 1.1, left. At time 1, the string is still sticking to the bow and the displacement of the string between the bridge and point 1 is increasing, whereas the displacement is decreasing on the other part of the string. Between time 1 and 2, the corner travels along the trajectory and when it passes under the bow, the string is released and begins to slip in the opposite direction. Until time 3, when the string is slipping, the corner reaches the bridge termination, is reflected, and begins to propagate toward the nut with an opposite displacement. At time 3, the corner passes under the bow and the string is captured again.

The described motion is an idealization of the observed vibrations. In particular, the corner between the two string segments can only be sharp with an ideal, flexible string. With real strings, it is rounded due to the stiffness of the string. However, all cases of bowed string motion characterized by an alternation between one sliding phase and one sticking phase during one nominal period of the string vibrations will be referred to as Helmholtz motion, in contrast to other possible vibrations of the string.

Theoretical inferences

Important results can be drawn from the simplified model described above. In the bowed-string instruments, the sound is radiated from the body, which is excited by the vibrations of the string transmitted via the bridge. The force acting on the bridge F_{bridge} can be deduced from the spatial derivative of Bernoulli's solution (Eq. 1.3)

$$F_{bridge}(t) = T_0 \frac{\partial y(x,t)}{\partial x}\Big)_{x=0} = \sqrt{T_0 \rho_L} \frac{v_b}{x_0} \sum_{n=1}^{\infty} \frac{2}{n\pi} \sin n\omega t \tag{1.5}$$

This expression corresponds to a perfect sawtooth function with linear ramps and steps. The maximal value of the ramp is

$$F_{max} = \sqrt{T_0 \rho_L} \frac{v_b}{x_0}$$

The amplitude of the vibration at the bridge, and hence the sound level, increases with increasing bow velocity and with decreasing bow-bridge distance[1].

Eq. 1.5 also gives an estimation of the spectrum of the sound. The amplitude of the n-th harmonic is

$$F_n = \frac{2}{n\pi}\sqrt{T_0\rho_l}\frac{v_b}{x_b}$$

The spectral slope is -6 dB/octave, which approximately corresponds to the measured spectrum of the force on the bridge. It will be seen in the next section that the highest partials are actually lower when playing with a low bow force. The -6 dB/octave slope corresponds to a limiting case corresponding to Helmholtz motion with a sharp corner, towards which the spectrum tends when the bow force increases. It should be noted that if the string is bowed at a nodal point, the corresponding partials would not be present in the spectrum. Due to the finite width of the bow complete cancellation does not occur, but the corresponding partials are strongly suppressed.

Effect of bow force

The previous analysis of the bowed string is an approximation based on free oscillations and on idealized representation of the observed motion of the string under the bow. It does not take into account the effect of external forces such as the frictional force applied by the bow. A complete description of the bowed string behaviour must include this effect. As every string player knows, the string cannot be bowed properly if the bow is not pressed hard enough against the string, and when the force is too high, the resulting sound becomes scratchy. As described above, playing closer to the bridge increases the amplitude of the driving force on the bridge and the sound level. However, a decrease in bow-bridge distance needs to be coordinated with an increase in the force with which the bow is pressed against the string (the bow force), in order to maintain the Helmholtz motion.

Studies including forced oscillations of the string were first carried out by Raman [65, 66]. He focused on the velocity waves travelling in opposite directions of the string and studied the different solutions that could be obtained, using a simple model with purely resistive terminations of the string. For the particular case of Helmholtz motion, he showed that the vibrations could not occur below a given value of bow force.

The bow force also influences the spectrum of the sound. The "brilliance" of the sound increases with increasing bow force, as experienced by any string player. However, with Helmholtz's idealized model as well as in Raman's analysis, no change in the string vibrations occurs as the bow force is increased. In particular,

[1] From a violin making point of view, it can be seen that the amplitude increases with increasing tension as well, which explains the transformations of the violin during the 19th century. For obtaining a more powerful sound, the tension of the string has been increased, involving longer strings and some modifications of the violin itself for supporting the increased load of the strings.

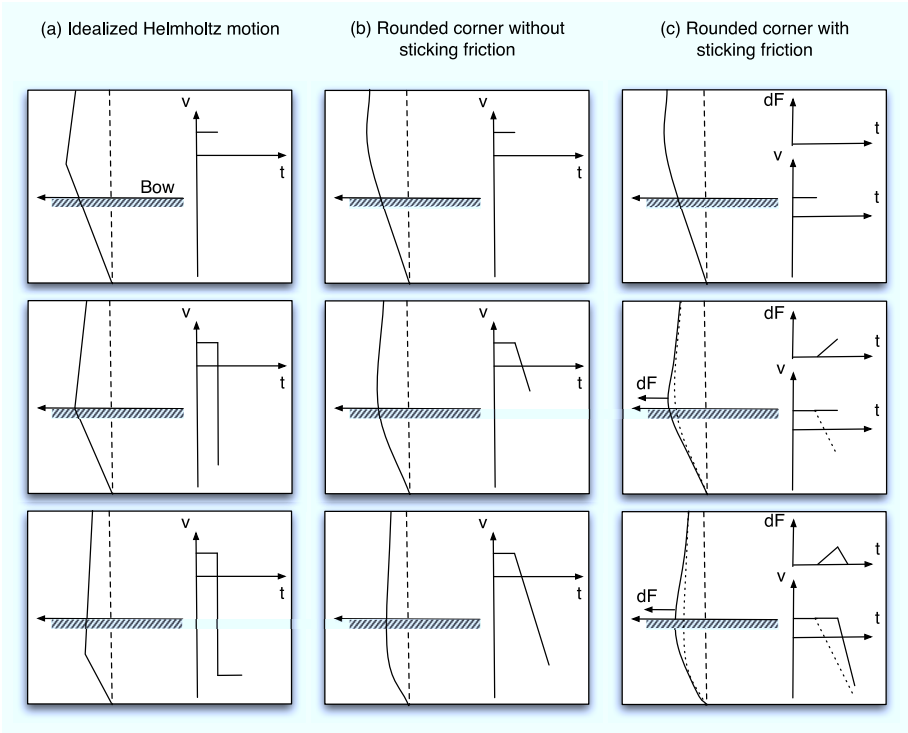

Figure 1.2: Effect of smoothing of Helmholtz corner. (a) Idealized motion of the corner described by Helmholtz. When the string passes under the bow, the sliding phase begins and the string velocity suddenly drops from a positive to a negative value. (b) A rounded corner produces a velocity ramp with constant rate if the friction force is not taken into account (for instance with a low bow force). (c) With the effect of friction force dF, the string is prevented from sliding until the maximum static force is reached. Consequently, the sticking phase lasts longer and the corner is sharpened. (After Cremer [19])

the bow force has no effect on the amplitudes of the string partials in Helmholtz motion.

A simple empirical observation gives an illustration of the effect of the bow force. When two objects are pressed against each other, the static friction between them increases with the pressing force. A higher transverse force is required for breaking the sticking contact between the objects and making them slide, which means that the limiting static force (i.e. the minimal transverse force for the sliding to occur) increases with the pressing force. Similarly, during sliding, the friction between the two objects increases with the normal force: it is more difficult to make a heavy object slide on a table than a light one. This gives a first indication of the effect of

bow force on the bowed string. The sticking phase will tend to last longer as bow force increases, and because the frictional force pulling the string in the bowing direction increases, the slipping phase tends to be shorter.

Cremer approached the problem by considering a smoothing of the sharp corner described by Helmholtz. If the corner is replaced by a rounded corner of finite length and constant radius, the string velocity at the bowing point decreases linearly instead of dropping suddenly (see Fig. 1.2a and b). Now, if the frictional force is taken into account, the string is prevented from sliding immediately as the "corner" passes under the bow (see Fig. 1.2c). The frictional force increases, preventing the string from sliding until the maximum static sticking force is reached, and the slipping phase starts. As a result of the build-up in frictional force, the rounded corner is sharpened as it passes under the bow.

As the maximum static force increases with increasing bow force, the sticking phase lasts longer, and the release of the string will be more abrupt. As a result the corner will be be more and more sharpened when the player presses the bow harder against the string. This effect provides an explanation to the increase in brilliance of sound with increasing bow force. If losses at the terminations are assumed to increase with frequency, the corner is rounded off during the reflections, which compensates for the sharpening under the bow at capture and release. Cremer analysed the conditions under which these effects balance each other.

1.2 Physical modelling of the bowed string

A physical description of the bowed string can be more or less detailed, depending on the purpose and the desired precision. A complete and physically realistic description needs to include a number of features, which often are far from straightforward to model. The present section aims at giving an overview of such a complete modelling. The different components and features of the mechanical system are presented together with related studies and usual ways of modelling.

First, we will examine a realistic model of the string including damping and stiffness. Then, we will shortly present the inclusion of external forces before discussing the modelling of the bow-string interaction. The modelling and effect of string terminations will be examined together with the coupling between the string and the body of the instrument. Finally, the torsional motion of the string will be addressed.

Real strings: Stiffness and damping

The wave equation for the ideal string was given in Eq. 1.1. With the flexible string, there is no limitation on the sharpness of the Helmholtz corner. However, real strings have some resistance to bending (stiffness) which needs to be taken into account in the method of rounded corners described by Cremer [19]. The main

effect of stiffness is to introduce some wave dispersion in the wave propagation on the string. Wave components with higher frequency propagate faster than lower frequencies, resulting in a slight inharmonicity of the partials of the freely vibrating string ("stretched spectrum").

The resistance to bending can be modelled by including a stiffness term in the string equation (see for example [24] or [84]). The string equation then becomes

$$\rho_L \frac{\partial^2 y(x,t)}{\partial t^2} = T_0 \frac{\partial^2 y(x,t)}{\partial x^2} - EI \frac{\partial^4 y(x,t)}{\partial x^4} \tag{1.6}$$

where E is Young's modulus and $I = \frac{\pi d^4}{64}$ the second moment of area for the cross section of the string, d being the string diameter. Eq. 1.6 leads to inharmonic frequencies of the string modes. If the string terminations are simply supported, the frequencies are given by

$$f_n = n f_0 \sqrt{1 + \frac{4\pi^2 EI\rho_L}{T_0^2}(n f_0)^2} \quad \text{with} \quad f_0 = \frac{1}{2L}\sqrt{\frac{T_0}{\rho_L}}$$

Real strings also show some damping. As the waves propagate along the string, energy is dissipated through several mechanisms, let alone the large losses at the terminations. Valette [84] made an extensive review of these mechanisms, including frictional losses due to the air, and internal damping due to viscoelasticity and thermoelasticity. The way of incorporating the losses in the string equation is not straightforward as they depend on frequency. A general formulation is

$$\rho_L \frac{\partial^2 y(x,t)}{\partial t^2} = T_0 \frac{\partial^2 y(x,t)}{\partial x^2} - EI \frac{\partial^4 y(x,t)}{\partial x^4} + R(\omega, y, t) \tag{1.7}$$

The term $R(\omega, y, t)$ can have different expressions, according to authors. For example, Hiller and Ruiz [41] introduced two terms in order to take into account heat dissipation and sound radiation as a function of frequency

$$R(\omega, y, t) = -2b_1 \frac{\partial y}{\partial t} + 2b_3 \frac{\partial^3 y}{\partial t^3}$$

In a slightly different way, Valette took the damping of each partial f_n into account by introducing quality factors $Q(f_n)$ in the general solutions of the string equation (Eq. 1.3)

$$y(x,t) = \sum_{n=1}^{\infty} a_n \sin\frac{n\pi x}{L} \sin(2\pi f_n t) \exp(-\frac{\pi f_n}{Q(f_n)} t)$$

Finally, we should mention the approach by Woodhouse, in which dispersion due to bending stiffness and dissipation due to all types of damping are simulated by "reflection functions" [87]. In this approach, the impulse response of the string at the bowing point is composed of an initial spike followed by incoming waves resulting from the reflections at the bridge and the nut. These reflection functions

contain all the information about dissipation and dispersion, including the losses at the string terminations (see Sect. 1.3).

Strictly speaking, the preceding description is only valid for strings made of a plain wire like the E string of the violin. Most real strings have a more complicated design. Wound strings are made of a core carrying the tension, around which mass is added by wrapping a fine wire. The design of strings and the influence on the string properties have been extensively discussed by Pickering [62][61]. However, as the design of wound strings basically sets the same mechanical properties as described above (linear density, damping, and bending stiffness), there is no real need to refine the previous description for homogeneous strings.

Other possible refinements of the analysis of the string include a three-dimensional description of the vibrations. In the previous descriptions, the string is assumed to move in a plane parallel to the bow. This is a reasonable simplification, but more elaborate descriptions of the vibration could take into account the motion in both the transverse directions and the longitudinal direction. In particular, the lengthening of the string during the vibration cycle includes variations in tension and leads to a non-linear coupling of the equations describing the motion in the three dimensions.

External forces

Until now, we have discussed string equations for free oscillations, i.e. with no external forces acting on the string. For describing the dynamics of the bowed string, we obviously need a way of incorporating the interaction with the bow. Two ways of taking external forces into account can be considered.

First, we can introduce a term depending on external forces in the string equation. Because the equation has the spatial derivative of force as unit, it will be necessary to consider the force distribution along the string (x-direction) $F(x,t)$. Then, the string equation for forced oscillation can be written as

$$\rho_L \frac{\partial^2 y(x,t)}{\partial t^2} = T_0 \frac{\partial^2 y(x,t)}{\partial x^2} - EI \frac{\partial^4 y(x,t)}{\partial x^4} + F(x,t) \tag{1.8}$$

An alternative view can be taken by considering the string as consisting of two parts $y_1(x,t)$ and $y_2(x,t)$ separated at the bowing position. Then, each part is described by the string equation for free oscillations, and some additional boundary conditions at the bowing position x_0 have to be defined. It is reasonable to assume a velocity continuity at x_0

$$\frac{\partial y_1(x,t)}{\partial t}\Big)_{x_0} = \frac{\partial y_2(x,t)}{\partial t}\Big)_{x_0} = v(t)$$

The additional velocity introduced by the external force F at x_0 can be written as

$$\delta v = \frac{F}{2Z_c}$$

where the characteristic impedance Z_c of the string is $Z_c = \sqrt{T_0 \rho_L}$.

The adequate method for introducing external forces in the model mainly depends on the method for simulating the motion of the string. As will be seen in Sect. 1.3 methods using travelling waves use additional boundary conditions at the bowing point, whereas it is easier to include external forces in the string equation in a modal description.

Bow-string interaction

When the bow is drawn across the string, a complicated interaction takes place. The bow-hair ribbon consists of more than 200 hairs (up to 400 for the double bass) attached to the wooden stick of the bow. The hairs form a multi-layer ribbon, which means that the number of hairs interacting with the string depends on the bow force. Moreover, the player can vary the number of hairs in contact with the string and modify the mechanical characteristics of the contact point by tilting the bow more or less. Finally, the bow itself is a dynamical system that interacts with the string. The coupling between the bow and the vibrating string can be felt through vibrations in the bow stick [6]. The vibrations in the bow hair, both in the transverse and longitudinal directions, may affect the interaction with the string.

The theoretical description of the frictional characteristics in the contact area is of primary importance in understanding bow-string interaction. Several models that explain the relation between the frictional force and the differential motion of the two bodies in contact, and quantify the limiting static force before sliding occurs, have been developed. General models and studies related to this topic are reviewed by Serafin ([76], chapter 2). Concerning the violin, a precise modelling would have to take into account the interaction of each bow hair in contact with the string, the particular surface of the hair, and the role that the rosin plays in the interaction. Such a precise modelling is not within reach, but fortunately less detailed, but experimentally justified, ways of describing the interaction have been found useful.

The basic way of modelling the interaction consists in neglecting the width of the bow and considering a single point contact between the bow and the string. The interaction of all hairs constituting the layer is replaced by an overall friction characteristic giving the friction force F_0 as a function of the bow force F_b and the relative velocity Δv between the string and the "bow"

$$F_0 = \mu(\Delta v) F_b \tag{1.9}$$

Early measurements by Lazarus [48] gave the standard shape for the friction curve $\mu(\Delta v)$. In his work, the static maximum friction coefficient $\mu_s = \mu(0)$ was found to be between 0.8 and 1.4 and the asymptotic value of the dynamical friction

$\mu_d = \mu(\infty)$ was around 0.2. Various expressions have been given for describing this curve

$$\mu(\Delta v) = \mu_d + \frac{\mu_s - \mu_d}{1 - \frac{\Delta v}{v_c}} \qquad \text{(hyperbolic model)} \tag{1.10}$$

$$\mu(\Delta v) = \mu_d + (\mu_s - \mu_d)e^{-C|\Delta v|} \qquad \text{(exponential model)} \tag{1.11}$$

Typical values used are $\mu_s = 0.8$ and $\mu_d = 0.3$. More recently, Smith and Woodhouse [81] fitted experimental data with

$$\mu(\Delta v) = 0.4e^{\Delta v/0.01} + 0.45e^{\Delta v/0.1} + 0.35 \qquad \text{(double exponential model)} \tag{1.12}$$

In addition, they observed an hysteresis behaviour of the friction curve which led them to consider modifications in the rosined interface between the string and the bow caused by variations in temperature during the stick-slip cycle. More elaborate models depending on relative velocity as well as temperature were developed and used for more accurate simulations [89].

Leaving aside specific studies on the friction characteristics in the interaction, improvements of the model could be made by including a finer description of the mechanics of the bow-string contact. Because of the finite width of the bow hair, effects could occur that are not taken into account in the single point contact model. Early works by McIntyre et al [52], in which the width of the bow was modelled with two single-point models separated by a short distance, showed that slipping could occur at the edge of the bow facing the bridge while the string is still sticking at the opposite edge, producing an irregular vibration in the part of the string between the bow and the bridge. This differential slipping was later explored in depth by Pitteroff [63] who proposed an efficient finite element model for simulating the contact across the full width of the bow hair.

An important improvement in the description of the bow-string interaction consists in adding compliance to the bow hairs. So far, the string has been assumed to be bowed by an object with a known velocity (stiff bow). But a real bow has inherent dynamical properties, including vibration modes of the stick and the elasticity of the bow hair. In combination they give rise to prominent transverse and longitudinal resonances in the bow, as seen by the string. The effective velocity of the bow hair at the contact point may consequently differ slightly from the velocity that the player imposes to the bow at the frog. In particular it may be modulated periodically by the resonances of the bow. Pitteroff introduced the compliance of the bow stick and the bow hair in his model, and showed how they affected differential slipping when the bow has a finite width.

A basic way of simulating the dynamical properties of the bow is shown in Fig. 1.3. In this approach, the bow hair is represented by a small mass, connected to a heavier mass (the stick) by springs and dampers, which define bow modes in the bowing direction and normal to the string. Control parameters of bow force and

velocity are applied at the heavy mass, and the actual values at the contact point are derived from the model [1].

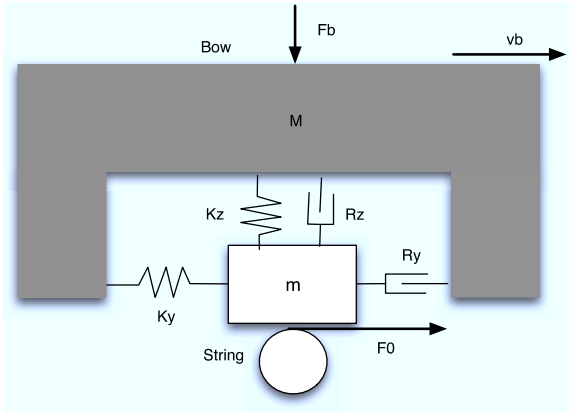

Figure 1.3: Basic model for simulating the dynamical properties of the bow (after Adrien [1]). The bow hair is represented by a small mass m connected to a heavier mass M representing the stick. The spring-damper systems connecting the two masses in the bowing direction (transverse to the string) and the normal direction (in the direction of the bow force) permit to simulate prominent vibration modes of the bow. Control parameters such as bow velocity and bow force are applied on the mass M, and corresponding variables at the bowing point are derived from the dynamics of the system interacting with the string.

Effect of the string terminations

In the previous sections we have only considered simply supported string terminations, or a purely resistive model in Raman's case. In reality, the string terminations have a strong influence on the vibration of the string. A striking illustration is the long decay of a violin pizzicato played on an open string compared to the very short pluck when the string is stopped by a finger. The finger apparently adds a substantial resistive part to the termination.

The influence of the bridge termination and the vibration transmission to the body of the instrument are of primary importance. Whereas for struck or plucked instruments the transmission of the string vibrations through the bridge must be determined by a trade-off between loudness and duration of the tone, the sustained excitation for bowed string instruments allows a much higher transmission of the strings vibrations to the body.

The resonances of the string given by Eq. 1.3 ($f_0 = \frac{1}{2L}\sqrt{\frac{T_0}{\rho_L}}$ and $f_n = nf_0$) were obtained by assuming rigid boundary conditions. However, the simplicity

of this relation is compromised by the effect of the terminations. If a complex admittance at the bridge Y_{br} is assumed, the (complex) angular frequencies of the string resonances become [84]

$$\Omega_n = 2\pi n f_0 \left[1 + \frac{2\pi^2 EI\rho_L}{T_0^2}(nf_0)^2 + \frac{T_0}{2\pi L} Im(Y_{br}) \frac{1}{nf_0}\right] \left(1 - j\frac{Q_n^{-1}}{2}\right) \qquad (1.13)$$

The term Q_n^{-1} represents all mechanisms contributing to the damping of the vibrations, including the real part of the complex bridge admittance $Re(Y_{br})$, which gives the energy transferred to the bridge. The equation also predicts a frequency correction of the harmonic series, to which the imaginary part of the bridge impedance $Im(Y_{br})$ contributes. When the imaginary part is positive, corresponding to a masslike impedance, the mode frequencies of the string are raised slightly, and when it is negative (springlike impedance) they are lowered. Fig. 1.4 shows the amplitude and the phase of a typical complex admittance measured at the bridge of a violin.

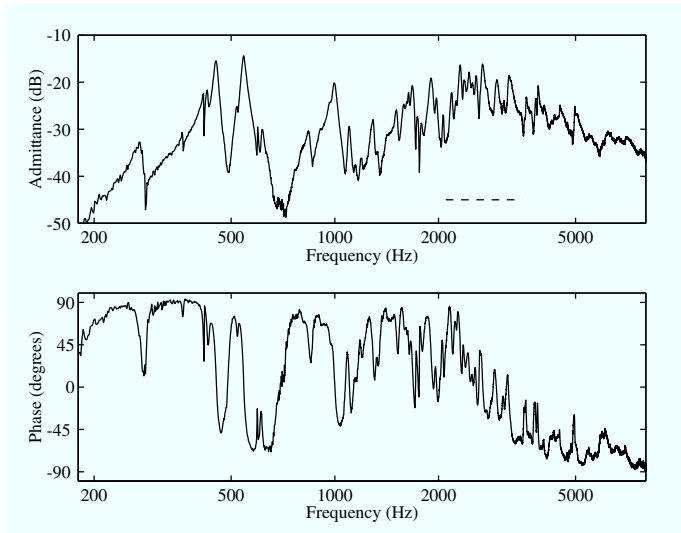

Figure 1.4: Input admittance of a violin. The upper panel shows the magnitude in dB re 1 m/s/N. Lower panel shows phase. (From Woodhouse [90])

Measurements of the mechanical admittance at the bridge can be used for computing the reflection coefficients. Another approach is to model the bridge and body as a lumped mechanical system. For instance, Cremer [19] used a spring-damper system for simulating a simple frequency-dependent bridge termination (see Fig. 1.5a).

The mechanical properties of the bridge itself are of specific interest because it constitutes the link between the two fundamental elements of the violin, the string and the body, which are separated by a large difference in mechanical impedance. In Fig. 1.5b and c, two mechanical models of the bridge are shown for comparison. The force F_{bridge} exerted by the string on the bridge is coupled to the violin admittance $Y_v(\omega)$ under the bridge through simple mechanical systems representing the bridge. In Fig. 1.5b, a mass spring system similar to Fig. 1.5a is used, whereas in Fig. 1.5c, a more complicated system acting on two points of the violin body is considered, simulating the effect of the bridge feet.

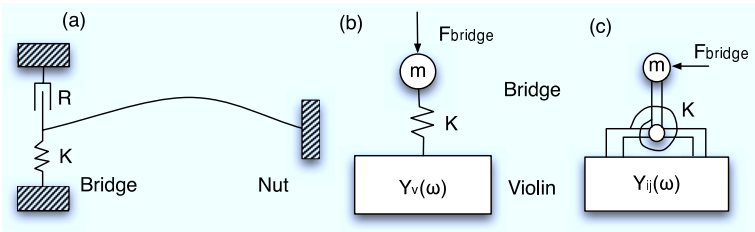

Figure 1.5: Different models of the bridge and the body. (a) Cremer's model for simulating a simple frequency-dependent termination at the bridge. (b) A simple mass-spring system is used to link the force acting on the bridge and the mechanical admittance of the violin under the bridge $Y_v(\omega)$. (c) A refined model of the bridge acts on two points of the violin body, corresponding to the feet of the bridge. (After Woodhouse [87, 90])

Torsional modes

Real strings have a finite diameter, and when the string is bowed, the friction force acting on the surface of the string causes a twisting in the bowing direction (Fig. 1.6). The effective string velocity under the bow (at $x = x_0$) is therefore composed of the transverse velocity $\dot{y}(x_0, t)$ at the center line of the string and the velocity at the surface due to torsional waves propagating on the string

$$\dot{y}_{eff}(x_0, t) = \dot{y}(x_0, t) + r\dot{\phi}(x_0, t)$$

where r is the radius of the string.

The wave equation for the torsional angle $\phi(x, t)$ can be written as

$$\frac{\partial^2 \phi(x,t)}{\partial t^2} = c_\phi^2 \frac{\partial^2 \phi(x,t)}{\partial x^2} \qquad c_\phi = \sqrt{\frac{G}{\rho}} \tag{1.14}$$

where ρ is the density of the string. For a plain string, the shear modulus G can be simply deduced from the Young's modulus E and the Poisson's ration ν

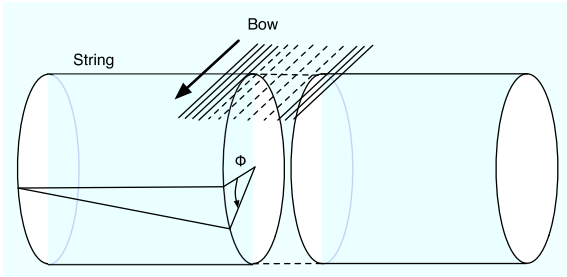

Figure 1.6: Illustration of the torsion of the string generated at the bowing point. The friction force acts at the surface of the string and causes a torsion ϕ in the bowing direction which propagates along the string with a greater velocity than transverse waves. The torsional modes contribute to the dissipation of energy in the string and influences the dynamics at the bowing position.

$$G = \frac{E}{2(1+\nu)}$$

The velocity of torsional waves is generally much higher than the velocity of transverse waves. Another difference is that torsional waves are highly damped. For this reason, they can be expected to have a small direct influence on the generated sound. However, the boundary conditions under the bow introduce a coupling between transverse and torsional waves, which influences the interaction with the bow and the shape of the friction characteristics. As torsional waves are highly damped due to the internal deformation of the string, they may contribute significantly to the overall damping of the transverse waves. Moreover, torsional waves have some effect on the sound by producing aperiodicities and jitter, as discussed by Bavu et al [8]. It can be noted that the torsional waves play an important role in the generation of oscillations with anomalous low frequencies (ALF), as shown by Guettler [32].

Previous sections have presented the different elements of a complete description of the bowed-string motion, including the coupling to the violin. In short, the elements included were string models with different levels of sophistication, a description of the interaction with the bow, and different boundary conditions describing the coupling to the violin body. Possible refinements of the models were presented in order to enhance the rustic character of the model that will be developed in Chapt. 2 and used in the following experiments of this work. Our model will consist of a stiff string with damping, vibrating in one direction only, and with simply supported boundary conditions at both ends. Torsion will not be taken into account. The bow is assumed to act as a rigid body at one point of the string, with a friction interaction described by the hyperbolic model.

Many of the features that were mentioned before will consequently not be taken into account. However, the simplicity of our bowed-string model is motivated by two reasons. First, an efficient algorithm is required in order to simulate the motion of the string in real time. Secondly, a main purpose of the present work is to examine how a realistic control of the model influences the realism of sound synthesis. Consequently, a naturally sounding synthesis obtained by refinements of the model is not a goal in itself in our work.

1.3 Techniques for simulating the bowed string motion

The last part of this introductory chapter is concerned with the solutions of the equations describing the bowed-string system. Usual methods for simulating the motion of the string can be divided in two main categories, depending on whether they aim at a direct solution of the string equation or apply the method of propagating waves. The differential equation describing the dynamics of the string can be solved using numerical methods like finite difference schemes or more elaborated mathematical tools like finite element analysis, but these methods are often considered as being expensive from a computational point of view. Other methods like the MSW algorithm or waveguides (both described below) use the D'Alembert solution of the flexible string equation for simulating waves propagating on the string. The computational cost of such methods is much lower, but solutions must be found for reproducing the effect of features not taken into account in the basic string equation, such as stiffness and damping.

In the following sections some of these methods are briefly described together with specific problems related to each of them.

Numerical solution of the string equation

Finite differences schemes

The basic way of solving the string equation numerically consists in rewriting the differential equation using discrete integration schemes. By choosing an adequate scheme, the displacement $y(i, j)$ of a point $x = i\Delta x$ at time $t = j\Delta t$ can be expressed as a function of displacements at various points on the string at previous times. This method was first presented by Hiller and Ruiz [41] for sound synthesis purposes. Eq. 1.6 can be written as

$$\rho_L \frac{1}{\Delta t^2}\Big[y(i,j+1) - 2y(i,j) + y(i,j-1)\Big] = T_0 \frac{1}{\Delta x^2}\Big[y(i+1,j) - 2y(i,j) + y(i-1,j)\Big] - EI\frac{1}{\Delta x^4}\Big[y(i+2,j) - 4y(i+1,j) + 6y(i,j) - 4y(i-1,j) + y(i-2,j)\Big]$$

which leads to (with $\Delta x = c\Delta t$)

$$\begin{aligned} y(i,j+1) = &- 6ay(i,j) + (1+4a)[y(i+1,j) + y(i-1,j)] \\ &- a[y(i+2,j) + y(i-2,j)] - y(i,j-1) \end{aligned} \tag{1.15}$$

with

$$a = \frac{EI}{T_0 \Delta x^2}$$

With this scheme, the displacement of each point $i\Delta x$ of the string at time $(j+1)\Delta t$ is entirely deduced from the displacements at previous times $j\Delta t$ and $(j-1)\Delta t$. Including damping will make the computation more complicated. For instance, with the damping term added by Hiller and Ruiz [41]

$$R(x,t) = -2b_1 \frac{\partial y}{\partial t} + 2b_3 \frac{\partial^3 y}{\partial t^3} \quad ,$$

the derivation of $y(i,j+1)$ gives an expression depending on $y(i,j+2)$, which makes it necessary to use a converging iterative algorithm. Alternatively, explicit recursion can be obtained with other discretization schemes [17] or other damping models. For example, Bensa [10] uses a term $2b_2 \frac{\partial^3 y}{\partial x^2 \partial t}$ in the string equation.

The effect of the string terminations can be taken into account by finding some other recursion relations that will be coupled with the recursion relation of the string displacement. If the terminations are rigid, we simply get $y(0,j) = y(N,j) = 0$ whatever the time j. Simple mechanical models of the bridge could also lead to recursion. In [41], the losses at the end supports were simulated by considering reflection coefficients a_{bridge} and a_{nut} at the two terminations. Then, the motion of the string could be obtained by coupling Eq. 1.15 with the termination relations

$$y(0,j+2) = (1 - a_{bridge})y(1,j+1) + a_{bridge}y(0,j)$$

$$y(N,j+2) = (1 - a_{nut})y(N-1,j+1) + a_{nut}y(N,j)$$

Note that these expressions were obtained by considering uniformly propagating waves on the string ($g_1(i+1,j) = g_1(i,j-1)$), which should be considered as an approximation for the stiff string case.

Whereas this discretization method has been widely used for simulating plucked and struck string instruments [9, 10, 17, 18, 12], applications for the synthesis of bowed string instruments are rare. To our knowledge, only Hiller and Ruiz in their seminal paper dealt with this problem. In their work, a very simplified model for the friction was considered. During the sticking phase, the velocity of the string was equal to the bow velocity, and during the sliding phase, friction was neglected and the string was therefore free to oscillate until it was moving again in the same direction as the bow. This very simple model was only used for constant bow force and constant bow velocity.

Decomposition into orthonormal functions

In order to avoid a discretization in space of the string equation (Eq. 1.6), it can be interesting to look for a decomposition of $y(x,t)$ into orthonormal functions. The general solution of the linear string equation for free oscillations can be written as

$$y(x,t) = \sum_{n=1}^{\infty} a_n(t)\phi_n(x) \quad \text{where} \quad a_n(t) = \int_0^L y(x,t)\phi_n(x)dx \tag{1.16}$$

If the basis $\phi_n(x)$ is assumed to be orthonormal, the external forces can be decomposed on the same basis

$$F(x,t) = \sum_{n=1}^{\infty} f_n(t)\phi_n(x) \quad \text{where} \quad f_n(t) = \int_0^L F(x,t)\phi_n(x)dx \tag{1.17}$$

After multiplying the string equation by $\phi_n(x)$ and integrating in space we obtain the modal equations

$$M_n\ddot{a}_n(t) + R_n\dot{a}_n(t) + K_n a_n(t) = f_n(t) \tag{1.18}$$

By using this analytical integration in space, it is therefore possible to simplify the differential equation depending on time and space in order to get an infinite number of equations depending only on time. A numerical method can then be used for integrating the equations in time. For computational convenience, the set of modal equations will be truncated to the N first modes.

This method has been applied to the bowed string by various authors with rather small differences, mainly in the numerical scheme for the time integration (see Antunes [2], Adrien [1], Doel [22] and Palumbi [59]). If the simplest case of the flexible string with simple supports at both terminations is considered, the orthonormal functions $\phi_n(x)$ can be written as

$$\phi_n(x) = \sqrt{\frac{2}{L}} \sin \frac{n\pi}{L}$$

and the modal equations are

$$\rho_L \ddot{a}_n(t) + T_0 \left(\frac{n\pi}{L}\right)^2 a_n(t) = f_n(t) \tag{1.19}$$

This method will be developed in the next chapter.

Travelling waves

As discussed before the general solution to the wave equation for the ideal string (Eq. 1.1) is composed of two terms, representing waves travelling in opposite directions (Eq. 1.2). The simulation of these travelling waves offers an interesting alternative to the numerical solution of the wave equation presented above. This approach is rather intuitive, simple to implement, and because the propagation can be modeled using delay lines, the computational cost is very low.

In the case of bowed strings, two methods can be considered: the McIntyre-Schumacher-Woodhouse algorithm [53] (MSW algorithm in the following) and the waveguide method. The two methods focus on incoming and outgoing waves under the bow. In both cases, outgoing waves are computed from incoming waves and the action of the bow. However, the two methods differs in the computation of the reflections from the terminations of the string (incoming waves). Effects of the propagation on the string (damping, inharmonicity) are reproduced by reflection functions in the MSW algorithm, whereas the waveguide method uses digital filters.

MSW algorithm

The principle of the MSW algorithm is developed in [53] and illustrated in [54] for the specific case of the bowed string. The string is separated in two parts by the bow. On the left part, the incoming wave q_{iL} propagates towards the bow and the outgoing wave q_{oL} in the other direction (towards the corresponding termination of the string). On the right part, the two corresponding travelling waves are denoted q_{iR} and q_{oR}. With these notations, the velocity q under the bow is equal to the sum of the incoming and outgoing waves on each part of the string and can be written as

$$q = q_{iL} + q_{oL} = q_{iR} + q_{oR} \tag{1.20}$$

Incoming waves are summed at the bowing point for obtaining their contribution to the string velocity.

$$q_h = q_{iR} + q_{iL} \tag{1.21}$$

This "historical" velocity represents the velocity that the string would have if no force was applied at the bowing point. The contribution of the friction force F_0 to the velocity can be computed from the characteristic impedance of the string.

$$\frac{1}{2Z_c}F_0 = q - q_h \tag{1.22}$$

The force F_0 and the velocity q must be determined from this expression together with the friction characteristic depending on the bow velocity q_b

$$F_0 = F_0(q - q_b, F_b) \tag{1.23}$$

Once the pair of values (F_0, q) is known, the outgoing waves are computed using Eq. 1.20 and Eq. 1.22

$$q_{oL} = q_{iR} + \frac{1}{2Z_c}F_0$$

$$q_{oR} = q_{iL} + \frac{1}{2Z_c}F_0$$

The critical point of this method lies in the description of the reflections at the string terminations. Once the outgoing waves are computed, they propagate along the string during a given time (which can give rise to some dispersion and dissipation), then they are reflected at the string terminations (where some of the wave can be transmitted or absorbed), and finally they propagate again towards the bow. It is therefore necessary to find a way of describing all the elements that characterize the propagation and the reflection, in order to compute the corresponding incoming waves. Reflections functions $r_L(t)$ and $r_R(t)$ are used, describing all the effects of the propagation on the left and right sections of the string. Incoming waves can therefore be computed as

$$q_{iL} = r_L * q_{oL} \tag{1.24}$$

$$q_{iR} = r_R * q_{oR} \tag{1.25}$$

where the asterisk denotes convolution. The influence of the reflection functions is drastic and has been studied in [54, 87, 88], among others. In [53], improvements of the previous model were also considered in order to take into account the torsional modes of the string, the compliance of the bow, and a two-points bow model for simulating the width of the bow. Pitteroff [63, 64] described in depth the contact between the bow and string and proposed a complete model in which a finite difference scheme was used for solving the system under the bow and the MSW algorithm for the remainder of the string. The model used by Guettler [33] is also based on this solution.

Waveguides

The MSW algorithm can be considered as a forerunner to the waveguide technique, which also uses the general solution of the string equation, composed of two propagating waves in opposite directions, as a starting point. The solution to the friction interaction is the same, as well as the principle of transforming the propagating waves. The main difference lies in the formulation of the waveguides which is more signal-processing oriented.

If c is the wave velocity on the string, D'Alembert's solution can be sampled in time with a period T and with an interval X in space such as $X = cT$. The discrete positions and times are denoted $x_m = mX$ and $t_n = nT$. Then, the displacement can be expressed as

$$y(t_n, x_m) = y_+(n - m) + y_-(n + m) \tag{1.26}$$

Note that the similar relations could be obtained in the same way for the string velocity and other variables such as the string acceleration or slope.

Without losses during the propagation, we have $y_+(n-m) = y_+((n-1)-(m-1))$ and $y_-(n+m) = y_-((n-1)+(m+1))$, which means that the displacement at any time t_n and any position x_m can be obtained from the values of the propagating waves y_+ and y_- at the preceding sampling time for adjacent discrete positions. In a more general way, the system can be represented with two rails representing delay lines for the waves y_+ and y_- propagating in opposite directions (see Fig. 1.7). The displacement can be computed by adding the outputs from the two delay lines at position m.

In Fig. 1.7, $1/z$ denotes a one-sample delay, and the value of the waves between two positions in the delay line is multiplied with a loss factor g for simulating dissipation during the propagation. At the terminations of the string, incoming waves y_- are converted into outgoing waves y_+. For the simplest case with a rigid string termination, y_- is simply reflected with opposite sign in order to get $y_+(n) + y_-(n) = 0$. For the bowed string, several effects need to be taken into account in order to obtain a realistic simulation. For example, frequency-dependent losses are introduced by inserting filters between adjacent positions in the delay line instead of a plain multiplication with g.

The main challenge using waveguides consists in designing filters that reproduce the desired features of the system. For instance, losses during the propagation can simply be simulated using a gain factor $\|g\| < 1$ between two sampling positions. Frequency-dependent losses can be implemented with zero-phase, finite impulse response filters $G(\omega)$. Serafin [76] simulated the frequency-dependent velocity of propagation by using three 4-th order allpass filters in cascade, and approximated the reflection functions described in [87] with second order low-pass IIR filters. The design of adequate filters has been described in depth by Smith [82].

In particular, Serafin [76] has developed a very complete model including torsional waves, improved friction model and a refined model of the bow hair inspired

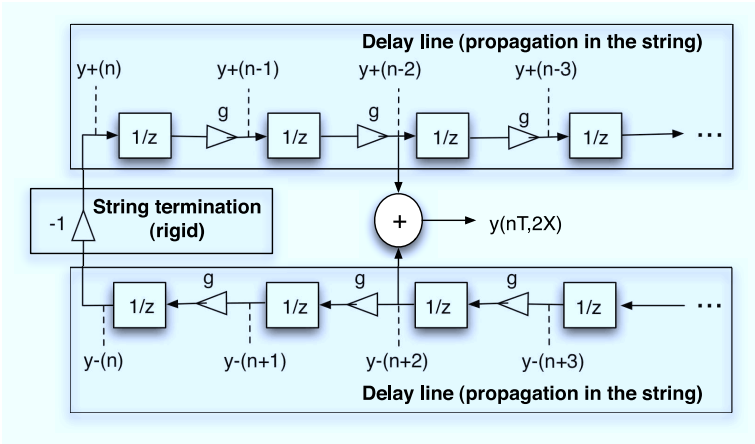

Figure 1.7: Block diagram of a basic waveguide string model including internal losses in the string and a rigid termination. The waves $y_-(n-m)$ (lower rail) propagate from right to left and the waves $y_+(n+m)$, from left to right. The boxes $1/z$ denote a one-sample delay and the triangles a multiplication with a loss factor g. At the string termination, the incoming wave y_- is simply reflected with opposite sign such as $y_+(n) + y_-(n) = 0$ at any time nT. The displacement at any point of the string can be obtained by summing the value of the two travelling waves at this point.

by Pitteroff's work [63]. A block diagram describing such a system is reproduced in Fig. 1.8.

1.4 Conclusions

The purpose of this first chapter was to provide all the necessary information for the reading of the following chapters. The fundamentals of the mechanics of the bowed string and the coupling to the instrument have been presented, as well as an overview of the problems related to the modelling and the numerical implementations. In the first section, basic derivations concerning the influence of the bowing parameters on the vibration were reviewed, based on Helmholtz's observations of the motion of the bowed string. The amplitude of the string vibration was found to be proportional to bow velocity and inversely proportional to bow-bridge distance. The argument of corner rounding was presented in order to offer an explanation of the effect of bow force on the spectral content of the vibration. In Chapter 3, these theoretical inferences will be compared with simulations, and in Chapter 5 and 6, we will present observations on the use of the bowing parameters by violinists, reflecting their control strategies for common bowing patterns in string playing

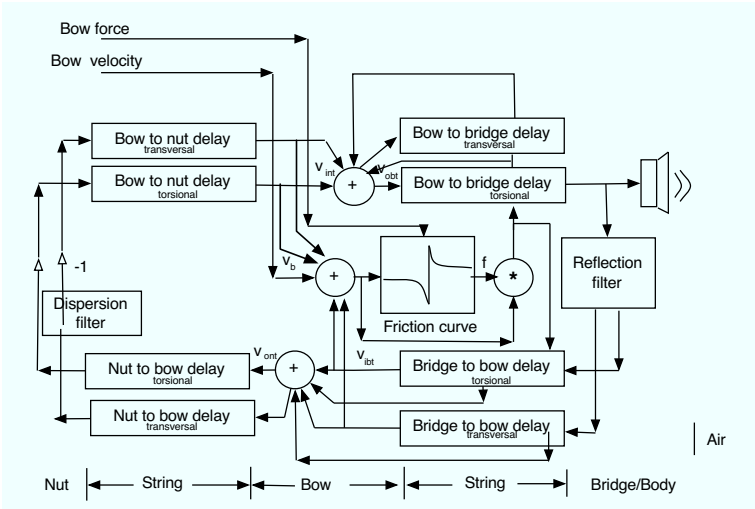

Figure 1.8: Block diagram of a digital waveguide model of a bowed string including torsional waves and allpass filters for stiffness simulation (after Serafin [76]).

In the following experiments and analyses, we will use a simple model of the bowed string, consisting of a stiff string with damping, simply supported at both terminations, and a bow modelled as a rigid body acting at a single point of the string. String torsion is not taken into account.

In the second section, the influence of string stiffness and damping were reviewed, which are necessary elements in a more complete model. Important elements of a complete violin model were presented, in particular related to the properties of the bridge and the bow, together with an overview of studies related to bowed-string instruments. Finally, different implementations of bowed string models were presented. The model that will be described in the next chapter is based on a modal solution of the string equation. However, we will often refer to other methods, for example when discussing the pros and cons of our model, or when comparing the computational cost of different methods.

Some fundamentals aspects of the bowed string were not included in this introductory chapter, but will be presented in the course of the following chapters. This applies to the playability of the model, i.e. the possible combinations of bowing parameters for obtaining Helmholtz motion. That will be the subject of Chapter 3 in which simulations will be observed in the light of the underlying theories.

Chapter 2

Modal formalism and numerical implementation for sound synthesis

In this chapter, a model for synthesising violin-like sounds is described. The model was developed and used throughout this work as a tool for testing bowing-gesture models and other aspects of the violinist's control of the sound. The first section presents the background and the underlying ideas on which the model was built. Section 2.2 describes the derivation of modal equations from the string differential equation. The formalism described basically aims at converting the string equation, depending on time and space, into a new set of equations depending only on time. Section 2.3 details the numerical solution of these equations, and their implementation for simulating a string with a friction interaction at the bowing point and a "finger" setting the pitch. The influence of the computation parameters (sampling frequency and number of modes) is illustrated by simulations in section 2.4. Finally we conclude by discussing some additional features that could be incorporated into the model.

2.1 Introduction

This section aims at giving some keys for understanding our approach to the subject and the ideas which drove the development of the model. We focused on a very simple model from a physical point of view, consisting of a string with stiffness and damping, vibrating in only one direction. This is rather far from the physically most relevant and elaborate description of the system, but some justifications can be found in the light of our objectives. We also chose a modal simulation for reasons that will be explained thoroughly. Finally, we will discuss the compatibility between the modal formalism and real-time implementation, and how computational cost considerations have influenced the development of the model.

Realistic physical modelling versus realistic sound synthesis

The realism of a physical model is often judged based on the number and refinement of the physical effects that are taken into account. Consequently, a large amount of work has been devoted to include more and more phenomena in the description of the motion of the bowed string, as described in the previous chapter (Sect. 1.2). Important contributions are the effect of bow-hair width, and the coupling between the vibrations in the bow and the string [63], the effect of torsional waves [8, 79], and detailed friction characteristics [89].

In our case, we decided to develop a model that was as simple as possible. Actually, it only consists of a string described by the classical string equation for small amplitudes in one dimension. The variations in string tension are neglected, the density is uniform, and the string is simply supported at both terminations. Except for the influence on the damping of the partials, no interaction with the body of the instrument is modelled. The bow is considered as a rigid body, controlled by a velocity and a force normal to the string. The bow acts at a single point on the string through a basic friction model.

Such a bias toward simplicity does not mean that all other elements mentioned above are assumed to have no influence on the string vibrations. However, in this work we were concerned with "realistic" sound synthesis of bowed string instruments rather than realistic physical modelling or detailed studies of the mechanics of the bowed string through simulations. The model will be tested in Chapter 3 in the light of theoretical and experimental studies in order to judge the realism of the simulated output, but it should be underlined that the model has never been intended to serve as a scientific simulation tool. In this work, we are focusing on the influence of a realistic control on the realism of the bowed string sounds. Such studies could be performed also with the use of more complex models. However, by using a very basic model we wanted to demonstrate that the realism of the sounds of the bowed string is hidden just as much in the control of the model as in the model itself.

On the choice of modal synthesis

In the previous chapter, we saw that the physical equations describing the dynamical behaviour of the bowed string can be simulated by different methods, including the use of travelling waves, finite difference schemes, or modal formalism. The choice of a specific technique is determined by several considerations, such as performance criteria that need to be fulfilled, computation cost when real-time synthesis is a goal, and the key characteristics of the system that is modelled. For instance, waveguides work well for nearly harmonic systems, whereas modal formalism could be preferred for more complex structures, especially for strong inharmonicity, as pointed out by Serafin [76]. A review and evaluation of physical modelling techniques can be found in [83]. For the particular case of bowed strings, the waveguide method as developed by Serafin [76], or the MSW algorithm used by Woodhouse

et al and Guettler [33], have shown to be the most efficient and accurate way of simulating the vibration of the bowed string for synthesis purposes.

Then, why would we use modal formalism for simulating the bowed string when other methods already have proved their efficiency for the case we are interested in? Two reasons have contributed to this choice. One reason was the scientific environment in which this work was performed, the *Acoustics of musical instruments* group at IRCAM. Through the works of Adrien [1] and Bensoam [11], a software (Modalys) for sound synthesis based on modal representation of vibrating objects was developed by the team, and many works since aimed at evaluating or incorporating new models in this framework. The idea was consequently to stay as close as possible to the research direction of the group. However, we did not wish to use Modalys directly in this work. Rather we preferred to develop a simpler simulation tool in order to facilitate experiments with different implementations and later development for real-time synthesis.

The second reason is related to the principles behind the different simulation methods. In the finite difference method, a model describing the string is defined and then solved by brute force of classical numerical schemes. It is consequently a pure physical modelling method. Each effect that is observed must have a corresponding cause in order to be included in the string equation or the boundary conditions, else it will not be reproduced. In contrast, waveguides simulate the effects more than the physical causes. Waveguides make use of the ideal string equation for deriving an exact solution, but the effect of stiffness and damping are reproduced using signal processing tools, including filters and delay lines. Modal synthesis is somewhere between the two: it allows a mathematically elegant way of solving the wave equation in order to derive the modal model. At the same time, some of the parameters can be freely set for obtaining a given effect. The choice between the different methods is a matter of scientific purpose.

On the influence of the real-time horizon

Modal synthesis is often considered as a computationally expensive way of simulating the motion of the bowed string. A few years ago, a real-time implementation of this method was certainly not within reach, but this limitation has been removed today. Even if the simulation of an ideal string could seem somewhat laborious with the modal formalism compared to the simplicity and elegance of waveguides, we will see that for more elaborate models of the string, modal formalism offers a straightforward and not so expensive way of solving the problem. For example, including bending stiffness or damping does not increase the computation cost, and spatial interpolations for accessing any point on the string are naturally included in the model.

Nevertheless, the development of the model has been influenced by the relatively high computation cost of the method. Computational considerations and the need for real-time implementation had to be balanced against the complexity of the model and numerical accuracy in the simulations.

2.2 General principle

A modal model is a description of the vibrating properties of a mechanical system. This description consists in a set of N natural frequencies ω_n with corresponding damping factors r_n, and a set of shape vectors $\phi_n(x)$ describing the associated spatial amplitude distributions of the modes of vibration (the displacements of points moving at the same frequency). The modal properties of a vibrating object can be deduced by analytical derivation (from a dynamical description) or by experimental investigation.

Modal analysis finds applications in the study of complex vibrating structures in the field of musical acoustics. But, as pointed out by Debut [20], this formulation has hardly been used in the case of self-sustained oscillations. The starting point of the development presented here is Adrien's work dealing with the use of modal decomposition for sound synthesis of bowed string instruments [1]. We will mainly refer to his work for emphasising differences. Contributions to the development have been made by Antunes et al [2].

In this section, we first derive the modal model from the equations describing the flexible string and the stiff string. Then, the inclusion of damping in the model is discussed, and we present some measurements for determining the values of the damping coefficients. Finally, we express the modal components of the forces representing the stopping finger (or the nut) and the bow, for the simplest case in which each of them acts at a single point on the string.

Derivation of the modal model

Ideal string

The string equation giving the displacement y along the string (axis x) for a simple flexible string is

$$\rho_L \frac{\partial^2 y(x,t)}{\partial t^2} - T_0 \frac{\partial^2 y(x,t)}{\partial x^2} = \sum_i F_i(x,t) \tag{2.1}$$

where ρ_L denotes the linear density of the string and T_0 the tension. The terms $F_i(x,t)$ represent the force densities acting on the string (i.e. forces distributed along the string).

For free oscillations ($F_i(x,t) = 0$) the solutions are

$$y(x,t) = (A \sin kx + B \cos kx) \exp(\pm j\omega t) \quad \text{with} \quad \rho_L \omega^2 = T_0 k^2$$

The values of k are determined by the boundary conditions. With a simple support at the two terminations of the string ($y(x,t) = 0$ at $x = 0$ and $x = L$), we find an infinity of particular solutions

$$y_n(x,t) = A_n \sin k_n x \exp(\pm j\omega_n t)$$

with

$$k_n = \frac{n\pi}{L} \quad \text{and} \quad \omega_n = \sqrt{\frac{T_0}{\rho_L}}\frac{n\pi}{L}$$

The spatial components $\sin k_n x$ of the solutions are of particular interest because they are orthogonal. By choosing an adequate normalization it is possible to get an orthonormal base of functions (eigenvectors) $\phi_n(x)$ on which the solutions of the string equation (Eq. 2.1) can be expressed. The normalization gives

$$\phi_n(x) = \sqrt{\frac{2}{L}} sin(n\pi\frac{x}{L}) \quad \Rightarrow \quad \int_0^L \phi_n(x)\phi_m(x)dx = \delta_{nm}$$

and the displacements $y(x,t)$ are written as

$$y(x,t) = \sum_{n=1}^{\infty} \phi_n(x)a_n(t) \qquad \Leftrightarrow \qquad a_n(t) = \int_0^L \phi_n(x)y(x,t)dx \tag{2.2}$$

A force $F(x,t)$ acting on the string can be expressed in the same base

$$F(x,t) = \sum_{n=1}^{\infty} \phi_n(x)f_n(t) \qquad \Leftrightarrow \qquad f_n(t) = \int_0^L \phi_n(x)F(x,t)dx \tag{2.3}$$

Combining equations 2.2 and 2.3 with the string equation 2.1, the partial differential equation including the two variables t and x is simplified into an infinity of ordinary differential equations depending only on time. Each modal coefficient $a_n(t)$ is the solution of a modal equation

$$\ddot{a}_n(t) + \omega_{0n}^2 a_n(t) = \frac{1}{\rho_L} f_n(t) \tag{2.4}$$

and the eigenvalues ω_n associated with the eigenvectors $\phi_n(x)$ are given by

$$\omega_n = \omega_{0n} = \sqrt{\frac{T_0}{\rho_L}(\frac{n\pi}{L})^2}$$

Stiff string

Following the same method, it is possible to include other features of the string. For instance, the resistance to bending can be included by adding a shearing force in the string equation, as seen in Chapt. 1.2

$$\rho_L \frac{\partial^2 y(x,t)}{\partial t^2} - T_0 \frac{\partial^2 y(x,t)}{\partial x^2} + EI \frac{\partial^4 y(x,t)}{\partial x^4} = \sum_i F_i(x,t) \tag{2.5}$$

where E is Young's modulus,, and $I = \frac{\pi d^4}{64}$ is the second moment of area for a circular cross section of the string, with d being the diameter of the string.

Solutions of Eq. 2.5 when $F_i(x,t) = 0$ are now

$$y(x,t) = (A\sin kx + B\cos kx + C\sinh kx + D\cosh kx)\exp(\pm j\omega t)$$

with the following dispersion relation

$$\rho_L\omega^2 = T_0k^2 + EIk^4$$

For simply supported boundary conditions at the string terminations $y(x,t) = 0$ and $\frac{\partial^2 y(x,t)}{\partial x^2} = 0$ at $x = 0$ and $x = L$, the spatial components of the solution remain the same as for the flexible string. The displacement and the force can be expressed on the previous eigenvectors $\phi_n(x)$ and the same modal differential equations (Eq. 2.4) are obtained. Only the dispersion relation changes and the eigenvalues ω_n are now

$$\omega_n = \omega_{0n} = \sqrt{\frac{T_0}{\rho_L}(\frac{n\pi}{L})^2 + \frac{EI}{\rho_L}(\frac{n\pi}{L})^4}$$

From the derivations of the modal equations we can stress an important advantage of the modal formalism: The case of the flexible string and the stiff string are formally very similar. In both cases, the solution is the same differential equation 2.4. Only the eigenvalues ω_n differ, but they are parameters of the simulation case, which will be computed only once at the beginning of the simulation. Consequently, the addition of stiffness in the physical description of the string does not increase the computational cost. This is in contrast to other simulation methods. For instance, the waveguide technique requires the use of extra filters to simulate string stiffness, and finite different schemes lead to additional terms in the recursion relation. This point will be developed in Sect. 2.3.

Discussion: On simplicity and the string terminations

In the previous section, expressions for the modal vectors and their eigenvalues were obtained. It must be emphasised that these expressions were obtained for simply supported boundary conditions, chosen for their simplicity. This is a somewhat arbitrary choice, not completely supported by the geometry and mechanical properties of the string terminations on the violin. For instance, they do not take the transmission of the string vibrations to the instrument body through the bridge into account, nor the damping induced by the finger on the fingerboard. Other boundary conditions could have been considered. For instance, Adrien [1] assumed that the string was clamped at both terminations ($y(x,t) = 0$ and $\frac{\partial y(x,t)}{\partial x} = 0$ at $x = 0$ and $x = L$) and obtained the following expressions for the modal vectors

$$n \text{ even:} \qquad \phi_n(x) = \frac{\cosh q_n x}{\cosh q_n \frac{L}{2}} - \frac{\cos k_n x}{\cos k_n \frac{L}{2}}$$

$$n \text{ odd:} \qquad \phi_n(x) = \frac{\sinh q_n x}{\sinh q_n \frac{L}{2}} - \frac{\sin k_n x}{\sin k_n \frac{L}{2}}$$

in which the values of q_n and k_n for even n (left) and odd n (right) are deduced from

$$\tanh q_n \frac{L}{2} = -\frac{k_n}{q_n} \tan k_n \frac{L}{2} \qquad \tanh q_n \frac{L}{2} = \frac{q_n}{k_n} \tan k_n \frac{L}{2}$$

with

$$q_n = \sqrt{k_n^2 + (\frac{T_0}{EI})^2}$$

The equations above must be solved numerically. Alternatively, by considering that $\frac{T_0}{EI}$ is much larger than k_n, they can be developed in order to find analytically approximated values of k_n, q_n and ω_n [84].

From the derivations above it is clear that the simplicity of the proposed formulation depends on the somewhat arbitrary choice of boundary conditions. Other solutions taking the mobility of the string at the bridge into account through a mechanical admittance function could be considered (see Chapt. 1.2). In that case, however, the functions $\phi_n(x)$ would not be an orthonormal base anymore for the solutions of the string equation, and the solution will not be as simple as for the simple supported case. The issue has been discussed by Kergomard et al [45] for the particular case of two resistive terminations, but it is not our intention to enter into this complicated problem.

Instead, our approach consisted in keeping the eigenvectors of the string as simple as possible, and transferred all additional features to forces acting on the string. This approach is illustrated in Fig. 2.1. Instead of computing the modal properties of the string using some specific well-motivated boundary conditions, we keep the simplest possible mathematical formulation by considering the "virtual" terminations simply supported, and the bridge and finger are considered as forces acting at their actual positions on the string.

It could be noted that this representation is not so far from a true description of the real string. The string is actually not directly attached to the bridge or the nut (or finger), but farther away, at the tailpiece and the tuning peg. The string is consequently divided into three parts, two of them not directly participating in the string vibration.

Including damping in the model

The solution to Eqs. 2.1 and 2.5 give undamped oscillations. Damping mechanisms have been shortly described in the previous chapter (see Chapt. 1.2), and different ways can be considered for including damping in the model. For instance, a real impedance modelling purely resistive terminations of the string could be used, but, as shown above, it would make the determination of the eigenvectors more complicated. Alternatively, it would be possible to keep the undamped string equation and use a damper for applying an external resistive force $F_1(t) = -R\dot{y}(x_1, t)$ at one point x_1 very close to one of the string terminations.

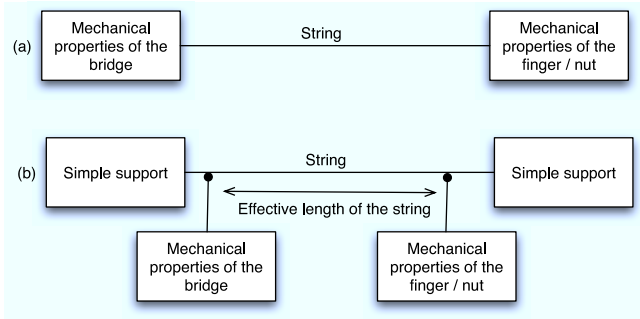

Figure 2.1: Alternative ways of taking the boundary conditions of the string into account. (a) The mechanical properties of the bridge and the finger (or nut) are used for computing the modal characteristics of the string, resulting in non-orthonormal eigenvectors. (b) The string is "virtually" simply supported at both terminations, the bridge and the finger being represented by forces acting at their actual positions on the string.

In this section, we describe the inclusion of a mechanical resistance depending on frequency in the string equation. Damping coefficients for the lowest modes are determined from experimental data and discussed.

Including damping in the string equation

A damping force proportional to the string velocity can be included in the string equation. Such a force is produced for example by the friction of the string in the air and the damping coefficient will be denoted $R_L(\omega)$ for stressing a potential dependence on frequency. The string equation becomes

$$\rho_L \frac{\partial^2 y(x,t)}{\partial t^2} + R_L(\omega)\frac{\partial y(x,t)}{\partial t} - T_0 \frac{\partial^2 y(x,t)}{\partial x^2} + EI\frac{\partial^4 y(x,t)}{\partial x^4} = \sum_i F_i(x,t) \qquad (2.6)$$

With $y(x,t) = \sum \phi_n(x) a_n(t)$, we obtain the modal equations

$$\ddot{a}_n(t) + 2r_n\dot{a}_n(t) + \omega_{0n}^2 a_n(t) = \frac{1}{\rho_L} f_n(t) \qquad (2.7)$$

where

$$r_n = \frac{R_L(\omega)}{2\rho_L} \quad \text{and} \quad \omega_{0n}^2 = \frac{T_0}{\rho_L}k_n^2 + \frac{EI}{\rho_L}k_n^4 \qquad (2.8)$$

The dispersion relation is obtained with $a_n(t) = e^{j\Omega t}$ and $f_n(t) = 0$ in Eq. 2.7

$$T_0 k_n^2 (1 + \frac{EI}{T_0}k_n^2) = \rho_L \Omega^2 (1 - j\frac{R_L(\omega)}{\rho_L \Omega}) \qquad \text{with} \quad k_n = \frac{n\pi}{L} \qquad (2.9)$$

This expression can only be solved analytically if the terms depending on stiffness and the mechanical resistance are assumed to be small compared to unity [84]. In this case, the frequencies are

$$\Omega_n \approx k_n \sqrt{\frac{T_0}{\rho_L}} \left(1 + \frac{EI}{2T_0} k^2 + j \frac{R_L(\omega)}{2\rho_L \omega}\right) \tag{2.10}$$

The frequency ω_n of the modes (real part of Eq. 2.10) does not depend on the damping parameter $R_L(\omega)$. Consequently, the determination of the modal damping values r_n is straightforward

$$r_n = \frac{R_L(\omega_n)}{2\rho_L} \qquad \text{with} \qquad \omega_n \approx k_n \sqrt{\frac{T_0}{\rho_L}} \left(1 + \frac{EI}{2T_0} k_n^2\right) \tag{2.11}$$

However, this way of introducing damping leads to approximate values of the frequencies, and it could be more appropriate to work directly with the modal damping values without considering the damping parameter $R_L(\omega)$. In that case, the damping r_n of each mode can be arbitrary set and the complex frequencies of the corresponding modes are deduced from Eq. 2.7

$$\Omega_n = \sqrt{\omega_{0n}^2 - r_n^2} + j r_n \qquad \omega_n = \sqrt{\omega_{0n}^2 - r_n^2} \tag{2.12}$$

The values of the modal damping coefficients r_n are chosen in order to damp different string modes more or less efficiently. They can be set empirically by listening to the resulting sound, or according to measurements, or according to a model describing the variation of the coefficients with frequency. For example, Adrien [1] assumed a quadratic variation of the coefficients with mode number

$$r_n = B_1 + B_2 (n-1)^2 \tag{2.13}$$

Estimation of damping coefficients from plucked string

The damping coefficients r_n were estimated from the decay times of the partials during the free decay of the string (violin steel D string). To obtain a pure pluck, a loop of thin wire was passed around the string. This wire was used for pulling the string until it broke and the resulting string velocity was recorded using a small magnet placed under the string[1].

The signal was first analysed with a high-resolution method [7] for extracting the frequencies and powers of the partials during successive time windows of 128 samples. In Fig. 2.2, the decrease in amplitude is illustrated for several partials, up to the 15th. As expected, the decay time decreases with increasing partial number, indicating a more prominent damping for highest harmonics.

The solutions of the string equation 2.6 for free oscillations are

[1] These measurements were cordially furnished by Erwin Schoonderwaldt

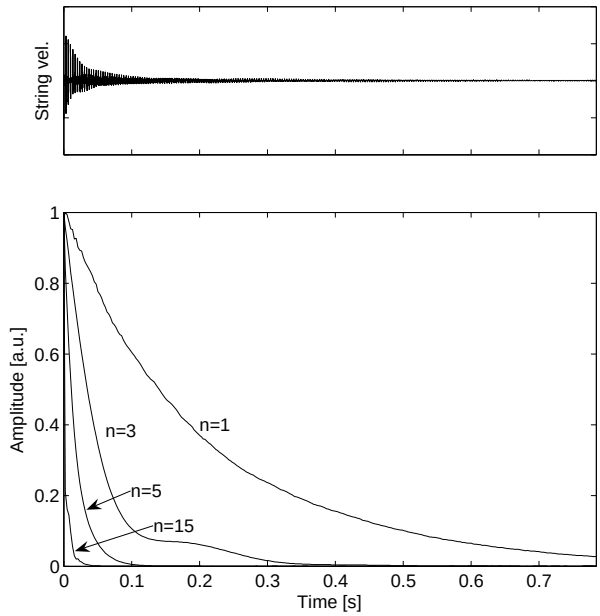

Figure 2.2: Illustration of the decay envelopes for some of the string partials when a violin D string is plucked.

$$y(x,t) = \sum_{n=1}^{\infty} a_n(t)\phi_n(x) \qquad \text{with} \qquad a_n(t) = A_n \sin(\omega_n t - \varphi_n)\exp(-r_n t)$$

where the parameters A_n and φ_n are determined by initial conditions.

The time evolution of the power of each partial can consequently be fitted with an exponential function $e^{-t/2\tau_n}$, the decay time $\tau_n = 1/r_n$ being determined for each partial using a linear fit (on a logarithmic scale) of the envelopes in Fig. 2.2.

Fig. 2.3 shows the resulting decay times τ_n computed for two different situations: an open D string (without finger), and a stopped D string. For the stopped string, all decay times were shortened compared to the open string, illustrating the added damping effect of the finger on the string.

Discussion

In the experiment above, we determined decay times τ_n resulting from a combination of all damping mechanisms. In particular, losses due to the bridge mobility and the stopping finger were included in the decay time, and taken into account in the resulting damping parameter $R_L(\omega)$. The effect of damping at the string

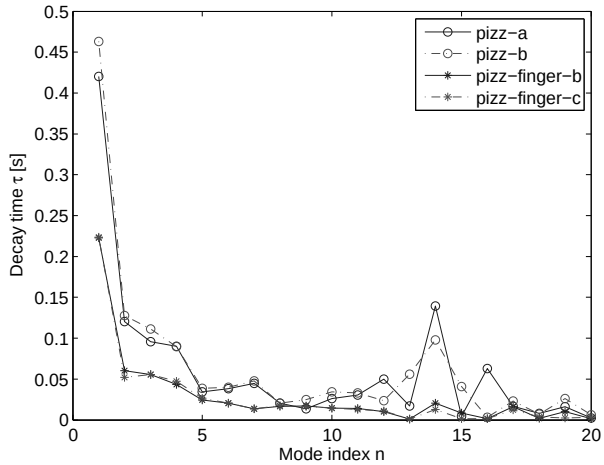

Figure 2.3: Decay times τ_n for the string partials of a D string (open and stopped). Each measurement was repeated two times for checking the reproducibility. The added damping of the finger is clearly illustrated by the shortening of all decay times when the string is stopped.

terminations is consequently incorporated in the string equation, as if it was due to internal damping.

This leads to a small difference compared to the actual effect of the termination. For instance, in the simplified case where the bridge acts as a simple resistance, the amplitude of a wave propagating along the string should decrease each time it is reflected at the bridge. When the effect of the bridge is included in the damping coefficient, the wave amplitude decreases continuously as it propagates along the string. However, if the waves are observed at a given point of the string, no difference between the two cases can be observed, even if they formally are very different.

External forces: Expression of the modal components and basic examples

With the modal formulation described before, there is no difficulty in making external forces acting on string. The modal components of the forces are derived from the projection of the linear forces $F(x,t)$ on the modal vectors $\phi_n(x)$

$$f_n(t) = \int_0^L \phi_n(x) F(x,t) dx$$

Under the assumption that each external force acts at a single point of the string, it can be represented with a dirac function $F_i(x,t) = F_i(t)\delta(x - x_i)$ and the modal

components can be written as a sum involving the effective force and the modal vectors

$$f_n(t) = \sum_i F_i(t) \int_0^L \phi_n(x)\delta(x - x_i)dx = \sum_i F_i(t)\phi_n(x_i)$$

The equations giving the modal components are consequently rewritten as

$$\ddot{a}_n(t) + 2r_n\dot{a}_n(t) + \omega_{0n}^2 a_n(t) = \frac{1}{\rho_L}\sum_i F_i(t)\phi_n(x_i) \tag{2.14}$$

The forces $F_i(t)$ contained in Eq. 2.14 are not known in advance and result from interactions with other more or less complex mechanical systems. Their instantaneous values are therefore determined from other dynamical equations coupled by contact conditions. In the case of the bowed string, we are interested in modelling the action of the finger and the bow. In this section, we will consequently restrict the description to a few examples that will or could be useful for our purpose.

The simplest mechanical system that could act on the string is a damped mass-spring system at a given position x_1. This could for example be used to represent a basic model of the bridge with only one resonance. In that case, $F_1(t)$ is given by the combination of Eq. 2.14 and

$$F_1(t) = -M\ddot{y}_1(t) - R\dot{y}_1(t) - Ky_1(t)$$

The two equations are linked by a contact condition at x_1, stating that the displacement $y(x_1, t)$ of the string at this position equals the displacement of the mass-spring system

$$y(x_1, t) = y_1(t)$$

A more essential example for the bowed string is the frictional force F_0 that acts on the string at the bowing point in order to drive it. In that case, the force must be determined from the string equation and a friction characteristics giving the force as a function of the velocity difference between the bow and the string, as seen in Chapt. 1.2. This interaction can be solved graphically as proposed by Frielander [26] and Keller [44]. The combination force-velocity $(F_0, v = \dot{y}(x_0))$ of the system is given by the intersection between the friction curve and a straight line described by

$$F_0 = 2Z_c(v - v_h) \qquad Z_c = \sqrt{T_0\rho_L}$$

For the modal formalism, we will see that the discretization in time leads to a similar relation where the characteristic impedance of the string Z_c is replaced by a numerical impedance Z_N.

Effect of the number of modes

The formalism described above leads to exact solutions as long as the number of modes is infinite. However, for obvious practical reasons, the modal space must be truncated to a finite number N. Some effects of such a truncation are discussed in this section.

Frequency response

The truncation reduces the number of resonances of the string to the number of modes. A sinusoidal driving force located at x_1 induces a frequency response $\chi_n(\omega)$ for each modal equation 2.14 according to

$$\chi_n(\omega) = \frac{\phi_n(x_1)}{\rho_L(\omega_{0n}^2 + 2jr_n\omega - \omega^2)}$$

Each modal equation corresponds to an oscillator with a resonance frequency $\omega_n = \sqrt{\omega_{0n}^2 - r_n^2}$. The global response $\chi(\omega, x)$ at a specific point x is obtained by summing the response associated with each mode

$$\chi(\omega, x) = \sum_{n=1}^{N} \phi_n(x)\chi_n(\omega) \tag{2.15}$$

Fig. 2.4 illustrates the effect of the truncation on the frequency response computed for $N = 20$ and $N = 50$. In the first case ($N = 20$), the absence of resonances above the 20th is clearly visible. In addition, there is a gap at each multiple of the fifth resonance. Because the driving force acts at a position $x_1/L = 0.2$, the contribution of eigenvectors $\phi_n(x)$ is zero when n is a multiple of $L/x_1 = 5$. Note that these gaps are slightly shifted for $N = 50$, due to the influence of the higher resonances.

Spatial spreading

The finite number of modes also leads to a spatial spreading of the forces. $F(x, t)$ can be computed from the modal components $f_n(t) = \phi_n(x_1)F(t)$ with

$$F(x, t) = F(t) \sum_{n=1}^{N} \phi_n(x_1)\phi_n(x)$$

The sum on the right side in the equation approaches a dirac delta at x_1 as N tends to infinity, but for a finite number of modes it gives a finite pattern around x_1 as shown in Fig. 2.5.

Consequently, the truncation tends to distribute the force along the string. The force does not act at a single point anymore, but shows a spatial width $2L/N$ and some oscillations along the string.

The single point interaction is a practical but rather unrealistic mathematical tool. From this point of view, the spatial extent of the force around a mean position on the string could be regarded as a more realistic situation. However, the small contributions along the string could have a drastic effect on the vibrations. If they become too prominent, the interaction with the bow will immediately influence any point on the string.

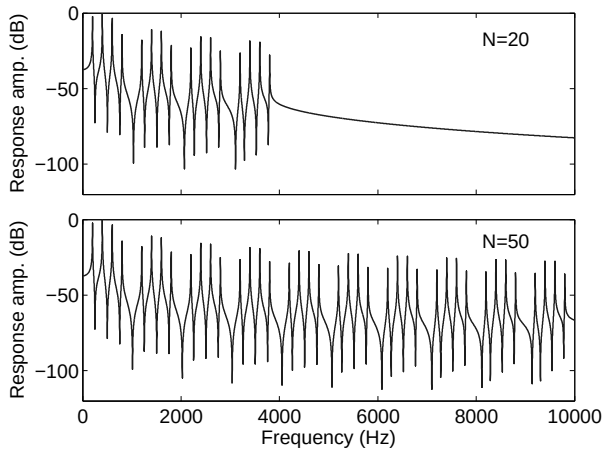

Figure 2.4: Frequency response of a string for two different truncations, $N = 20$ (top) and $N = 50$ (bottom), computed with Eq. 2.15. The string is flexible, with constant damping coefficients $r_n = 5$ and a fundamental frequency of 200 Hz. The driving force is applied at $x_1/L = 0.2$ and the response is observed at the same position $x = x_1$. The number of resonances equals the number of modes used for the computation. Because the string is driven at a node of the fifth mode ($L/x_1 = 5$), gaps can be observed at each multiple of the fifth resonance.

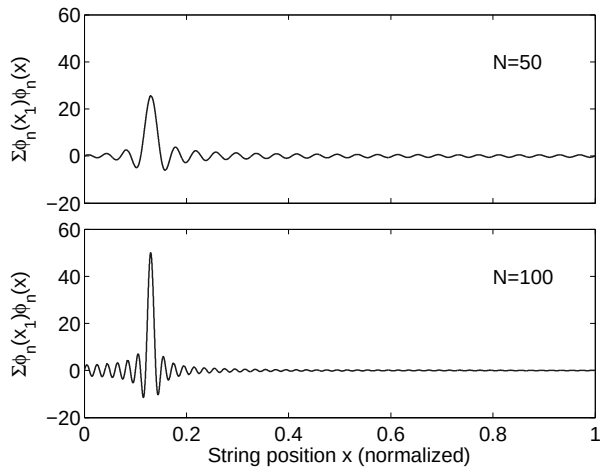

Figure 2.5: Effect of mode truncation on the spatial extension of the forces for two number of modes: $N = 50$ (top) and $N = 100$ (bottom). The shape of the reconstructed "dirac" function becomes narrower as the number of modes increases.

For example, from Eq. 2.7, the impulse response for each modal component of the displacement is

$$h_n(t) = \frac{\phi_n(x_1)}{\rho_L \omega_n} \sin(\omega_n t) \exp(-r_n t)$$

The impulse response for the displacement at any point x of the string can then be written as $h(t,x) = \sum \phi_n(x) h_n(t)$. An example of such a response is shown in Fig. 2.6, for a position x different from the interaction point x_1 ($x/L = 0.3$ and $x_1/L = 0.13$). The three figures corresponding to different truncations show a rather similar shape of the response. The string is displaced as successive reflections of the initial impulse arrive from the two string terminations and pass the observation point. Initially, the impulses are propagated in both directions out from x_1 towards the two terminations, i.e. the bridge and the nut. The observation point x is first displaced by the velocity impulse travelling toward the nut, obtaining a positive displacement. A short time later the displacement is returned to zero by the reflected impulse arriving from the bridge. The displacement becomes negative as the reflection from the nut arrives. Observing the details, it can be noticed that the string begins to vibrate before the arrival of the incoming wave, due to the spatial spreading of the force. This precursory vibration becomes smaller and smaller as the number of modes increases.

2.3 Numerical resolution and sound simulation

The vibration of the string as modelled in the previous section can be simulated by solving the modal equations 2.14. In this section, we will first describe two key points that have to be considered for the numerical solution: the integration scheme permitting to obtain the new modal components at each time step, and the algorithm for the interaction with external forces (frictional force and finger). Then, more pragmatic procedures will be considered in order to compute a "sound" from the force acting on the string termination representing the bridge. Finally, the computation cost of the proposed resolution will be discussed and compared with other methods.

Integration scheme

Different methods can be considered for simulating the time evolution of the modal components given in Eq. 2.14. For instance, Adrien [1] and Antunes [2] used an Euler scheme and a Verlet integration algorithm, respectively. Another approach was proposed by Doel [22] who expressed the solutions by using a numerical convolution of the external force with impulse responses of the modal equations and obtained a second order recursion equation for the new modal components.

The disadvantages of Euler schemes are well known. For example, they introduce some numerical damping in the simulations, they can become unstable and they are less accurate than other techniques such as Runge-Kutta methods. For

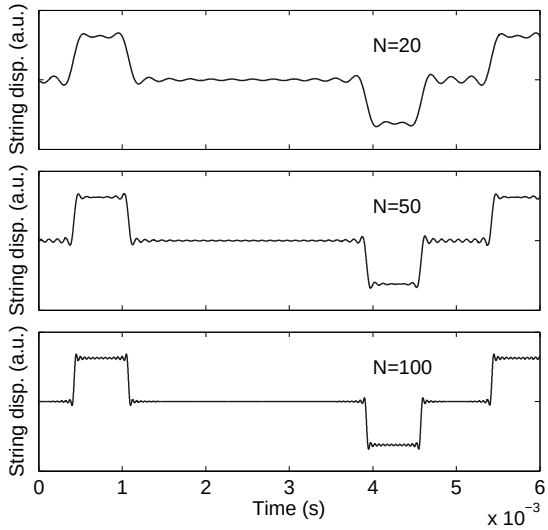

Figure 2.6: Impulse response of the displacement at an observation position at $x = 0.3L$, different from the interaction point at $x_1 = 0.13L$. String with no damping and no stiffness included; fundamental frequency $f_0 = 200$ Hz. The impulse responses are computed for different number of modes $N = 20$, 50, 100 in order to highlight the influence of the mode truncation on the details of the string vibrations.

the specific case we are interested in (a second order linear ordinary differential equation), the analytical solution is obvious and can be used directly. The modal displacements at time $t_1 = t_0 + dt$, with modal forces $f_n(t)$ and initial conditions $a_n(t_0)$ and $\dot{a}_n(t_0)$, are

$$a_n(t_1) = X_{1n} a_n(t_0) + X_{2n} \dot{a}_n(t_0) + \frac{1}{\rho_L} \int_{t_0}^{t_1} f_n(t_1 - t') h_n(t') dt' \tag{2.16}$$

where $h_n(t)$ is the impulse response deduced from Eq. 2.14 as

$$h_n(t) = \frac{1}{\omega_n} \sin \omega_n t \exp(-r_n t)$$

and the coefficients X_{1n} and X_{2n} are

$$X_{1n} = (\cos \theta_n + \frac{r_n}{\omega_n} \sin \theta_n) R_n \tag{2.17}$$

$$X_{2n} = \frac{1}{\omega_n} \sin \theta_n R_n \tag{2.18}$$

with $\theta_n = \omega_n dt$ and $R_n = \exp(-r_n dt)$.

The time discretization is consequently included in the integration of the force whose shape is not known in advance. The integral could be computed with a numerical method over the time step dt between t_0 and t_1. However, in our case, $h_n(t)$ has a sine shape that can be easily integrated and it seems more relevant to approximate the function $f_n(t)$ by considering a simple form between each time step. For instance, if $f_n(t)$ is simply supposed to have a constant value $f_n(t_1)$ during the interval $[t_0\ t_1]$, we obtain:

$$\int_{t_0}^{t_1} f_n(t')h_n(t_1 - t')dt' = \frac{1}{\omega_{0n}^2}(1 - X_{1n})f_n(t_1)$$

Consequently, equation 2.16 becomes

$$a_n(t_1) = X_{1n}a_n(t_0) + X_{2n}\dot{a}_n(t_0) + X_{3n}f_n(t_1) \tag{2.19}$$

or

$$a_n(t_1) = a_n^h + X_{3n}f_n(t_1)$$

with

$$X_{3n} = \frac{1}{\rho_L \omega_{0n}^2}(1 - X_{1n})$$

Alternatively, it is possible to consider a linear variation of the force between the two time steps expressed by

$$f_n(t) = f_n(t_0)(1 - \frac{t}{dt}) + f_n(t_1)\frac{t}{dt}$$

In that case, we would obtain

$$\int_{t_0}^{t_1} f_n(t')h_n(t_1 - t')dt' = \frac{1}{\omega_{0n}^2}\big((1 + C)f_n(t_0) + (-R_n \cos\theta_n - C)f_n(t_1)\big)$$

with

$$C = \frac{1}{\omega_{0n}^2 dt}(2r_n(R_n \cos\theta_n - 1) + \frac{r_n^2 - \omega_n^2}{\omega_n}R_n \sin\theta_n)$$

In this work, we considered a constant force during intervals between time steps. This bias is based on the simplicity of the computations and expressions, and additionally, on the idea that the friction force should theoretically be discontinuous at the transition between the two friction states (sticking and slipping), which would not be reproduced with a linear variation of the force.

In order to solve the friction interaction, we are more interested in the string velocity than in the displacement. The first derivative of the modal components can be derived in a similar way and we obtain

$$\dot{a}_n(t_1) = Y_{1n}a_n(t_0) + Y_{2n}\dot{a}_n(t_0) + Y_{3n}f_n(t_1) \tag{2.20}$$

or

$$\dot{a}_n(t_1) = \dot{a}_n^h + Y_{3n} f_n(t_1) \tag{2.21}$$

with

$$Y_{1n} = -(\omega_n + \frac{r_n^2}{\omega_n}) \sin \omega_n dt \exp(-r_n dt) \tag{2.22}$$

$$Y_{2n} = (\cos \omega_n dt - \frac{r_n}{\omega_n} \sin \omega_n dt) \exp(-r_n dt) \tag{2.23}$$

$$Y_{3n} = -\frac{1}{\omega_{0n}^2 \rho_L} Y_{1n} \tag{2.24}$$

In Eq. 2.21, $\dot{a}_n^h$ represents the "historical" value of the modal component, i.e. the exact value that would have been obtained if no force was applied on the string (free oscillation).

The modal displacements and the modal velocities are both interesting for our purpose because they will be used for solving the interaction with the "finger" and the bow, respectively. Note that similar relations could be obtained for the modal components of the acceleration which could be useful if we were considering the action of a mass on the string.

Action of external forces

The model representing the bowed string is composed of a string with mathematically convenient properties, a friction interaction at the bowing point of the string, and a "finger" permitting to set the pitch of the sound. In this section, we will consider the two forces acting on the string. The first one (F_1) represents the finger and should prevent the string from vibrating at a specific position. The second one (F_0) models the frictional force of the bow on the string and excites the string.

In our specific case with $f_n(t) = \phi_n(x_0)F_0(t) + \phi_n(x_1)F_1(t)$, Eqs. 2.19 and 2.21 can be rewritten as

$$a_n(t_1) = a_n^h + \alpha_{0n} F_0(t_1) + \alpha_{1n} F_1(t_1) \tag{2.25}$$

$$\dot{a}_n(t_1) = \dot{a}_n^h + \beta_{0n} F_0(t_1) + \beta_{1n} F_1(t_1) \tag{2.26}$$

with

$$\alpha_{in} = \phi_n(x_i) X_{3n} \qquad \beta_{in} = \phi_n(x_i) Y_{3n} \qquad i = 0, 1$$

The general principle consists in using these discrete equations for the modal components in order to deduce a linear expression giving the force $F_i(t_1)$ as a function of the string displacement or velocity at a given position. It is then possible to use these relations for solving the interaction with the other mechanical systems (the finger and the bow). This will first be illustrated with a simple modelling of the finger, then with the more sophisticated case of the bow-string interaction. At the end of this section, some problems related to the derivation of the solution for the friction force will be discussed.

Determination of the "finger" force

The effect of the finger consists in shortening the vibrating part of the string in order to change the fundamental frequency. This is achieved by forcing the transverse displacement to zero at a given point x_1 on the string. The force that prevents the string from moving at x_1 will be called F_1 in the following and will be derived from Eq. 2.25. The displacement at x_1 can be expressed as

$$y(x_1) = y_1^h + A_{01}F_0 + A_{11}F_1 \quad \text{with} \begin{cases} y_1^h &= \sum_{n=1}^{N} \phi_n(x_1) a_n^h \\ A_{01} &= \sum_{n=1}^{N} \phi_n(x_1) \alpha_{0n} \\ A_{11} &= \sum_{n=1}^{N} \phi_n(x_1) \alpha_{1n} \end{cases} \tag{2.27}$$

Assuming $y(x_1, t) = 0$ in Eq. 2.27, F_1 can be directly deduced from the values of y_1^h and the force F_0

$$F_1 = -\frac{1}{A_{11}}(y_1^h + A_{01}F_0) = C_{11}y_1^h + C_{12}F_0$$

An alternative way of forcing the string displacement to zero at the finger position consists in modelling the finger with a very stiff spring. The force F_1 is then determined by the equation of the spring $F_1 = -Ky(x_1)$ combined with Eq. 2.27

$$F_1 = C_{11}y_1^h + C_{12}F_0 \quad \text{with} \begin{cases} C_{11} &= \frac{-K}{1+KA_{11}} \\ C_{12} &= A_{01}C_{11} \end{cases} \tag{2.28}$$

From this expression, it can be noticed that the determination of the friction force F_0 is necessary for computing the finger force F_1. In spite of the different locations of the two forces, there is a weak coupling due to the truncation of the number of modes as discussed before, and to the time discretization. Consequently, forces applied on the string have a non-negligible effect over the entire length of the string, in particular at the positions of other interactions.

Fig. 2.7 illustrates the effect of the number of modes and the finger position x_1 on the coefficients A_{11} and A_{01}. The string is bowed at a position $x_0 = 0.13L$. Whatever the finger position x_1, the cross coefficient A_{01} tends to zero when the number of modes is larger than 150. Under this value, A_{01} is more and more affected when the finger gets closer to the bowing point ($x_1 = 0.16L$ and $x_1 = 0.14L$). For more usual positions such as $x_1 = 0.9L$ and $x_1 = 0.3L$, the coefficient is almost equal to zero and could be neglected. However, in order to not endanger the exactness of the simulation, these coefficients will be kept in the solution.

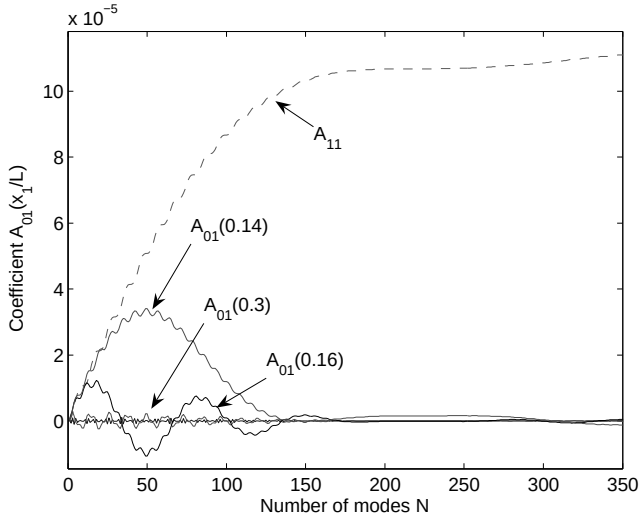

Figure 2.7: Effect of the number of modes on the cross coefficients A_{01} for a force applied at $x_0 = 0.13L$ and $dt = 1/44100$ s. For comparison, the coefficient A_{11} appearing in Eq. 2.27 is shown as well. The contribution of the friction force at the finger position increases when the finger gets closer to x_0 and tends to disappear with increasing number of modes.

Determination of the friction force

The string velocity at the bowing position $\dot{y}(x_0, t)$ is expressed as

$$\dot{y}(x_0) = v_0^h + B_{00}F_0 + B_{01}F_1 \quad \text{with} \begin{cases} v_0^h &= \sum_{n=1}^{N} \phi_n(x_0)\dot{a}_n^h \\ B_{00} &= \sum_{n=1}^{N} \phi_n(x_0)\beta_{0n} \\ B_{01} &= \sum_{n=1}^{N} \phi_n(x_0)\beta_{1n} \end{cases} \tag{2.29}$$

Replacing F_1 with Eq. 2.28, we obtain

$$F_0 = C_{01}(\dot{y}(x_0) - v_0^h) + C_{02}y_1^h \quad \text{with} \begin{cases} C_{01} &= 1/(B_{00} + B_{01}C_{12}) \\ C_{02} &= -B_{01}C_{11}C_{01} \end{cases} \tag{2.30}$$

Two different cases have to be considered for determining the friction force: sticking and slipping of the string.

During the sticking state, the force F_0 must be computed from a continuity condition, normally equal velocity of the string and bow. Inserting $\dot{y}(x_0) = v_b$ in

Eq. 2.30, the computation of F_0 is straightforward

$$F_0 = C_{01}(v_b - v_0^h) + C_{02}y_1^h \tag{2.31}$$

The friction state changes when F_0 is greater than the maximal friction force computed as $F_{max} = \mu_s F_b$ where μ_s is the static friction coefficient in the friction characteristic, and F_b the bow force. This is illustrated in Fig. 2.8d.

During the slipping state, the friction force F_0 is determined by the intersection between Eq. 2.30 and the friction characteristic depending on the relative velocity between the bow and the string ($\Delta v = \dot{y}(x_0) - v_b$). Eq. 2.30 can be expressed as a function of Δv

$$F_0 = C_{01}(\Delta v + v_b - v_0^h) + C_{02}y_1^h \tag{2.32}$$

To avoid long computations due to iterative algorithms, the hyperbolic expression of the friction curve is used. This choice permits a direct determination of the combination $(\Delta v, F_0)$ during the sliding part of the motion.

The friction characteristic is determined by three parameters (μ_s, μ_d and v_0) and is given by

$$F_0 = \mu(\Delta v)F_b \quad \text{with} \quad \mu(\Delta v) = \mu_d + \frac{\mu_s - \mu_d}{1 - \frac{\Delta v}{v_c}} \tag{2.33}$$

with

$$v_c = \begin{cases} v_0 & \text{if} \quad v_b > 0 \\ -v_0 & \text{if} \quad v_b < 0 \end{cases}$$

$$F_c = \begin{cases} F_b & \text{if} \quad v_b > 0 \\ -F_b & \text{if} \quad v_b < 0 \end{cases}$$

This characteristics is used with Eq. 2.32 in order to obtain a second order equation where Δv is unknown

$$c_2\Delta v^2 + c_1\Delta v + c_0 = 0 \quad \text{with} \quad \begin{cases} c_2 &= -\frac{C_{01}}{v_c} \\ c_1 &= C_{01}\frac{v_c - v_b + v_0^h}{v_c} + \mu_d\frac{F_c}{v_c} - C_{02}\frac{y_1^h}{v_c} \\ c_0 &= C_{01}(v_b - v_0^h) + C_{02}y_1^h - \mu_s F_c \end{cases} \tag{2.34}$$

The existence of Δv (related to the value of the discriminant $\Delta = c_1^2 - 4c_0c_2$) gives one of the two following situations, and provides a first condition for determining if the string is still sliding.

- if there is no solution ($\Delta < 0$), the friction state has changed and the string is now sticking to the bow (see Fig. 2.8b).

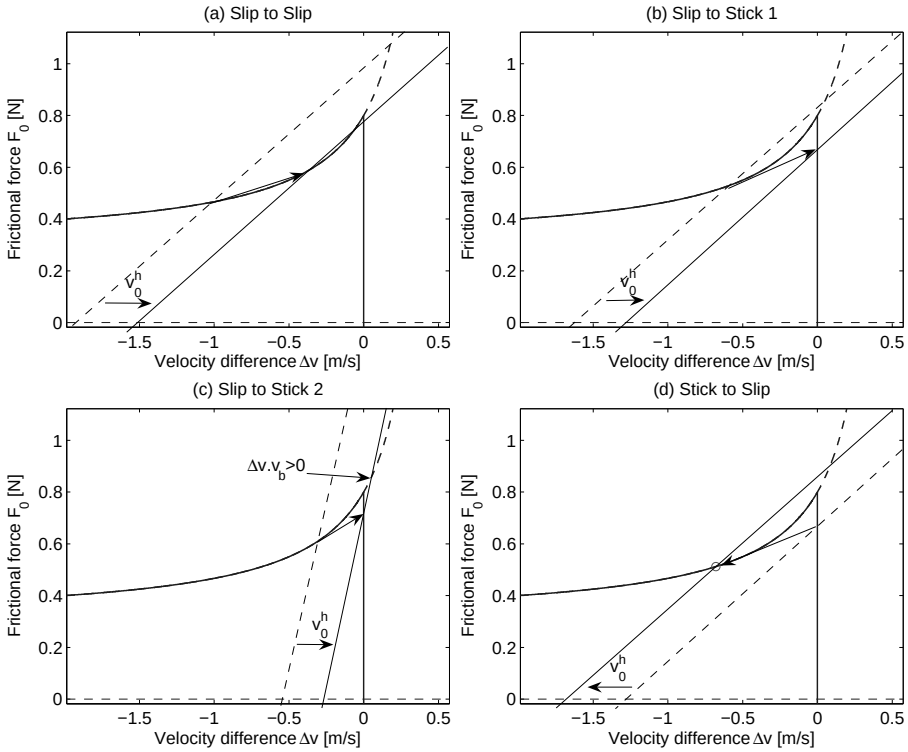

Figure 2.8: Illustration of the situations that can occur when solving the friction interaction. (a) The string keeps slipping. (b) No solution ($\Delta < 0$), then the string begins to stick. (c) The solution is outside the range in which the friction curve is defined ($\Delta v * v_b > 0$). The string sticks. (d) The string sticks but the next force value is above the maximal force and the string begins to slip.

- if at least one solution exists ($\Delta \geq 0$), Δv is computed using the following expression, corresponding to Fig. 2.8a

$$\Delta v = \frac{-c_1 + \sqrt{\Delta}}{2c_2}$$

However, the sign of Δv should be tested in order to determine if the solution is acceptable or not. The friction curve is valid for $\Delta v < 0$ when $v_b > 0$, but Eq. 2.34 does not take this restriction into account, which can lead to unacceptable solutions, like in Fig. 2.8c. Consequently, if $\Delta v * v_b < 0$, the solution is acceptable and the string is still sliding, and in the opposite case, the string is sticking and $\Delta v = 0$, which gives a second condition for the string to keep sliding.

The friction force is computed with the friction characteristics (Eq. 2.33) and an equation describing the response of the string to the external force F_0 (Eq. 2.32). In the following sections, two aspects of this approach to the numerical solution will be discussed. First, we underline the similarity between Eq. 2.32 and the theoretical situation using the characteristic impedance of the string. Then, the importance of the friction characteristic in the direct solution of the equations will be discussed.

On the numerical impedance

Previously we have discussed the effect of truncation on the coefficients A_{01} and A_{11} related to the displacement at the finger position. The same kind of discussion could be applied to the coefficients B_{00} and B_{01} related to the velocity at the bowing position. However, it will be more interesting to focus on the coefficient C_{01} which gives the connection between the force and the velocity (Eq. 2.30).

This equation is indeed very similar to the equation used by Friedlander [26] and Keller [44] for determining the combination force-velocity graphically from the friction curve. The principle is exactly the same, but the characteristic impedance of the string $Z_c = \sqrt{\rho_L T_0}$ has been replaced by a "numerical impedance" depending on the number of modes and the time step dt. Neglecting the influence of the cross-coefficients B_{02} and C_{02} in Eq. 2.30, we can write

$$F_0 = 2Z_N(\dot{y}(x0) - v_0^h) \quad \text{with} \quad \frac{1}{2Z_N} = \sum_{n=1}^{N} \phi_n(x_0) Y_{3n}$$

The dependency of this factor $1/2Z_N$ versus the number of modes N is illustrated in Fig. 2.9 for an ideal string. As a comparison, the numerical impedance that would be obtained with an implicit Euler scheme is shown as well. It can be seen that these coefficients tend toward the theoretical $1/2Z_c$ as the number of modes increases.

This is an important feature of the numerical scheme. From a theoretical point of view, the velocity and the friction force at the bowing position should be discontinuous at the transitions between the sticking and slipping states. When the number of modes is too low, the slope $2Z_N$ of the line becomes steeper and the discontinuity tends to disappear. In contrast, if the slope was too low, the discontinuity would become larger and larger, much larger than the theoretical prediction.

On the friction model and the influence on computational complexity

The hyperbolic model offers a straightforward way of solving the interaction in an implicit scheme, as seen above. An alternative proposed by Adrien [1] consists in using a simplified version of the friction curve during slipping. In order to allow a direct solution of the friction interaction, the curve was approximated by successive straight lines with different slopes, depending on the relative velocity between the

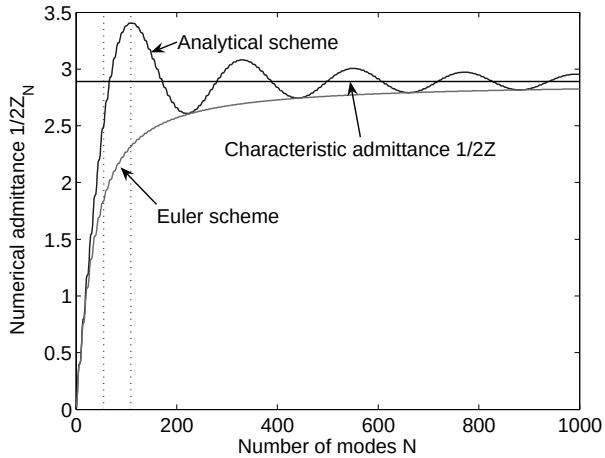

Figure 2.9: Effect of the number of modes on the numerical admittance $Y_N = \frac{1}{2Z_N}$ for the numerical scheme described in text ("analytical scheme") and for an implicit Euler scheme. The horizontal line represents the admittance deduced from the characteristic impedance of the string.

string and the bow. The non-linearity of the curve was then transformed into several different slipping states and some try-and-test procedures for determining the current slipping state of the interaction.

Other analytical friction models than the hyperbolic model offer two alternatives:

- Solving the interaction by looking for the intersection with the friction curve. In that case, a recursive algorithm such as the Newton-Raphson method is needed for approaching the solution. However, with such a solution method, the computation cost will increase significantly and the real-time implementation could become problematic.

- Using an explicit scheme in which the forces acting on the string are computed from the velocities and positions corresponding to the time step before. This solution can be used with an exponential friction model as in [2], and seems to give a non-significant error in the simulations. However, in that case, the use of an explicit scheme seems to make the analysis of the sticking state more problematic. Using the velocity at the previous time step for computing the friction force does not lead to the same velocity of the bow and string. Antunes [2] solved this problem by "attaching" the string to the bow with a very stiff spring during the sticking part of the motion.

Sound signal

In the previous sections, we focused on the numerical solution of the string equation. Our point of departure was in string physics for deriving the wave equation of the string and deriving the modal formulation, then numerical methods were applied for solving the modal equations.

This procedure can be used to compute the modal components, and consequently the displacement or the velocity at any point of the string, in order to simulate the vibration of the string. In this section, we will be interested in more pragmatic arguments that permit to transform the string vibrations into more or less convincing sounds. It means that we will add some "ad hoc" features that are not contained in the physical equations described before, but that contribute to the realism of the sound.

Computing the bridge force

The output signal of the simulation can be the string displacement or velocity at any position on the string, computed using Eq. 2.2. In a real violin, the string acts on the bridge which transmits the vibrations to the body of the instrument, and it will be relevant to base our output signal from the force on the bridge. The bridge force is obtained from the modal components as

$$F_{bridge}(t) = T_0 \frac{\partial y(x,t)}{\partial x}\Big)_{x=0} - EI \frac{\partial^3 y(x,t)}{\partial x^3}\Big)_{x=0}$$

Consequently, with $y(x,t) = \sum_{n=1}^{N} a_n(t)\phi_n(x)$, we obtain

$$F_{bridge}(t) = \sqrt{\frac{2}{L}} \sum_{n=1}^{N} a_n(t)\Big(T_0 \frac{n\pi}{L} + EI\big(\frac{n\pi}{L}\big)^3\Big) \tag{2.35}$$

Obtaining an "acoustic" signal

The bridge force gives a signal that contains all the dynamical characteristics that make it possible to recognize a vibration produced by a bowed-string instrument. But this signal still does not show some of the spectral characteristics of a real violin sound. Typically, the bridge signal sounds metallic and the result is very close to the sound of a string mounted on rigid supports (monochord), or to a recording of the string vibrations. It is therefore necessary to add the effect of the violin body in order to obtain a more convincing sound.

The most straightforward way of including the effect of the violin body in the model consists in filtering the bridge force with an impulse response of a violin. With this approach, the violin body is considered as a filter responding to a given source signal. The mechanical effects on the string vibration resulting from the coupling between the string and the violin body are ignored. Apart from this

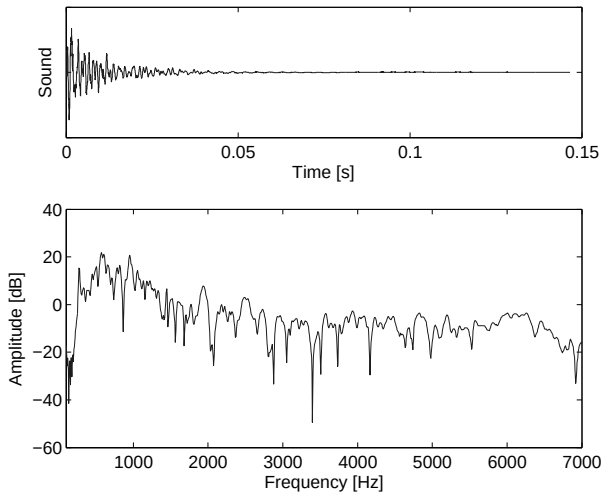

Figure 2.10: Impulse response of a violin (top) and corresponding spectrum (bottom) measured by striking the bridge with an impact hammer. The resulting acoustical signal was recorded close to the player's left ear.

restriction, the approach has shown satisfying results from a perceptual point of view and for sound synthesis purposes [27, 47, 30].

The impulse responses were measured by striking the edge of the bridge with a small impact hammer and recording the radiated sound pressure with a microphone. The resulting response and spectrum are illustrated in Fig. 2.10. The response depends on several parameters, including the position of the microphone relative to the violin, and the acoustics of the room. For sound synthesis purposes, a powerful way of simulating different situations can be obtained by filtering the bridge signal with impulse responses corresponding to different violins, different positions around the violin, and different acoustic environments.

Adding noise

The sounds of instruments generating sustained notes such as the violin are composed of a harmonic part and a noise component. The noise component is illustrated in Fig. 2.11. As pointed out by Chafe [16], the noise is crucial for the realism of the sound. Basic examples are the sound of the bow as it is drawn across the string, which is clearly audible close to the violin, or the turbulent noise from the tone holes of wind instruments.

As seen in Fig. 2.11, the noise component shows a strong correlation with the slipping part of the motion and appears as pulses at each stick/slip transition. This instabilities have been attributed to the sliding of the string along the bow-hair which has a certain roughness. Consequently, Chafe [16] proposed to incorporate a

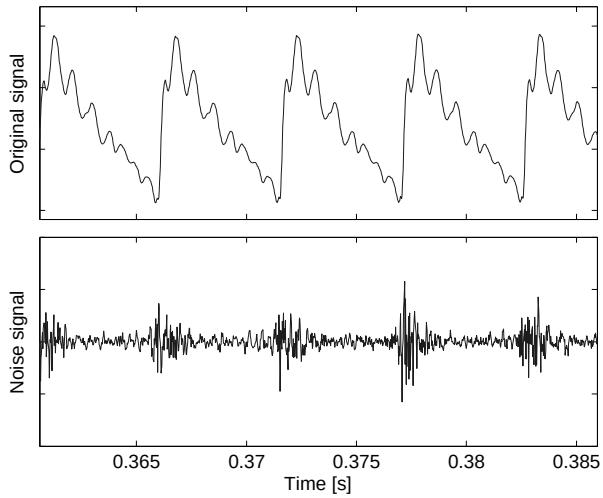

Figure 2.11: Illustration of the noise component during the steady part of a real violin tone. Top: The string vibration at the bridge measured by a piezoelectric sensor under the string. Bottom: After analysis of the signal, the noise component can be computed by subtracting the harmonic part from the original signal, showing noise pulses concentrated at the slipping phases.

stochastic component into the model during the slipping periods. For that purpose, the friction characteristic can be perturbed by multiplying with a random number given by

$$N(t) = \begin{cases} O + Gu(t) & \text{if} \quad u(t) > P \\ 1 & \text{otherwise} \end{cases}$$

where u is a uniform positive noise, O an offset term, G a scaling factor and P a value setting the amount of samples that are perturbed.

Following Chafe (and a number of other authors), we incorporated noise during the slipping periods by scaling the friction curve randomly. However, we used a simpler model given by

$$N(t) = 1 - A_{noise}u(t)$$

where $u(t)$ is random noise with values between 0 and 1, and A_{noise} is a coefficient controlled by the user for setting the amplitude of the noise. This approach ensures that the perturbed friction curve is lower than the original curve in order to avoid difficulties that could occur at the slip/stick transitions with values greater than 1.

The generation of noise using this procedure is illustrated in Fig. 2.12 which shows strong similarities with the noise pulses observed in recorded signals (Fig. 2.11).

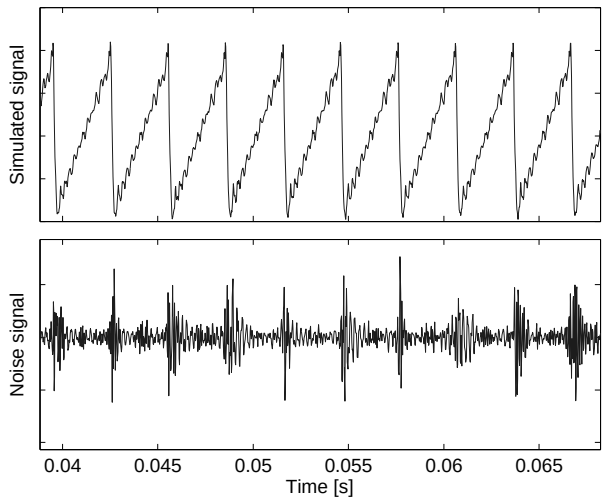

Figure 2.12: Illustration of the noise component during the steady part of a simulated note using the noise model described in text. The simulated bridge force including noise (top) has been analysed for extracting the noise component (bottom). The noise track shows bursts of noise similar to the recorded signals in Fig. 2.11.

General description of the algorithm

The numerical implementation of the algorithm is summarized in Fig. 2.13. At the beginning of the computation, all coefficients that will be used are initialized with the different parameters (string parameters, computation parameters, etc). Then, the procedure consists in:

- computing the "historical" variables v_0^h and y_1^h at the interaction points x_0 and x_1
- determining the velocity difference Δv and the friction force F_0 for the current bowing state. During slipping, the tests for changing the state are performed when computing Δv. During sticking, the test is done at the end, once the force is computed.
- computing the "finger" force F_1 with F_0, then the new modal components with F_0 and F_1.
- computing the bridge signal and making the convolution with the impulse response.

The control parameters x_0 and x_1 representing the bow and the finger position can be changed in real time during the simulation but necessitate a reinitialisation

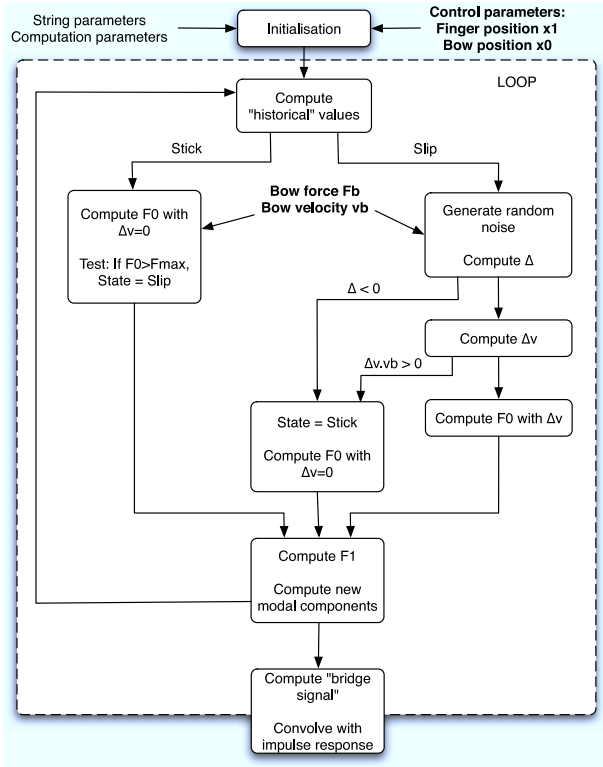

Figure 2.13: Schematic representation of the complete algorithm for synthesising violin sound.

of some coefficients. However, for efficiency some partial initialisations have been implemented. The same applies to the string parameters. Some of them do not require a complete initialisation of the coefficients, and changing their values gives rise to smaller initialisations for computational economy. In contrast, the two other control parameters (bow force and bow velocity) act only inside the loop and do not require any update of the variables.

On the computation cost

For real-time implementation, it is important to have a rather low computation cost. This cost can be estimated from the preceding description of the model. In this section, we will first quantify the cost of the modal synthesis by emphasising the expensive parts of the resolution, then we will estimate the cost of other algorithms, for comparison.

Estimation of the computation cost

To estimate the computation cost, we focus on the loop which performs the computation of the next output sample, without the final convolution of the signal. Considering a number of N modes, we can follow the schematic representation of the algorithm (Fig. 2.13) and quantify the cost of each step:

- Computation of the historical values: The computation of the two following expressions gives twice $3N$ multiplications and $2N$ additions

$$a_n^h = X_{1n} a_n(t_0) + X_{2n} \dot{a}_n(t_0) \qquad y_1^h = \sum \phi_n(x_1) a_n^h$$

$$\dot{a}_n^h = Y_{1n} a_n(t_0) + Y_{2n} \dot{a}_n(t_0) \qquad v_0^h = \sum \phi_n(x_0) \dot{a}_n^h$$

- Computation of the forces: The cost depends on the friction state of the string. For free oscillations, $F_0 = 0$ and no extra operation is required. If the string is sticking, $\Delta v = 0$ is already known, and then we have to compute F_0 with Eq. 2.30, i.e. 3 operations. Finally, if the string is slipping, we also have to compute the force (3 operations), but Δv has to be determined before through about 25 operations. Because the number of operations during this procedure is generally less than the mode number N, and because it will be about the same for all the algorithms compared (providing they all use the same model of friction), we do not take this cost into account in the estimation.

- Computation of the new modal components with Eqs. 2.25 and 2.26: Twice N multiplications and N additions.

- Computation of the next sample for the signal (bridge force) with Eq. 2.35: N multiplications and N additions.

The computation cost of the loop is consequently around $9N$ multiplications and $7N$ additions. It should be noticed that these values do not depend on the characteristics of the string: the flexible string, the stiff string, and the damped string will all give the same computation cost. The case of free oscillations can be reduced to $3N$ multiplications and $2N$ additions, because the computation of the modal components of the velocity $\dot{a}_n$ is not required. The values above are summarized in Table 2.1, and in the next section they will be compared with the performance of other algorithms.

Computation cost of other algorithms

In this section, we discuss the computation cost of other simulation methods including finite difference schemes and digital waveguides. The number of operations during one loop is estimated without taking into account the determination of the

external forces, as discussed above (the cost of this computation can be considered to be about the same for all the methods).

The method using finite different schemes has been described in Chapt. 1 and the following estimation will be based on the description by Hiller and Ruiz [41]. The string equation is solved numerically for a set of N points along the string whose displacement is given by a recursion relation. For a flexible string, the recursion is

$$y(i, j+1) = y(i+1, j) + y(i-1, j) - y(i, j-1)$$

This relation requires 2 additions for each point during the loop, corresponding to about $2N$ additions for the entire string.

For the stiff string, the recursion becomes

$$\begin{aligned} y(i, j+1) = -6ay(i, j) + (1+4a)[y(i+1, j) + y(i-1, j)] \\ - a[y(i+2, j) + y(i-2, j)] - y(i, j-1) \quad , \end{aligned}$$

which requires 4 additions and 4 multiplications for each point, if the factors before each variable y are computed in advance.

The case of the damped string depends on the model used for describing the losses. By adding a term depending on $\partial y/\partial t$, all variables are already contained in the previous equation and no extra operation is needed, as only the coefficients contained in the equation change. However, as this case introduces similar losses at all frequencies, a more sophisticated model is required.

Following Hiller [41] and introducing frequency-dependent losses through the term $\partial^3 y/\partial t^3$, the recursion becomes implicit (the value of the displacement at time $t+2$ must be known in order to compute the value for time $t+1$). However, with a small approximation, the scheme can be made explicit [17], and the recursion then requires about $7N$ additions and 5N multiplications per sample (without taking into account specific recursion relations in the vicinity of the terminations). The computation costs for the finite difference scheme and for the modal synthesis are then very similar.

For comparison, we give a rough estimation of the computation cost for a similar model using the waveguide method. This estimation is based on the description of Serafin's model [76] and does not take possible optimizations of the algorithm into account.

The propagation is simulated with four delay lines, two at each side of the bowing position. If the cost of delay lines is neglected, the computation only requires 3 additions and 2 multiplications for the flexible string in order to determine q_h, q_{oL} and q_{oR} at the bowing position (see Chapt. 1.3 for the notations). In addition, it is necessary to compute the output signal, which can be done with only one addition. The computation cost is consequently much lower than for the two preceding methods. The method takes advantage of this computational efficiency, and reproduces

	Modal Synthesis	Finite Differences	Waveguides
Free oscillation	3N / 2N	0 / 2N	2 / 4
Ideal string	9N / 7N	0 / 2N	2 / 4
Stiff string	9N / 7N	4N / 4N	27 / 24
With damping	9N / 7N	7N / 5N	37 / 32

Table 2.1: Estimation of the number of operations during one loop for different simulation methods (number of additions/number of multiplications). The estimation does not take into account the computation of the friction force and neglects the cost of delay lines.

the propagation effects in real strings (stiffness, damping) by filtering the travelling waves, which can increase the initial cost significantly.

The simulation of dispersion is obtained by using allpass filters in each delay line. However, for computational efficiency, the filters are located at one termination of the string, as in [76], where the reflection at the nut takes the dispersion into account. Using three 4-th order allpass filter in cascade such as

$$H(z) = \frac{a_0 + a_1 z^{-1} + a_2 z^{-2} + a_3 z^{-3} + a_4 z^{-4}}{a_4 + a_3 z^{-1} + a_2 z^{-2} + a_1 z^{-3} + a_0 z^{-4}} \quad ,$$

the extra cost consists in 9 multiplications and 8 additions for each filter. Note that this cost can be reduced as discussed by Bensa at al [10].

The damping of the string is reproduced by designing lowpass filters. In [76], second order low-pass IIR filters are estimated and used at the nut and the bridge terminations. Filters such as

$$H(z) = \frac{b_0 + b_1 z^{-1} + b_2 z^{-2}}{1 + a_1 z^{-1} + a_2 z^{-2}}$$

add 5 multiplications and 4 additions, which must be multiplied by the number of terminations.

The computation costs for the three methods in terms of additions and multiplications are summarized in Table 2.1. As expected, the number of operations for the digital waveguide method is much lower than for the others. For comparison, considering 50 modes or 50 points on the string, respectively, the modal synthesis requires 800 operations per sample and the finite differences scheme 600, whereas the waveguide method requires only around 70 operations. It is important to notice that the computation cost remains constant in the case of modal synthesis, whereas it increases significantly with the other methods. A more accurate comparison should be based on reproducibility of the vibration characteristics for a given computation cost as done in [10].

2.4 Illustration and influence of computation parameters

The previous sections have presented the theoretical base and the implementation of the tool that we will use to simulate the vibration of the bowed string. The simulated motion will in turn be used to synthesize the sound. The ingredients of the model are expected to be sufficient to reproduce the vibrations of the string well, but that remains to be shown. In this section we will consequently first check that the simulated string motions are realistic, and that the vibrations match empirical observations. Then we will illustrate the influence of the computation frequency and the number of modes on the simulations. Typically for a real-time implementation of the model, the computation frequency is set by the standard audio sampling frequency (44.1 kHz) and a reasonable number of modes is considered (e.g. less than 80). In the following simulations, a violin D string was used with fundamental frequency $f_0 = 294$ Hz, inharmonicity factor $B = 2.10^{-4}$, decay time $\tau_1 = 0.3$ s for the first mode and $\tau_n = 1/(3 + 3(n-1)^2)$ s for the others. The bowing position was $x_0 = 0.12L$, the bow speed 0.1 m/s and the bow force between 0.2 and 0.6 N.

We will first show an exemplary simulation in order to illustrate the time evolution of the string motion. Then the influence of computation parameters will be evaluated separately for the steady part of the vibration (corresponding to the Helmholtz motion) and the attack. Finally, we discuss some ideas that can be considered when choosing the value of computation parameters.

Example: Motion of the string

In the first chapter, we have described the basic motion of the bowed string observed by Helmholtz [40]. The string does not vibrate uniformly in Helmholtz motion, and the observed envelope of the string vibration is produced by a corner dividing the string in two segments and travelling around a parabolic trajectory. It can therefore be instructive to observe if our model produces this type of motion with appropriate control parameters.

Fig. 2.14 shows the time evolution of the displacement along the string under steady control parameters (constant bow force $F_b = 0.6$ N, bow velocity $v_b = 0.1$ m/s and bow-bridge distance $x_0 = 0.12L$) during two periods of a simulation. The values of bowing parameters are typical of real violin playing. At the bowing position, the displacement increases linearly during the sticking phase, and then suddenly drops at string release. In the foreground, it can be seen that the shape of the displacement along the string is composed of two straight lines linked with a rounded corner. The corner travels along the string toward the nut, then toward the bridge with opposite sign after reflection at the nut, forming the predicted parabolic shape. The string release occurs as the corner passes over the bowing position.

It is reassuring that the expected string motion is obtained qualitatively with "default" choice of computation parameters. No reliable criteria could be found beforehand in order to determine adequate parameter values and their choice is a

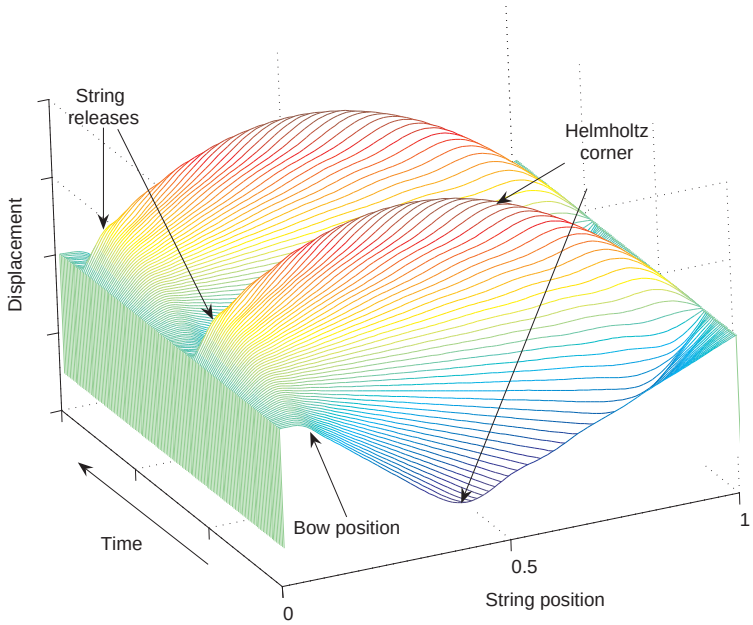

Figure 2.14: Motion of a string bowed at $x_0 = 0.12L$. The figure shows the time evolution of the displacement vs. string position. The maximum of the displacement (Helmholtz corner) travels along the string, forming a parabolic shape similar to the motion observed by Helmholtz.

tricky issue. However, it can be assumed that, provided that the parameter values stay within reasonable ranges, changes in the computation parameters give rise to only small modifications in the vibrations. In the next sections, we will have a closer look at the vibrations of the string and examine how the computation parameters influence some details of the motion.

Influence of computation parameters on the steady motion

To illustrate the influence of the number of modes, simulations with constant bow force $F_b = 0.2$ N and constant velocity $v_b = 0.1$ m/s were performed with 10, 30, 60 and 150 modes. Usual values will be 30 or 60 modes, but, for comparison, a very small number of modes ($N = 10$) as well as a large number ($N = 150$) were tested. The results are presented in Fig. 2.15, showing the spectrum of the bridge force (Fig. 2.15b), and typical velocity patterns during the slip phase (Fig. 2.15a).

Concerning the spectrum, we can observe a cut-off frequency corresponding to the number of modes, as expected. For instance, with $N = 10$, the 10 first partials are between 0 and -30 dB, whereas all the others are below -50 dB. For $N = 30$,

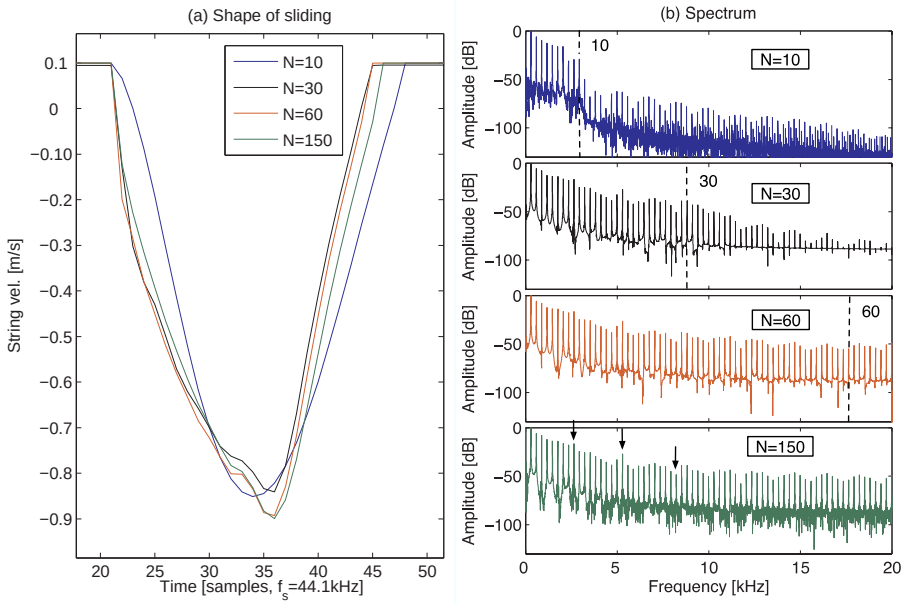

Figure 2.15: Influence of the number of modes on the sustained part of the simulation. (a) Typical string velocities under the bow during slip for $N = 10$, 30, 60 or 150 modes. (b) Corresponding spectra of the force on the bridge. Dashed vertical lines indicate the harmonic corresponding to the number of modes in the simulations. The two first arrows indicate common peaks in the spectra and the third a common gap.

the cut-off is less obvious, but we can compare with the spectrum obtained with 60 modes to conclude that the harmonics are smoothly disappearing above harmonic 30. Because the 60th harmonic is very close to 20 kHz (Nyquist frequency), no real difference can be observed between $N = 60$ and $N = 150$.

Except for these differences in the spectrum above the partial corresponding to the number of modes, it is interesting to notice how the envelopes of the spectra are very similar for $N = 30$, 60 and 150. For instance, in all cases, we observe the same small peaks around the 9th and 18-19th partials, and a similar gap at the 30th partial (indicated with arrows in Fig. 2.15b).

In Fig. 2.15a, the velocity shapes of the string during the slip are shown. The slipping velocity patterns are very similar in amplitude and time (the shift at the moment of capture is less than 0.1 ms) and do not show any particular tendency depending on the number of modes. However, it can be observed that the release is somehow rounded for $N = 10$. From our previous discussion about the numerical impedance (Sect. 2.3), it is not a surprise. With a small number of modes, the slope of the line intersecting with the friction characteristics is high, resulting in a

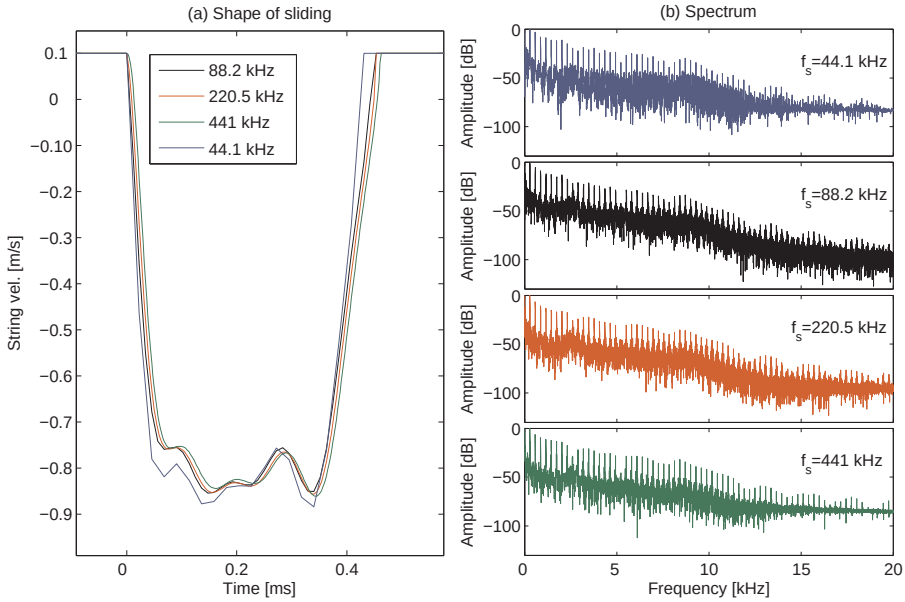

Figure 2.16: Influence of the computation frequency on the sustained part of the simulation. (a) Typical string velocities under the bow during slip for f_s=44.1, 88.2, 220.5 and 441 kHz. (b) Corresponding spectra of the force on the bridge.

smaller discontinuity when the string is released by the bow.

The computation frequency does not show a stronger influence than the number of modes on the simulation results. In the following simulations, the bow force was 0.6 N, the velocity 0.1 m/s, the number of modes 30, and the frequency was set successively to 44.1, 88.2, 220.5 and 441 kHz. As expected, no obvious differences could be observed in the shape of the spectrum (Fig. 2.16b), which is mainly dependent on the number of modes. The velocity during the slipping phase (Fig. 2.16a) also showed very similar patterns. As the computation frequency increases, the velocity is more continuous and smooth because of the increasing number of samples during the slipping phase, but without any significant change in the shape. It can be noted again that the release is slightly rounded for $f_s = 44.1$ kHz for the same reason as before.

In conclusion, the number of modes seems to have a greater influence than the computation frequency during the steady part of the vibration, especially on the resulting sound, because it changes the envelope of the spectrum. In general, the two computation parameters do not seem to have any drastic influence on the characteristics of the vibration, at least not in the chosen ranges and for this exemplary simulation. The differences were limited to small details, they did not change the

type of string vibration, and even not the characteristics of the interaction at the bowing point.

However, it should be noted that these simulations were performed for a standard set of string parameters and at a reasonable bowing position ($x_0 = 0.12L$). It is clear that when the bowing position is set to more extreme values, for example very close to the bridge, we will observe a different influence of the computation parameters. As the duration of the sliding phase decreases, the number of samples during the phase decreases as well. A critical limit may be reached beyond which the sliding cannot be described well with use of the friction characteristic. Such an effect could yield very different behaviour of the string vibrations for rather small changes in computation frequency.

Influence of parameters during attacks

During the sustained part of the sound, the computation parameters influence mainly the spectral content of the sound, as shown above. In contrast, dynamic parts of the simulations like the attacks may be significantly more influenced by these parameters. The number of modes, and the computation frequency, change the mechanical response of the model (for example, the impulse response, Sect. 2.2, or the numerical impedance, Sect. 2.3). Extra slips can be produced, which changes the quality of the attack. The three following sets of simulations illustrate the effect of changes in the computation parameters on the attack.

In the two first sets of simulations, we examine the effect of the computation frequency and the number of modes on a "standard" situation. The string is bowed at a rather large distance from the bridge ($\beta = 0.12$). The bow force is kept constant during the attack ($F_b = 0.3$ N), and the velocity is linearly increased from 0 to 0.1 m/s in 0.08 s. The same violin D string was used ($f_0 = 293$ Hz) and the computation parameters were varied from one simulation to the other. Control parameters were chosen to give a perfect attack (regular triggering of the slip phase from the first period) with $f_s = 44.1$ kHz and $N = 30$.

Fig. 2.17 illustrates the influence of the computation frequency on the simulations. The string velocity under the bow is shown (Fig. 2.17a) as well as the resulting force on the bridge (Fig. 2.17b). The initial computation frequency ($f_s = 44.1$ kHz) is multiplied by in turn 2, 5 and 10 ($f_s = 88.2$, 220.5 and 441 kHz). No significant differences can be observed between the simulations. A regular Helmholtz motion is maintained in all four cases, and slip triggerings occur at the same positions with the same amplitude. The details of the string velocity during slip reveals the behaviour that was observed before: shapes are very similar but, because the number of modes is kept constant, the string velocity at the transition between stick and slip becomes more and more rounded as the frequency increases, due to an increasing numerical impedance.

The influence of the number of modes is illustrated in Fig. 2.18, in which simulations obtained with $N = 10$, 30, 60 and 150 are shown. It is interesting to notice that an extra slip occurs around time 0.04 s for all simulations except for N

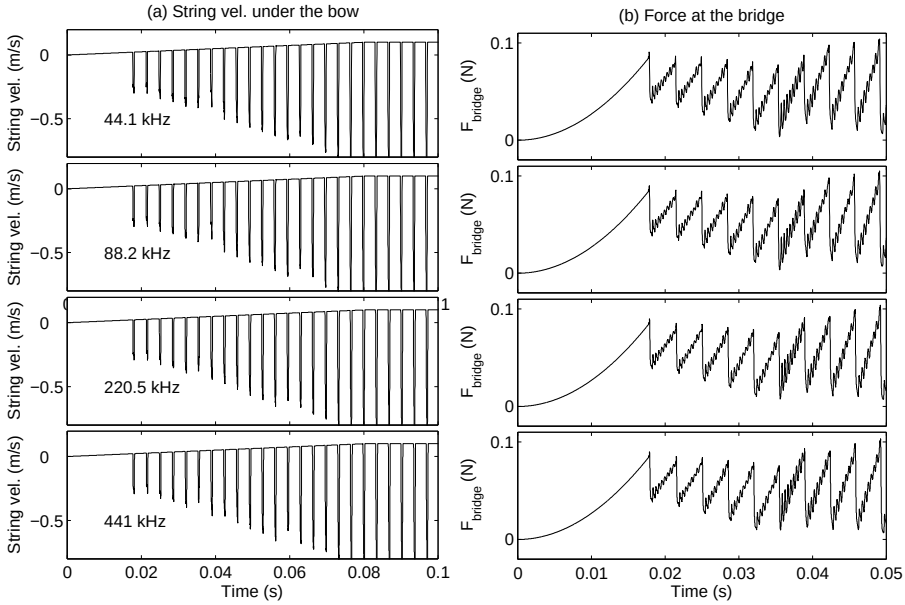

Figure 2.17: Attacks on a violin D string for different computation frequencies (from top: $f_s = 44.1$, 88.2, 220.5 and 441 kHz). The bow force is kept constant ($F_b = 0.3$ N) while the velocity is increased from 0 to 0.1 m/s in 0.08 s. The bow-bridge distance β is set to 0.12. No significant changes are observed in (a) showing the string velocity under the bow, or in (b) giving the force on the bridge.

$= 30$. However, the extra slip does not have a drastic influence on the string motion: the regular triggering is maintained despite this "accident". The string velocities obtained with $N \geq 30$ are very similar in amplitude and timing. For $N = 10$, the simulation show some differences, but we cannot expect the string behaviour to be well reproduced with such a small number of modes. Similarly, the driving forces on the bridge are very similar, except for $N = 10$, for which high frequencies are lacking.

In the previous sets of simulations, no strong qualitative differences could be observed when the number of modes and the computation frequency were varied. The overall motion of the string was the same, showing a periodic triggering of the string velocity under the bow. However, in some situations, the oscillation of the string can be strongly influenced by the computation parameters.

In the next set of simulations, a shorter bow-bridge distance was used ($\beta = 0.06$). The bow force was kept constant ($F_b = 0.3$ N) and the velocity was increased from 0 to 0.1 m/s in 0.2 s. Two computation frequencies were used ($f_s = 44.1$ kHz and 441 kHz) and for each frequency, the number of modes was first set to $N = 30$ and then

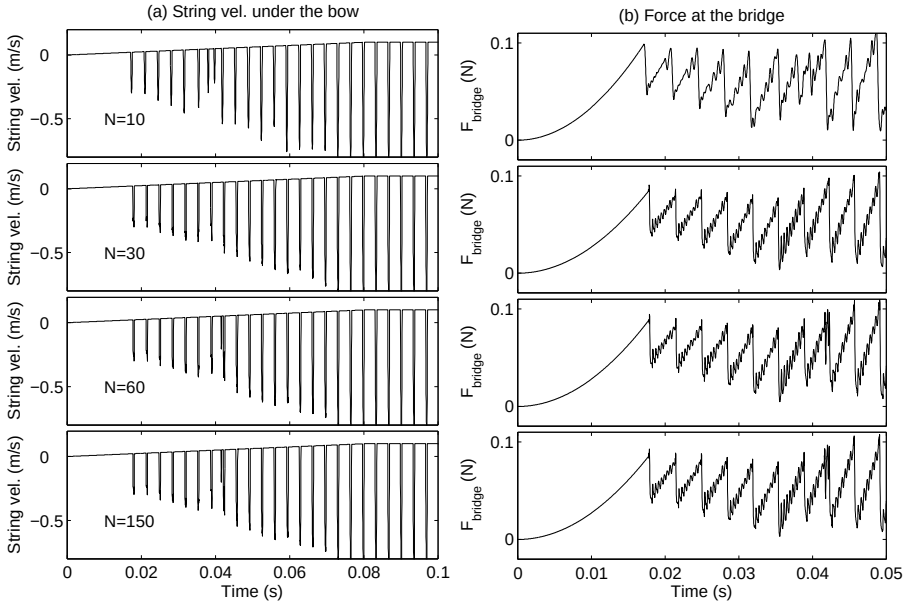

Figure 2.18: Attacks on a violin D string for different numbers of modes (from top: $N = 10$, 30, 60 and 150). The bow force is kept constant ($F_b = 0.3$ N) while the velocity is increased from 0 to 0.1 m/s in 0.08 s. The bow-bridge distance β is set to 0.12. (a) String velocity under the bow and (b) force on the bridge. An extra slip appears around time 0.04 s but the overall motion of the string is unchanged. Higher frequencies can be observed in the bridge force when the number of modes increases, as expected.

to 300. The resulting simulations are shown in Fig. 2.19. The string vibrations are seen to vary strongly depending on the computation frequency. With $f_s = 441$ kHz, a regular triggering is obtained during the entire duration of the attack, whereas $f_s = 44.1$ kHz produces a non-periodic oscillation. In contrast, the number of modes seems to have a weaker influence on the simulations and no qualitative differences can be observed for a given computation frequency.

Choice of the computation parameters

In the two previous sections, we have illustrated the influence of the computation frequency and the number of modes on the string motion during the sustained part of the simulation and during attacks. We have observed small variations in the spectral content of the resulting sound, and in the motion of the string due to the influence of the computation parameters on the mechanical properties of the virtual string. In particular, the simulations obtained in Fig. 2.19 resulted in

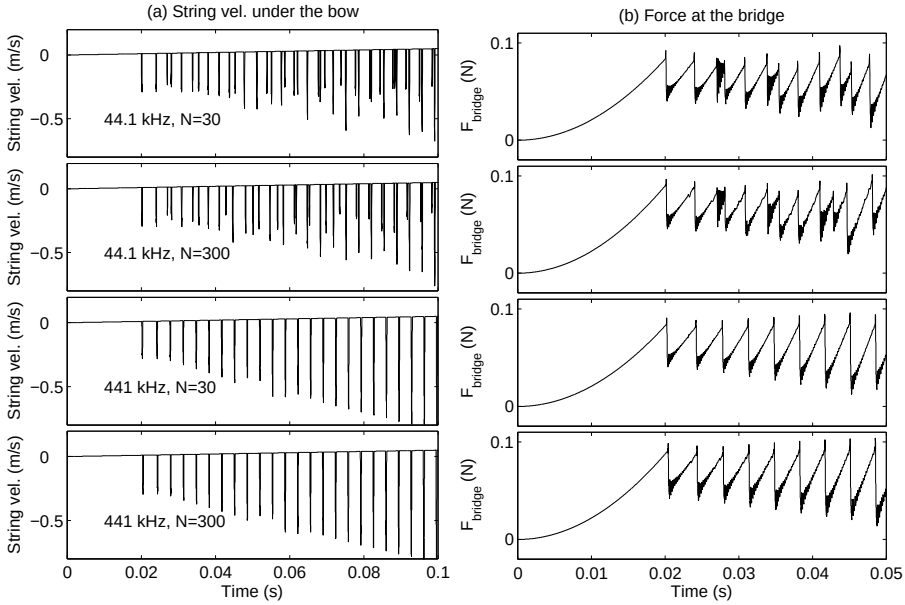

Figure 2.19: Attacks on a violin D string for different combinations of computation parameters (from top: $f_s = 44.1$ kHz with $N = 30$ and 300, then $f_s = 441$ kHz with $N = 30$ and 300). The bow-bridge distance is short ($\beta = 0.06$). The computation frequency is seen to have a strong influence on the result. With $f_s = 441$ kHz a regular triggering is reached, which is not the case with $f_s = 44.1$ kHz. The bow force is kept constant ($F_b = 0.3$ N) while the velocity is increased from 0 to 0.1 m/s in 0.2 s. (a) String velocity under the bow and (b) force on the bridge.

different string motions when the computation frequency was varied. Consequently, the computation parameters have to be carefully chosen when an accurate solution of the string equation is required, giving a detailed and realistic picture of the bow-string interaction.

Some influences of the computation parameters have been discussed in the course of this chapter. The number of peaks in the response of the string depends on the number of modes, a spatial spreading of the external forces can be observed, and the effective impedance of the string is changed with the computation frequency and the number of modes. However, no satisfying criteria could be found for setting these parameters, and here only some empirical considerations regarding this choice can be given.

For real-time purposes, it seems reasonable to set the computation frequency to the normal audio sampling frequency ($f_s = 44.1$ kHz) and choose a moderate number of modes, typically lower than 80. More precisely, if an harmonic signal is

assumed with a fundamental frequency f_0, the number of modes will be limited by the Nyquist frequency and

$$N < \frac{f_s}{2f_0}$$

In order to ensure that the maximal frequency component in the simulated signal is below this limit, we usually set the computation frequency to half this value. For example, with the D string used previously ($f_0 = 293$ Hz), this criterion leads to $N = 37$.

However, this criterion is only motivated by computational efficiency reasons, and there is no correlation between the criterion and the mechanical properties of the string that could set the optimal values of the computation parameters. For example, simulating a high D on the E string ($f_0 = 1174$ Hz) requires less than 18 modes with this criterion, which probably not is sufficient for reproducing the string vibrations properly. In that case the duration of the slip phase, when the string is bowed at a reasonable distance from the bridge (e.g. $\beta = 0.1$), is theoretically around $\beta/f_0 = 0.085$ ms, which would give only 3-4 computation steps during the slip phase. It can therefore be useful to increase the computation frequency in order to obtain a better description of the slip phase during the simulation.

This argument can also be used for explaining the results obtained in the previous sets of simulated attacks (Fig. 2.19). With $\beta = 0.06$, there are only 9 time steps during the slipping phase for $f_s = 44.1$ kHz and more than 98 time steps with $f_s = 441$ kHz. In the first case, the simulation of the bow-string interaction, in particular the transitions between sticking and slipping, is less precise. For example, unwanted peaks in the friction force may be produced, which, when propagated along the string, can endanger the regularity of the slip triggering. As a result, a regular Helmholtz motion was obtained for $f_s = 441$ kHz, whereas extra slips were produced with $f_s = 44.1$ kHz.

In contrast, no strong qualitative differences could be observed when the number of modes was varied: the overall motion of the string was the same, showing a periodic triggering of the string velocity under the bow (Fig. 2.18). This result can be explained by inspecting the frequency response of the string, shown in Fig. 2.20, top. The higher modes are more and more damped and no significant peak can be found in the response above the 15th mode. Starting from 5000 Hz, the response is lower than -60 dB, which could explain the differences between the simulations for $N = 10$ and $N \geq 30$. Note that the damping was very strong for the set of string parameters used in the simulation. For comparison, the mechanical response of a less damped string ($r_n = 0.3 + 0.2(n-1)^2$) is shown in Fig. 2.20, bottom. In that case, a much higher number of modes would be required in order to simulate the motion of the string properly.

As mentioned before, no analytical criteria could be found for choosing the computation frequency and the number of modes. In most of the simulations, the default parameters defined before has been used ($f_s = 44.1$ kHz and $N = f_s/4f_0$).

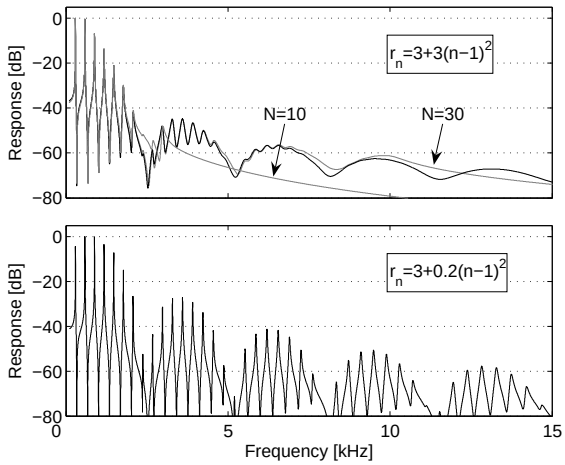

Figure 2.20: Frequency response of a violin D string bowed at $\beta = 0.12$ for different damping coefficients of the modes. The damping coefficient of mode n is determined according to $r_n = B_1 + B_2(n-1)^2$. Top: Strongly damped system with $B_1 = 3$ and $B_2 = 3$. The reference frequency response is obtained with $N = 1000$. With $N = 10$, the response is not well reproduced, whereas $N = 30$ gives only small deviations from the reference. Bottom: Less damped system with $B_1 = 3$ and $B_2 = 0.2$. In this case, more modes are required for the simulation. The response can be used for choosing an adequate number of modes to take into account.

It must be kept in mind, however, that both pitch and bow-bridge distance have an important influence on the exactness of the solution when the computation frequency is kept unchanged.

To conclude, the preceding discussion of the number of modes provides an empirical way of setting the computation parameters. The inspection of the frequency response of the string can be used for choosing an adequate number of modes N, and then the computation frequency can be determined from $f_s = 4f_0N$.

2.5 Concluding discussion

In this chapter, the model used for simulating the motion of the bowed string has been described in detail. We have presented the principle, which is based on the solution for each mode of the string equation, the numerical implementation, the solution of the bow-string interaction, and some empirical features that were added for improving the realism of the sound (noise generation during slip phases and convolution of the driving force on the bridge with a violin impulse response). In the last section, simulations were performed in order to compare the simulations

with observed motions of the bowed string, and to illustrate the influence of the computation parameters. Practical arguments for setting these parameters were discussed, and empirical guidelines proposed.

The model presented is not claimed to be original. Modal formalism is the base of bowed-string models developed by Adrien [1], Antunes [2] and Palumbi [59]. However, slight differences can be found between authors. For instance, Adrien introduced a discretisation in space with which he obtained a matrix formulation of the modal equations. However, this discretisation led to numerical inharmonicity of the modes. Some other models do not take bending stiffness explicitly into account, and just mention that there is no difficulty in including it in the formalism. Stronger differences can be found in the numerical schemes used to solve the modal equations and in the solution of the friction interaction. However, it should be noted that the comparison is sometimes made difficult by the lack of detailed description of the models in the literature.

In contrast, we tried to make the description of our model as complete and detailed as possible, in order to allow a straightforward implementation by other researchers. To our knowledge, the influence of computation parameters such as the number of modes and the computation frequency has never been discussed before. The numerical scheme that we used is also considered to be original within the field of bowed-string models using modal formalism.

Some possible improvements of our modelling of the bowed string and violin can be considered. As mentioned several times, the model presented in this work is very simple and not very realistic from a mechanical point of view. Several improvements could be foreseen and all of them would not require the same increase in computational complexity. For instance, a coupling with the violin body could be obtained by considering a resonant mechanical system at the position corresponding to the bridge. The simplest of these systems would be a mass-spring-damper system described in the first chapter (Sect. 1.2), but more elaborate models could be incorporated and easily solved, for example by defining another modal structure interacting with the string.

Similarly, the vibration of the string in several directions (normal to the bow, longitudinal and torsional modes) could be considered. As a first approximation, the system can be linearized in order to obtain independent string equations for each direction. In that case, the vibrations are only coupled under the bow and at the string terminations. Under the bow, the effective velocity is composed of the transverse velocity and the torsion component, and a conversion between waves in the two transverse directions could occur.

Changing the bow modelling or the friction interaction may be more difficult under real-time constraints. Modelling the bow as a vibrating structure would be rather straightforward and not too expensive. Other friction models in contrast, would require iterative algorithms for solving the interaction, which would greatly increase the computation cost. In the same way, a two-point bow model could be considered for simulating the finite width of the bow. In that case, the solution of two independent non-linear interactions is necessary, which again will require an

iterative procedure. Further, due to the spatial spreading described in Sect. 2.2, the number of modes would need to be carefully chosen in order to avoid mutual interaction of the friction forces at the two bowing points.

A main purpose of our work with the bowed-string model was to separate the properties of the model that are sufficient for obtaining an acceptable violin synthesis, from the demands necessary for obtaining a realistic modelling of the mechanics of the bowed string. It should be emphasized that our model has not been developed to be a scientific simulation tool for detailed studies of the bowed string, and in many cases it will not meet the demands of such a tool. However, in the light of our objectives, it is considered to perform perfectly satisfactorily, allowing perceptually convincing simulations of bowed-string sounds.

Chapter 3

Observations on the playability and sound properties of the model

In this chapter, simulations are performed in order to examine some important aspects related to the control of the bowed-string model. Like for a real instrument, different combinations of input parameters representing the musician's control will give rise to different types and qualities of the string vibrations. For instance, the sound can be more or less loud, "scratchy", or "brilliant".

In classical violin playing, the musician normally tries to obtain a stable tone, corresponding to Helmholtz motion (see Chapt. 1). The establishment and dynamical control of such a tone is a main objective in the player's musical education. As Helmholtz motion depends on the combination of the three main bowing parameters (bow force, bow velocity and bow-bridge distance), a considerable experience of the response of the bow-string interaction has to be gained in order to drive the bow-string system reliably. For instance, comparing a beginner and an experienced violinist, one is immediately struck by the skilled player's ability to obtain an acceptable tone, whatever the quality of the instrument.

Besides acquiring a purely motoric skill that enables the player to control the bowing parameters by basic gestures, the musician develops an ability for generating a proper Helmholtz motion by intuitively correcting the bowing gestures in the right direction depending on the resulting sound. This ability also includes how to obtain different and subtle properties of the tone quality according to the musical context and the musical intentions. An evaluation of the playability of the described model for sound synthesis has therefore to include two main tasks: (a) observing the actual playability properties, i.e. the input parameter space in which Helmholtz motion is produced, and (b) observing changes in sound properties that are significant for the player and relevant from a musical point of view. In addition, we should check that these control spaces are similar to those representing the playing of a real instrument.

The expected benefit of such a study concerns the control of the model. If the

observations correspond approximately to what is observed for the real instrument, then it would be possible for an experienced player to quickly acquire a subtle control of the model, provided that an adequate real-time control interface is used (e.g. graphical tablet [78], bow controller [80, 93], or similar devices [77]).

However, another interesting application of such a synthesis tool consists in offering the possibility of producing violin-like sounds for people who have little (or no) experience in violin playing, and therefore no dedicated gesture skills. In that case, a systematic exploration of the sound properties and the playability in the control parameter space could offer a way of making the control easier by limiting this space to produce classes of sounds (e.g. Helmholtz motion). Different classes of sound could be produced by offering qualitative different alternatives in the control. For that purpose, the consistency between observations and theoretical predictions of the behaviour of the bowed string for a given combination of control parameters would be of great interest. For example, it would spare us systematic explorations of the model when string parameters are changed.

The observations of the performance of the model are organised as follows. First some preliminary considerations about the motivations and the procedure are described (Section 3.1). Then simulations are reported, addressing three aspects. The first (Section 3.2) deals with the onset of the vibration and the conditions that lead to a good attack of the note. In the second one (Section 3.3), the conditions for maintaining Helmholtz motion will be examined. The last aspect, section 3.4, deals with the tonal properties which are studied in order to describe the effect of control parameters on the sustained vibration of the string (effect of bow force on string spectrum, flattening effect). Finally (Section 3.5), some applications for improving the control of the model are proposed.

3.1 Preliminary considerations

Point of departure

The introduction to this chapter has given the motivations to performing the simulations. In order to avoid confusion, it could be useful to clarify the purpose of this chapter further, and especially what we don't intend to do.

First of all, we have developed a tool for synthesizing violin-like sounds, nothing more. Consequently, we don't want to evaluate the model as a simulation tool dedicated to studies of the mechanics of the bowed string. Such an attempt would require more detailed simulations to check that the model behaves like it should in physical terms. In addition, the analysis of the resulting string motion would need to be done carefully, and compared with experimental results from studies of the bowed string when driven under controlled conditions by a bowing machine. Instead, we are interested in studying some high-level behaviours of the model, such as the type of vibration, the fundamental frequency and spectral content, and verify that the observations approximately fit with the experiences of players, and what can be inferred from basic theoretical considerations.

This approach is justified by some practical considerations. As explained in the previous chapter, the model has intentionally been made as simple as possible, in order to test the effect of realistic input parameters on the realism of the sound. Consequently, we cannot expect a very good agreement with detailed experimental results, which only could be explained by phenomena that are not taken into account in the model. Moreover, the choice of the computation parameters (sampling frequency and number of modes) has been made empirically (based on real-time synthesis considerations). An application for accurate simulation of the mechanics of the bowed string would require either to choose the values of these parameters in such a way that they would have no limitation on the realism of the simulation, or to find physically-based criteria for choosing them.

Secondly, because we are interested in the control of a virtual instrument, the simulations will be examined with the focus on the control parameters. Consequently we will not explore the mechanical parameters of the bow-string system, and we will not proceed to a systematic evaluation of their influence. Detailed analyses of this aspect have been reported by Guettler [36] and Serafin [76].

This approach can be questioned because the string parameters do not only determine the basic properties of the vibrations of the string, like fundamental frequency or inharmonicity. By influencing the excitation conditions of the string, these parameters also have a far from negligible impact on the control of the model. A more complete study would require to explore this aspect as well, which, however, would require a huge number of simulations. We have adopted the following strategy: A set of string parameters will be chosen so as to fit with properties of a "realistic" string, and these parameters will be used in all simulations. Only if the simulations do not give reasonable results, we will examine the influence of varying relevant parameters.

Procedure

The synthesis model is governed by a set of parameters describing the string properties and the friction between the bow and the string. In addition, computation parameters such as the number of modes and the computation time step may have a drastic effect on the simulations. As mentioned before, it is obviously not possible to explore the whole parameter space in order to obtain a detailed picture of the behaviour of the model. A choice of a limited set of parameter combinations has to be made in order to check the consistency of the simulations with empirical and theoretical results.

The simulations presented hereafter result from the use of a violin G string with parameters listed in Tab. 3.1. Computation parameters were determined by the constraints set by real-time simulations with $f_s = 44100$ Hz and a "reasonable" number of modes (given by $f_s/4f_0 = 56$). The length of the string between the nut and the bridge was set to 330 mm. Most of the remaining string parameters come from measurements by Pickering ([61], G string, Pirastro Eudoxa). As Young's modulus was not directly given in Pickering's data, the value was esti-

Parameter	Unity	Remarks	G string
Tension T_0	N	From Pickering	39.15
Length L	m	Measured	0.33
Diameter d	mm	From Pickering	0.8
Density ρ_L	g/m	From Pickering	2.34
Young's modulus E	Pa	Deduced from Pickering	$4 \cdot 10^9$
Damping B_1	1/s	Deduced from measurements	3.12
Damping B_2	1/s	Deduced from measurements	7
Sampling frequency f_s	Hz		44100
Number of modes N		$f_s/4f_0$	56
Frequency f_0	Hz	$f_0 = \sqrt{T_0/\rho_L}/2L$	196
Impedance Z_c	kg/s	$Z_c = \sqrt{T_0\rho_L}$	0.30
Inharmonicity factor B		$B = \pi^3 E d^4/64TL_0^2$	$1.86 \cdot 10^{-4}$
Quality factor Q_0		$Q_0 = \pi f_0 \tau_0$	197
Equivalent resistance R	kg/s	$R = Z_c \coth(\pi/2Q_0)$	38

Table 3.1: String and computation parameters used for the simulations. The data come from measurements by Pickering ([61], G string Eudoxa) or own measurements. The five last rows indicate some physical characteristics of interest.

Order of harmonics	1	2	3	4	5	6	7	8
Freq. deviation (in cents)	0.2	0.6	1.4	2.6	4	5.8	7.9	10.2
Freq. deviation from [61]		1	4	3	4	6	11	14
Decay time (ms)	320	98	32	15	9	6	4	3
Quality factor	197	122	59	37	27	21	17	14

Table 3.2: Table illustrating some properties of the G string used for the simulations. The two first rows show the agreement between the frequency deviation of the partials given by Pickering [61] and the values obtained with $E = 4 \cdot 10^9$ Pa for Young's modulus. The two last rows gives the decay time and the quality factor of the modes in order to illustrate the damping.

mated from the partial frequencies for plucked notes. The value $E = 4 \cdot 10^9$ Pa gives frequency deviations for the 8 first harmonics that approximately correspond to the measurements (see Tab. 3.2). The damping coefficients were set using data measured on the D string in the previous chapter. B_1 and B_2 were chosen to give a decay time of 0.3 s for the fundamental, and 0.01 s around the fifth harmonic ($r_n = 1/\tau_n = B_1 + B_2(n-1)^2$). These values give Q factors that are a bit lower than normally used, especially for the highest harmonics (see Tab. 3.2).

3.2 Onset of the vibration: The attack

Before reaching the periodical oscillation that characterizes the normal bowed-string motion, the string must be set in vibration. During the short time when the oscillations build up, other frequencies than the harmonics of the fundamental are excited, resulting in an aperiodic and sometimes noisy part. The sound of transients is of primary interest for the perceptual identity of the instrument [70], and their reproduction is therefore an important feature for the realism of the synthesized sounds. Note that the onset of the vibration is naturally produced by the physical model used and controlled by the time evolution of the input parameters, in contrast to other synthesis methods like spectral models.

Depending on the combination of bowing parameters applied at the beginning of a bow stroke, the transient can sound differently and have substantially different durations. For instance, a too high initial bow pressure generally gives rise to a "choked/creaky" sound, according to Guettler's terminology [37], whereas a too low pressure, which can be the case when the stroke is begun "from the air", will give a "loose/slipping" attack. The different ways of attacking the note are an integral part of the musical discourse, and in analogy with speech production the attacks are often compared with consonants, the steady part of the motion being the "vowels".

In this section, we are interested in describing the relation between the onset of the vibration and the time evolution of the bowing parameters at the beginning of the stroke. Two basic situations can be considered, corresponding to two contrasting ways of exciting the string. In an attack from the string, the bow is pressed on the string before beginning to move (initial velocity null), whereas in an attack from the air, the bow lands on the string while already moving (initial bow force null). We will focus on the attack from the string, because it is the most documented situation and it will allow comparisons with theoretical results.

In a first section, we will present Guettler's experimental and theoretical results, then simulations of the initial transient will be shown and discussed under the light of the theory.

Background: Experimental and theoretical results

A large number of studies have described the steady oscillation of the bowed string, but very few have been concerned with the attack. Apart from a few remarks on the question, Schelleng [71] only considered the problem of the "shape of the attack", i.e. the amount of energy that is necessary for making the steady oscillation grow. In a way, he considered the attack as a quick crescendo, without focusing on the conditions for setting the string in steady vibrations.

More recently, Guettler and Askenfelt [37] reported a pioneer work on the subject. They collected a database of different types of attacks produced by a bowing machine, and a panel of string players were asked to judge the quality of the attacks. The acceptance limits for the duration of the pre-Helmholtz transient was found to be 50 ms for "choked" attacks and 90 ms for "loose" attacks. Waveforms

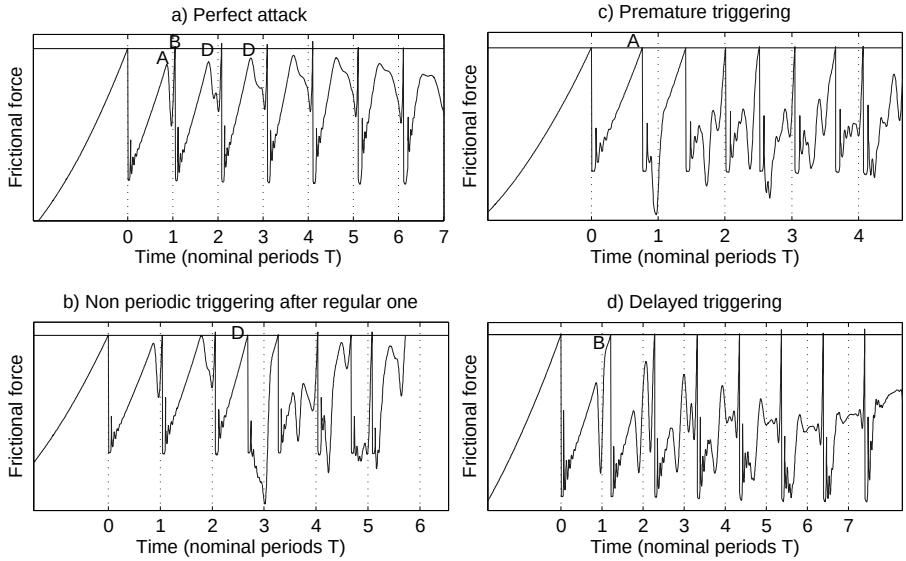

Figure 3.1: Frictional force during the very first periods of the attack, illustrating different situations for the onset of the vibration. Slip triggerings occur when the frictional force reaches the limiting static force represented by a horizontal line. Nominal periods are represented on the x-axis for comparison. (a) Perfect attack: The intervals between slip triggerings are equal to the nominal period from the first triggering. (b) After two triggerings occurring at the nominal periods, the regular onset is perturbed by a force peak in between (corresponding to condition D, Eq. 3.4). (c) Premature triggering: A triggering occurs before the first nominal period (condition A, Eq. 3.1). (d) Delayed triggering: The period between slip triggerings is greater than the nominal period during the first periods (condition B, Eq. 3.2).

of the velocity under the bow showed that choked attacks correspond to prolonged periods, whereas loose attacks correspond to additional slips during the nominal period ("multiple slips"). By analysing attacks produced during real performances, they showed that most of them fell within the acceptance limits.

The theoretical conditions for establishing the periodical motion were investigated later by Guettler [34], for the specific case of attacks performed from the string. From an analysis of the propagating velocity waves during the transient, he deduced the conditions for the operative parameters, bow force F_b and bow acceleration a_b, which give a quick build-up of the oscillation.

Fig. 3.1 presents some simulations illustrating the limitations considered by Guettler. Frictional forces during the attack are shown, together with the limiting static force (horizontal line). When the frictional force reaches this limit, the string begins to slip. In Fig. 3.1a, the slip triggering occurs at each nominal period T

from the very beginning of the attack. This illustrates the situation that Guettler referred to as a "perfect attack". A perfect attack was found to depend on four equations, describing two kinds of conditions: The two first ones (A and B) for establishing the motion from the very first slip, and the two other ones (C and D) for maintaining a periodic motion.

Fig. 3.1c illustrates the first condition for obtaining the "perfect attack". The first frictional force maximum after the first slip, at $t = (1-\beta)T$ (point A, resulting from the return of the velocity wave travelling towards the nut) must be less than the maximum static force in order to avoid premature slipping of the string. If this slip occurs (as in Fig. 3.1c), the interval between the two first slips is less than the nominal period and the attack is not perfect. This condition is formalized by

$$a_b < \beta(1-\beta)F_b\Big[(3-4\beta)\mu_s - \mu_d - 2\sqrt{(1-2\beta)(2(1-\beta)\mu_s^2 - \mu_s\mu_d}\Big]\left[(1-2\beta)TZ_c\right]^{-1} \tag{3.1}$$

where μ_s and μ_d are the static and dynamic friction coefficients, Z_c the characteristic impedance of the string, T the nominal period and β the bow-bridge distance relative to the string length.

Secondly, after the period T (point B) a second slip must occur, i.e. the friction force at that point must surpass the maximum static friction force. In Fig. 3.1d, the static force is not reached after the nominal period T, resulting in delayed slip triggering. The condition for this slip to occur is given by

$$a_b > \beta(1-\beta)F_b\frac{3\mu_s - \mu_d - 2\sqrt{2\mu_s^2 - \mu_s\mu_d}}{TZ_c} \tag{3.2}$$

These two equations give the conditions for getting a nominal period between the two first slips. Consequently, they are also necessary conditions for getting a "perfect attack". But there is no warranty that the next intervals will have the desired motion and some additional conditions are necessary for the right triggering to be maintained. Guettler identified two critical points in the time evolution of the frictional forces.

First, the reflection of the first slip pulse travelling between the bow and the nut must not cancel the friction force maximum after a time T/β (point C in Guettler's article, not represented here). The resulting condition is

$$a_b > \beta^2(1-\beta)F_b\Big[(1-1.5\beta)(C+\lambda^{1/\beta})(\mu_s - \mu_{d1}) + \beta\mu_s - \sqrt{(2\beta - 3\beta^2)(C+\lambda^{1/\beta})(\mu_s^2 - \mu_s\mu_{d1}) + \beta^2\mu_s^2}\Big]\left[2(1-1.5\beta)^2TZ_c\right]^{-1} \tag{3.3}$$

where λ is the reflection coefficient at the nut, μ_{d1} and μ_{d2} refer to the sliding friction coefficients at the first slip and the last one[1], and $C = (\mu_s - \mu_{d2})/(\mu_s - \mu_{d1})$.

Finally, some of the friction force peaks observed at times $t_i = i(1-\beta)T$ (points D) could become higher than the static friction force maximum, which would result in premature slip triggering between the nominal periods, illustrated in Fig. 3.1b. Guettler observed that the point at $i \approx 1/3\beta$ was particularly critical for maintaining the periodical triggering.

$$\begin{aligned} a_b \leq 9\beta^2(1-\beta)F_b\Big[&(2-3\beta^2)\mu_s - (2-4\beta+3\beta^2)\mu_d \\ &-2\sqrt{(2\beta-3\beta^2)\big[(2-2\beta)\mu_s^2 - (2-4\beta+3\beta^2)\mu_s\mu_d\big]}\Big] \\ &.\big[(8-44\beta+104\beta^2-132\beta^3+90\beta^4-27\beta^5)TZ_c\big]^{-1} \end{aligned} \tag{3.4}$$

In a bow force-acceleration parameter space, these limitations define a triangular region in which the onset of the vibration is theoretically optimal. Simulations for various values of β, F_b and a_b were performed by Guettler and plotted in force-acceleration diagrams, which showed very good agreement with the theoretical predictions.

Simulations of initial transients: Procedure and results

Our model was tested in the light of these theoretical results. Simulations were performed using the open G string defined before. During the attack, the force was kept constant whereas the velocity was increasing with a constant acceleration a_b. Successive simulations were performed with the acceleration varying from 0.1 to 10 m/s^2 (200 values), and the force from 0.1 to 2 N (40 values), representing 8000 simulations per bow-bridge distance β. Ten bow-bridge distances β were used, from 1/25.4 to 1/6 (11 mm to 55 mm from the bridge).

For each simulation, the ten first slip triggerings were computed. The regularity of the slips was analyzed in order to determine the first triggering from which a regular vibration with the nominal period occurred and which lasted until the end of the simulation.

Results are shown in Fig. 3.2. The number of slips before regular triggering is reached is shown on a grey color scale, from white (first slip) to black (more than 5 slips). Triangular regions giving an optimal onset of the vibration are recognizable and seem to be in agreement with Guettler's predictions: For a given force, the maximum acceleration giving a "perfect attack" increases with bow-bridge distance, and at the same time, the optimal region becomes wider. It can be noted that for small bow-bridge distances (here, for $\beta = 1/25.4$ and $\beta = 1/22$), the region in which the regular triggering occurs from the first slip is very narrow. Moreover, it

[1] As the relative velocity increases during the attack, μ_d may have decreased significantly since the first slip.

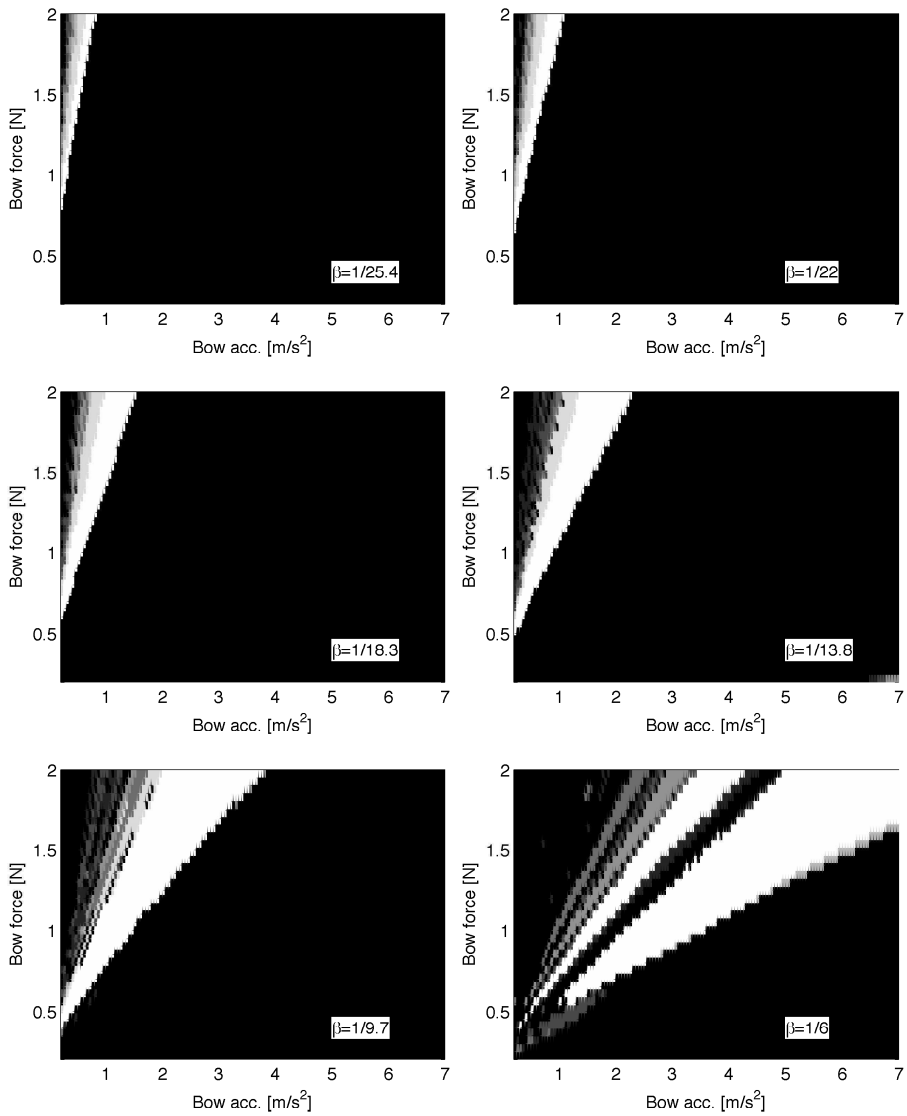

Figure 3.2: Simulated attacks with the bowed-string model. The figures show in grey scale the number of slips occurring before a regular triggering is obtained at the nominal period T, from 0 (white) to 5 and more (black). Simulations were performed with bow forces varying from 0.1 to 2 N and accelerations between 0.1 and 10 m/s^2 representing 8000 simulations per plot. Ten bow-bridge distances were used, six of them being shown here.

is interesting to note that beyond this region (for higher accelerations), no regular triggering is observed at all, whereas for lower accelerations, the regular triggering can be reached after several slips.

Discussion and comparison with theoretical results

In order to compare the results with Guettler's equations (Eqs. 3.1, 3.2, 3.3 and 3.4), simulations were done with a flexible string (Young's modulus $E = 0$). Guettler used only an ideal string for analysing the starting transient. The more elaborate model including stiffness could lead to deviations that would not be very easy to anticipate.

Fig. 3.3 shows the simulations obtained for three bow-bridge distances β (1/25.4, 1/15.7 and 1/11.4). On the right is shown the number of slips occurring before a regular oscillation at the nominal period, lasting throughout the simulation, was obtained (referred to as *regular triggering*). In addition, we looked for the first interval between two successive slips occurring with the nominal period (referred to as *first triggering*). This additional analysis does not tell whether the motion is maintained or not, but permits making a comparison with the conditions for obtaining a first interval equal to the nominal period (equations 3.1 and 3.2). In all figures, the number of slips is represented on a grey scale, from white (first slip) to black (fifth slip and higher).

The theoretical expressions are plotted with color lines in the figures. Eq. 3.1 and 3.2, describing the conditions for obtaining a nominal period between the two first slips, are represented with red lines. Equations 3.3 and 3.4, describing conditions for maintaining the regular triggering, are plotted with green lines. Because of the slope of the hyperbolic friction, the coefficient μ_d at the instant of the release may vary slightly with bow force F_b. For this reason, the lines were obtained by computing μ_d as the intersection between the line $F_0 = 2Z_c(v_b - v_h)$ and the characteristic friction for $v_h = -\mu_s F_b/2Z_c$, corresponding to the instant of string release.

Looking at the left hand panel, Eqs. 3.1 and 3.2 seem to be in very good agreement with the first triggerings at nominal period that were found. The red lines fit rather well with the white triangular regions corresponding to a nominal period appearing from the first slip (white sections). It could be noticed that these regions seem slightly wider than predicted by the theoretical limits. This is probably due to the analysis of the data: A tolerance of 5 % was used for determining if the time between two slips was equal to the nominal period.

A comparison with the right-hand panel gives information about the maintaining of the oscillation. For $\beta = 1/25.4$, it can be seen that no regular, lasting triggering with the nominal period was obtained from the very first slip to the end of simulation (right figure), whereas an initial triggering after the first nominal period T was obtained (left figure). This indicates that some phenomenon breaks the periodic triggering of the slips.

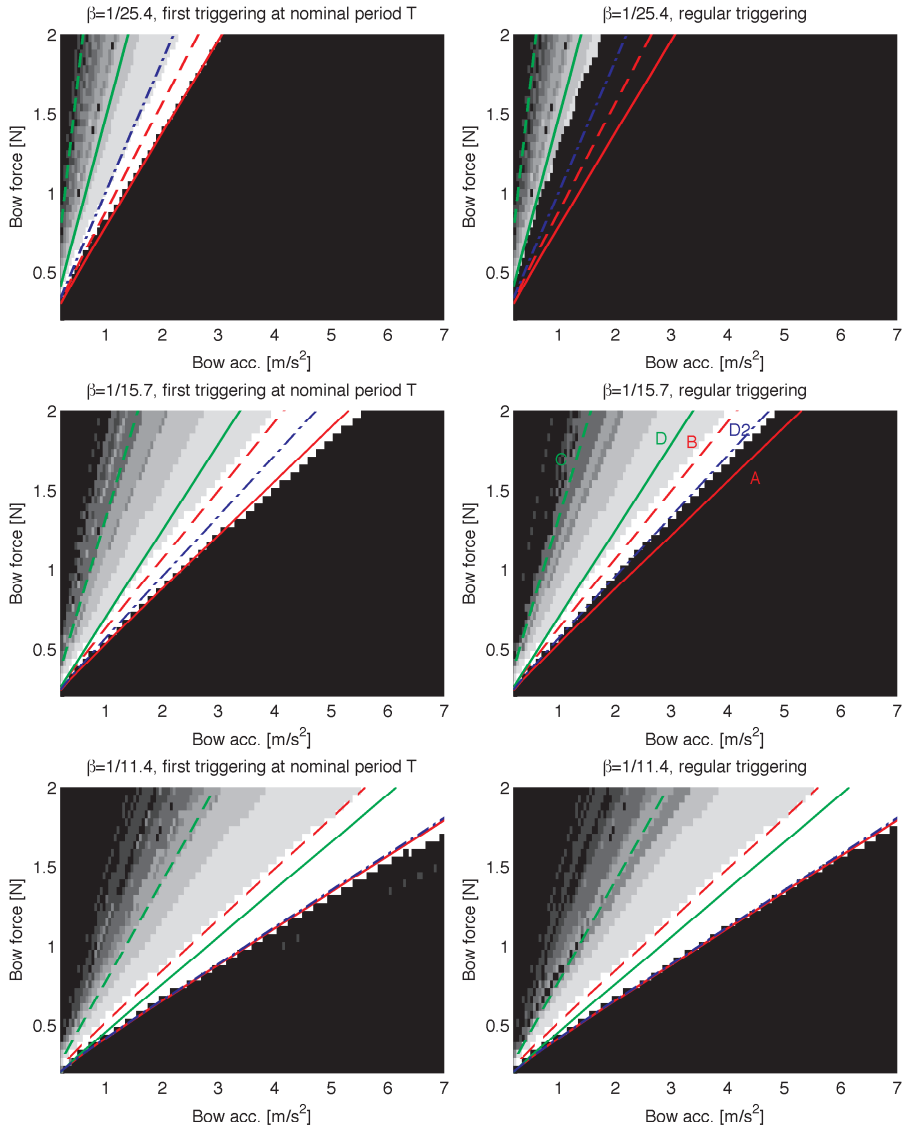

Figure 3.3: Comparison between simulated attacks for a flexible string and theoretical relations A (Eq. 3.1), B (Eq. 3.2), C (Eq. 3.3) and D (Eq. 3.4) obtained by Guettler. D_2 (blue line) represents Eq. 3.5 with a fitted coefficient $i = 1/11\beta$. Left: Number of slips occurring before a first interval with nominal period is obtained. Right: Number of slips occurring before a regular triggering at nominal period is obtained which lasts until the end of the simulation. The three bow-bridge distances illustrate different situations concerning the maintaining of the regular triggering.

The three bow-bridge distances illustrate different situations in this respect. For $\beta = 1/25.4$, none of these potentially "perfect attacks" are maintained until the end of the simulation. For $\beta = 1/15.7$, only the part corresponding to the lowest accelerations are maintained, and for $\beta = 1/11.4$, almost all periodic attacks are maintained. In Guettler's analysis, such a truncation should occur, determined by the limitation D: For a given force and a given acceleration to give rise to a "perfect attack", the acceleration must be higher than both B and C and lower than both A and D. However, in our case, it can be seen that condition D does not give the expected limitation. Otherwise there would be no perfect attack at all for $\beta = 1/15.7$ (no intersection between the regions delimited by the green lines and the region delimited by the red lines).

As pointed out by Guettler ([34], Annex A5), the determination of this relation is to some degree empirical. The general limitation consists in saying that the force maxima occurring at $t = i(1-\beta)T$ after the first release should be lower than the static limiting force, this general condition being given by

$$\begin{aligned} a_b \leq \frac{F_b \mu_s}{T Z_c} \beta(1-\beta) \Big[& (1-\beta+2i-3\beta i + \frac{\mu_d}{\mu_s}(1-\beta-2i+\beta i) \\ & -2\sqrt{(1-\beta-\beta i)\big[2i-2\beta i+\frac{\mu_d}{\mu_s}(1-\beta-2i+\beta i)\big]}\Big] \\ & . \Big[(1-\beta-\beta i)(1-\beta-2i+\beta i)^2\Big]^{-1} \end{aligned} \tag{3.5}$$

The coefficient i depends on the bow-bridge distance β and the friction characteristic through the ratio μ_d/μ_s. From observations on the frictional force during the attacks and a comparison between the maximal acceptable acceleration at D depending on i and the maximal acceleration at A, Guettler concluded that the most restrictive limitation could be found at $i = 1/3\beta$, which gave equation 3.4. In other words, the critical force maxima were found to be at i periods $(1-\beta)T$ after the first slip, with i varying from 2 to 8 for bow-bridge distance varying from 1/6 to 1/24. However, in our case, most of the premature slip triggerings corresponding to this limitation were found to be at lower i (typically less than 2). In Fig. 3.3, it can be seen that equation 3.5 gives a good agreement with the observed data for $i = 1/11\beta$ (blue line, denoted D2).

Concerning limitation C, it does not seem to play an important role in our simulations as it always was outside the region determined by A and B. Note that this was the case in Guettler's simulations as well, except for the largest bow-bridge distance.

In this section, we focused on the attacks in order to observe the parameter space in which a regular vibration of the string is quickly obtained. In the simulations, optimum regions can be identified, varying qualitatively as expected from Guettler's analysis. For example, the maximum possible acceleration for a given

bow force increases with increasing bow-bridge distance. A more precise comparison showed a good agreement with Guettler's theoretical inferences: The conditions for obtaining a first triggering at the nominal period fit well with the corresponding region in the simulations. The conditions for maintaining a regular triggering were found to be slightly different but gave the expected qualitative behaviour. From these observations, we should consequently be able to predict the quality of attacks according to control parameters, or produce the right time evolution in order to control the model.

During the attack, the relevant control parameters are the bow-bridge distance, the bow force and the bow acceleration. An adequate choice of these parameters will lead to the desired vibration state of the string, i.e. Helmholtz motion. In the next section, we will perform simulations in order to observe the behaviour of the model under steady control parameters. In particular, we will be interested in how to maintain the Helmholtz motion for various bow-bridge distances, bow forces, and bow velocities.

3.3 Maintaining Helmholtz motion: Schelleng diagrams

At the beginning of this chapter, we pointed out that a major element in a violinist's education consists in learning the adequate control strategies for obtaining and maintaining a Helmholtz motion. For a given bow velocity and bow position, pressing too hard on the string produces a raucous sound, which is of little musical interest. At high bow forces, and certain combinations of bow-bridge distance and velocity, periodical vibrations below the fundamental frequency can be obtained, in which torsional waves play an important role in the triggering of the slips. Such anomalous low frequencies (ALF) are not used in traditional classical music [32], but they can be of interest in contemporary music [46]. In contrast, a very light pressure on the string gives rise to a "surface sound" with higher string modes excited. This type of string vibrations is characterized by the presence of more than one slip during a nominal period, and is therefore referred to as multiple-slip motion. This motion is difficult to control, as it requires a very light and constant bow pressure, but it is sometimes used for musical purposes, like when the violinist plays *sul ponticello* ("on the bridge"). It can be noted that multiple slips can be obtained far from the bridge, but a small bow-bridge distance makes it easier.

In this section, the model will be used to simulate string vibrations under "steady-state" conditions, using various sets of control parameters. By examining the resulting oscillations, we will be able to identify the different types of motion, define the regions in the control parameter space where the model can be used, and make a comparison with theoretical predictions. First a background is given reviewing the experimental studies describing the playable region and theoretical values for minimum and the maximum bow force.

Background: Experimental and theoretical studies

The requirement for a minimum bow pressure was first investigated by Raman [66]. He found experimentally that this limit was varying in proportion to bow velocity, except for low velocities for which it was tending to a finite minimum. Further he showed that the minimum force was varying inversely as the square of bow-bridge distance for constant speed. He also observed that the minimum bow force was related to the resonances of the violin body. Additional experiments by Kar et al. [43] (cited by Schelleng [71] and Hiller [41]) corrected the variation with bow-bridge distance, indicating that the minimum bow force was varying simply inversely with bow-bridge distance.

These observations were confirmed by Schelleng [71] who gave a theoretical expression for the minimum and maximum limits of bow force. He considered two requirements for the Helmholtz motion to be maintained. First, the frictional force should reach the static limiting force after a nominal period T, when the velocity discontinuity created by the last slip arrives from the nut. If the limiting static friction force ($\mu_s F_b$) is too high, the slip will not occur. This situation is illustrated in Fig. 3.4, right. At the beginning, the oscillation looks like Helmholtz motion, but as the limiting force is too high the period is lengthened, and then the vibration develops into a rather chaotic behaviour. This condition imposes a maximum bow force

$$F_{max} = \frac{2Z_c}{\beta(\mu_s - \mu_d)} v_b \tag{3.6}$$

Secondly, the frictional force should not reach the limiting static force between the two slip triggerings determining the nominal period. In Fig. 3.4, left, the frictional force grows between the two main slips and gives rise to an additional slip triggering after about half the nominal period. After a few periods the vibration would develop into the multiple-slip vibration described above. The minimum bow force can be expressed as

$$F_{min} = \frac{Z_c^2}{2\beta^2(\mu_s - \mu_d)R} v_b \tag{3.7}$$

assuming that the terminating impedance at the bridge is a pure mechanical resistance R.

As can be seen, these equations give zero limit for a zero bow speed. Actually, μ_d depends on the relative velocity between the bow and the string, and for small bow speeds, these expressions can be corrected using a friction model. With the hyperbolic model described before, the difference between static and dynamic friction coefficient can be expressed as $\mu_s - \mu_d = \frac{v_b}{v_b + \beta v_0}(\mu_s - \mu'_d)$, with μ'_d the asymptotic limit of the friction characteristic. Then, Schelleng's requirements become

$$\frac{Z_c^2}{2R(\mu_s - \mu'_d)} \frac{v_b + \beta v_0}{\beta^2} < F_b < \frac{2Z_c}{(\mu_s - \mu'_d)} \frac{v_b + \beta v_0}{\beta} \tag{3.8}$$

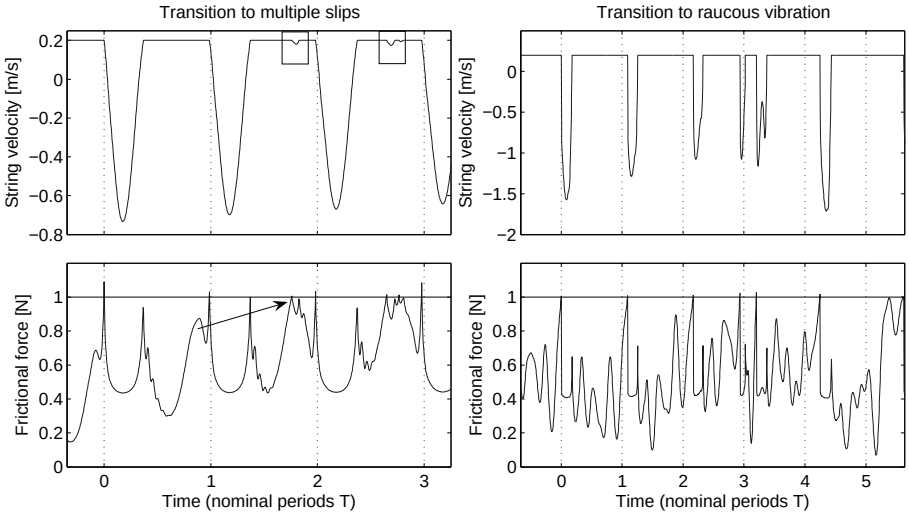

Figure 3.4: Illustration of situations in which the Helmholtz motion is interrupted. Left: An increase in frictional force during the interval between the two slips occurring at the nominal period gives rise to an additional slip marked with the boxes (multiple slip). Right: The frictional force after a nominal period is not high enough for launching the slip triggering. The period is first lengthened, then the vibration becomes raucous. Note the different time scales.

These conditions determine a region for maintaining Helmholtz motion in the bow-bridge distance, bow force space for each bow velocity. This is illustrated in Fig. 3.5, showing the original diagram presented by Schelleng [71].

After Raman's and Kar's experiments very few studies followed trying to determine the maximum and minimum bow forces experimentally. Askenfelt gave approximate estimations of the upper and lower force limits for a violin G string, based on measurements of sustained notes performed by professional violinists [4]. Schumacher [75] reported some determinations of maximum bow force using a bowing machine as well as simulations. Recently, Galluzzo [29] determined Schelleng diagrams for a cello D string using a bowing machine. Schoonderwaldt [72] used a bowing machine for systematically studying the influence of bowing parameters and damping on the bow force limits for violin D and E strings. Concerning the use of bowed-string models, Serafin [76] has studied playability in terms of Schelleng diagrams. The purpose was mainly to test different configurations of a physical model (with and without torsional waves, or different friction models) and to observe how they influence the playable control parameter space.

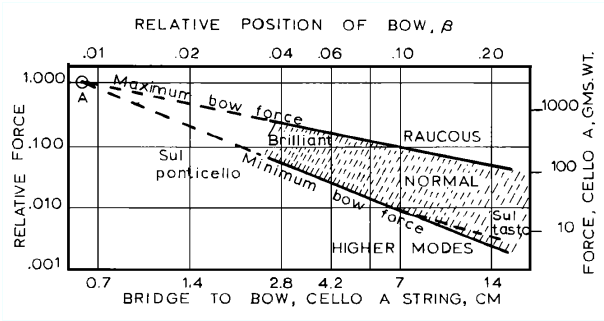

Figure 3.5: Schelleng diagram, from [71]. The figure shows the maximum and the minimum bow force limits for Helmholtz motion vs. bow-bridge distance, at a given bow velocity. Usual descriptions of the tone color are indicated in different regions.

Procedure

Simulations with different bow forces, bow velocities and bow-bridge distances were performed with the model in order to systematically explore the parameter regions in which Helmholtz motion is obtained. The vibration of the string is very sensitive to the time evolution of bowing parameters, and the same set of parameter values can give different kinds of vibration depending on the way the target values are approached. Multiple slips, for instance, can be maintained very long even for a bow force greatly above Schelleng's minimum force, if they are initiated during the attack. This hysteresis rule was pointed out by McIntyre [55]. The initial part of the bow stroke will consequently be of primary importance for the resulting vibration.

As seen in the previous section, we should be specifically careful in simulations with small bow-bridge distances for which the acceleration limits during the attack are particularly narrow. A procedure has to be defined, ensuring that the simulations are performed under best possible conditions. This means that Helmholtz motion should be reached very soon after the beginning of the bow stroke, and be maintained as long as possible. The following procedure was adopted.

For each bow-bridge distance, the Guettler diagram was first computed with simulations. A combination of bow force F_{b1} and acceleration a_{b1} used during the attack of a note must satisfy the following requirements: (a) Be located in the region where the conditions for obtaining Helmholtz motion is optimal, and (b) lead to a velocity v_{b1} for which the combination force-velocity fits in the theoretical Schelleng triangle. More precisely, this last requirement is expressed as follows: The velocity is supposed to be reached after a given time, for instance 10 nominal periods, which can be expressed as $v_{b1} = 10Ta_{b1}$. This relation is used to plot the lines $F_{max}(a_{b1})$ and $F_{min}(a_{b1})$ in the Guettler diagram, defining a region in which $(v_{b1} = 10Ta_{b1}, F_{b1})$ is inside the theoretical Schelleng's limits. A combination force-acceleration is then determined graphically (see Fig. 3.6, left) by finding a

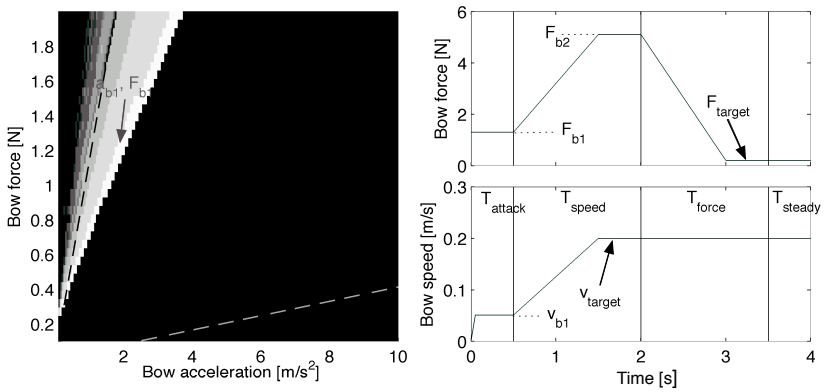

Figure 3.6: Procedure for defining the profiles of bow velocity and bow force in the simulations when computing the Schelleng diagrams. Left: The slope of the attack is determined using simulated Guettler diagrams. The lines represent Schelleng minimum and maximum bow forces for $v_b = 10Ta_b$. A combination of bow force and acceleration is selected that satisfy both the requirements of the Guettler diagram and Schelleng's limits for force and velocity at the end of the attack. Right: Illustration of the profile of a bow stroke. Provided that the previous procedure is followed, Helmholtz motion is obtained during the first interval T_{attack}. Then the target velocity is approached during a coordinated variation in bow force (interval T_{speed}). Finally, the bow force is slowly changed to its target value. This procedure ensures that Helmholtz motion is maintained during the bow stroke before reaching the target bow force.

combination that is both in the simulated Guettler's triangle and in the region determined by the two lines.

The Helmholtz motion is maintained 0.5 s for this combination (F_{b1}, v_{b1}), and then the velocity is increased to the target value v_{target}. In order to maintain the Helmholtz motion during this transition phase, a coordinated change in bow force is made to a value F_{b2}:

$$F_{b2} = \frac{F_{b1}}{F_{max}(v_{b1})} F_{max}(v_{target})$$

After a new plateau at (F_{b2}, v_{target}), the force is then slowly decreased to the target value F_{target}. This procedure ensures that Helmholtz motion is quickly reached and maintained until the force has reached the target value. An example of a bow stroke profile is illustrated in Fig. 3.6, right.

Four bow velocities were studied: 5, 10, 20 and 50 cm/s. The same grids for bow force and bow-bridge distance as in Schoonderwaldt's study [72] were used, defined by logarithmically equally spaced values (20 values for bow force between

49 mN and 3 N, and 10 values for bow-bridge distance between 1/25.4 and 1/6). These values are typical of the control parameters used in real violin playing.

A simple algorithm based on the analysis of the 20 last slip triggerings of the simulations was used to determine the type of string vibrations. From the time intervals between successive slips, the mean value and the spread were computed, allowing to make a basic classification of the vibrations in: slip only (no stick period during the interval considered), raucous (large spread), Helmholtz motion (small spread around the nominal period T), multiple slips (small spread around one or two periods shorter than T, typically $T/2$) and ALF (small spread around one or two periods larger than T, typically around nT).

Results and discussion

The resulting diagrams are presented in Fig. 3.7, each plot representing one bow velocity. For comparison, theoretical limits for minimum (Eq. 3.7) and maximum bow force (Eq. 3.6) are included. As we were mainly interested in the determination of the region in which the Helmholtz triggering occurs, other types of vibration that occur outside this region were not analyzed in detail (missing values in the diagram).

The region in which the Helmholtz motion is maintained seems to be in very good agreement with the theoretical values, especially with regard to the upper force limit. Above this limit, several types of ALF vibrations can be observed. The results should be compared with measurements by Schoonderwaldt [72], which gave slightly different results: Above the maximum bow force limit, mostly raucous vibrations were observed with some small regions of anomalous low frequencies. One reason for this difference lies in the simple model that we used for the bowed string. Some phenomena that were not taken into account, in particular torsion of the string and finite width of the bow, could facilitate or prevent the development of such vibrations. Another reason could be that the generation of ALF vibrations necessitates a very fine and constant control of the input parameters, difficult to maintain in real playing or with a bowing machine (Schoonderwaldt report fluctuations of 20-30 mN in the bow force and 5 mm/s for the velocity). With simulations, the parameters are strictly constant, which may facilitate a long-lasting establishment of such vibrations.

Concerning the lower limit, the Helmholtz motion seems to be maintained rather long under the theoretical force value. This may be explained by the simulation procedure. During the first part of the simulation, the Helmholtz motion was established in order to reach the target values (v_b, F_b) at a stable Helmholtz condition. In the last part of the simulated stroke when the parameters were kept constant, the remaining Helmholtz vibration was gradually decaying in the cases when the combination of force and velocity was not sufficient for maintaining the vibrations. Sometimes, even with a steady part lasting more than 2 seconds, this was not enough for making the remaining vibrations disappear entirely. However, in most of the cases that were checked, the decay seemed to be very slow and the oscillation could be considered to have reached a steady motion.

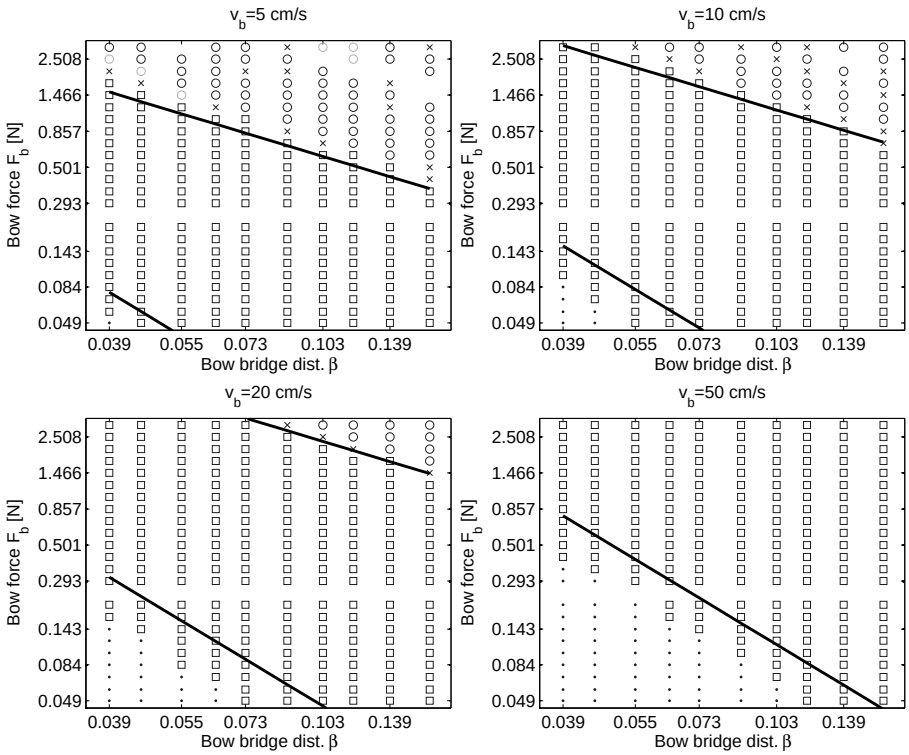

Figure 3.7: Schelleng diagrams representing the different kinds of vibration obtained for a given set of gesture parameters. The four figures represent four different bow speeds (v_b =5, 10, 20 and 50 cm/s). Bow-bridge distance is represented on the x-axis and bow force on the y-axis (both with logarithm scales). The different vibrations obtained are: Helmholtz motion (□), constant sliding (·), multiple slips (+), raucous (x) and anomalous low frequencies (o). The lines represent the theoretical minimum and maximum bow force according to Schelleng (Eq. 3.7 and 3.6).

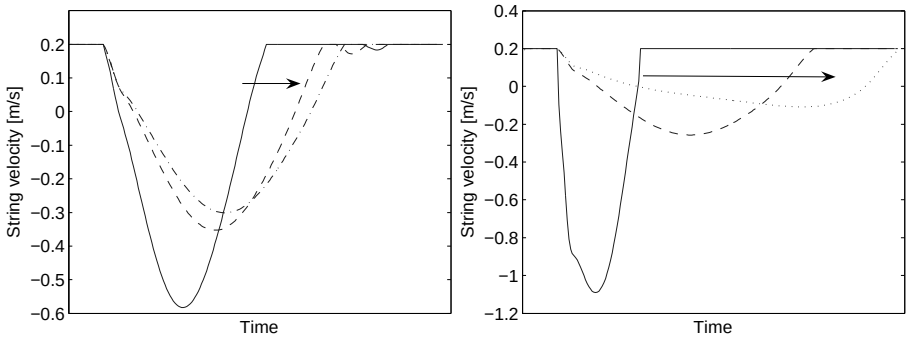

Figure 3.8: Illustration of the changes in the slip phase under the minimum theoretical bow force in Fig. 3.7 when the force is slowly decreased. Left: An additional slip appears at about half the nominal period but the lengthening of the main slip triggering prevents it to develop. Right: For very low bow forces, the lengthening can increase until occupying the whole nominal period, giving a constant sliding. These two phenomena prevent multiple slips to develop under the minimum bow force, between the Helmholtz region and the region with constant sliding.

Secondly, it can be observed that no multiple slips were found under the theoretical lower force limit. The fact that Helmholtz triggering was established early during the stroke seems to facilitate a maintaining of the oscillation and a direct transformation into a steady slipping state, without multiple slips occurring in between. This is very similar to the effect that was pointed out by Woodhouse [88] for models with narrow reflection functions. Woodhouse's analysis of minimum bow force for such models predicted (also confirmed with simulations) that the minimum bow force would be very small and could not be anticipated using Schelleng's analysis:

> "If the bow force is slowly reduced once a stable Helmholtz motion is established, the Helmholtz corner becomes more and more rounded, and the slipping time occupies a larger and larger proportion of the entire period length. Eventually, slipping occupies the entire period length. (...) the motion may then decay slowly to a state of steady sliding without oscillation."

This is illustrated in Fig. 3.8. Actually, at some time in the simulation, an additional small slip may appear (Fig. 3.8, left), but the lengthening of the main slip period makes it disappear and the oscillation degenerates into some kind of Helmholtz motion with a very long slipping period.

This effect seems to depend strongly on the damping of the first string mode. In the previous simulations, damping parameters were set to $B_1 = 3.12$ and $B_2 = 7$, resulting in a decay time $\tau = 320$ ms for the first mode. If only the first mode is

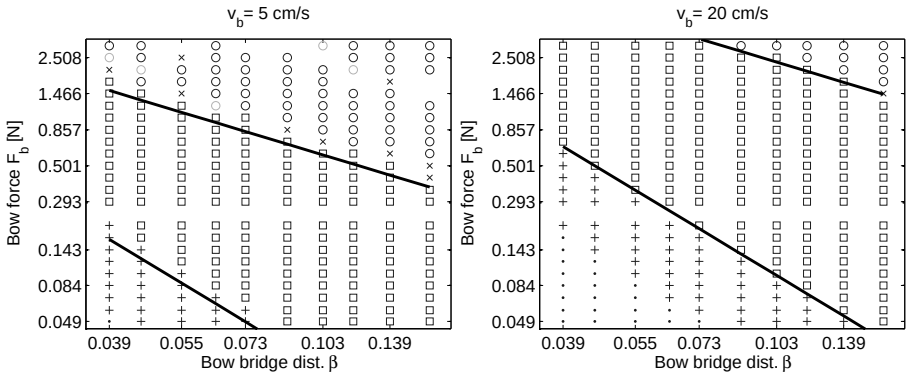

Figure 3.9: Schelleng diagrams obtained with the same string parameters as in Fig. 3.7, except for the damping coefficient of the first mode that is multiplied by two. The changing of this factor introduces a multiple-slip region under the theoretical minimum bow force.

changed by reducing its decay time to half the value ($B_1 = 6.4$), the simulations show a very different behaviour. In the lower part of Fig. 3.9 (under the lower force limit), it can then be seen that multiple slips occur between the Helmholtz region and the steady sliding state region. In that case, the theoretical minimum bow force seems to be in better agreement with the simulations.

In conclusion, the bowed-string model has been used to simulate the string vibration for various sets of steady-state control parameters. Different kinds of string vibrations were obtained. Regular Helmholtz motion was found to constitute homogeneous and continuous regions in the control parameter space. These regions corresponded well with the theoretical definitions given by the minimum and maximum bow force vs. bow-bridge distance for a given bow velocity. This is reassuring concerning the behaviour of the model. In particular, we can expect a conformity between the usable regions for control parameters of the model and realistic bowing parameters used by players.

The control of the bowed string in real violin playing does not only consist in finding the right combination of bowing parameters in order to obtain an acceptable vibration of the string. The playable region offers a wide variety of sound colors which the violinist utilizes according to musical purposes. The next step in the exploration of the model will consequently deal with the description of the main sound properties within the playable region of the control parameter space.

3.4 Influence of gesture parameters on the sustained part of the vibration

In this section, we will describe variations of some qualities of the sound during the steady part of the vibration, i.e. in the Helmholtz region of the Schelleng diagram. Three properties of the sound are of primary interest from the player's point of view, and can be controlled by combining the bowing parameters accordingly

- The sound level: The player must be able to generate different dynamic levels, from a very soft (*pianissimo*) to a powerful loud level (*fortissimo*).
- The tone color, also referred to as brilliance: String players are able to produce a variety of sound colors. For instance, they generally use a rather long bow-bridge distance (*sul tasto*) for obtaining a soft and spectrally poor sound, whereas they slow down the bow, press harder on the string and play closer to the bridge for producing a brilliant and rich sound.
- The pitch: Close to the upper bow force limit, the vibration period will increase ("pitch flattening") due to a hysteresis effect in the bow-string interaction. This is not exactly a means of expression, but the player has to take it into account when playing with high bow forces. The pitch flattening effect provides an interesting point of comparison with other studies and measurements.

The simulations obtained in the previous section for compiling the Schelleng diagrams were analyzed in order to describe them in terms of the three properties of the sound. In the analyses, we will consider the bridge force as the output signal, without taking into account the filtering effect of the violin body and the frequency dependence of the radiation. The sound could have been computed as described in Chapter 2, incorporating pulsed noise and simulation of the radiation by the body of the instrument. However, the force on the bridge will be assumed to give a first good approximation of the resulting sound properties.

Effect on dynamic level

In a first approximation, the level of the sound radiated by the violin is dependent on the amplitude, or peak value, of the force exerted by the string on the bridge. In Helmholtz's and Raman's theories, this force is simply proportional to the amplitude of the string displacement, controlled by the bow velocity and the bow-bridge distance ($F_{bridge} \propto v_b/\beta$), with a negligible effect of the bow force. According to Schelleng [71]: "Bow force is important primarily as the catalytic agent that make possible a correct reaction between bow speed and bow position".

However, Cremer [19] notes that "the peak value does not determine the perceived loudness". He reports the following observation:

> "As already mentioned, the strength of the tone does not correspond to the displacement of the string. A basic example is, for example, to bow a cello string with low bow pressure and relatively high bowing speed: it is easy in this way to achieve a displacement so great that the string nearly hits the adjacent ones. The tone is dull and not very loud. Now, if the bow is moved more slowly and with somewhat more pressure, the tone becomes brighter, and somewhat louder, and so it carries to greater distances. In this case, however, the displacement is considerably smaller than before."

Consequently, the influence of the spectral content of the vibration plays an important rule in the perception of the sound level. Askenfelt [4] reported measurements in which players seem to prefer changing bow force and bow position rather than bow speed for increasing dynamic level. In a paradoxical way, players were found to decrease the velocity for increasing the volume of the sound. As pointed out by Guettler [35], "raising the bow velocity alone would decrease the relative content of high partials, which to some extend would counteract the perception of increased loudness."

This effect can be confirmed by simulating the vibration of the string by only increasing the bow velocity. Whereas the amplitude grows, the result does not produce a real feeling of increased dynamic level. In contrast, when both bow velocity and force are increased, a more realistic crescendo is perceived.

In the following, we will focus on the total energy of the string vibration, including all harmonics, rather than the peak value of the vibration. The energy is computed as

$$L = \sqrt{\frac{1}{N}\sum_{i=1}^{N} \|x_i\|^2} \tag{3.9}$$

where x_i are the samples of the force on the bridge F_{bridge}, and the vibration level in dB is computed with

$$L_{dB} = 20\log_{10}(\sqrt{2}L) \tag{3.10}$$

The resulting plots are shown in Fig. 3.10 for the four bow velocities. Comparing the four figures, it can be observed that higher sound levels are obtained with higher bow velocities. For example, the level difference between $v_b = 5$ cm/s and $v_b = 50$ cm/s is around 15 dB for the same bow-bridge distance and bow force. The bow velocity thus allows a substantial increase in dynamic level. However, the bow force is seen to have a profound effect as well. For a given bow-bridge distance, the level increases with increasing bow force, the difference being around 10 dB between the minimal and maximal bow force.

These results are consistent with the control of the sound level as experienced by players. For a given bow position, the level can be slightly increased by pressing

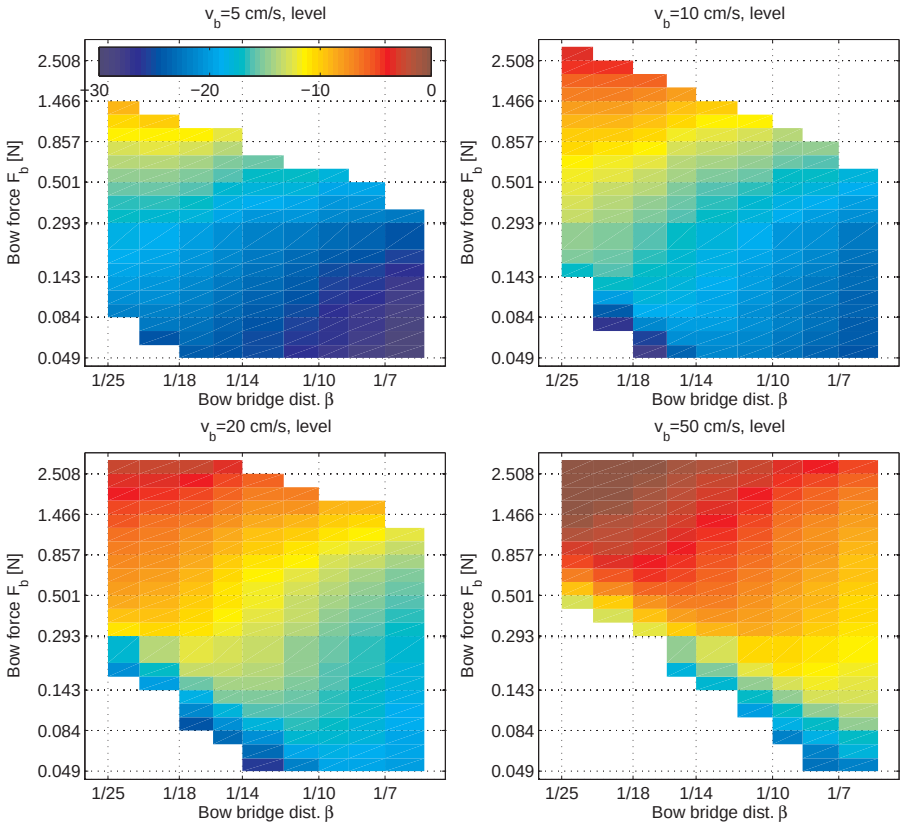

Figure 3.10: Effect of bowing parameters on the dynamic level for four bow velocities (v_b =5, 10, 20, 50 cm/s). Simulations obtained when determining the Schelleng diagrams (Section 3.3) were used for computing the energy of the resulting vibration as a function of bow-bridge distance and bow force. The plots demonstrate the influence of bow force and bow-bridge distance on the energy of the string vibration, and in turn the perceived level of the sound. Level scale runs from zero (red) to -30 dB (blue).

harder on the string, but the effect is more obvious when combined with bowing closer to the bridge. Increasing the bow velocity makes the effect stronger, but on the other hand, it requires a better ability of controlling the bowing gesture. Pressing hard and bowing fast is not so easy to achieve, especially because it makes the control of the bow-bridge distance more difficult. Moreover, bow velocity is usually not a parameter which is free to control. The available length of the bow hair and thus the velocity has always to be determined according to musical and technical constraints such as the duration of the note.

The variations in the simulated levels can be compared with measured dynamic levels of violin sounds. Meyer [57] reports the dynamic range of the violin to be about 40 dB from *pp* to *ff*. Askenfelt found a variation of 37 dB for a G string "between the softest and loudest possible playing" [4]. These results seem to be in line with our simulations. Unfortunately, there are no systematic measurements of violin sound levels versus bowing parameters available. This makes it difficult to assess the realism of the obtained level differences in the simulations. However, we can refer to Askenfelt's measurements, who recorded the vibration of the top plate for determining the level, for an approximate comparison. When violinists were playing long notes at different dynamic levels, he reported variations in the bow force from 0.5 to 2 N and in bow-bridge distance from 40 mm to 20 mm between *piano* and *forte* levels. The bow velocity was kept rather constant (between 20 and 30 cm/s), and the variation of dynamic level was found to be 9 dB. By using these values for interpolating the level in the simulations with a bow velocity of 20 cm/s, the resulting level variation is 10 dB, which is surprisingly close to Askenfelt's measurement. Note that this result would probably have been better if we had considered a bow velocity of 30 cm/s: By interpolating from the level at 50 cm/s, the difference becomes 7.6 dB.

Effect on spectrum

Variations in the tone color were already mentioned by Schelleng [71] (see Fig. 3.5). In his famous diagram, he reported three regions associated with different tone qualities when playing violin: *sul tasto*, *normal* and *brilliant*. These sound qualities were indicated in relation to the bow-bridge distance and bow force, but with no considerations on their respective influence.

Considering the vibration at the bridge as an idealized sawtooth waveform, Schelleng and Cremer deduced a first approximation of the instrument spectrum: the decrease in amplitude of successive harmonics n should be proportional to $1/n$, i.e. a slope of -6 dB per octave. This envelope can be considered as a good first estimation, but as noted by Schelleng: "This statement has to be modified for actual vibrations, which follow the rule for the lower several harmonics but deviate in higher orders according to the bow position and bow force".

Fig. 3.11 illustrates the spectrum obtained in simulations for different bow-bridge distances, and with two bow forces (F_b = 143 and 1025 mN), both at a constant bow velocity (v_b = 20 cm/s). The amplitudes of the first 60 harmonics

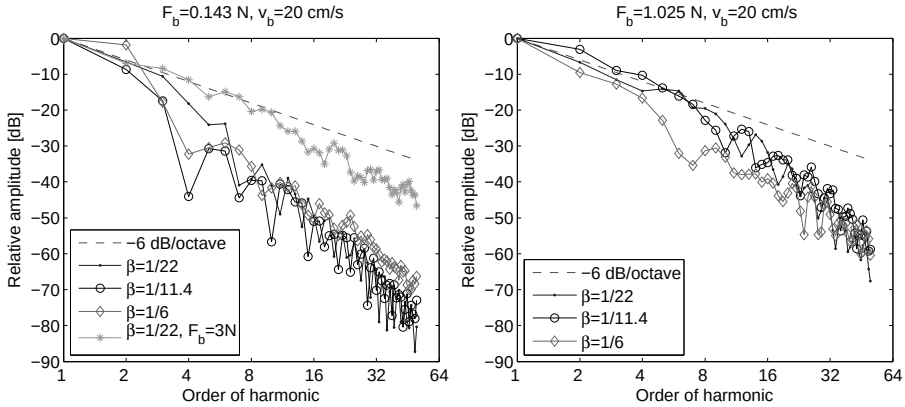

Figure 3.11: Spectrum of the force on the bridge obtained for simulations with a bow velocity of 20 cm/s. Left: Low bow force (F_b = 143 mN) for different bow-bridge distances β. Right: The same cases with a higher bow force (1025 mN). The dashed line corresponds to theoretical spectrum slope of -6 dB/octave inferred by Cremer and Schelleng. In the left figure, a limiting case with a very high bow force (3 N) corresponding to the maximum force in the Schelleng diagram, has been included in order to illustrate the idea that the theoretical spectrum corresponds to a limiting case obtained at the upper force limit.

of the force on the bridge are plotted. It can be seen that the simulated spectra follow the theoretical shape quite well for the first harmonics, up to the 7th for the high bow force, and up to the 3rd for the low force. The highest components in the spectra become weaker with decreasing bow force, meaning that the spectra deviate more and more from the theoretical slope as the force is decreased. As a comparison, a limiting case with a very high bow force (3 N) is included in Fig. 3.11, left, showing that the spectrum follows the predicted slope rather well up to a high harmonic number. In the simulations, the theoretical shape of the spectrum seems to correspond to a limiting case, occurring when the bow force is very close to its maximum value given by Schelleng.

Recently, Guettler [36] proposed some more precise indications of the variation of tone coloring in the Schelleng diagram. He concluded that the tone coloring is dependent on the force relative to limit forces defined by Schelleng more than on absolute force. Moreover, from considerations about the sharpening of the Helmholtz corner under the bow [36] obtained from simulations and measurements [39], he suggested that the amplitude of the highest harmonics does not depend on the bow-bridge distance for a given bow force and bow velocity. This is approximately observed in Fig. 3.11.

The brightness, or sharpness of the tone color, often referred to as “brilliance”, is related to the relative strength of low and high frequencies and can be described

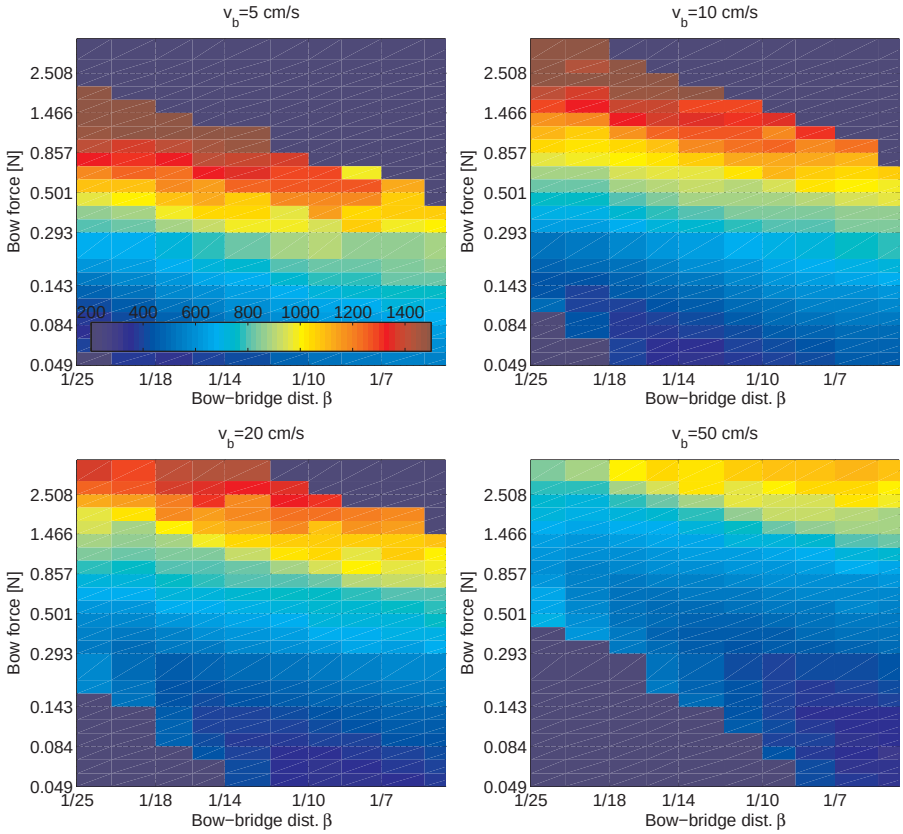

Figure 3.12: Variation of brilliance in the Schelleng diagram. The figures show the spectral centroid of simulations with varying bow-bridge distance and bow force for four bow velocities (v_b=5, 10, 20 and 50 cm/s). The spectral centroid (in Hz) was computed from the force on the bridge. Frequency scale runs from 200 Hz (blue) to 1500 Hz (red).

by the spectral centroid of the bridge force [31, 14]. The amplitude A_n and the frequency f_n of the 50 first harmonics were extracted from the spectrum of the bridge force, and the spectral centroid was computed as

$$SC = \frac{\sum A_n f_n}{\sum A_n} \tag{3.11}$$

The results are shown in Fig. 3.12. The centroids are represented in a color log scale vs. absolute force and bow-bridge distance, for the four bow velocities. It can be seen that for a given bow-bridge distance, the centroid increases with bow force, as expected. For instance, at $\beta = 1/13.8$ and $v_b = 10$ cm/s, the variation

reaches about 700 Hz for a change of 1 N. Moreover, the centroid is found to increase faster as high bow forces are reached. More precisely, the logarithm of the centroid was found to increase linearly with the logarithm of the bow force. For example, with $v_b = 20$ cm/s and $\beta = 1/14$, the centroid varied according to $\log(SC) \propto 0.34 \log(F_b)$.

A bit more surprisingly, the centroid was found to decrease with decreasing bow-bridge distance for a given bow force. This could seem contradictory to Guettler's result [39] and to what is experienced by players. As described before, string players tend to bow closer to the bridge for obtaining a more brilliant sound. However, the players often compensate a bowing position closer to the bridge by pressing harder on the string, which explains the increase in brilliance. The decrease due to changes in bow-bridge distance seems to be related to the lowest string modes (see Fig. 3.11), typically the 10 first modes. The effect is rather weak compared to the effect of bow force.

In a next step, the spectral centroid was plotted in a similar diagram, but replacing the absolute force by the force relative to the minimal and maximal bow force, as suggested by Guettler [36]. This can be achieved by dividing the bow force with a reference force corresponding to the intersection between the theoretical minimal and maximal forces (upper-left point of the Schelleng triangle). This reference value is given by $F_{ref} = 8Rv_b/(\mu_s - \mu_d)$. Diagrams with relative forces are the same for the different bow velocities and can be used to compare the variation of the spectral centroid inside the Helmholtz region, independently of the bow velocity.

Such a comparison is shown in Fig. 3.13. The same data as in Fig. 3.12 are represented in the relative Schelleng diagram ($\beta, F_b/F_{ref} \propto F_b/v_b$) defined above. In this representation, the Helmholtz region (between the two black lines) is the same for the four velocities, and the variations in the spectral centroid are very similar for the four cases. Close to the maximal bow force, the spectral centroid falls between 1200 and 1500 Hz, whereas close to the minimum bow force it decreases to about 200 Hz.

Flattening effect

We conclude this section about the effect of bowing parameters on the string vibrations by illustrating the variations of pitch between the maximum and minimum bow force. The frequency of the bowed string is rather constant in the region defined by these limits, which means that the player can use a large part of the playable region without having to compensate for frequency variations. However, when the bow is pressed strongly on the string, the vibration frequency tends to decrease. This flattening effect appears in a region below the theoretical maximum bow force and imposes a practical maximum force to the player.

The mechanism of this phenomenon has been explained by McIntyre and Woodhouse [54] by providing a solution to Frielander's ambiguity. Frielander pointed out that for some shapes of the friction characteristic the determination of the friction

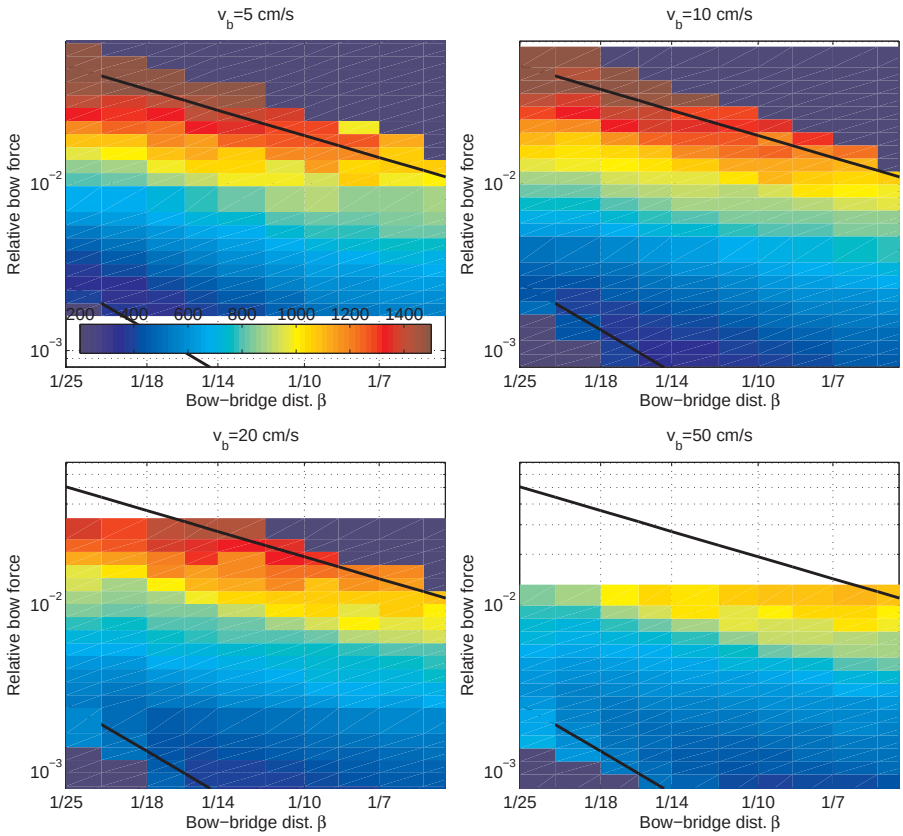

Figure 3.13: The same data as in Fig. 3.12 shown in a Schelleng diagram with relative force scale, defined in the text. The representation of the spectral centroid between the minimum and maximum bow force limits shows the same variations independent of the bow velocity, suggesting that the spectroid varies with relative bow force. Frequency scale runs from 200 Hz (blue) to 1500 Hz (red).

force could give three solutions (one for $\Delta v = 0$, corresponding to the sticking, and two for intersections with the friction curve). In order to solve this ambiguity, McIntyre formulated a hysteresis rule in the evolution of the sliding force. As long as the string is sticking and the maximum static friction is not reached, it continues to stick to the bow, and as long as the string is sliding, it continues to slide, until no solution can be found anymore. As a consequence, the friction force does not follow the same path at the beginning of the slip triggering and at the end. When the force is increasing at the end of the triggering, the path is longer, resulting in a lengthening of the period. The flattening effect has been investigated analytically, and by measurements and simulations by Schumacher [74][75], Faure [23] and Boutillon [13].

In the simulations, the vibration frequency was computed and plotted in the Schelleng diagram. The frequency variations (in cents, relative to the nominal frequency of the free string $f_0 = 196$ Hz) are shown in Fig. 3.14. The variation is indicated in color scale, from -30 cents to +20 cents. In the main part of the diagram the frequency is the same, around 20 cents above the nominal frequency. Note that the frequency of the forced oscillations imposed by the bow differs from the frequency of the free oscillations, as expected. However, the frequency suddenly drops as the bow force gets closer to the maximum bow force and reaches a maximum flattening of around -20 cents (i.e. a variation of 40 cents relative to the forced oscillation for low forces).

The effect sets in rather close to the upper bow force limit, the frequency being approximately constant everywhere else. Note that the logarithmic scale used for the bow force contributes to this impression. The region in which flattening occurs is not as narrow as it seems in Fig. 3.14. In Fig. 3.15, the variations are shown vs. bow force on a linear scale and the decrease in frequency is seen to be more uniform. In Fig. 3.15a, the frequency variation is shown for one bow velocity ($v_b = 20$ cm/s) and several bow-bridge distances. The effect is weaker for small distances, which seems to be in line with recent measurements by Schoonderwaldt. In Fig. 3.15b, the variation is shown at $\beta = 1/11.4$ for the four bow velocities. It can be seen that the greatest flattening is obtained with a small velocity ($v_b = 5$ cm/s), and that the slope of the variations decreases with increasing bow velocity.

In this section, we have explored the behaviour of the model under bowing conditions aiming at establishing and maintaining Helmholtz motion. We also studied properties of the sound that the player consciously controls by choosing the appropriate set of bowing parameters during performance: the sound level and the spectral content of the sound. These simulations were performed in order to verify that the model gave a realistic synthesis, i.e. that the model behaved as expected in the control parameter space.

Both the sound level and the spectral content were found to vary in line with predictions and with the experiences of players. The sound level increased with increasing bow velocity and decreasing bow-bridge distance as predicted, and the effect was substantially emphasized when coordinated with an increase in bow force.

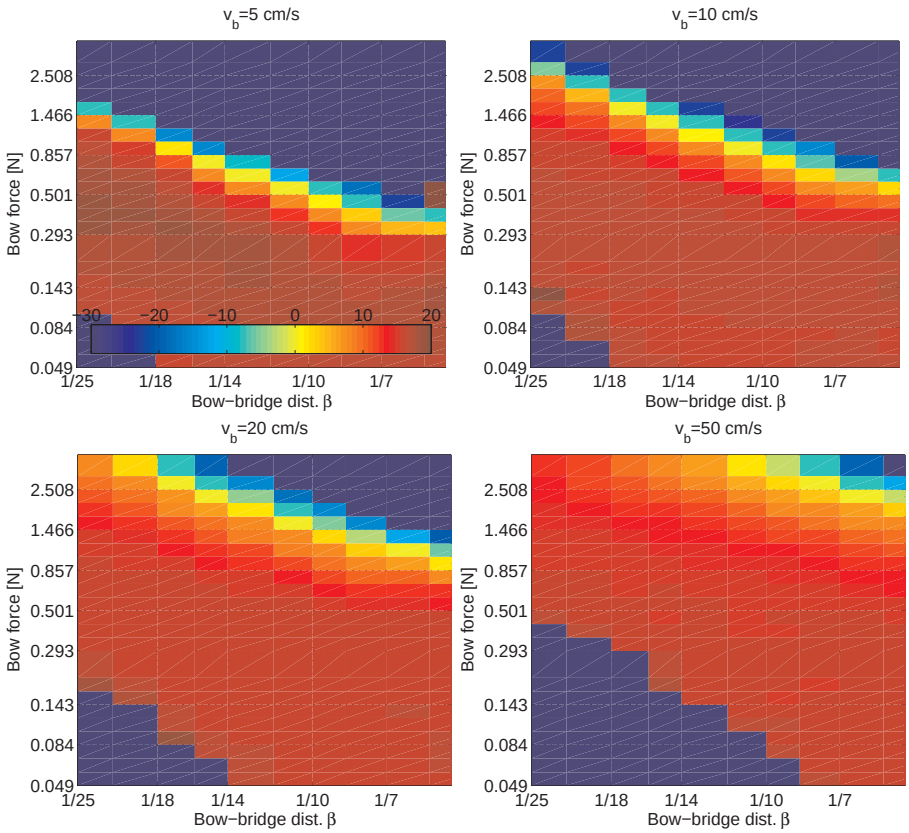

Figure 3.14: Observation of the flattening effect in the Schelleng diagram. The variation of the playing frequency (in cents) in shown in color scale vs. bow-bridge distance and bow force. Pitch scale runs from 20 cents (red) to -30 cents (blue) relative to nominal string frequency (197 Hz).

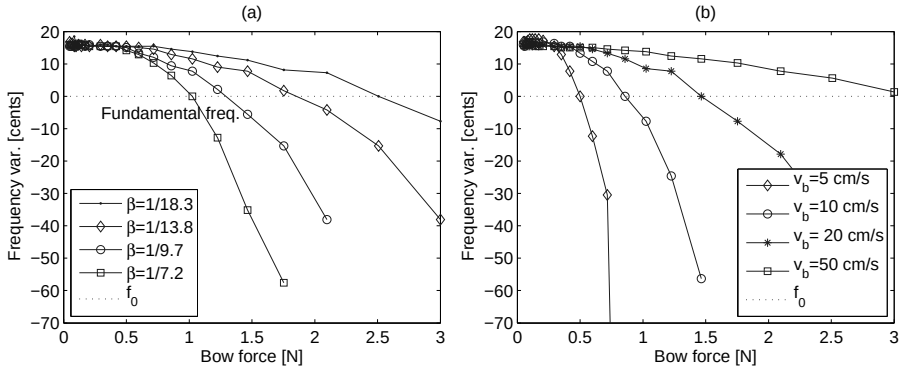

Figure 3.15: Observation of the flattening effect vs. bow force, on linear scale. (a) Frequency variation at a given bow velocity $v_b = 10$ cm/s for different bow-bridge distances. (b) Frequency variation at a given bow-bridge distance ($\beta = 1/11.4$) for various bow velocities.

The spectral centroid increased with bow force. In all, the simulations showed a satisfactory agreement with experimental observations and theoretical expectations.

3.5 Conclusions and applications

This chapter has tackled aspects of string playing that are pertinent from a control point of view: the attack of the sound, the establishing of a stable Helmholtz motion, and the control of the sound properties during the sustained part of the note. Simulations have been performed to examine the behaviour of the bowed-string model in the control parameter space. Optimal regions have been deduced for rapid development of regular slip triggering (with slowly varying bowing parameters), and for maintaining an established periodic motion with constant parameters. The behaviour of the model during attacks and steady-state parts of the tone was found to be in good agreement with predictions by Guettler and Schelleng, verifying a region of fast establishment of Helmholtz motion through close to "perfect" attacks, as well as the famous Schelleng triangle for sustained Helmholtz motion. The examination of the sound level and the spectral content and their dependence on bow-bridge distance, bow velocity and bow force has enabled an accurate description of the sound properties which the player controls during performance and their relation to the bowing parameters. Such an exploration is required for an understanding of the behaviour of the model under a given set of control parameters, and useful for controlling the synthesized sound in a predictable manner.

All simulations were performed on a violin G string defined at the beginning of the chapter. Some variations in the model behaviour can be expected for a string with different mechanical properties. Actually, a systematic exploration of the kind

described in this chapter should be performed for a variety of strings. However, we have seen that the behaviour of the exemplary string followed theoretical expectations quite well. Some important features for the control of the model can be deduced from these observations:

- Guettler's relations give an idea of the region in which good attacks can be obtained. With our simulations some of the conditions were found to be slightly different, especially for short bow-bridge distances. However, the relations A, B and C (Eqs. 3.1, 3.2 and 3.3) provide an useful information about the combination acceleration-force that have to be used at a given bow-bridge distance.

- The playable region for the sustained part of the note is well described by Schelleng's maximum and minimum bow force limits during the steady part of the sound. The simulations were performed with a carefully designed time evolution of the bowing parameters in order to establish a stable Helmholtz motion quickly and maintain it as long as possible when approaching the target value in force. The playable region may be smaller if the preceding attack is not optimal.

- The variation of the spectral centroid was found to increase linearly on logarithmic scale with the bow force between the minimum and maximum bow force. The sound level increased proportionally to the bow speed and inversely to the bow-bridge distance. However, it is important to keep an adequate bow force by not decreasing the level of the relative bow force when increasing the dynamic level.

These rules can be used in order to obtain an initial description of the behaviour of the bowed-string model, independently of the values of the string parameters. The rules give precious information for the control of the model. We will conclude by describing some possible applications of our observations.

The model can be controlled in real time with an adequate interface, as mentioned at the beginning of this chapter. However, some technical skills and knowledge of the model behaviour are necessary to drive it properly. In a first approach, a simple mapping on a realistic parameter space can be considered. For example, the bow force and the bow velocity can be limited to a range from 0 to 2 N and 0 to 1 m/s, respectively. The control may still be problematic for inexperienced users, and it could be simplified by restraining the parameter space to the playable region. For example, based on the actual values of the velocity and bow-bridge distance, the bow force could be mapped between the minimum and maximum bow force. As a consequence, the novice would not need to focus on the technical problem of obtaining a good tone, but could concentrate on the tone color and the sound level.

Other applications can be imagined. For example, the rules above could be interesting when adapting the control parameters to different strings or to other

instruments. Questions like the following could be answered: If a given time evolution of the sound properties is obtained with a certain set of bowing parameters on a violin A string, which transformation is needed to obtain the same effect on a cello C string? Or how should the parameter variations during the attack be changed in order to obtain the same quality for the different bowed string instruments?

Finally, the results obtained provide helpful information in order to make the relation between bowing parameters and sound properties clear. With physical models, the user does not control the perceptually relevant aspects of the sound directly. In real playing, the violinist is implementing musical intentions that are communicated through the variations in sound such as level and brilliance, which in turn are controlled through appropriate combinations of bowing parameters. The choice of the bowing parameters is a matter of practicing and building an intuitive mapping between the bowing gesture and the behaviour of the instrument. The previous analysis gives access to this intuitive correspondence between the features of the bowing gesture and the resulting characteristics of the sound. For example, a given time evolution of the control parameters which defines the profile of the bowing parameters during the bow stroke, could be changed with simple rules in order to obtain similar bow strokes with different levels or brightness.

Chapter 4

Measuring bowing parameters in violin performance

A principal aim of this work was to study the violinist's control of the instrument in normal playing, in order to formulate general rules and describe characteristic features which could be used to obtain realistic control of violin synthesis. For that purpose, the development of dedicated measurement devices for recording the bowing parameters has been a key point of the work.

An inspiration to start this work was the Augmented Violin project developed at IRCAM [25][67]. That device did, however, not register the bow force, and bow velocity was reconstructed from measurements of the acceleration of the bow, using an additional setup [73]. The development of a robust sensor for measuring bow force without interfering with normal playing conditions was thus required. In this chapter, two submitted manuscripts are reproduced, presenting the bow force sensor that was developed during this work (Paper I), and the integration of the force sensor with an optical motion capture system which enabled measurements of complete sets of bowing parameters in violin performance (Paper II). The setup allowed measurement of the three main bowing parameters (bow force, bow velocity and bow-bridge distance), as well as bow tilt and bowing angles relative to the violin (skewness and inclination). In addition, accelerometers placed on the bow provided more detailed information for studying rapid bowing gestures, such as bow changes and strong accents.

First an introduction is given explaining the interest in measuring the real control parameters in playing in the context of realistic violin synthesis ("virtual violin"). Following, an introduction to Paper I will describe the specific problems associated with the development of a bow force sensor for musical performance purposes. The introduction to Paper II describes the context in which the bow force sensor and motion capture method were combined into a complete measurement system for control parameters in violin playing.

4.1 Introduction: On physical modelling and the control

In Chapter 2, a model allowing a simulation of the motion of the bowed string was described in detail. The parameters setting the behaviour of the model can be divided into three classes: model parameters (such as the string length and tension, and friction parameters), computation parameters (computation frequency and number of modes), and control parameters (bow force, bow velocity, and bow-bridge distance). In Chapter 3, simulations of a violin G string were described using realistic string parameters. The behaviour of the model for largely different sets of control parameters was explored in detail and compared with expected results from theory. In particular, we focused on the onset of the string vibrations (attacks, Guettler diagrams), on how an established Helmholtz motion was maintained ("steady-state", Schelleng diagrams). Variations in perceptually important characteristics of the vibrations within the "playable region" (spectral centroid, sound level and variation in pitch) were studied as well.

However, setting the right parameters describing the string and instrument is not sufficient for obtaining a realistic sound synthesis. When the control parameters are kept strictly constant, as was the case in the verification of the Schelleng diagrams (Chapt. 3.3), the simulations sound artificial. In contrast, the simulations of attacks were much more satisfying from a perceptual point of view, despite the simplistic profile for the variation in the bow velocity used. The time evolution of the control parameters is consequently of primary importance and requires adequate descriptions.

Regarding the evolution over time of the control parameters, two kinds of variations with in general different time constants can be identified. Smaller variations on a short time scale are introduced by the human control of the bowing parameters through the motions of the arm, hand and fingers. Consequently, when a player is asked to perform a task with constant bowing parameters, unintended variations on a low level in bow force, bow velocity and bow-bridge distance will always be observed. These variations are perfectly natural ingredients in string playing, reflecting the characteristics of human motor control. Flaws in the playing technique may exaggerate the variations to much higher levels. A constant bow velocity during a full bow stroke will for example require a delicate coordination between the motions of the elements of the arm and hand. A constant bow-bridge distance is dependent on that the bow is drawn exactly in the longitudinal direction of the bow, which is not easily achieved, in particularly not over a long bow stroke. The bow force is difficult to keep perfectly constant because of the resonant properties of the bow, which easily are excited and induce variations in force. Further, the way the bow force is supplied gives rise to an interesting control problem in itself. The player applies a torque at the end of the bow (the frog), which makes the bow force against the string dependent on the distance between the contact point with the string and the frog. Drawing a note with constant bow force therefore requires a continuous adaptation of the torque to the bow position, and the constancy of the bow force is to a large extent judged by the resulting sound quality. It is important

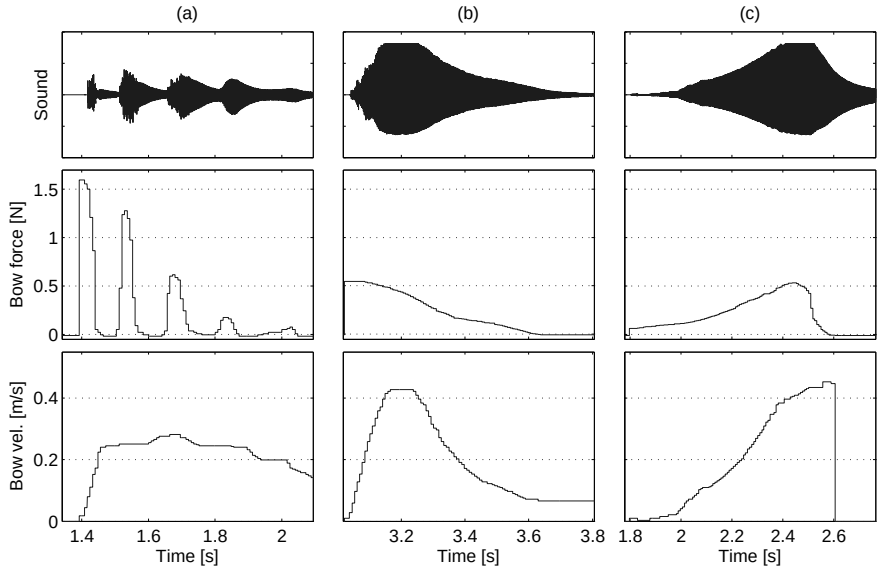

Figure 4.1: Templates for the bowing parameters imitating various bow strokes. Synthesized sound, bow force and bow velocity (top to bottom). The bow-bridge distance was constant ($\beta = 0.093$). (a) Bow thrown on the string (*gettato*) imitated by successive peaks in bow force. (b) *Martelé*. (c) *Crescendo.*

to stress that the human limitations in the control of the bowing parameters are not "errors" or unwanted contributions. They represent natural variations of the bowing parameters, which in turn contribute significantly to the perceptual quality of "naturalness" of the sound.

Keeping the control parameters perfectly constant has little musical significance as such. In contrast, keeping perceptual quantities like loudness, tone quality and pitch approximately constant can often be motivated by musical purposes, but may require continuous changes in the bowing parameters as the contact point moves from frog to tip during a stroke. On a longer time scale, an evolution of the control parameters is therefore demanded by musical purposes. Basic examples are changes in dynamic level and sound color over a phrase, or the performance of various accented or bouncing bow strokes such as *martelé, staccato* or *spiccato.*

Templates for the evolution of the control parameters can be obtained by simply watching violin player's behaviour, in order to imitate various bow strokes like in Fig. 4.1. In Fig. 4.1a, the bow force is composed of successive peaks with decreasing amplitude while the bow velocity is slowly decreasing after the attack, imitating several rebounds as if the bow was thrown on the string (*gettato*). In Fig. 4.1b, the bow force decreases continuously during the stroke, while the bow velocity exhibits a peak followed by a decay to a small constant value. This produces a kind of

martelé with a rather short and strong attack followed by a slow decay in sound level. In contrast, Fig. 4.1c shows a *crescendo* cartooned by increasing the bow force and velocity strongly during the stroke.

Control of a bowed-string model based on generalized templates obtained by imitations, such as those illustrated in Fig. 4.1 has several limitations. Even an experienced violin player may not have the necessary ability to quantify the bowing gestures in terms of relevant control parameters. Direct measurements of the effective control of the bowing parameters during actual performance provide a much more promising direction for the control of a virtual violin. Based on the performer's experience of violin playing, and provided that the virtual violin (physical model) and the real instrument behave quite similarly, it is possible to obtain a great variety of exemplary evolutions for the control parameters and deduce typical rules for the control strategies in playing.

4.2 Introduction to Paper I: The bow force sensor - from the laboratory to the stage

Paper I:

M. Demoucron & R. Caussé: *Measuring bow force in bowed string performance: Theory and implementation of a bow force sensor*

Submitted for publication in Acta Acustica, September 2008.

A basic part of this work concerned the development of a robust bow force sensor that could be attached to any bow with minimal modifications. Based on the principle described by Askenfelt [3, 4], sensors were placed on the bow for measurement of the transverse forces at the terminations of the bow hair. The core element of the sensor was a thin leaf spring of steel. The displacement of the spring under loading of the deflected bow hair was measured by strain gauges.

A complete description of the sensor, its principle, design and calibration are detailed in Paper I. The sensor has been used in the experiments reported in Chapt. 5 and 6 for measuring complete sets of bowing parameters in violin performances.

Some composers and musicians were interested in using the bow force sensor in a musical context. The bow force signal can for example be used for controlling digital processing of the violin sound, or for obtaining information about the performance of the musician. Some design problems arise from the use of the device in live musical performance. Whereas the comfort of the musician can be disregarded to a certain extent in scientific experiments, it becomes of primary importance when the player has to perform on stage and interpret a demanding score during a rather long time. The following section provides some details concerning the development of a bow force sensor suitable for musical purposes.

The device developed at the very beginning of this work is shown in Fig. 4.2. Two sensors were used, one at each termination of the bow hair. The sensor at the frog was clamped to the flat side of the ferrule, under the bow hair (Fig. 4.2b).

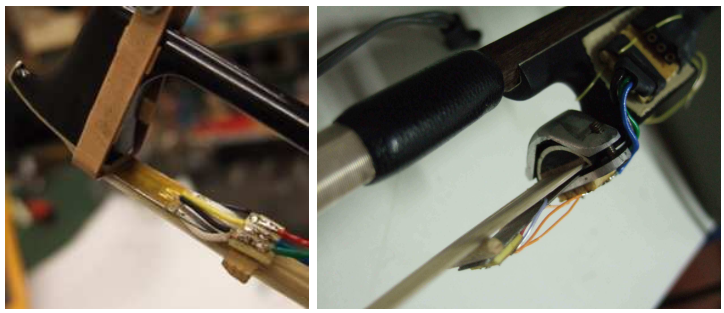

(a) (b)

Figure 4.2: An early version of the device for measuring bow force using two sensors. The two signals representing the transverse forces at the tip and at the frog due to the deflection of the bow hair are used for computing the bow force and bow position. (a) Sensor at the tip. The sensor is clamped between the bow hair and the ivory plate at the tip. A thin metal fixation around the head prevents the sensor from moving. (b) Sensor at the frog. The V shaped design of the ring permitted to clamp the sensor to any bow.

The sensor at the tip was clamped between the bow hair and the ivory plate at the tip (Fig. 4.2a). The sensors provided two complementary signals that were used for measuring bow force and bow position. This version of the device was used in some preliminary experiments with standard types of bow strokes such as *détaché*, *spiccato* and *martelé* [21]. However, the sensor at the tip and the wires along the bow stick added a considerable weight to the bow, which was not desirable under real performance conditions.

In order to reduce the discomfort for the player, a device using only one sensor at the frog was developed. Two versions of the system are shown in Fig. 4.3. The player holds the bow just above the sensor and the added weight is therefore almost negligible compared to the weight of the frog. However, as the sensor signal depends on both bow force and bow position, an additional device measuring the bow position is necessary in order to obtain accurate measurements. A solution consisting in combining the sensor with a motion capture system will be presented in Sect. 4.3. Here we will only describe some design considerations for making the force sensor usable in musical performances.

The sensor shown in Fig. 4.3a is obviously more suitable than the two-sensor device described above (Fig. 4.2). The additional weight is concentrated at the frog, the weight of the clamping ring has been reduced, and the size of the electronic board is minimized. However, also this version included some parts under the frog which reduced the accessible length of the bow hair, and also could be a hindrance in vigorous playing close to the frog.

The last version of the sensor (shown in Fig. 4.3b) was modified in order to

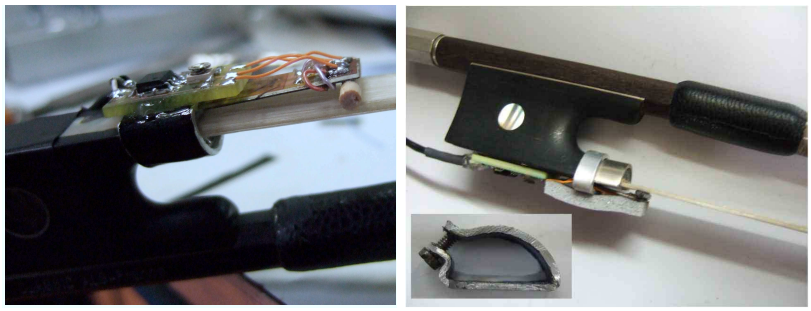

(a) (b)

Figure 4.3: Two versions of the device with only one sensor attached to the frog. (a) Sensor used for measuring the bow force in laboratory conditions. The ring clamping the sensor covers the width of the ferrule. (b) Sensor developed for musical performance. The width of the ring is reduced in order to move the sensor farther away from the hair termination.

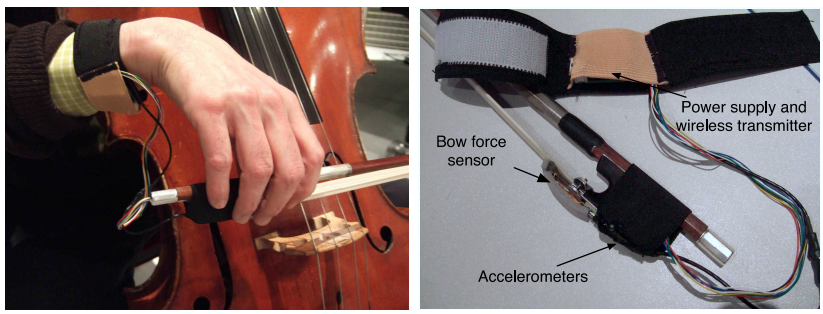

(a) (b)

Figure 4.4: Acquisition system used for the creation of *StreicherKreis* for string quartet by composer Florence Baschet. The sensor is connected to an electronic board containing three accelerometers and three gyroscopes. A small battery attached to the forearm provides power supply, and data are sent via a wireless transmission. (a) Device mounted on the player. (b) Overview of the device, showing the bow force sensor (old version), accelerometers and the wristband containing the battery.

make the performance safer for both the instrument and the sensor. In order to reduce the thickness of the sensor, the electronic board was placed behind the ring (and not under the ring, as in Fig. 4.3a), and only one strain gauge was glued to the strip. The length of the strip under the bow hair was minimized by moving the ring farther from the ferrule. This was achieved by reducing the width of the ring and clamping the strip partially on the gauge. In the last version, less than 3 mm of the bow hair was not usable. A protective material was glued over the entire length of the sensor for minimizing the damages in case of accidental contact between the sensor and the violin.

A complete set of these sensors has been developed on the occasion of composer Florence Baschet's creation *StreicherKreis* for augmented string quartet. The sensors were connected to an electronic board containing three accelerometers and three gyroscopes. The complete set of signals was sent to a computer via wireless transmission. Power supply was provided by a small battery attached to the forearm of the players. The complete setup is shown in Fig. 4.4.

4.3 Introduction to Paper II

Paper II:

E. Schoonderwaldt & M. Demoucron: *Extraction of bowing parameters from violin performance combining motion capture and sensors.*

Submitted for publication in J. of Acoustical Society of America, July 2008.

The bow force is one of the three main bowing parameters together with bow velocity and bow-bridge distance. In order to obtain a complete description of a player's bowing, it is therefore necessary to have access to equipment which provides data on the momentary position of the bow relative to the strings. With such a device, the bow force can also be measured with only one sensor at the frog as described above, and bow position data are used for correcting the force sensor signal.

During this work, experiments using an optical motion capture system at Input Devices and Music Interaction Laboratory (IDMIL), McGill University, Montreal were performed. A complete setup including a thorough calibration and correction of the force sensor signals was developed together with Erwin Schoonderwaldt during a short stay in June 2007. Pilot experiments were performed during this visit and numerous measurements were done by Schoonderwaldt during the autumn.

Paper II is the result of this collaboration. It describes the measurement setup used during the sessions, consisting of the optical device (Vicon system), accelerometers on the bow, and one bow force sensor. In particular, the paper details the computation of the bowing parameters from motion capture data, and the calibration of the bow force sensor using optical-based measurements. In the paper, the sections related to the calculation of bowing parameters based on motion capture data are due to E. Schoonderwaldt. My own contribution concerns the measure-

ment of bow force including the comparison between the sensor-based and the optical-based method for force measurement (Sect. IV, Appendix B and C).

Most of the measurements presented in the following come from the pilot experiment. During this session, more than 60 acquisitions lasting about one minute were performed by a professional violinist. The acquisitions were divided into six categories:

- Simple *détaché* with various durations (from whole notes to 1/32 notes), with the whole bow and at different bow positions for the fast *détaché*.
- Sustained long notes at different dynamic levels (from *pp* to *ff*) and *crescendo-diminuendo.*
- Sixteenth notes at different dynamic levels and various bowing patterns ("normal", accented, *staccato*, *portato*, controlled and natural *sautillé*)
- Transitions between notes and attacks. *Martelé.*
- Continuous and stepwise *accelerando. Tremolo*
- Musical examples

Not all categories were used for the analyses included in this thesis.

Paper I

Measuring bow force in bowed string performance: Theory and implementation of a bow force sensor

Abstract

A sensor has been developed which allows measurement of the force exerted by the bow on the string (bow force) during violin performance. The bow force is deduced from measurement of the transversal force at the termination of the bow hair at the frog. The principle is illustrated with an experiment that demonstrates how the bending of the stick and variations in bow hair tension influence the measurements. The design of the sensor is described and performance characteristics are discussed. A thorough calibration procedure is described and tested. Finally, the use of the sensor is demonstrated through measurements in real playing situations.

I. Introduction

Bow force is one of the three main control parameters in bowed string playing, the two others being bow velocity and bow-bridge distance. In particular, a rapid establishment of Helmholtz motion during the attack is dependent on the coordination of bow force with acceleration and bow bridge distance [6][11]. Also, for the control of timbre, bow force is the main parameter, bow-bridge distance playing a secondary role [7].

The interest for measuring control parameters in playing is encouraged by the advancements in the study of musical instruments by physical modeling. One advantage of this approach is that the control parameters of the model become the same as for the real instrument. On the other hand, measuring the control parameters in normal playing without interfering with normal playing conditions presents a challenge, in particular for wind instruments. The bowed stringed instruments are seemingly straightforward to approach as the string and bow are of reasonable size and the motions associated with bowing are accessible for measurement. Application of motion capture techniques is an obvious approach for measuring bow velocity and bow-bridge distance in playing, while bow force measurements will require application of sensors to the bow or the violin.

The first reliable measurement of control parameters in violin playing during real performance were made by Askenfelt [1], [2]. A bow was modified to measure bow position, bow velocity, bow-bridge distance and bow force. Bow position refers to the position of the contact point between bow hair and string relative to the frog or tip. The bow position was measured by a resistance wire running among the hairs in the outer layer of the bundle of bow hair contacting the string. The string divided the wire in two parts which were used in a branch of a Wheatstone bridge. Bow-bridge distance was measured in a similar manner, using the parts of the string on each side of the bow (wire) in a second Wheatstone bridge. Bow velocity was obtained from the bow position signal through differentiation. Bow force was measured by gluing the bow hair to two metal strips at the frog and at the tip, respectively, and measuring the deflection of the strips by strain gauges.

Later, Young used the bending of the bow stick to estimate the force on the string in playing. Two pairs of strain gauges were glued to the stick in order to measure the bow force (normal to the string) as well

as the lateral force component (in the string direction) [13]. Recently, the present author [4] proposed an improvement of Askenfelt's work by designing detachable sensors which could be attached to any bow, and treating the sensor signals from the frog and tip independently. Later implementations of this idea for real-time measurements have been presented by Guaus et al [5]. The following presentation gives a description of the basic idea, theory, design, and calibration of a detachable bow force sensor.

II. Introductory experiment and theoretical considerations

The basic idea of the force sensor was to determine bow force indirectly by measuring the resulting transversal forces at the bow hair terminations. In this section, the principle is illustrated and the influence of the mechanical behaviour of the bow is analysed. A simple model based on measurements is used to quantify the contributions from the bending of the bow stick and changes in bow hair tension to the observed behaviour.

A. General description of the bow

The bow consists of a bow hair ribbon fastened to the head of the bow stick at one end and to the frog at the other end (see Fig. 1a). As the bow hair is brought up to tension by turning the frog screw, the hair pulls the head back, and the initial camber of the stick is reduced. Keeping the frog fixed horizontally, the tip is lowered until an initial displacement h_t^0 has been reached, at which the restoring force resulting from the straightening of the stick counteracts the static hair tension (see Fig. 1b). The displacement of the tip is measured relative to a horizontal reference line extending from the underside of the frog, as if the frog was resting on a table (see Fig. 1).[1]

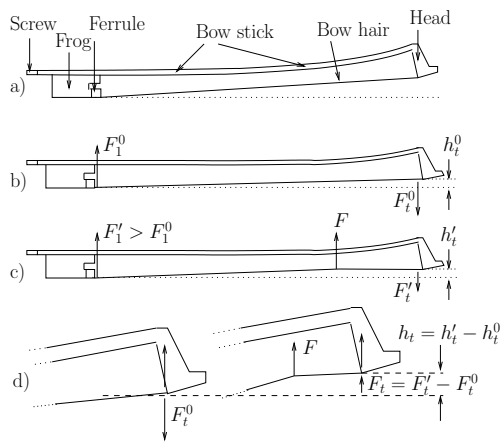

Fig. 1: Description of the bow geometry and definition of forces and displacements: (a) Bow hair not tightened, (b) bow hair tightened, (c) bow force F applied at the bow hair. F_1' represents the transversal force acting at the frog, and $-F_t'$, the transversal force acting at the tip. The reaction of the bow-stick resulting from the straightening is indicated by F_t'.

[1]Superscript 0 will be used to denote the condition with the bow hair at playing tension and no bow force applied, and prime symbols to indicate playing condition with bow force applied.

When the bow is pressed against the string, the bow hair is deflected at the contact point, resulting in a bow force F normal to the string. Associated transversal reaction forces act at the frog F_1, and at the tip F_t, respectively (see Fig. 1c). At the frog, the change in force is visible through the change in bow hair angle relative to the reference line, and at the opposite end through changes in the displacement of the tip h'_t (see Fig. 1d). The deflection of the bow hair due to the applied bow force relaxes the transversal force on the tip ($F'_t < F^0_t$), because the slope of the bow hair at the tip will be directed more upwards. As a result, the bow stick regains some of the initial camber. Simultaneously, the bow hair tension will tend to increase.

In the following, T_0 will be used to indicate the initial tension set by the player, and T the effective tension that may vary when applying the bow force. Normalized bow position is denoted by γ, indicating the ratio of the distance x_b between the frog and the contact point with the string (bow position), and the length of the bow hair L_b ($0 < \gamma < 1$). All variables will be expressed relative to the configuration in which the bow hair is tightened and no bow force applied

$$F_1 = F'_1 - F^0_1 \quad , \quad F_t = F'_t - F^0_t \quad , \quad h_t = h'_t - h^0_t \tag{1}$$

B. Experiment

A test bench was designed for the initial experiments. With the bow hair tightened, the bow was rigidly clamped upside-down at the frog, with the tip being free to move. A force transducer (HBM model U1A, compliance 0.028 mm/N, frequency range 0 - ca 200 Hz) was used to measure the transversal force component F_1 of the hair close to the frog. This was done by letting the bow hair run on top of a small wheel, mounted on the facing of the transducer (see Fig. 2). At the free end of the bow, a digital caliper was used to measure the tip displacement h_t. From repeated measurements the accuracy was estimated to ± 0.2 mm.

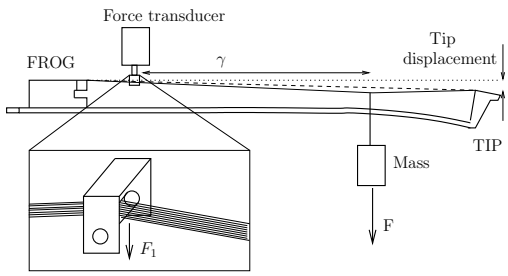

Fig. 2: View of the experiment for determining transversal forces at the bow hair terminations. The bow is clamped upside-down at the frog. Bow forces were simulated by hanging masses on the bow hair. The resulting transversal forces are measured by a force transducer close to the frog and by the displacement of the tip.

Loads, simulating different bow forces F, were applied by hanging weights with known mass at six positions distributed across the entire length of the bow hair. Three masses were used, 54, 100 and 154 g (approximately 0.5, 1, and 1.5 N). The values were chosen to cover the typical bow force range in normal playing, from 0.5 to 1.5 N [1]. Each measurement series was repeated three times.

C. Results

1) Force at the tip: Tip displacements for the three loads are shown in Fig. 3a. Each load case includes three curves corresponding to the repeated measurements. For a given load the tip displacement increases with bow position γ, and for a given position, with increasing load.

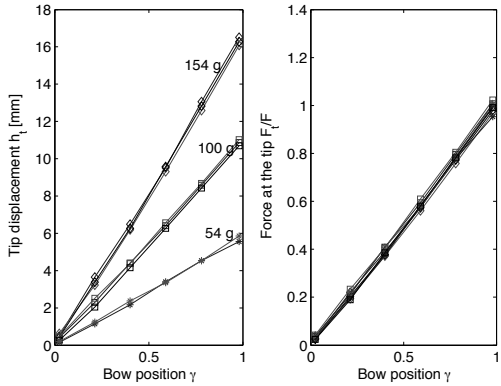

Fig. 3: (a) Measured tip displacement vs. normalized position for a load on the bow hair (54, 100 and 154 g), equivalent to applying bow forces of 0.5, 1, and 1.5 N at different bow positions γ. Each series was repeated three times. (b) Calculated transversal force at the tip F_t normalized by bow force F from equation 2 using $K_b = 91$ N/m.

The displacements are due to the transversal force acting at the tip when the bow hair is loaded. The data in the figure indicate that the assembled, tightened, bow can be well described by a transverse stiffness K_b. The force acting on the tip can then be calculated from the tip displacement

$$F_t = K_b h_t \tag{2}$$

An estimation of the transverse stiffness K_b was obtained by taking the average of the three tip displacements at the tip ($\gamma = 1$), giving a value of 91 N/m. The resulting force at the tip F_t for relative bow positions was computed using this value and equation 2 (see Fig. 3b). The force values have been normalized relative to the bow force F. As seen, the normalized force at the tip can be well approximated by a linear increase from 0 to 1 as function of γ

$$F_t = \gamma F \tag{3}$$

2) Force at the frog: The force measurements from the transducer at the frog vs. normalized load position are shown in Fig. 4. The data points of the three repeated measurements merge, indicating a high reproducibility in the experiment.

The force at the frog F_1 is seen to increase with increasing load position (moving away from the frog), which may seem surprising. Intuitively the expected behaviour would be that the force gets lower as the tip is approached, due to the decreasing angle of the bow hair at the frog. With the mass placed at the transducer ($\gamma = 0$), the measured force would correspond to the applied weight, and as the loading point moves closer to the tip, the force at the frog would approach zero. The simplified case in which the bow

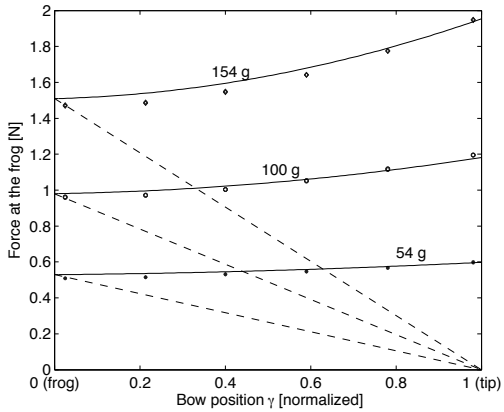

Fig. 4: Transversal force at the frog F_1 vs. position of a load on the bow hair (54, 100 and 154 g), equivalent to applying bow forces of 0.5, 1, and 1.5 N at different bow positions γ. The forces measured by the transducer close to the frog are indicated by data points. The dashed lines represent a simplified bow model with a completely rigid stick. The full lines correspond to a realistic model (equation 11), accounting for tip displacement and variations in bow hair tension. Data were fitted with $T_0 = 50.2$ N and $\alpha_T = 8.1$ N/N.

stick is completely rigid gives

$$F_1 = (1 - \gamma)F \tag{4}$$

The results obtained with such a rigid model are included in Fig. 4 (straight dashed lines). The measurements are far from following this simple behaviour. In fact the measured force at the frog increases substantially when the load is moved farther away, and surprisingly the force at the frog is greater with the load at the tip than at the frog. In the following section two factors that explain this behaviour, tip displacement and bow hair tension, are analyzed.

D. Analysis

In the following analysis, a simple model is used to represent the bow. The assembled bow when tightened is supposed to act as a spring in the transverse direction, with stiffness K_b at the tip. The bow hair ribbon is represented by a single string with tension T and length L_b. The displacement of the hair at the bow position is denoted by $h(\gamma)$. The transversal force at the frog can then be written as

$$F_1 = T\frac{h(\gamma)}{\gamma L_b} \tag{5}$$

1) Tip displacement: A study including the bending of the stick has been presented by Pitteroff [8], aiming at a description of the transverse stiffness along the bow hair. He considered that the force acting at the tip was γF, which is in line with our measurements (see Fig. 3).

Using this assumption, Pitteroff found the displacement of the hair at the bowing point γ to be composed of two terms, the first one representing the deflection of bow hair under loading when the bow tip does not move, and the second one taking the global displacement of bow hair due to the tip displacement h_t

(equation 2) into account

$$h(\gamma) = \frac{\gamma(1-\gamma)L_b}{T}F + \frac{\gamma^2}{K_b}F \tag{6}$$

The force acting at the frog is obtained from equations 6 and 5

$$F_1 = \left[1 - \gamma(1 - \frac{T}{K_b L_b})\right] F \tag{7}$$

The effect of stick bending reduces the slope of the dashed line in Fig. 4 representing the transversal force at the frog, and the force does not reach zero at the tip, as was the case with the rigid model. The reason is that when the contact point is moved towards the tip, the decrease in angle of the bow hair at the frog is more than compensated by the bending of the bow, which lowers the position of the hair termination at the tip.

The stick bending can dominate the displacement of the bow hair at the contact point and give an increasing force at the frog when approaching the tip. From equation 7, this will be the case if the tension is greater than $K_b L_b$

$$T \geq K_b L_b \Rightarrow \frac{\partial F_1}{\partial \gamma} \geq 0 \tag{8}$$

In our case with $K_b = 91$ N/m and $L_b = 0.53$ m this will occur when the bow hair tension exceeds 48 N. For comparison, Askenfelt [3] and Pitteroff [8] reported typical tensions to be around 60 N, with an estimated practical lower limit of 45 N which was considered "very loose" but still playable. The conditions for a considerable influence of the bending of the stick are thus at hand with the bow hair taught to normal playing conditions.

The theoretical behaviour of the transversal force at the frog partly matches the observed data in Fig. 4, explaining the observed increase in force with increasing γ. The model does not, however, succeed in explaining the non-linear variation with γ. It is therefore necessary to examine the influence of the hair tension T in equation 7, and how it can contribute to a complete explanation of the observed data.

2) Variation in bow hair tension: Accurate measurement of bow hair tension for the assembled bow is not straight-forward to perform without instrumenting the bow. In studies of the bow, the tension is generally described as "low", "normal" or "high". Askenfelt [3] reported a simple estimation of acceptable bow hair tensions using a dynamometer. The player was first asked to tighten the bow with the screw, the position of the frog on the bow stick was then measured, and, the screw being removed, the frog was then pulled to the same position with a dynamometer allowing an estimation of the hair tension. More accurate estimations can be made by clamping the bow rigidly at the frog and tip and measure the (small) deflection of the bow hair when loaded at the middle by a suitable weight. By making the measuring point electrically conductive by a small piece of cupper tape to indicate in-contact condition, an accuracy of 0.05 mm can be reached in the measurements using a dial gauge.

In this study, we took advantage of the unused part of the bow hair between the frog and the force transducer. A second force transducer (transducer 2) was placed in the middle of the unused part, pressing slightly on the bow hair (see Fig. 5). Provided that the facing of transducer 1 is rigid, the signal from

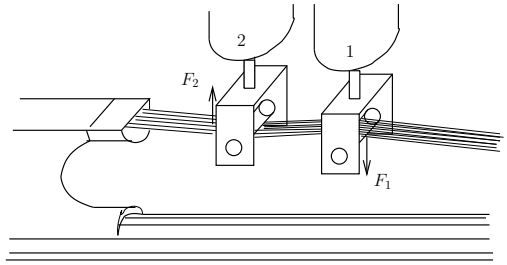

Fig. 5: Two force transducers were used to measure the variation in bow hair tension during loading of the bow hair. Provided that the facing of transducer 1 is rigid, transducer 2 is sensitive to tension variations only.

transducer 2 is sensitive only to variations δT in the static bow hair tension T_0

$$F_2 \propto T_0 + \delta T \tag{9}$$

In the experiment, the support at transducer 1 approximated a rigid termination well with a nominal displacement of the facing of 0.028 mm/N.

The setup was used to quantify variations in bow hair tension when loading the bow. It was not possible to make an absolute calibration of the force variations with the assembled bow, but the ratio between the variations and the static signal with no loading applied gave the relative tension variation. The results are plotted versus bow position for the three loads (see Fig. 6, left).

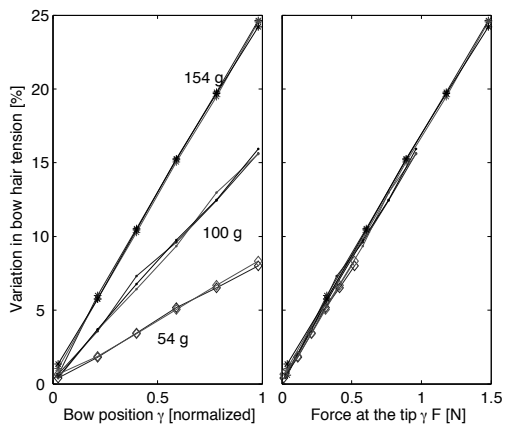

Fig. 6: Left: Variation in bow hair tension vs. normalized position γ of a load on the bow hair (54, 100 and 154 g). Right: The same variations in bow hair tension vs the calculated transversal force at the tip $F_t = \gamma F$.

The curves corresponding to the different loads are seen to be well separated and almost linear. The variations in bow hair tension during playing are often assumed to be rather small, but in the present case they reached 25% of the initial tension for the highest load (154 g) at the tip.

In the following, it is assumed that the variations in hair tension are mainly related to the tip displacement, neglecting the elongation of the hair under loading. An experiment, in which the stick was prevented from moving at the tip, was made in order to confirm this assumption. The tension variation was then less than 1% with 1 N load at the middle of the hair, but increased to around 10% when the bow stick was released at the tip and free to bend. As a good approximation, the tension variation due to the deflection of the bow hair under loading can be considered not significant compared to the variation due to tip displacement. Tension variation can then be expressed as a function of the transversal force at the tip $F_t = \gamma F$. As seen in Fig. 6 (right), the variation in tension can be approximated by a linear relation

$$T = T_0 + \alpha_T \gamma F \tag{10}$$

where α_T is a coefficient quantifying the combined effect of bow force and bow position.

With the use of Eq. 10, equation 7 becomes

$$F_1 = \gamma^2 \frac{\alpha_T}{K_b L_b} F^2 + (1 - \gamma + \gamma \frac{T_0}{K_b L_b}) F \tag{11}$$

The ratio between α_t and T_0 was found to be 0.16% (Fig. 6, right). Using this value in equation 11 together with $K_b = 91$ N/m and $L_b = 0.53$ m, the measured force at the frog in Fig. 4 can be well fitted with $T_0 = 50$ N and $\alpha_T = 8$ N/N (see Fig. 4 full lines)

Equation 11 gives an analytical relation between the transversal force at the frog and the bow force. This result will be used later to justify the way the force sensor will be calibrated and to interpret some of the observed results.

III. Design of a bow force sensor

A sensor for measuring the bow force in normal playing was designed, based on the principle described above by estimating the transversal force at the hair termination at the frog. The sensor was attached to the frog where the added weight gave minimum influence on the playing properties of the bow. The sensor was designed as a detachable unit, which could easily be moved to any bow without damaging the frog or hair.

A. Description

The force sensor consisted of a thin leaf spring of steel to which two strain gauges were glued (see Fig. 7). The steel strip was fixed to the flat side of the ferrrule by a clamping ring. The free end of the strip made contact with the bow hair through a light cylindrical bearing piece of wood. The bending of the strip generated a signal which after correction gave an accurate estimation of bow force. The strip was mounted on the lower side of the hair (the side facing the string), and a static down-ward bending was established as the hair was brought up to tension. When the bow was loaded in playing, the bending was reduced.

The strain gauges were glued to the upper and lower side of the strip and connected in one branch of a Wheatstone bridge (Vishay CEA series, 7 x 14 mm, 1000 ohm, gauge factor 2.1). Using this configuration, the output voltage will be linearly related to the resistance variations, and temperature changes will be

Fig. 7: Bow force sensor. A thin steel strip is clamped to the flat side of the ferrule. The strip bends as the deflected bow hair presses at the free end via a wooden bearing piece. The bending is measured by two strain gauges glued to the strip. A Wheatstone bridge and conditioning amplifier is integrated in the sensor.

compensated for. The resulting voltage variations were amplified using an operational instrumentation amplifier (gain 1000) integrated with the sensor. The electronics were connected to a battery and data aquisition board via a thin cable. The sensor was light, total mass 3.8 g including electronics and the clamping ring, which should be compared with the mass of the frog(17 g including screw). The mass of the steel strip (0.6 g) and wooden bearing piece (0.02 g, diameter 2.5 mm) was low compared to the bundle of bow hair (about 5 g).

The strain ϵ and the deflection of the free end δy of the steel strip when loaded by a transversal force F_L at the free end is given by the equations for a bar with rectangular cross section clamped at one end

$$\epsilon = \frac{6F_L b}{Ywt^2} = 201F_L \ [\mu\text{m/m}] \qquad \delta y = \frac{4F_L L^3}{Ywt^3} = 0.14F_L \ [\text{mm}] \tag{12}$$

where $w = 8.5$mm, $L = 20$ mm, and $t = 0.5$ mm are the width, length and thickness of the strip, $b = 15$ mm is the distance from the free end to the position where the strain is measured (center of the strain gauge,$b \leq L$), and $Y = 210$ GPa is Young's modulus. The width of the strip is limited by the width of the bow hair, while *L, b* and *t* are used to obtain a suitable sensitivity. For practical reasons in playing, *L* should not be longer than about 3 cm. The diameter of the bearing piece (2.5 mm) was set by sensitivity considerations (see Sect. 3.2.3).

The deflection of the steel strip in playing is small. For a typical bow force of 1 N at the middle of the bow, the transversal force on the strip F_L can be estimated from Fig. 4 to be of about the same value, which deflects the free end around 0.1-0.2 mm. Even for very heavy loading with a bow force of about 1.5 N at the tip of the bow, the strip deflection will only be around 0.3 mm. (Actually, the sensor operates in a reversed mode as mentioned, the deflection decreasing for increasing load.)

In order to check and calibrate the sensor, the bow was held as normal and pressed against a string-like facing (T shaped piece, diameter 1 mm) on a calibrated load cell. A comparison of the signals is shown

in Fig. 8. The responses are very similar with the exception of the smallest details, which have been smoothed slightly in the sensor signal.

An upper frequency limit for the dynamic response of the sensor was estimated from the resonance frequency, which was found experimentally to be around 400 Hz.This was considered fully acceptable for the purpose of studying dynamical features of bow force related to the player's control of the bow.Vigorous spiccato playing on a completely rigid force transducer (BK8001, compliance $4 \cdot 10^{-6}$ mm/N) showed that the force signal did not include any significant components above 150-200 Hz (-40 dB). In real violin playing the compliant string will lower this frequency further.

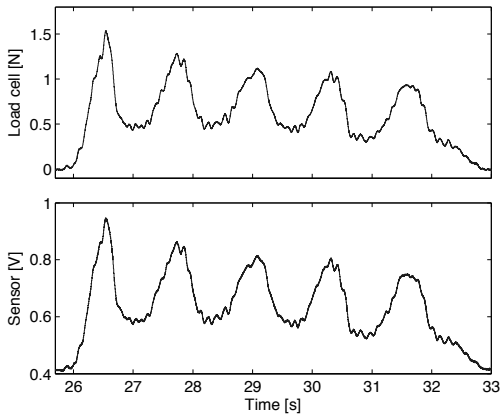

Fig. 8: Illustration of the performance of the bow force sensor. The bow is repeatedly pressed against a calibrated load cell (top). The signal from the force sensor (bottom) replicates the force signal except for some minor high-frequency details.

B. Design considerations

1) Theoretical sensor sensitivity: The force that bends the strip is not identical to the transversal force at the frog F_1. The short distance x between the frog and the bearing piece (where the bending force is applied), as well as the resulting deflection of the strip influence the estimation of F_1 and have to be taken into account.

In the following, the sensor is supposed to act on the bow hair as a simple spring K at a distance x from the frog and the bow hair is modelled as a single string with tension T. The rest position of the spring y_0 is set by the diameter of the bearing piece. Using this simple model described in Fig. 9, the corrected force F_L acting at the free end of the strip can be computed as

$$F_L = \frac{1}{T + Kx} \left[-KxF_1 + TKy_0 \right] \tag{13}$$

and, from Eq. 12, the deformation measured by the strain gauges can be expressed as

$$\epsilon = \frac{3bt}{2L^3} \left[\frac{-xF_1 + Ty_0}{T + Kx} \right] \qquad K = \frac{Ywt^3}{4L^3} \tag{14}$$

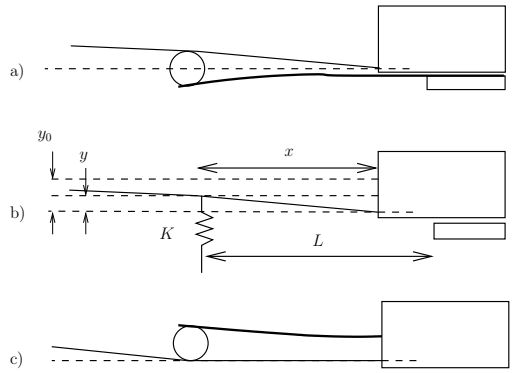

Fig. 9: (a) Schematic view of the sensor. The steel strip experiences maximum deflection when the bow is unloaded. As bow force is increased the strip straightens. (b) Model used to derive the sensitivity. The strip is modeled as a spring (stiffness K, rest position y_0) acting on the bow hair at a distance x from the frog. The bow hair is modelled as a single string with tension T. (c) Alternative design for minimizing y_0 with the strip mounted at the opposite of the bow hair.

It follows from Eq. 13 that the strain of the steel strip when placed under the bow hair is smaller than for the fixed-free condition, given by $\frac{3bt}{2KL^3}F_1$. Second, the strain is strongly non-linear as a function of L. For the free strip, the strain increases linearly with strip length (equation 12 with $b \propto L$), but the behaviour of the sensor strip under the bow hair is more complex.

In Eq. 14, the main design parameters L, b, t, x and K are constants. The tension T is, however, set by the player and varies when a bow force is applied (up to 25 % of the static tension, according to Sect. 2). The transverse sensitivity $\partial\epsilon/\partial F_1$ of the sensor is given by

$$\frac{\partial \epsilon}{\partial F_1} = \frac{3bt}{2L^3}\left[-\frac{x}{T+Kx} + \frac{F_1 x}{(T+Kx)^2}\frac{\partial T}{\partial F_1} + \frac{Ky_0 x}{(T+Kx)^2}\frac{\partial T}{\partial F_1}\right] \tag{15}$$

Equation 15 gives the keys to the choice of design parameters for the sensor in order to reach maximal sensitivity and avoid strong non-linearity.

Focusing on the first term, the linearity of the response can be improved by increasing the stiffness K which reduces the dependence on tension variations. If the actual tension is written $T = T_0 + \delta T$ with T_0 the static tension set by the player, and if the maximal tension variation is δT_{max}, a criterion for minimizing the influence of δT is given by

$$\frac{\delta T_{max}}{T_0} \ll 1 + \frac{Kx}{T_0} \tag{16}$$

A sufficiently high stiffness can consequently make the deformation practically independent of variations in bow hair tension and give the desired linear dependence of the transversal force at the frog. The influence of the static tension T_0 can be neglected provided that $K \gg T_0/x$, i.e. $K \gg 2500$ N/m with $x = 20$ mm and $T_0 = 50$ N. In the current design of the sensor K is about 7000 N/m, and a maximal increase of the tension of 25 % as observed in Fig. 6 would lower the sensitivity with about 6 %. Increasing the stiffness further reduces the strain and a compromise has to be found between linearity and sensitivity.

The second and the third term in Eq. 15 are directly dependent on the variations in bow hair tension. If the stiffness is high enough, the second term can be neglected. In the third term, the diameter of the bearing piece will influence the response through y_0. In order to reduce the non-linearity due to tension variations, it is desirable to make y_0 as small as possible, but that will reduce the maximum force that can be measured in the current configuration (strip mounted under the bow). An alternative design with the sensor mounted on the opposite side of the bow hair would minimize the influence of the third term (see Fig. 9, bottom).However, this configuration makes it necessary to fix the strip inside the frog, which is more radical operation when attaching the sensor to the ferrule.

2) Strip length: For the fixed-free strip, the strain ϵ increases with the strip length. In contrast, the sensitivity of the sensor, given in Eq. 15, shows a different behaviour and, under some conditions, increasing strip length can surprisingly reduce the sensitivity.

If tension variations are neglected in Eq. 15, the maximal sensitivity at $b = L$ is written as

$$S = \frac{\partial \epsilon_{max}}{\partial F_1} = \frac{3t}{2L^2} \frac{x}{T_0 + Kx} \tag{17}$$

Fig. 10 illustrates the sensitivity given in Eq. 17 for a strip length L varying from 0 to 5 cm and $x = L$ (full straight line). For comparison, the sensitivity of the fixed-free strip is shown (dashed line), varying linearly with the plate length. Between 0 and 2 cm, the sensitivity of the sensor increases somewhat slower than the sensitivity of the fixed-free strip. Then it reaches a maximum value and slowly decreases from 3 to 5 cm. In this region, the sensitivity is consequently reduced with increasing strip length.

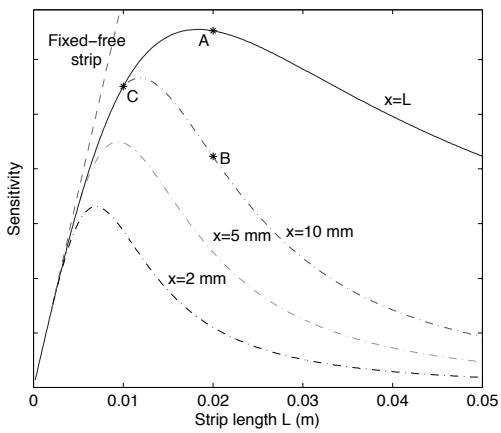

Fig. 10: Variation of the sensor sensitivity with strip length L (full line, $x = L$). Other parameters are Y= 2.1 MPa (steel), w=5 mm, t= 0.4 mm and T_0=50 N. For comparison, the sensitivity of the fixed-free strip is shown (dashed line), as well as alternative sensor designs with $x < L$ (dashdot lines, marked $x = 2$, $x = 5$ and $x = 10$ mm).

The fixation of the strip can be moved back on the ferrule in order to decrease the distance x between the outer edge of the sensor and the frog, while keeping the same strip length and the same stiffness (see Fig. 9b). The idea of such a modification was to improve the playability (by decreasing the unused part of

the bow hair) without modifying the mechanical response of the sensor. However, it can be seen in Fig. 10 that the sensitivity is significantly reduced. For example, with $L = 20$ mm, the sensitivity decreases from A ($x = 20$ mm) to B ($x = 10$ mm). Surprisingly, the response is even lower than the response of a strip with length 10 mm (point C).

3) Bearing piece: As shown above the diameter of the cylindrical bearing piece should be as small as possible in order to minimize the non-linearity, but on the other hand it must at least touch the bow hair at the highest applied bow force. The diameter and position (2.5 mm at x =20 mm from the ferrule) was empirically determined by observing the displacement of bow hair for a realistic maximal bowing force near the frog.

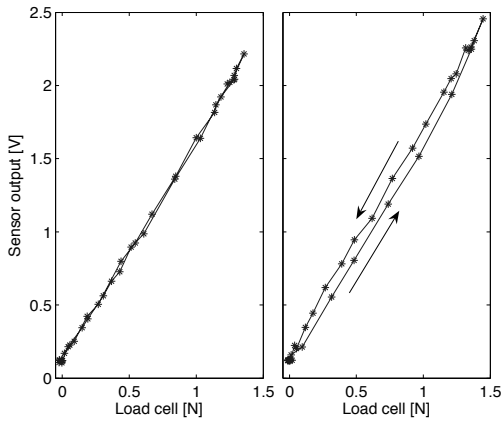

Fig. 11: Effect of gluing the bearing piece to the strip. Left: Bearing piece wedged between the steel strip and the bow hair. Right: Bearing piece glued to the strip, resulting in hysteresis.

In order be sure that the bearing piece stayed in place even in vigorous playing, it was glued to the strip in the initial experiments. However, this step of precaution introduced a hysteresis (see Fig. 11, right), resulting in higher sensor output when the bow force was decreasing compared to when it was increasing. This effect could be related to a torque at the end of the strip. With the bearing piece glued, the contact with the strip is relatively strong. When the bow is pressed down, the hair stretches slightly, exerting a longitudinal force on the bearing piece in the direction towards the tip. The resulting couple on the strip counteracts the deformation due to the transversal force. When the bow force is reduced, the longitudinal force acts towards the frog, again counteracting the deformation change due to change in transversal force. When the bearing piece was held in position only by wedging between the strip and the bow hair, the hysteresis disappeared (see Fig. 11, left).

IV. Calibration

The sensor output reflects the transversal force exerted by the bow hair at the frog, which in turn depends on the bow force and bow position. The calibration procedure aimed at determining the coefficients that relate the sensor signal to the actual bow force. As the sensitivity was slightly dependent on the support of the bow, the calibration procedure was designed to be as close as possible to real playing conditions.

This would also allow fast repeated calibrations during measuring sessions in order to take changes in hair tension into account.

A. Calibration procedure

The calibration was performed by pressing the bow against a load cell. The subject (violinist) was asked to hold the bow as in normal playing and apply equal bow force at successive bow positions, from the frog to the tip. The force signal from the load cell F_{LC} which gave a calibrated reference of the bow force, was recorded together with sensor signal s_F. A typical calibration session is illustrated in Fig. 12.

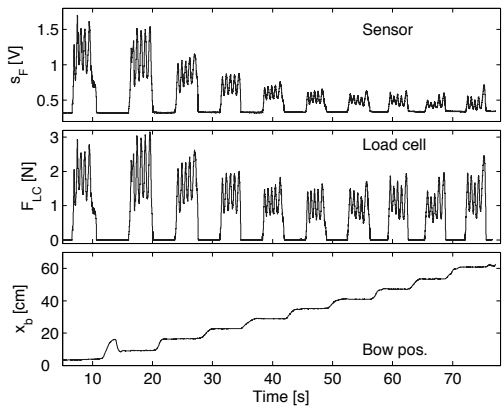

Fig. 12: Calibration procedure. The bow is pressed against a calibrated load cell at 10 bow positions. At each position the bow force is varied periodically five times. Bow positon (bottom), bow force as measured by the load cell (middle), and force sensor signal (top).

In this example, ten successive bow positions were used, from the frog (x_b=35 mm) to the tip (x_b=610 mm). At each position, the bow force was varied periodically five times between about 1-2 N, each cycle lasting 1 s approximately. The variation range in bow force was approximately the same for the ten positions, but the signal from the force sensor decreased when approaching the tip due to the position of the sensor.

B. Calibration coefficients

The signals were segmented in order to get calibration data for each bow position x_b. Calibration curves were obtained by fitting a second order polynomial to the data

$$s_F = b_2(x_b)F_{LC}^2 + b_1(x_b)F_{LC} \tag{18}$$

Fig. 13 shows an example with three calibration curves for a violin bow, corresponding to bow positions at the frog, middle and tip.

Fig. 14 shows the fitted calibration coefficients b_1 and b_2 plotted as function of bow position for three repeated calibrations. The calibration procedure is seen to give good reproducibility. The figures suggest that b_1 can be well approximated by a linear fit, whereas b_2 requires quadratic interpolation.

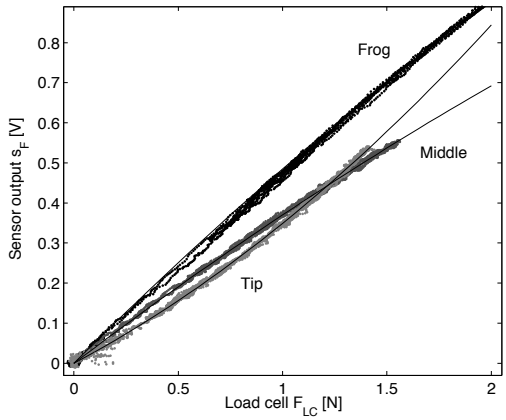

Fig. 13: Calibration curves for a violin bow corresponding to bow positions near the frog, middle and tip. Fitted second-order polynomials are shown with solid lines.

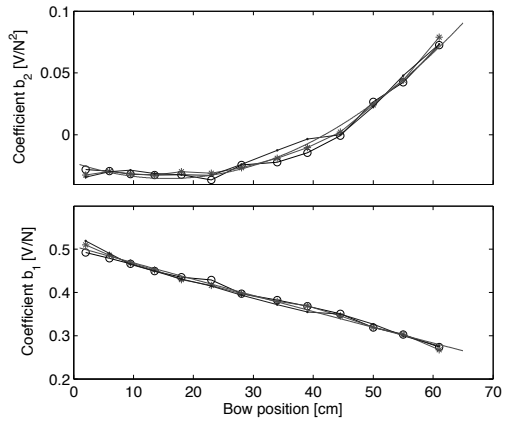

Fig. 14: Calibration coefficients b_2 and b_1 plotted as function of bow position x_b for three repeated calibrations.

The correspondence with the analytical expressions derived in Sect. 3 is good. From equation 11, with $\gamma = x_b/L_b$, it could be predicted that b_2 and b_1 should show the observed dependence on bow position

$$b_2(x_b) \propto x_b^2 \frac{\alpha_T}{K_b L_b^3} \tag{19}$$

$$b_1(x_b) \propto 1 - \frac{x_b}{L_b}(1 - \frac{T_0}{K_b L_b}) \tag{20}$$

C. Bow force reconstruction

During measurements, bow force is calculated from the sensor signal and bow position. Using equation 18, the actual bow force F can be reconstructed as

$$F = \frac{-b_1(x_b) + \sqrt{b_1(x_b)^2 + 4b_2(x_b)s_F}}{2b_2(x_b)} \tag{21}$$

Of the two possible solutions to Eq. 15 this was chosen because it has the necessary properties for the reconstruction: When b_1 is positive (which is always the case), F will be zero when $s_F = 0$. Moreover, whatever the sign of b_2, this function is increasing when s_F increases.

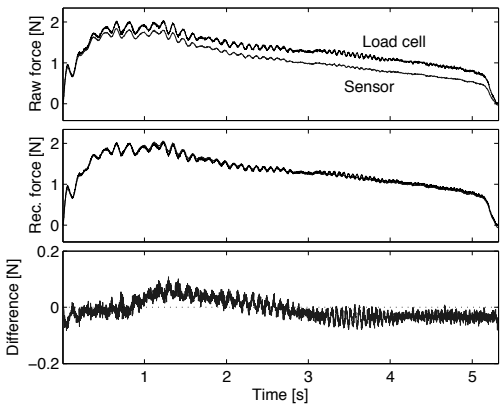

Fig. 15: Test of the reconstructed bow force during a full down-bow from frog to tip. The bow was moved with constant velocity on a wheel mounted on the load cell. Bow position was interpolated linearly between the beginning and end of stroke. Top: Comparison between load cell output and raw sensor signal. The sensor signal has been normalized using b_1 and b_2 at the frog. Middle: Comparison between the load cell signal and reconstructed bow force. Bottom: Difference between the reconstructed bow force and load cell output.

In order to check the reconstruction using interpolated calibration coefficients $b_2(x_b)$ and $b_1(x_b)$, the bow was 'played' on a wheel mounted on the calibrated load cell, using full bow strokes with constant velocity (see Fig. 15). The load cell signal and the reconstructed bow force are seen to almost coincide, the difference being only ± 0.05 N centered around zero. This value can be considered as a typical error in the bow force estimation under standard conditions (slow variations of the bow force between 0.5 and 2 N).

D. Factors influencing the calibration

The output of the bow force sensor is sensitive to several conditions, and it is not straight-forward to estimate the effect and compensate for the effect of all of them. In this section, three factors are discussed, including the mechanical action of the bow, hair tension, and tilting of the bow, and their influence on the calibration coefficients illustrated.

1) Influence of the mechanical action of the bow: More than 20 bows were tested with the sensor, from violin bows to double bass bows. Most of them showed the characteristics shown in Fig. 13: The calibration curves for different bow positions lie rather close together, and the curve for the tip steepens rapidly for higher bow forces. Further, the output from the sensor is typically higher for bow positions at the tip than at the middle of the bow. Some bows, however, showed a different behaviour as illustrated in Fig. 16 where the bow in Fig. 13 is compared with a bow which behaves quite differently. Here the calibration curves are widely separated, and the response close to the tip is weak for bow forces below 1 N. For some very stiff bows, like double bass bows, this behaviour is easily understandable, as the bow can be represented by the rigid model described in Sect. 2. For violin bows, however, the comparison between calibration curves and measurements of the transversal stiffness of the bow did not show a specific relationship. In these cases, the weak response below 1 N seems to be related to some more elaborated property of the bow.

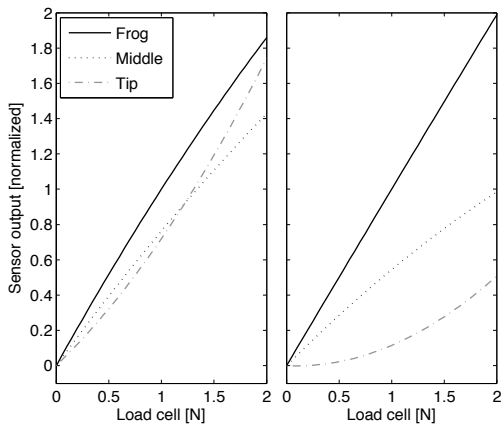

Fig. 16: Calibration curves for two violin bows with different mechanical action. Left: Bow 1, corresponding to Figs. 13 and 14. Right: Bow 2, with a stiffer stick of carbon fibre which gives widely separated calibration curves with a much lower sensitivity at the tip than at the frog.The curves have been normalized using the sensor output for 1 N force at 5 cm from the frog as reference.

The calibration procedure will take such differences in mechanical action between bows into account, but the accuracy in the reconstruction of low bow forces will be reduced. For example, at bow forces between 0.5 and 1 N, a measurement error in the sensor output of 1% would give an error of about 3% in the reconstructed bow force for bow 1, but as high as 15% for bow 2. At 1.5 N the errors have reduced to 1.8 % for bow 2 and 0.7 % for bow 1. In short, some bows will be more suitable for precise bow force measurements with this design of the sensor than others because of their mechanical properties.

2) Influence of bow hair tension: The tension of bow hair set by the player influences the transversal force at the frog (see Section 2) and the response of the sensor (see Section 3). The combined effect of changes in hair tension was quantified in a calibration with three largely deviating tensions; very low, normal, and very high, the two extreme values not being suitable for playing. The results are shown in Fig. 17.

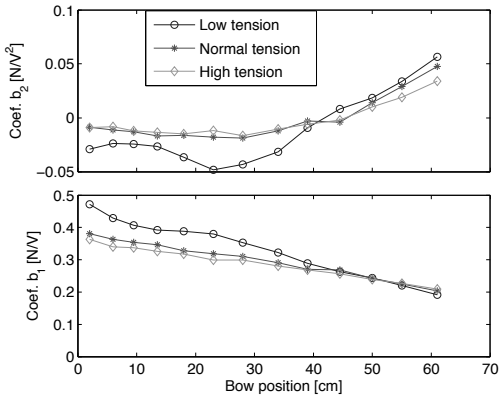

Fig. 17: Influence of the bow hair tension on the calibration coefficients for three values; low, normal, high. The high and low tensions were not suitable for playing.

The results for bow positions at the frog follow the expected behaviour. Close to the frog the stick does not bend and tension can be supposed to be constant during loading ($T = T_0$). Equations 11 and 14, with $\gamma \to 0$, predict that b_1 will be inversely proportional to T_0, which is in line with the observations.

An interpretation of the results close the tip would require knowledge about the mechanical behaviour of the particular bow. Here it is sufficient to note that the values of calibration coefficient b_1 for different tensions merge when approaching the tip.

The observed changes in b_2 and b_1 are seen to be rather limited, even for extreme values of tension. Typical differences in preferred tensions between players are much smaller and will be handled accurately by the calibration procedure. However, repeated calibrations during a measurement session are desirable in order to take natural changes in hair tension during playing into account.

3) Influence of bow tilt: String players tilt the bow in playing in order to reduce the effective width of the bow hair in contact with the string. Typically the bow is tilted much in soft playing, and more so when playing near the frog than at the tip. While the mechanical characteristics (stiffness) of the bow as well as changes in tension are taken into account by the calibration as discussed above, bow tilt is an external parameter which not easily can be handled in the measurements.

The tilting influences the bow force measurement in two ways. First, the sensor measures the force applied in the direction perpendicular to the steel strip, whereas the bow force by definition is applied perpendicular to the string. This results in an underestimation of the bow force, related to the tilt angle. For instance, an angle of 20° would give 6 % lower transversal force acting on the sensor (proportional to $\cos\theta_{tilt}$), compared to the case with the bow hair flat on the string.

Secondly, the bending of the strip, and thus the response of the sensor, will be affected when the transversal force from the hair is not evenly applied across the bearing piece. In addition to bending the strip will twist. The profile of the transversal deflection of the bow hair as it crosses the bearing piece is not easily predicted. However, as the ribbon of bow hair is composed of several layers, a force which is applied mainly at one edge of the ribbon will be distributed approximately linearly across the width of

the bearing piece (see discussion in [8][9])

The uncertainties in the estimation of bow force due to tilting were found to be limited. Calibrations performed when tilting the bow at various degrees showed that the influence was noticeable only for bow positions close to the sensor. The deviation between the calibration curves with and without tilting the bow could then reach more than 30 %. From the second calibration point at about 8 cm from the frog and further towards the tip the deviation was found to be less than 10 %. In order to measure bow force correctly also in tilting, a possible solution would be to split the strip along the centerline and apply two sets of strain gauges, one on each side. In this way the amount of tilting could be estimated and a correction for the influence on bow force taken into account.

V. Applications in playing

The use of the bow force sensor is illustrated in two applications. In the first example, one sensor was placed at the frog as described above, and motion capture technique [10][12] was used to measure bow position in order to reconstruct the bow force. Alternative methods for measuring bow position include a simple solution using a resistive wire placed among the bow hairs and connected in a Wheatstone bridge [1], [2], and more complex systems based on a capacitive principle with an antenna placed behind the bridge of the violin and a resistive strip along the bow stick [13]. In the second application example, two sensors are used, one at the frog and one at the tip. In this configuration, the difference between the sensor signals could be used to calculate bow position and no extra measurement devices were needed.

In the experiments two violinists were asked to play two types of bow strokes; sustained, separated notes (detaché) in which the bow force was supposed to be held rather constant, and long strokes with strong accents at the beginning of each note, which would require large variation in bow force.

A. One bow force sensor and motion capture

Examples using one bow force sensor and motion capture are given in Fig. 18, showing audio signal, bow force, bow position and bow velocity, for a G4 note played without vibrato on the D string. In Fig. 18a showing detaché , it is apparent from the audio signal that each note was played with a slight crescendo. This was accomplished by an increase in bow velocity from about 30 to 60 cm/s during each stroke. The reconstructed bow force was approximately constant at about 600 mN, except local increases prior to the bow changes at the frog. The raw force sensor signal, which decreased as expected when approaching the tip, illustrates the magnitude of the compensation for bow position in the reconstruction of bow force.

The compensation is more promounced in Fig 18b showing the bow strokes with accents: In up-bows (negative velocity), the raw sensor signal is almost flat, whereas the reconstructed bow force shows the same large variation as in down-bows. The accented initial part of each note is obtained through a coordination of high bow velocity reaching about 80 cm/s and high bow force, up to 2 N. The sustained softer parts are played with a comfortable bow velocity around 20 cm/s, requiring about 0.5 N bow force.

B. Two bow force sensors

An alternative system was developed in order to allow bow force measurements without an additional device for measuring bow position. The solution was based on a second force sensor at the tip. This

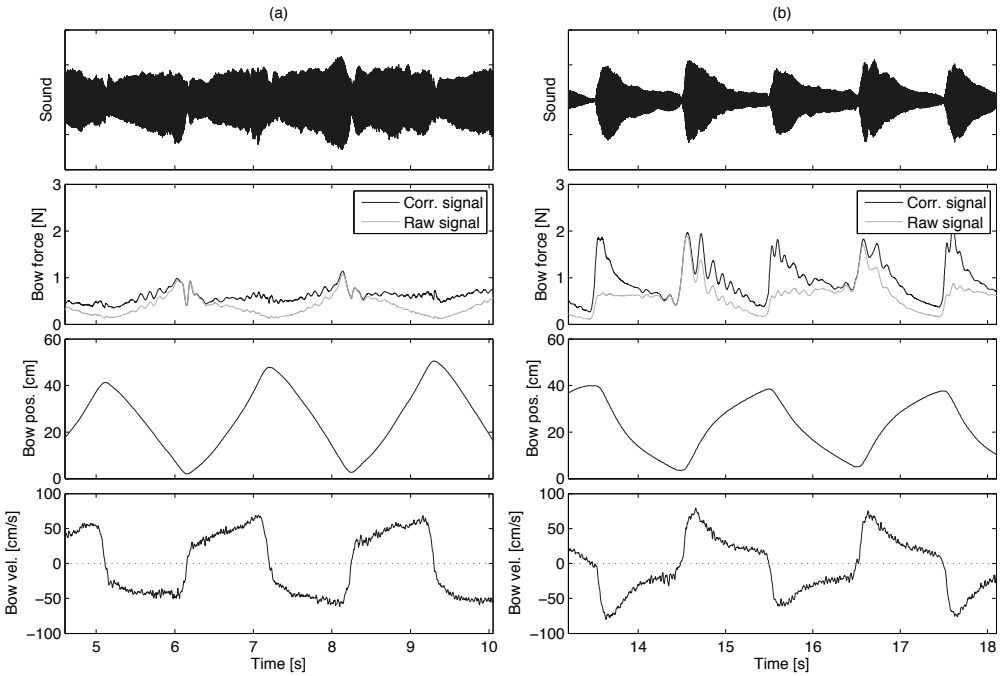

Fig. 18: Measurements using one bow force sensor and motion capture showing audio signal, reconstructed bow force, bow position and bow velocity (top to bottom). The raw sensor signal is included in the bow force panel (gray curve) in order to illustrate the effect of bow position on the reconstruction. Bow velocity was derived from the bow position signal. The player performed (a) sustained, separated notes (detaché), and (b) long strokes with inital accents on each note.

configuration was originally used by Askenfelt [1], [2], but he used the two sensors (four strain gauges) together in a full Wheatstone bridge for bow force. The sensitivities of the frog and tip branches were adjusted to obtain a constant signal for a given bow force at all positions along the bow hair.

In the current application the two sensors were used independently to obtain the transversal force at the frog and tip, respectively. When a certain bow force is applied somewhere along the bow, the outputs from the sensors will be dependent on the actual bow position. The difference between the signals can be used to estimate the bow position. By simultaneous calibration of bow force and bow position it is thus possible to obtain both parameters from the output of the two force sensors.

The second sensor was clamped between the bow hair and the ivory plate at the tip. A thin metal fixation around the head prevented the sensor from moving.

1) Calibration: A coordinated calibration of bow force and bow position was performed by pressing the bow hair against the load cell at different bow positions as described in Sect. 4. Signals obtained from the sensor at the frog (F_{c1}) and at the tip (F_{c2}) were used to compile a calibration grid from which bow force and bow position could be interpolated (see Fig. 19, left). The grid gives the bow force and bow position for equally spaced values of F_{c1} and F_{c2}. An analytical expression as for the case with one force

sensor (see Eq. 21) was not considered due to the complex relation between the rotation of the head and the output of the sensor at the tip.

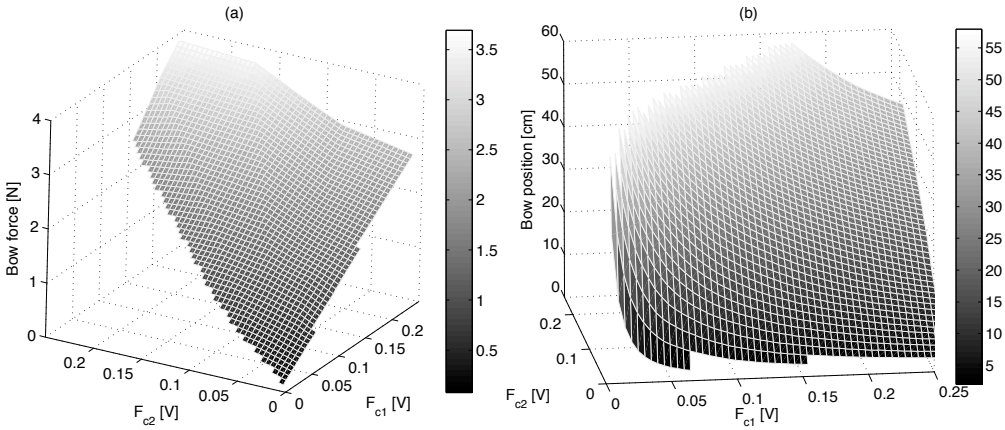

Fig. 19: Coordinated calibration surfaces for (a) bow force and (b) bow position using one sensor at the frog F_{c1} and one at the tip F_{c2}.

As seen in Fig. 19a, the force calibration surface is delimitated by two edges originating from the origo of F_{c1} and F_{c2}, the right-going corresponding to a bow position at the frog and the left-going to a position near the tip. Near the frog, the variations in F_{c1} are large as the bow force is varied, whereas the tip sensor provides a signal F_{c2} with very small variations. However, near the tip, F_{c2} variations are much stronger, and F_{c1} still has appreciable variations. This is in agreement with the observations in the previous sections, showing that the frog signal response does not tend to zero when bowing near the tip. A similar calibration grid was computed for bow position, giving bow position as a function of F_{c1} and F_{c2} (see Fig. 19b).

Recordings of the two sensor signals were used to determine bow force and bow position from two-dimensional interpolations on the calibration surfaces. It should be noted that as the slope of the bow position surface was very steep near the origin, bow position determination can be supposed to work better for high bow forces than for lower.

2) Measurements: As before, a violinist was asked to play sustained bow strokes with and without accents. The examples were played on the open G string, and the bridge force signal was recorded by a transducer on the bridge. Bow position was computed from the sensor signals and calibration grid. The resulting bow position signal was rather noisy, and a Savitzky-Golay filter (polynomial order 2, frame size 61) was used for smoothing before calculating the bow velocity.

The results are shown in Fig. 20. It is satisfying to notice the good agreement in bow position and velocity with the corresponding curves in Fig 18, obtained by motion capture. The bow position curves are almost triangular for the detaché notes, whereas the accentuated examples show asymmetrical patterns due to the high velocity during the attack of the note. The bow velocity curves show very convincing similarities, including the peak velocities around 80 cm/s. Further, the velocity peaks are well correlated

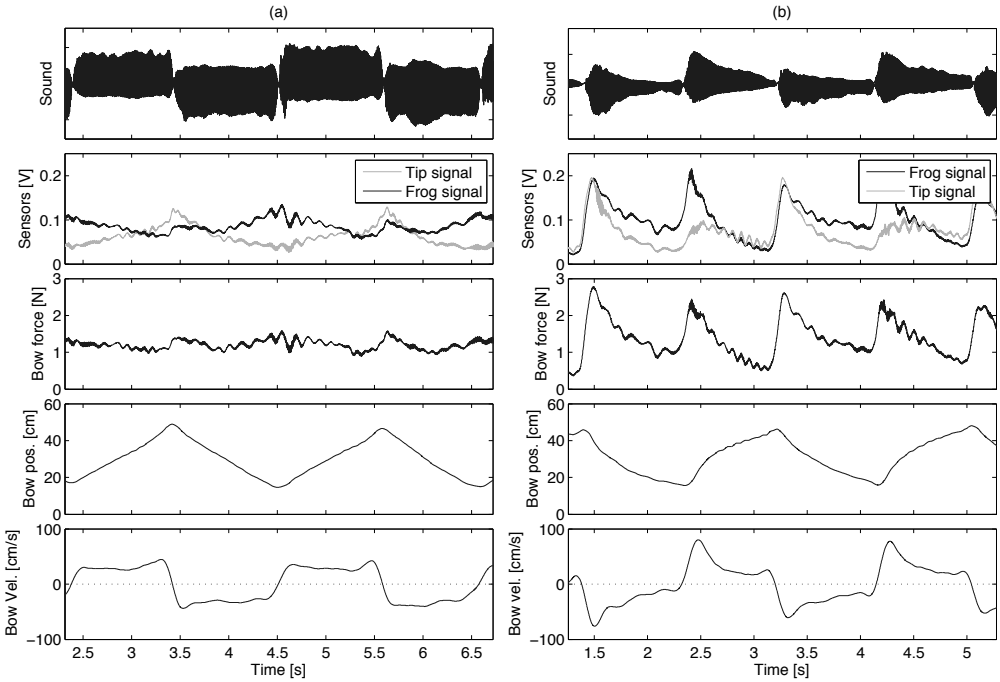

Fig. 20: Measurements using two force sensors, one at the frog and one at the tip, showing bridge force, output from the two force sensors (frog, black line; tip, grey line), interpolated bow force, bow position and bow velocity. Bow velocity was derived from the bow position signal. The player performed (a) sustained, separated strokes (detache') , and (b) long strokes with initial accents on each note.

with the bow force peaks. In both cases, each maximum in bow force occurs just before the corresponding velocity maximum, the shift being between 0 and 100 ms (cf. Figs. 18 and 20).

In the detaché example (see Fig. 20a), the bow velocity was lower than in the previous example (see Fig. 18a), about 30 cm/s and with a short period of acceleration before the bow changes at the tip. The bow force was almost constant as in Fig 18 but higher, above 1 N. The two raw sensors signals are shown separately for comparison. The signal variations are seen to be in opposite phase; the tip signal increases and the frog signal decreases in down-bows (positive velocity), and inversely in up-bows. After the reconstruction, the interpolated bow force signal is rather flat, with a mean value around 1.2 N.

In the accentuated example (see Fig. 20b), both bow velocity and bow force are of similar magnitude as in Fig. 18b. As the bow force was varied, the two sensor signals followed each other close in phase. It could be noted that the tip signal is much stronger when the attack is played close to the tip in up-bows (negative velocities), whereas the signal from the frog sensor has almost the same amplitude in accents played at the tip as at the frog. Again, this is related to the fact that the response of the frog sensor does not go down to zero when playing near the tip.

The comparisons between the examples measured with the motion capture (Fig. 18) and two force sensors (Fig. 20) suggest that the configuration with two force sensors offers a satisfying alternative for

measuring bow position as well as bow force. In many cases there is thus no need for dedicated extra equipment for position measurement.

SUMMARY AND CONCLUSIONS

The principle and implementation of a sensor that can be used to measure the bow force during violinists' performances are presented. The sensor is based on measurement of the transversal forces at the bow hair terminations when the bow is pressed against the string. The principle was tested in laboratory experiments, in order to verify the influence of bow position and hair tension on the forces at the terminations. Somewhat unexpected, it was found that the transversal force at the frog termination could increase when the loading point on the bow hair was moved closer to the tip. By measurements of variations in bow hair tension and the displacement of the tip due to stick bending, a simple model describing the mechanical behaviour of the bow could be developed, which predicted the measured force at the frog well.

The design of the sensor was described in detail. The sensor is light (total mass < 4 g) and easily detachable, causing no damage to the bow. It consists of a thin leaf spring of steel that is fixed at the ferrule and contacts the bow hair through a light bearing piece. The steel strip is deformed due to the hair deflection, and the deformation is measured using strain gauges glued on both sides of the strip.

A procedure for calibrating the sensor under conditions resembling normal playing was described. The player presses the bow against a calibrated force transducer at successive positions along the bow, and varies the bow force periodically. Two calibration coefficients were derived that are used to reconstruct the bow force from the sensor signal and the bow position. The reconstructed bow force was found to be accurate. The typical error in bow force estimation under standard conditions (slow variations between 0.5 and 2 N) was about 0.05 N. The influence of the mechanical properties of the bow, hair tension, and tilting were illustrated and quantified.

Measurements of bow force in normal violin playing were illustrated for two applications of the sensor. The first used only one sensor at the frog and requires another device for measuring the bow position in order to reconstruct the bow force. In the second application two sensors were used, one at the frog and one at the tip, in order to measure both bow force and bow position. The bow force sensor was found to perform satisfactorily in both applications, giving realistic measurements.

In summary, the described bow force sensor is a robust and accurate device for simple measurements of bow force in string playing using the player's own bow, and without interfering with normal playing conditions.

ACKNOWLEDGEMENTS

This work is part of the CONSONNES project, funded by the French Agence Nationale pour le Recherche. Stays at IDMIL, McGill University, Montreal, and at the Dept. of Speech, Music and Hearing, Royal Institute of Technology (KTH), Stockholm, were funded by the Cost 287-ConGas action and the Swedish Institute. Special thanks go to Emmanuel Fléty and Alain Terrier for their valuable help in developing the sensors and very special thanks go to Anders Askenfelt and Benoît Fabre for their invaluable comments and corrections during the writing of this manuscript.

REFERENCES

[1] A. Askenfelt. Measurement of bow motion and bow force in violin playing. *J. Acoust. Soc. Am.*, 80(4):1007–1015, 1986.

[2] A. Askenfelt. Measurement of the bowing parameters in violin playing II. *J. Acoust. Soc. Am.*, 86(2):503–516, 1989.

[3] A. Askenfelt. Observations on the dynamic properties of bows. *Speech Transmission Laboratory Quarterly Progress and Status Report, Dept. of Speech, Music and Hearing, Royal Institute of Technology (KTH) Stockholm, STL-QPSR*, 4:43–49, 1992.

[4] M. Demoucron, A. Askenfelt, and R. Caussé. Mesure de la pression d'archet des instruments à cordes frottées, application à la synthèse sonore. In *8ème Congrès Français d'acoustique*, Tours, France, 2006.

[5] E. Guaus, J. Bonada, A. Perez, E. Maestre, and M. Blaauw. Measuring the bow pressing force in a real violin performance. In *Proceedings of International Symposium on Musical Acoustics*, Barcelona, Spain, 2007.

[6] K. Guettler. On the creation of the Helmholtz movement in the bowed string. *Acta Acustica*, 88(6):970–985, 2002.

[7] K. Guettler, E. Schoonderwaldt, and A. Askenfelt. Bow speed or bowing position - which one influences spectrum the most? In *Proceedings of the Stockholm Music Acoustics Conference (SMAC 03)*, pages 67–70, Stockholm, August 2003.

[8] R. Pitteroff. *Contact mechanics of the bowed string*. PhD thesis, University of Cambridge, 1995.

[9] R. Pitteroff and J. Woodhouse. Mechanics of the contact area between a violin bow and a string. Part III: Parameter dependence. *Acta Acustica*, 84:929–938, 1998.

[10] N. Rasamimanana, D. Bernardin, M. Wanderley, and F. Bevilacqua. String bowing gestures at varying bow stroke frequencies: A case study. In *Gesture Workshop*, Lisbon, Portugal, 2007.

[11] J. C. Schelleng. The bowed string and the player. *J. Acoust. Soc. Am.*, 53(1):26–41, 1973.

[12] E. Schoonderwaldt, S. Sinclair, and M. Wanderley. Why do we need 5-DOF force feedback? An analysis of violin bowing. In *4th International Conference on Enactive Interfaces (ENACTIVE07)*, Grenoble, France, 2007.

[13] D. Young. the hyperbow controller: real-time dynamics measurement of violin performance. In *Proc. of the 2002 Conference on New Instruments for Musical Expression (NIME-02)*, Dublin, Ireland, 2002.

Paper II

Extraction of bowing parameters from violin performance combining motion capture and sensors

E. Schoonderwaldt
KTH-Computer Science and Communication, Dept. of Speech Music and Hearing
Lindstedtsvägen 24, SE-100 44 Stockholm, Sweden[a)]

M. Demoucron
IRCAM, Centre Pompidou, CNRS UMR 9912
1 Place Igor Stravinsky, 75004 Paris, France

A method is described for measurement of a complete set of bowing parameters in violin performance. Optical motion capture was combined with sensors for accurate measurement of the main bowing parameters (bow position, bow velocity, bow acceleration, bow-bridge distance and bow force) as well as secondary control parameters (bow angles: skewness, inclination and tilt). In addition, other performance features (moments of on/off in bow-string contact, string played, and bowing direction) were extracted. Detailed descriptions of the calculations of the bowing parameters, features and calibrations are given. The described system is capable of measuring all bowing parameters without disturbing the player, allowing for detailed studies of musically relevant aspects of bow control and coordination of bowing parameters in bowed-string instrument performance.

PACS numbers: 43.75.De, 43.75.Yy

I. INTRODUCTION

The interaction between the performer and the instrument is a fascinating subject of study. Technological developments have led to ways of capturing this interaction, shedding more light on sound control and musical performance aspects in general. An important example is the computer-controlled grand piano, such as Yamaha's Disklavier, which offers built-in technology for capturing key played, hammer timing and key velocity, the main parameters for studying piano performance.[1]

In most other instruments the sound production process is controlled by many more parameters and therefore more difficult to quantify. The sound is often generated via direct contact between the player and the instrument, e.g. the lip-mouthpiece interaction in wind instruments or finger-string contact in plucked string instruments. This type of interaction can be considered *endogenous* and is typically difficult to model or quantify. In many instruments sound production is controlled by movements. This type of interaction is *exogenous*, and therefore easier to observe. A typical example is the bowed string instruments, and as an extreme case the Theremin.

In violin playing, sound generation originates from the bow-string contact. The sound is controlled mainly via three basic bowing parameters: bow velocity, bow-bridge distance and bow force. The control exerted by the player is transferred to the instrument via the bow, making the control parameters relatively easy accessible for measurement. The interfacing function of the bow might partly explain the relatively large number of studies on bowing in comparison with other types of player-instrument interaction.[2–8]

The first detailed study of bowing gestures was performed in the 1930s by Hodgson,[9] who measured the spatial trajectories of the bow and the player's bow arm using cyclegraphs (a photographic record of the track covered by a moving object). The first complete setup for measuring the main bowing parameters bow position, velocity, force and bow-bridge distance was developed by Askenfelt and used to study typical bowing patterns in violin playing.[7,8] Since then, several sensor-based systems have been developed for quantitative measurement of bowing gestures,[10–13] both suitable for analysis of bowing gestures[14,15] and control of live performance.[16]

Other studies of violin performance have been performed using 3D motion capture techniques. The generally high spatio-temporal resolution makes these techniques suitable for analysis of timing and coordination in instrument performance.[17,18] Studies of kinematics and kinetics related to development of vocational injuries in musicians are also important applications.[19–21] More recently, a 6 degrees-of-freedom electromagnetic-field-based motion tracker has been used for measuring bowing parameters in violin playing.[22]

The major goal of the current study was to provide a complete and accurate method for measurement of bowing parameters in violin performance. The method was based on motion capture techniques, augmented with sensors for bow force and acceleration. An important requirement was that a regular bow and instrument could be used, allowing for a normal playing situation. In addition to measurement of the three main bowing parameters (bow velocity, bow-bridge distance and bow force), the angles of the bow relative to the violin (tilt, inclination and skewness) were included. The bow angles could be considered as secondary control parameters operating on two levels. The angles are used for controlling details of the note played, like the effective width of the bow

[a)] Electronic address: schoondw@kth.se

hair, and which string is being played. On a higher level they play an important role in the pre-planning of the upcoming bowing gestures, like bow changes and changes in dynamic level.[23]

After a short description of the experimental setup in Sect. II, the measurement of position and orientation of the violin and the bow will be discussed in Sect. III. Kinematic models for straightforward and accurate calculation of spatially defined bowing parameters, including bow-bridge distance and bow velocity, are described. Further, it will be shown how the violin model can be extended for the determination of other features, such as bowing direction and string played.

Optical motion capture was combined with sensors on the bow for measurement of bow force and acceleration. In Sect. IV it will be explained how motion capture and sensor data can be used in a complementary way for sensor calibration and reconstruction of bowing parameters. Special attention will be given to the measurement of bow force. An idea brought forward by Maestre et al.,[22] suggesting that bow force could be measured from motion capture data only will be further explored and compared with sensor-based measurement of bow force.

II. EXPERIMENTAL SETUP

A. Motion capture and audio

A Vicon 460 system with six M2 cameras (max. res. 1280×1024 pixels) was used for optical motion capture.[24] The cameras were positioned around the subject at distances of about 3-4 m.[25] The frame rate was 250 Hz.

Middle-sized reflective spherical markers (10 mm diameter, mass < 1 g) were attached to the bow and the violin using a special adhesive goop (Schertler Audio) leaving no traces on the varnish. Markers were positioned so that the sound would not be influenced (e.g. markers on the bridge were avoided). Extra markers used during calibrations were small half-spheres (diameter about 5 mm), which could be positioned accurately on the violin and bow (estimated positioning error about 0.5 mm).[26] Details of the marker configurations will be discussed in Sect. III.A.

Audio was recorded as analog data in synchrony with the motion capture data, using an acquisition card connected to the Vicon processing unit (sample frequency 40 kHz).

B. Bow force and acceleration

Sensors were mounted on the bow for accurate measurement of bow force and acceleration. A 3-axis accelerometer (STMicroelectronics LIS3L02AS4) with a linear measurement range of ± 60 m/s^2 and frequency range down to DC was used for measuring bow acceleration in the longitudinal and vertical direction ($\hat{\mathbf{x}}_b$ and $\hat{\mathbf{z}}_b$ in Fig. 3). The wide measurement range was needed for reliable acquisition of bowing acceleration. In a pilot study bow accelerations up to about 60 m/s^2 were observed in forte semi-quaver passages.

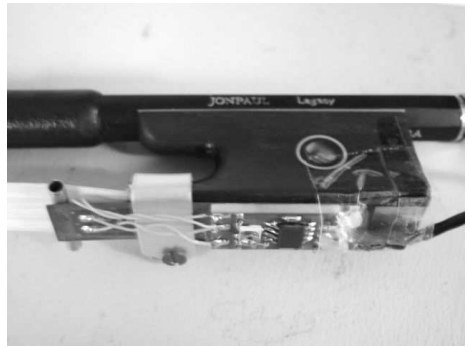

FIG. 1. Bow force sensor mounted at the frog. A metal leaf spring with strain gauges on both sides measures the deflection of bow hair at the frog. The electronic board under the frog integrates a Wheatstone bridge and an instrumentation amplifier.

Bow force was measured using a custom-made sensor which registered the deflection of the bow hair at the frog.[27,28] The sensor consisted of a leaf spring with strain gauges on both sides. The sensor was mounted rigidly to the frog and connected to the bow hair via a cylindrical bearing piece (see Fig. 1). Details about the calibration are given in App. B. To prevent possible damage to the violin due to the pieces under the frog, the violin was equipped with a plastic C bout protector.

The bow force sensor was calibrated using a miniature load cell with a capacity of about 25 N (Transducer Techniques MDB-5). The load cell in turn was calibrated using a set of standard weights (mass 10-200 g).

The sensor signals were recorded at a sample rate of 10 kHz using a National Instruments acquisition card (NI PCI-4472B).

C. Synchronization of motion capture and sensor data

Motion capture and sensor data were synchronized by providing a pulse with a push button at the beginning and the end of each trial. The synchronization signal was recorded on both data acquisition devices, allowing for accurate a posteriori synchronization.

D. Playing comfort

The total mass added to the bow was estimated to about 10 g (force sensor 5 g, accelerometer 3 g, markers 2 g), mostly concentrated at the frog, where it influenced playing properties like moment of inertia relative to the hand of the player the least (the weight of the frog is about 17 g). The wires from the sensors were taped to the the player's arm to keep them out of the way. After a short period of familiarization all participating players

(about ten) confirmed that they felt comfortable in playing. One player commented on the stiffness of the wires, which he could notice during spiccato playing.

III. MOTION CAPTURE OF BOWING GESTURES

A. Kinematic models and marker configurations

The Vicon iQ software used for processing the motion capture data facilitates the use of kinematic models. A kinematic model typically consists of segments interconnected with joints with a certain number of degrees-of-freedom (DOF). The segments are typically associated with one or more markers, making up the marker configuration of the kinematic model. The simplest type of kinematic model, consisting of one free segment, can be used to model a rigid body, and more complex models can be built with segments interconnected with different types of joints (e.g., a human skeleton model).

In the software templates can be used for general classes of objects. A particular object model can be obtained via calibration. A kinematic fit procedure is then used to obtain positions and orientations (6 DOF) of the segments of the model, based on measured marker positions.

The local reference systems of the kinematic models of the violin and the bow were chosen to make the calculation of bowing parameters and feature extraction straightforward and easy to interpret. For this reason the models included important landmarks used in the calibrations to define the origin and the axes of the local reference systems. On the violin the landmarks were the string terminations at the bridge and nut, and on the bow the hair terminations at the frog and tip. As markers at these positions would either be in the way of the player or problematic to track due to frequent occlusions, a reduced marker configuration was used during the measurements. The positions of the landmarks were reconstructed by fitting the models to the measured positions of the present markers.

Four main criteria were taken into account in the design of the models and marker configurations: (1) at least three non-collinear markers are needed for measurement of position and orientation (6 DOF) of a rigid body; (2) a wide spread between marker positions and addition of redundant markers improve the accuracy of the kinematic fit in the presence of noise;[29] (3) optimal visibility of the markers under normal playing conditions; and (4) the markers should not impede normal playing.

The marker configuration and kinematic model used for the violin is shown in Fig. 2. The violin is modeled as a rigid body (one segment). Five markers are used for tracking the position and orientation of the violin. Two extra calibration markers are located at the middle of the bridge (*BridgeMid*) and at the nut *NutMid* between the D and the A string. In the kinematic model the origin corresponds to *BridgeMid*, and the y-axis corresponds to the line between *BridgeMid* and *NutMid* (virtual string). The x and z-axis are defined by an additional constraint that the markers at the upper C bouts (*RBDist* and *LBDist*) share the same z-coordinate in the local reference system.

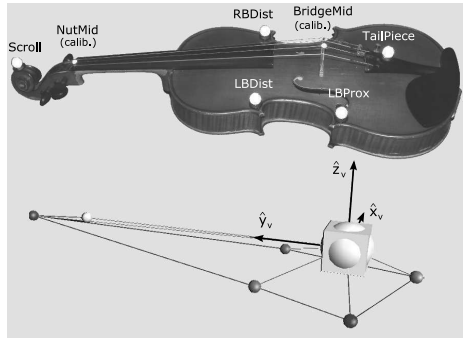

FIG. 2. Marker configuration for the violin, and the corresponding kinematic model as implemented in the Vicon software. The five markers used for tracking the position and orientation of the violin are labeled *Scroll*, *RBDist*, *LBDist*, *LBProx*, and *TailPiece*. The two calibration markers *BridgeMid* and *NutMid*, indicating the positions of the bridge and the nut between the D and the A string, are only present during calibration. The violin is modeled as one segment (rigid body), where the origin, indicated by the cube, coincides with *BridgeMid*. The orientation of the local reference frame is indicated by the basis vectors ($\hat{\mathbf{x}}_v$, $\hat{\mathbf{y}}_v$, $\hat{\mathbf{z}}_v$).

For the bow, a rigid body approximation is not appropriate as the stick can bend considerably under normal playing conditions.[30,31] Depending on tilt bending can take place in two directions. Torsion of the stick can be neglected, as the mechanical lever (height of the tip) is much smaller than that for bending (length of the stick).

The bow was modeled as compound of two (rigid) segments, the frog (root segment) and the stick, connected with a two degrees-of-freedom joint (Fig. 3). The joint coincided with the origin of the root segment (marker *Frog* at the ferrule), securing a fixed distance between the frog and tip (length of the bow hair). The frog segment included the lower, thick part of the stick from the frog screw (*Screw*) to some centimeters in front of the wrapping (*Stick*). In order to avoid a collinear configuration and to achieve a better spread between markers, two markers were placed on short antennas mounted on the stick. This configuration allowed for a complete measurement of the orientation of the bow, including bow tilt (rotation around the x-axis). The orientation of the stick segment relative to the frog segment was determined by a single marker (*Tip*). Two extra calibration markers were located on the bow hair ribbon close to the frog (*Frog*) and the tip (*TipHair*). The calibration marker *Frog* defines the origin of the model, and the line between *Frog* and *TipHair* defines the x-axis. The y and z-axis are established via the constraint that both *Stick* and *Screw* must lie in the x-z plane ($y = 0$) in the local reference system.

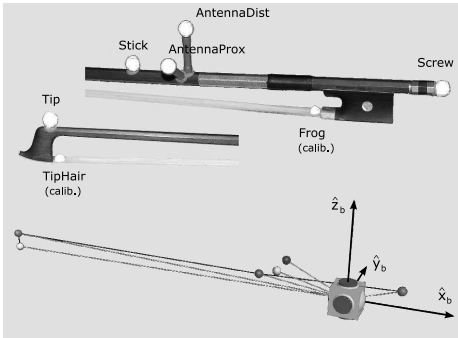

FIG. 3. Marker configuration for the bow, and the corresponding kinematic model. The frog segment, indicated by the cube, is considered as a rigid body and is connected to four markers: *Stick*, *AntennaProx*, *AntennaDist* and *Screw*. The 2 DOF joint, used for modeling bending of the stick coincides with the origin of the frog segment (defined by *Frog* marker). The orientation of the stick segment relative to the frog is determined by the *Tip* marker. The two calibration markers *Frog* (frog segment) and *TipHair* (stick segment) indicate the positions of the hair terminations at the frog and tip. The orientation of the bow is indicated by the basis vectors ($\hat{\mathbf{x}}_b$, $\hat{\mathbf{y}}_b$, $\hat{\mathbf{z}}_b$).

B. Position and orientation of the bow and the violin

The position and orientation of the violin and the bow were determined by fitting the kinematic models to the measured 3D marker positions using the kinematic fit facilities in the Vicon iQ software, and exported for further processing in Matlab.[32] The orientations (Euler angles) were converted to rotation matrices.[33] The rows of these rotation matrices correspond to the basis vectors of the local reference systems expressed in world coordinates.[34] These basis vectors were extensively used in the calculations of the bowing parameters, as will be shown in the following.

C. Calculation of bowing parameters

Having defined the local reference systems of the bow and the violin, the bowing parameters can be calculated based on these 6 DOF representations, instead of the 3D positions of individual markers. In Fig. 4 the geometric relations used for the calculation of bowing parameters is shown. The bow-string contact point P is defined as the intersection between the line corresponding to the (virtual) string (direction $\hat{\mathbf{y}}_v$) and the bowing plane BPP' (see App. A.1 for calculations). The point P' is the projection of P on the bow.

Bow-bridge distance is calculated as $\overrightarrow{VP}$, projected on the string direction, where V is the origin of the violin (marker *BridgeMid* at the top of the bridge, see Fig. 2)[35]

$$y_{bb} = (P - V) \cdot \hat{\mathbf{y}}_v \,. \tag{1}$$

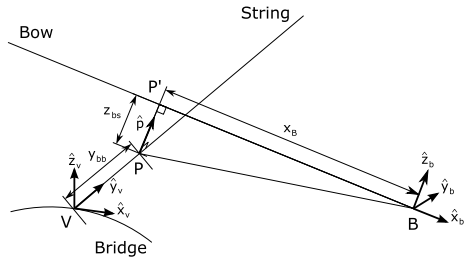

FIG. 4. Geometric relations for calculation of bow-string contact point, bow position (x_B), bow-bridge distance (y_{bb}) and bow-string distance (z_{bs}). The points indicated are the local origins of violin V (marker *BridgeMid* in Fig. 2) and bow B (marker *Frog* in Fig. 3), the contact point on the string (P) and its projection on the bow (P'). Unit vector $\hat{\mathbf{p}}$ is perpendicular to both the bow and the string. Also basis vectors of the local reference systems of the violin (subscript v) and the bow (subscript b) are indicated.

The bow-string distance (the distance of the bow above/below the string) is defined as

$$z_{bs} = (B - V) \cdot \hat{\mathbf{p}} \,, \tag{2}$$

where B is the origin of the bow (marker *Frog* at the ferrule, see Fig. 3) and $\hat{\mathbf{p}}$ the unit vector perpendicular to both the bow and the string.

Bow position (the distance between the contact point and the frog) is defined as

$$x_B = (B - V) \cdot \hat{\mathbf{x}}_b \,, \tag{3}$$

which corresponds to the distance between P' and B. It should be noted that the calculated distances above can become negative, as they are projections on non-static axes.

Regarding the basis vectors of the bow the kinematic model used offers the choice between the frog and the stick segment. Typically, the basis vectors of the stick are preferred for the calculation of the bowing parameters, because they correspond better to the line of the bow-hair ribbon when the stick is bent, and they can be measured more accurately (see Sect. III.G). However, in some cases it might be worthwhile to include the bending of the stick in the evaluation, e.g., for estimation of bow force. In such cases the basis vectors of the frog segment are more appropriate (see Sect. IV.C).

Bow velocity is defined as the velocity of the bow relative to the violin projected on the x-axis of the bow

$$v_B = \frac{\mathrm{d}\,(B - V)}{\mathrm{d}t} \cdot \hat{\mathbf{x}}_b \,. \tag{4}$$

Even if bow velocity can only be considered meaningful as a bowing parameter when the bow is in contact with the string, the above definition of bow velocity is more general and allows for studying anticipatory movements of the bow in the air, like in bouncing bowing techniques such as spiccato.

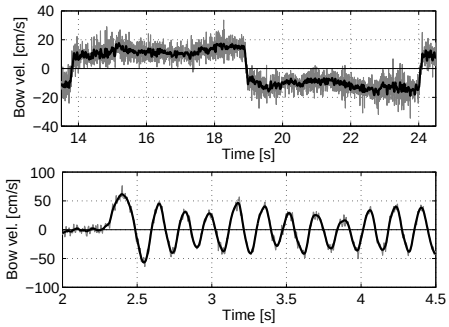

FIG. 5. Two examples of bow velocity signals before and after filtering using a second-order Butterworth filter (cut-off freq. 18 Hz). Top: Slow bowing (crescendo-decrescendo); bottom: Fast bowing (excerpt of N. Paganini, Caprice No. 5).

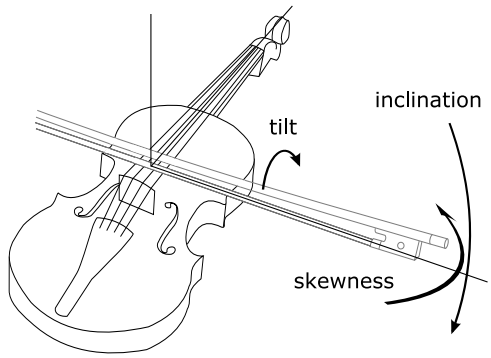

FIG. 6. Bow angles skewness (φ), inclination (ϑ) and tilt (ψ). The arrows indicate the positive direction according to the definitions.

For the numerical differentiation a central difference algorithm was used. The velocity signal can become rather noisy due to amplification-by-differentiation of the noise present in the measured positions. The quality of the velocity signals can be improved by low-pass filtering without loosing essential details. It was found that a second-order Butterworth filter with a cut-off frequency of 18 Hz (applied back-and-forth to avoid phase shift) effectively filtered the noise, while preserving the shape of the velocity profile in fast bowing (see Fig. 5).

It could be noted that Eq. (4) is theoretically similar to $v_B = \mathrm{d}x_B/\mathrm{d}t$, but it was found that the velocity signal was less noisy when differentiation was performed before taking the dot product. The explanation is that amplification of the noise introduced by $\hat{\mathbf{x}}_b$ due to differentiation is avoided in this way.

D. Calculation of bow angles

The three angles of the bow relative to the violin, *skewness* (φ), *inclination* (ϑ) and *tilt* (ψ), were defined in a way which reflect basic concepts in bowing, as shown in Fig. 6.[36]

Skewness is defined as the deviation of the bowing direction from orthogonality to the string. Considering angling the frog away from the player as the positive direction, it can be calculated as

$$\varphi = \frac{\pi}{2} - \arccos\left(\hat{\mathbf{y}}_v \cdot \hat{\mathbf{x}}_b\right) . \tag{5}$$

Inclination is the angle associated with playing different strings. Assuming the convention that inclination increases from the lower to the higher-pitched strings it can be expressed as

$$\vartheta = \arccos\left(\hat{\mathbf{z}}_v \cdot \hat{\mathbf{x}}_b\right) - \frac{\pi}{2} . \tag{6}$$

Tilting is used to change the contact properties of the bow hair with the string by controlling the effective width of the bow hair in contact with the string, and introducing a bow-force gradient across the width of the bow-hair ribbon. Here, tilt is defined as the angle between a plane parallel with the length axis of the bow ($\hat{\mathbf{x}}_b$) and the string ($\hat{\mathbf{y}}_v$), and a line with direction $\hat{\mathbf{y}}_b$. For convenience, the tilt direction used in classical playing with the stick turned towards the fingerboard is taken as the positive direction. Tilt is zero when the hair is flat on the string. The expression for tilt then becomes

$$\psi = \arccos\left(\frac{\hat{\mathbf{x}}_b \times \hat{\mathbf{y}}_v}{|\hat{\mathbf{x}}_b \times \hat{\mathbf{y}}_v|} \cdot \hat{\mathbf{y}}_b\right) - \frac{\pi}{2} . \tag{7}$$

E. Extending the instrument model

The geometrical model of the violin as described above features only one virtual string between the *BridgeMid* and *NutMid* markers. For a more complete definition of the violin model including four strings an additional calibration is needed. The string-crossing angles specific of an instrument can be obtained from a so-called *tuning trial*, in which the three double-string combinations (G-D, D-A and A-E) are played slowly using the whole bow (see Fig. 7). The string-crossing angles can then be calculated by taking the average inclination for each combination of strings. The standard deviations provide angular intervals, which can be useful for further feature extraction (see Sect. III.F). When double strings are played softly (*pp*) the inclination of the bow is rather constrained in order to make both strings speak properly. However, the measured standard deviation will to a certain extent depend on the skill of the player.

An important drawback of the one-string model is that the bow-string distance as calculated by Eq. (2) deviates from the actual value depending on which string is played. The dependence of the bow-string distance on bow inclination can be determined via slow, whole bow arpeggios across all four strings (Fig. 8). It was found that the relation was well described by a second-order polynomial. The coefficients obtained by a least-square

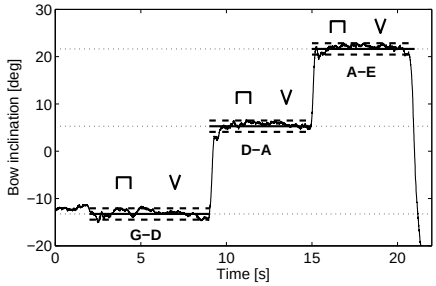

FIG. 7. Tuning trial used for the estimation of string-crossing angles (mean and st. dev.). The three double-string combinations (G-D, D-A, A-E) are played slowly down bow and up bow, using the whole length of the bow. The calculated mean values and 99% confidence bounds of the string-crossing angles are indicated by the horizontal lines.

fit can be used for improving the estimation of bow-string distance, as demonstrated in Fig. 8 (c).

Also the other actual distances (bow position and bow-bridge distance) can deviate from those calculated using the one-string model, and correction should be applied when an exact estimate is required. Regarding bow-bridge distance, a non-zero skewness of the bow results in a deviation of the calculated contact point along the string depending on which string is played. For example, at a skewness angle of ten degrees the deviation of bow-bridge distance amounts to about 2.5 mm for the outer strings. As skewness angles of this order can be observed in certain playing situations (see, e.g., Ref.23) compensation might be needed, using knowledge of which string is played (see Sect. III.F).

Given the specific string-crossing angles, the positions of the four strings relative to the local reference system of the violin can be determined when the distances between the adjacent strings are known (see App. A.2). For most violins the separation between the strings at the bridge is about 11 mm. The calculated (or measured) string positions may be used as alternative origins for the calculation of bowing parameters, removing the need for additional corrections. However, a serious drawback of the use of multiple origins in the calculations is the presence of discrete jumps at the moments of string crossings, causing artifacts in, e.g., calculated bow velocity. Furthermore, the choice of the origin is dependent on the, sometimes uncertain, decision of which string is played. In the following the one-string model is therefore preferred, applying corrections afterward when necessary.

F. Feature extraction

With the use of the calculated bowing parameters and the bow-instrument model, extraction of performance features such as bowing direction, string contact and string played becomes straightforward.

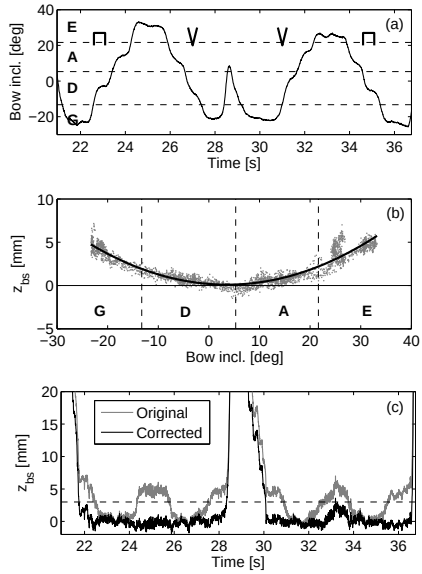

FIG. 8. Open-string arpeggios (played down bow, up bow and reversed) used for the estimation of bow-string distance correction parameters. (a) Inclination of the bow versus time. The inclination ranges corresponding to the four strings are indicated by their pitches. (b) Bow-string distance as calculated by Eq. (2) versus bow inclination and fitted parabola; (c) estimated bow-string distance (corrected and uncorrected). The dashed line indicates a possible threshold for the determination of bow-string contact.

Bowing direction (up bow, down bow) is simply determined by the sign of the bow velocity (down bow for positive and up bow for negative velocity). For detection of zero bow velocity a threshold is needed (about 1-1.5 cm/s with the current setup), taking the noise fluctuations into account. Further, it might be desirable to set the bowing direction to zero when the bow is not in contact with the string, as bowing direction has no meaning in that case.

To determine if the bow is in contact with the string a threshold criterion is applied to the corrected bow-string distance. A threshold in the range of 3-5 mm above the string gave satisfactory results in most cases (dashed horizontal line in Fig. 8 (c)). Additional criteria with regard to the relative position and orientation of the bow and the violin could be added to avoid possible misdetections.

The string played is determined by bow inclination (Eq. (6)). Also in this case a threshold method is used based on the specific string-crossing angles of the instrument. Detection of double-string playing is tricky, as this involves angular regions of finite width around the string-crossing angles. The width of the transition region is a trade-off between sharpness in the detection of string crossings and robust identification of double-string pas-

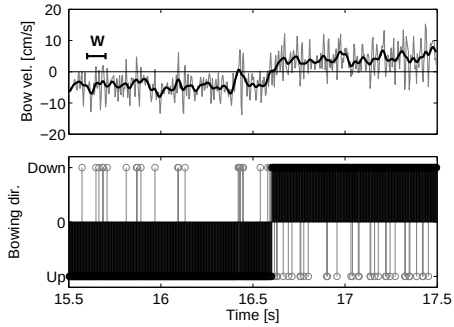

FIG. 9. Effect of a median filter with a window of 100 ms (indicated by W) on the detection of change in bowing direction. Top: Bow-velocity signal (unfiltered and low-pass filtered with a Butterworth filter, cut-off 18 Hz); bottom: Detected bowing direction (up/down) applied directly to unfiltered bow velocity signal (gray stems) and after median filtering (black stems).

sages. A useful way to define the width is based on the measured standard deviation of the string-crossing angles in the tuning trial. Preliminary tests indicated that at least a 99% confidence interval (obtained by multiplying the standard deviation by a factor 2.58) was needed for satisfactory identification of double stops.

A complicating factor in the detection of double string playing is that stopping of the string can significantly influence the actual string-crossing angle due to lowering of the string. The discrepancies are largest when one of the strings is open and the other stopped. This effect is not accounted for in the current model. Compensation would require knowledge of the distance between the string and the fingerboard and the fingering used by the player.

As all the above threshold methods are applied to more or less noisy signals there will be noise present in the detection results. This noise can be reduced by applying a running median filter with a time window in the order of the shortest expected note duration. The effect of such a filter is demonstrated in Fig. 9. It can be seen that small misdetections due to noise are effectively filtered out, while the moment when the bowing direction is reversed is preserved.

G. Accuracy assessment

1. Noise

Noise estimations were made from the slow four-string arpeggio (see Fig. 8). The RMS noise of each coordinate were calculated after filtering the slowly varying signals using a high-pass filter (Butterworth, order 4, cut-off 8 Hz). The noise distributions of the coordinates and angles were well described by a Gaussian distribution.

The RMS noise, averaged across markers and coordinates, are displayed in Tab. I. The RMS noise was well

TABLE I. Average noise RMS of the measured markers and the local origins and orientations of the fitted kinematic models. For the orientation of the frog segment the values for roll (rotation about the length axis) and the other Euler angles (yaw and pitch) are specified separately.

Model/segment	Average noise RMS		
	Markers [mm]	Local origin [mm]	Orientation [deg]
Bow/frog	0.47	0.38	0.64/0.25
Bow/stick	0.32	n/a	0.05
Violin	0.34	0.21	0.10

below 0.5 mm, corresponding to peak-to-peak values of less than 3 mm. The RMS noise associated with the frog segment was somewhat larger, mainly due to the *Screw* marker, which was detected by less cameras as it was shadowed by the players hand. As expected, the noise in the positions of the origins of the fitted models was somewhat less. The RMS noise in the orientation (Euler angles[37]) of the violin was 0.1 degrees. For the frog segment of the bow distinction was made between roll (rotation about the length axis of the bow, roughly corresponding to tilt) and the other Euler angles yaw and pitch (roughly corresponding to skewness and inclination, respectively). The first is more noisy due to the marker configuration for the bow: as the mounted antennas are short compared to the length of the frog segment (distance between *Stick* and *Screw*) the rotation about the length axis is more sensitive to noise in marker positions. For the stick segment only the noise in yaw and pitch was considered, as the roll is constraint to the orientation of the frog segment. The noise in the angles of the stick segment was much lower compared to the frog segment, the reason being that they are based on data from the entire length of the bow. Due to the lower noise content the orientation of the stick segment is preferred to the frog segment for the calculation of bowing parameters.

Table II indicates how the noise in position and orientation is propagated to the calculated bowing parameters. As tilt is associated with roll (rotation about the length axis of the bow) it is more noisy than the other bow angles. The noise RMS of the relative distance measures remained below 0.5 mm. For clarity the peak-to-peak noise is also displayed, which can be obtained by multiplying the RMS value by a factor 6.18 (99.9% interval of the noise distribution).

In order to assess a possible influence of bow velocity on the accuracy of marker positions, the distance between the *Stick* and the *Screw* markers on the bow was analyzed in a highly dynamic trial with bow velocities of more than 2 m/s and accelerations of 60 m/s^2 (a semi-quaver passage in Preludio of the third Partita for solo violin, J.S. Bach). No systematic relation was found between marker distance and bow speed. The total (unfiltered) noise RMS of distance was 0.77 mm (cf. 0.94 mm for the distance between the same markers in the arpeggio trial used in Tab. I). These results indicate that marker

TABLE II. Average noise RMS and peak-to-peak values of the bow angles tilt, inclination and skewness and distances between the bow and the violin.

Bowing parameter	RMS	peak-to-peak
Tilt [deg]	0.64	4.0
Inclination [deg]	0.17	1.0
Skewness [deg]	0.08	0.5
Bow pos. [mm]	0.36	2.2
Bow-bridge dist. [mm]	0.46	2.8
Bow-string dist. [mm]	0.31	1.9

TABLE III. Fit results with 95% confidence bounds of bow-bridge distance tests. The linear fit model was $y = b_1 x + b_0$, with x the set bow-bridge distance and y the measured bow-bridge distance.

Bow pos.	b_1	b_0 [mm]	R^2
Middle	1.0 (0.97, 1.03)	−0.3 (−1.3, 0.7)	0.9994
Tip	1.0 (0.95, 1.02)	0.3 (−0.8, 1.3)	0.9994

positions could be accurately measured even for extreme bow velocities and accelerations.

2. Bow-bridge distance

As there is some degree of uncertainty in the placement of the calibration markers on the violin and bow, there might be a systematic error in the measured bow-bridge distance. To investigate the magnitude of the systematic errors, static trials were performed using a test bench equipped with a ruler. The dimensions and marker configuration of the test bench were similar to those of the violin.

Static trials were performed for six bow-bridge distances (0-5 cm in steps of 1 cm) and two bow positions (middle and tip). Bow-bridge distance was set with respect to the middle of the bow hair ribbon, corresponding to the placement of the calibration markers. The fit results of measured bow-bridge distance versus set bow-bridge distance are displayed in Tab. III. Only minor, non-significant offsets were found, indicating that the systematic error could be neglected, provided that the calibration markers are carefully positioned. The (human) error in positioning the latter was estimated to be about 0.5 mm.

Another error in measured bow-bridge distance during playing arises from bow tilt. When the bow is tilted, the center line of the part of the bow-hair ribbon which is in actual contact with the string, will deviate from the bow-hair line in the model. The deviation is dependent on tilt angle and bow force. In an extreme case with a tilt angle of 45 degrees and a very low bow force (one hair in contact with the string) the deviation can reach about 3.5 mm. However, under normal playing conditions the deviation will be smaller than 1 mm in most cases.

All the errors discussed above are small compared to the width of the bow hair ribbon (8-10 mm), which forms a fundamental uncertainty in the determination of bow-bridge distance.

IV. MEASUREMENT OF ACCELERATION AND BOW FORCE

Sensors were attached to the bow for measuring bow acceleration and bow force. The data obtained via motion capture and sensors could be considered complementary. For example, the signal-to-noise ratio of the second derivative of position data is usually rather poor and requires a fair amount of smoothing. The accelerometer signal contains much finer details, and is therefore preferred in studies of transients, e.g. during changes of bowing direction (bow changes). One the other hand, the advantage of motion capture systems to measure position and orientation of objects accurately can be used in calibrating the accelerometer and other sensors. In addition, this gives a possibility to correct the sensor signals for influence of external conditions like gravity and bow tilt. In this section it will be explained how the combination of motion capture and sensors was exploited to obtain reliable, quantitative data from the sensors.

A. Acceleration

1. Calibration and correction

Besides measuring the actual bow acceleration, the accelerometer was sensitive to the inclination of the bow due to the influence of gravity. As the inclination θ (in world coordinates) is measured by the motion capture system this information can be used to (1) calibrate the accelerometer, and (2) remove the gravity component ($a_0(\theta) \approx -9.81 \sin\theta$ m/s^2) from the acceleration signal. The calibration was performed by rotating the bow slowly, varying the inclination of the two accelerometer axes ($\hat{\mathbf{x}}_b$ and $\hat{\mathbf{z}}_b$). The calibration coefficients (gain k and offset s_0) needed to convert the accelerometer signal s to acceleration was found by fitting

$$s = \frac{a_0(\theta)}{k} + s_0 \,.$$

The calibrated bow acceleration a including the correction for inclination is then calculated as

$$a = k(s - s_0) - a_0(\theta) \,.$$

2. Illustration and comparison with motion capture acceleration

The correction of the bow acceleration signal is illustrated in Fig. 10, showing sustained loud notes played on the four strings. The bow inclination (bottom) starts at a high value for the E string and approaches zero (horizontal) for the G string. The correction for inclination in the accelerometer data (middle) is about 7 m/s^2 for the E string and almost zero for the G string.

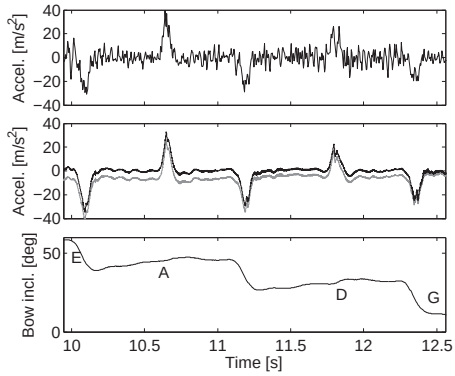

FIG. 10. Illustration of the correction of bow acceleration for inclination. Long sustained notes are played on the four strings (E A D G). The accelerometer is sensitive to bow inclination θ due to the influence of gravity, $a_0(\theta) = -9.81 \sin\theta$. The inclination measured with the motion capture system was used for correcting the acceleration. Top: Acceleration computed from the bow velocity obtained by motion capture; middle: Calibrated accelerometer signal without correction (gray) and with correction for inclination (black); bottom: Bow inclination (in world coordinates).

For comparison, the bow acceleration as computed from the bow velocity measured with the motion capture system (low-pass filtered, cut-off 18 Hz) is included (top). The loss in details is evident. In particular, the accelerometer signal provides more details at the peaks corresponding to the bow changes. The bow change actually gives rise to double acceleration peaks which merge in the smoothed acceleration signal provided by motion capture. The loss in detail is due to the combined effect of several factors, including a lower sampling frequency (250 Hz), the spatial resolution of the optical system, and the smoothing filter. The benefit of combining the motion capture system with an accelerometer is particularly obvious in cases like this, offering a higher time resolution of rapid changes.

3. Computing bow velocity from acceleration

Calculation of bow velocity from acceleration over a longer time span is typically problematic due to the presence of drift in the integrated signal. The correction for inclination described above improves the situation somewhat, but drift cannot be completely compensated for. A possible solution, proposed by Schoonderwaldt et al.[38] is to apply piece-wise integration of the acceleration signal between breakpoints where the bow velocity is known to be zero (bow changes) and remove the linear trends (drift) between the break points to obtain a continuous signal.

The quality of the computed velocity signal is primarily dependent on the density of breakpoints and the smoothness of the acceleration signal. The method is rather sensitive to small time deviations of the detected breakpoints, especially for quick bow changes characterized by peak-like accelerations. Further, movements of the violin might cause discrepancies as the accelerometer measures the acceleration of the bow relative to the world coordinate system, not to the instrument. For these reasons the computation of velocity is generally more reliable in faster passages, as illustrated in Fig. 11.

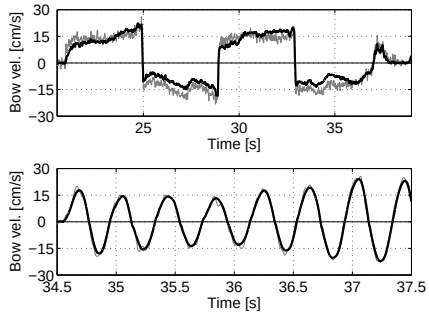

FIG. 11. Computed bow velocity signals obtained by piecewise integration of bow acceleration between bow changes for sequences of whole notes (top) and semi-quavers (bottom). The gray curves show bow velocity obtained by motion capture.

B. Bow force

1. Calibration procedure

The bow force sensor registers the deflection of the bow hair at the frog. The deflection is dependent on bow force as well as bow position. Typically, the deflection decreases when the contact point approaches the tip at a constant bow force. This effect needs to be compensated for in the calibration.

The calibration of the bow force sensor was performed using a calibrated load cell mounted on a small wooden board, which was held by the player in a violin-like manner (see Fig. 12). The player was asked to hold the bow as normal with the hair flat on the load cell (no tilt), and perpendicular to the measuring direction of the cell. The player pressed the bow against the load cell at ten equally spaced positions from the frog to the tip, modulating the force at each position.

The position and orientation of the bow and the calibration board was tracked with the motion capture system, allowing for calculation of bow position and angles in a similar way as for the violin. The bow position was used for the calculation of the calibration coefficients. The measured bow angles were used to check if the calibration was performed correctly, as these might influence the quality of the calibration (see Sect. IV.B.2). For a detailed description of the calibration of the bow force sensor and computation of bow force, see App. B. As

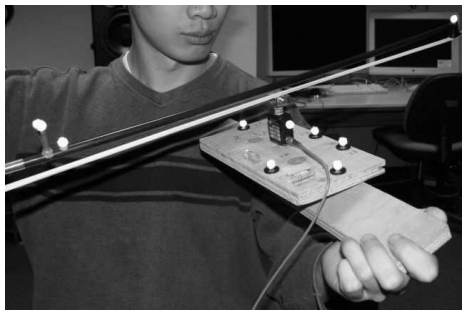

FIG. 12. Load cell mounted on wooden board used for bow force calibration. Bow position is obtained by motion capture.

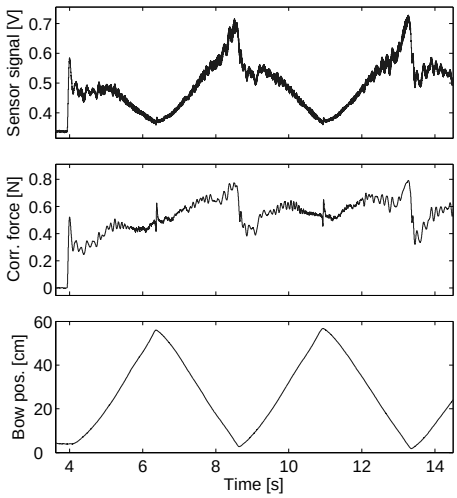

FIG. 13. Illustration of bow force calibration and correction for bow position. Long notes were played using the whole length of the bow. Top: Uncalibrated force sensor signal; middle: Calibrated bow force; bottom: Bow position obtained by motion capture.

the calibration coefficients will slightly change over time due to changes in bow hair tension, the calibration procedure needs to be repeated at regular intervals during longer sessions.

An example of a calibrated bow force signal is shown in Fig. 13 for long notes played using the whole bow, with a rather constant bow force. It can be clearly seen that the uncalibrated force sensor signal (upper panel) decreases when approaching the tip. This is effectively compensated for in the calibrated bow force (middle panel).

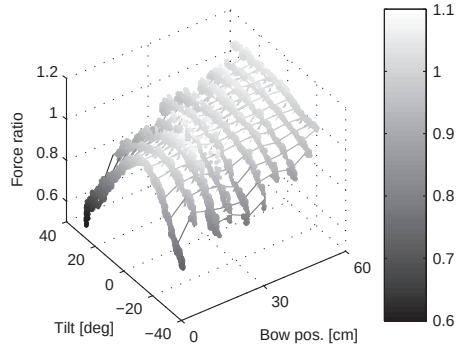

FIG. 14. The bow pressure sensor is sensitive to the bow tilt. For determining this influence, the bow was pressed against a load cell at ten positions along the bow, and tilted at different angles. The resulting ratio between the measured force (after calibration) and the actual bow force according to the load cell is plotted versus bow position and tilt angle. The interpolated surface can be used to compensate for the influence of tilt.

2. *Influence of bow tilt*

In many situations players tilt the bow for obtaining a lighter contact of the hair on the string, especially close to the frog. As a result the amount of bow hair in contact with the string is decreased, giving the player a finer control of bow force due to the increased compliance of the bow.

The force measured by the sensor is influenced by the bow tilt in two ways. First, the transversal force exerted by the bow on the string is no longer normal to the bow force sensor. Second, there will be a force gradient across the width of the bow hair ribbon, resulting in a non-uniform deformation of the leaf spring of the sensor. As a result, the measured bow force will deviate from the actual bow force.

For assessing the influence of bow tilt a test was performed, pressing the bow on the load cell with an approximately constant force and slowly tilting the bow back and forth (about ± 30 degrees). The bow force was computed using the calibration coefficients obtained from a normal force calibration.

In Fig. 14, the ratio between the measured bow force and the actual bow force measured by the load cell is plotted versus bow tilt at ten equally spaced positions along the bow. As could be expected, the discrepancy was largest close to the frog, where bow force measured by the sensor was underestimated by about 40% at a tilt angle of 30 degrees. Towards the tip, the effect of the tilt diminished giving a deviation of about 20% at the middle and 5% at the tip. The deviation was not entirely symmetric with respect to tilt direction; the deviation tended to be slightly less for negative angles (stick leaning towards the bridge) than for positive angles. This asymmetry can be due to variations in the tension of individual bow hairs, and the placement of the sensor or

the bearing piece between the sensor and the bow hair.

As the effect of tilting on measured bow force showed a regular behavior, it can be compensated for. This is illustrated in Fig. 15 for two positions close to the frog and the tip, respectively. The correction factor was obtained by interpolation of the force ratio data (surface in Fig. 14).

C. Reconstruction of bow force from motion capture data

1. Principle

The data collected in this study was used to evaluate the possibility to reconstruct bow force from motion capture data as suggested by Maestre et al.[22]

When the bow is pressed against the string the reaction force F_B causes two visible effects: (1) deflection of the bow hair, (2) bending of the stick. Deflection of the hair results in a distance d_{stick} between the actual bow-string contact point and the straight line between the frog and the tip (x-axis of the stick segment), given by

$$d_{stick} = \frac{\gamma(1-\gamma)L}{T} F_B \,, \tag{8}$$

where γ is the normalized bow position ($\gamma = x_B/L$), L the length of the bow hair, and T the effective tension of the bow-hair ribbon.

Bending of the stick can be measured as the angle between the x-axes of the stick and the frog segment in the kinematic model of the bow (see Sect. III.A). The amount of bending depends on the transversal stiffness K_b of the bow stick. The combined effect of the hair deflection and stick bending results in a distance d_{frog} between the actual bow-string contact point and the x-axis of the frog segment

$$d_{frog} = \left(\frac{\gamma(1-\gamma)L}{T} + \frac{\gamma^2}{K_b} \right) F_B \,. \tag{9}$$

In addition, the string is deflected under influence of bow force. The bow-string distance z_{bs} calculated by Eq. (2), with $\hat{\mathbf{x}}_b$ the x-direction of the frog segment will include contributions from all three effects, which means that motion capture data could in principle be used to calculate bow force. This possibility will be further explored in the following.

A detailed description of the calibration and reconstruction of bow force using the string-distance method is provided in App. C.1. The influence of string deflection on the reconstructed bow force is explained in App. C.2.

2. Force reconstruction and comparison with the bow force sensor

For illustration of the reconstruction of bow force from motion capture data and comparison with the results obtained by the bow force sensor an experiment was conducted. A small wheel was mounted on the facing of the load cell. Short bow strokes were played on the wheel, using about 10 cm of the bow near the frog and at the tip, respectively. The load cell gave a calibrated reference signal, which was compared with the reconstructed bow force using bow-string distance data, and the output of the bow force sensor after calibration (see Fig. 16). As the reconstructed force signal was rather noisy, a low-pass, zero-phase filter with a cut-off frequency of 5 Hz was applied.

As seen, the bow force sensor provided a good description of the actual bow force. The sensor signal followed the load cell signal well, including a high degree of detail. The bow force reconstructed from motion capture data was rather noisy and did not reproduce the same amount of details. At best, it gave a reasonable overview of the bow force, following the slow, global variations, which may be sufficient for certain purposes, e.g. in some types of synthesis control.

V. DISCUSSION

A. Example

An illustration of the capability of the described system is given in Fig. 17 showing a complete set of bowing parameters in a solo violin performance. The combined panels provide a complete overview of the relevant aspects of bowing, including bow distribution (bow position), the use of the main bowing parameters (bow velocity, bow-bridge distance, bow force and bow acceleration) and secondary control parameters (bow angles tilt and skewness). The bottom panel combines the extracted features 'string played' and 'bowing direction,' showing the choices of the player and providing a rudimentary link to the score. Analyses of an extended collection of violin and viola performances using the described system will be reported elsewhere.

B. Calculation of bowing parameters using kinematic models

In the described method the calculation of bowing parameters is based on fitted kinematic models of the violin and bow (position and orientation of segments), rather than on individual marker positions. This approach gives two important advantages. First, the calculated bowing parameters become less sensitive to noise and gaps in the marker trajectories. Second, the use of kinematic models allows for a general geometric definition of bowing parameters and bow angles, as described in Sect. III.

The current work relied on kinematic fit facilities implemented in Vicon software (Vicon iQ), but the described methods can be generalized to other motion capture systems, both optical (active and passive) and electromagnetic field tracking (e.g., Polhemus[39]). For motion capture systems measuring 3D positions of markers alternative kinematic fit methods could be used, e.g., the least-square method described by Veldpaus et al.[29]

The kinematic models and calculations described in this study are specific to the violin and the viola. For measurement of cello and double bass bowing the same

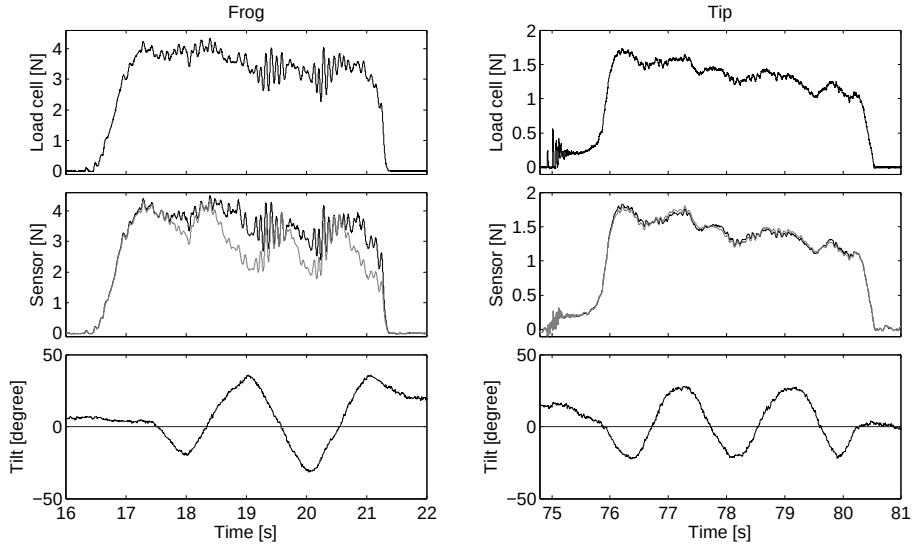

FIG. 15. Illustration of the correction for influence of tilting on bow force. The surface in Fig. 14 is used for interpolating correction factors for tilt. Top: Actual bow force measured by the load cell; middle: Calibrated signal from the bow force sensor without correction (gray), and with correction for bow tilt (black); bottom: Tilt angle. The correction for influence of tilt is more important at the frog (left) than at the tip (right).

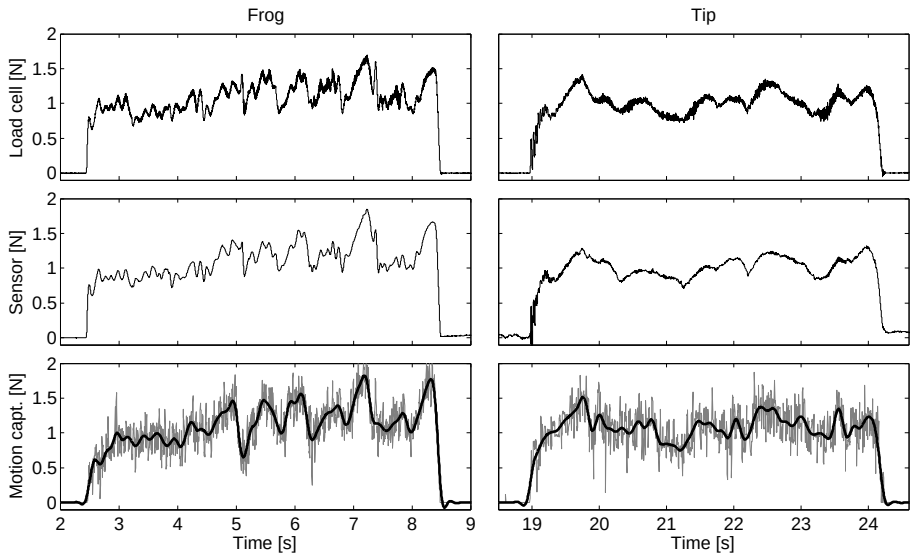

FIG. 16. Comparison of bow force data measured by the bow force sensor and reconstructed force from motion-capture data. The bow is moved back and forth on a small wheel mounted on a load cell, near the frog (left) and near the tip (right). Top: Reference signal measured by the load cell; middle: Calibrated force signal from the bow force sensor; bottom: Reconstructed bow force using motion-capture data on bow-string distance, unfiltered (gray) and low-pass filtered (black).

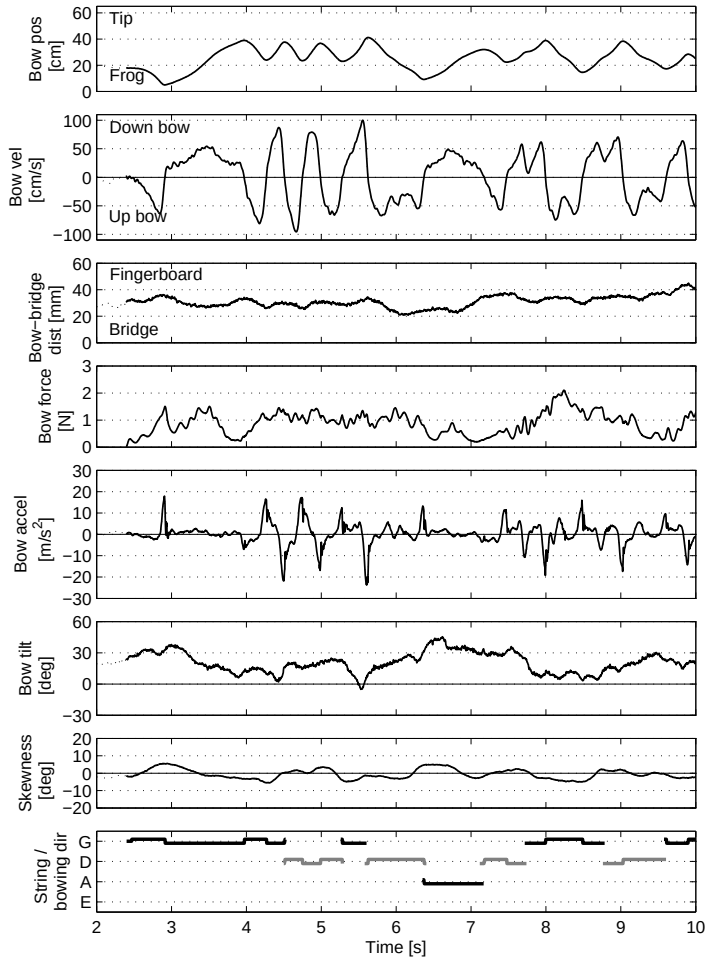

FIG. 17. Example of a full set of bowing parameters versus time measured with the described system. The musical fragment consisted of the first 1 1/2 bars of the Allemande of the 2nd Partita for solo violin by J. S. Bach. The bowing parameters shown, from top to bottom, are: *bow position*, *bow velocity*, *bow-bridge distance*, *bow force*, *bow acceleration*, the bow angles *tilt* and *skewness*, and the combined features *string played* (vertical position) and *bowing direction* (vertical offset, positive for up bow and negative for down bow).

principles can be applied, but some adaptations are necessary due to the reversed orientation of the bow relative to the instrument.

C. Combination with sensors

The complementary nature of motion capture techniques and the use of sensors attached to the bow offers several advantages. First, it provides practical and accurate calibration procedures for both acceleration and bow force. Second, it allows for correction of the influence of bow inclination on acceleration (gravity component in accelerometer signal), as well as for the influence of tilt on bow force.

In Sect. IV.A a procedure was discussed for computation of bow velocity from acceleration. The advantage is that the integrated velocity profiles offer more detail and a higher temporal resolution compared to those obtained from motion capture data, mainly due to the smoothing required to obtain acceptable noise levels. However, the reliability of the computed velocity signal is somewhat limited, and normally bow velocity obtained from motion capture data is preferred. Using the accelerometer signal for estimating bow velocity may, however, form an interesting alternative in combination with less expensive

motion tracking techniques based on normal video.[38]

D. Measurement of bow force

Bow force could be accurately measured with the force sensor over the whole length of the bow. The bow force tended to be underestimated when the bow was tilted, especially close to the frog. However, it was shown that this effect could be compensated for, given the amount of tilt measured with the motion capture system.

An alternative method for bow force reconstruction entirely based on motion capture data proposed by Maestre et al.[22] was explored and compared with sensor-based measurement of bow force. The proposed method gave reasonable force reconstructions in the upper half of the bow where the bending of the stick under influence of bow force is considerable. In the lower half the reconstruction became less reliable, mainly because the change in bow-string distance due to bending of the bow is much smaller and harder to estimate reliably. Further complications are due to the deflection of the string under influence of bow force and stopping of the string. These deviations are, however, small and close to the spatial resolution of the motion capture system, and therefore hard to take into account.

The two methods for determination of bow force could to a certain extent be considered as complementary: the sensitivity of the sensor is highest in the lower part of the bow, as opposed to the motion-capture-based force, which is most reliable in the upper part. In some cases, depending on the properties of the bow or incorrect placement of the bow force sensor, problems might be experienced with the determination of bow force from the sensor when approaching the tip. In such cases the motion-capture-based bow force could be used to replace the sensor-based bow force in the upper part of the bow.

E. Applications

The described methods for determination of bowing parameters allow for detailed measurement of bowing gestures and in-depth analysis of players' control and coordination of bowing parameters, set in relation to the produced sound. In addition, motion capture can be extended to include body movements of the player, allowing study of biomechanical aspects of playing, anticipatory movements and the influence of posture. This type of studies will deepen our understanding of bowed-string instrument performance, not only from a scientific point of view but also from the player's perspective. Especially in combination with effective visualizations, motion capture and other measurement techniques have interesting potential for pedagogical use.[9,40–43] Another promising application is gesture-based sound synthesis, where this type of measurements will be helpful in the development of parametric control models.[44–46]

VI. CONCLUSIONS

In this study motion capture techniques have been applied to build a complete system for measurement of bowing parameters in violin playing. Kinematic models for the violin and bow have been developed which can be used to calculate the main bowing parameters, bow position, bow velocity, and bow-bridge distance. In addition, the angles of the bow relative to the violin, inclination, skewness and tilt, which do not control the sound generation directly, but reflect the pre-planning and coordination of parameters in bowing gestures are measured.[47] Bow force is measured with a custom-designed sensor, integrated with the frog, allowing for accurate measurement of bow force in combination with motion capture data. Bow acceleration is measured in two directions with an accelerometer mounted on the frog, allowing for detailed study of transients during bow changes or attacks.

In addition, the system allows automatic extraction and visualization of three basic performance features; bowing direction, moments of on/off in bow-string contact, and determination of which string is played. These features are necessary for musically relevant analyses of bowing parameter data. Such analyses will give an understanding of how a certain bowing gesture is composed from basic elements of motion, and allow comparison of bow control strategies between players.

An interesting approach for estimation of bow force from motion capture data describing the bending of the bow stick is explored, and compared with measurements by use of the bow force sensor.

The described system is capable of measuring all bowing parameters in violin performance without disturbing the player. The system is robust, and accuracy and signal quality are high. In combination with the extracted features, the system allows for detailed studies of musically relevant aspects of bow control and coordination of bowing parameters in bowed-string instrument performance.

Acknowledgments

This work was partly supported by the Swedish Science Foundation (contract 621-2001-2537) and the Natural Sciences and Research Council of Canada (NSERC-SRO). The bow force sensor was developed as part of the CONSONNES project, funded by the French Agence Nationale pour le Recherche. The collaboration was stimulated by two short-term scientific missions (Erwin Schoonderwaldt at IRCAM, Paris; Matthias Demoucron at IDMIL, McGill University, Montreal) funded by the Cost 287-ConGas action. Important part of the work was realized at IDMIL, McGill University, Montreal. Part of the work was performed during Matthias Demoucron's stay at the Dept. of Speech, Music and Hearing, Royal Institute of Technology (KTH), Stockholm supported by the Swedish Institute. Special thanks go to Emmanuel Fléty and Alain Terrier for their valuable help in developing the sensors, Nicolas Rasamimanana and Frédéric

Bevilacqua with whom this work has been initiated, Marcelo M. Wanderley for his inspiring support and advice, and Lambert Chen for his invaluable contribution as a violin and viola player.

APPENDIX A: GEOMETRIC CALCULATIONS

1. Calculation of contact point

The contact point P in Fig. 4 was determined as follows.

The unit vector perpendicular to both the bow and the string, was calculated as

$$\hat{\mathbf{p}} = \frac{\hat{\mathbf{x}}_b \times \hat{\mathbf{y}}_v}{|\hat{\mathbf{x}}_b \times \hat{\mathbf{y}}_v|} .$$

The normal vector of the bowing plane was then calculated as

$$\hat{\mathbf{n}}_b = \hat{\mathbf{x}}_b \times \hat{\mathbf{p}} .$$

Subsequently, the intersection P between the virtual string

$$\begin{pmatrix} x \\ y \\ z \end{pmatrix} = \lambda \hat{\mathbf{y}}_v + V$$

and the bowing plane

$$\hat{\mathbf{n}}_b \cdot \left[\begin{pmatrix} x \\ y \\ z \end{pmatrix} - B \right] = 0$$

can be found by solving λ:

$$\lambda_P = -\frac{\hat{\mathbf{n}}_b \cdot (V - B)}{\hat{\mathbf{n}}_b \cdot \hat{\mathbf{y}}_v} .$$

The contact point P on the string is then given by

$$P = \lambda_P \hat{\mathbf{y}}_v + V . \tag{A1}$$

2. Calculation of string positions

Given the string-crossing angles, obtained from the tuning trial and the measured inter-string distances, the positions of the four strings on the bridge can be calculated in local coordinates (Fig. A1). The inter-string distance d_s is usually the same for all adjacent strings on an instrument, typically about 11 mm for violins.

In the local reference system of the violin the bridge is located in the x-z plane ($y = 0$). The rotation matrix for a rotation about the y-axis by an angle ϑ is

$$R(\vartheta) = \begin{bmatrix} \cos\vartheta & 0 & -\sin\vartheta \\ 0 & 1 & 0 \\ \sin\vartheta & 0 & \cos\vartheta \end{bmatrix} .$$

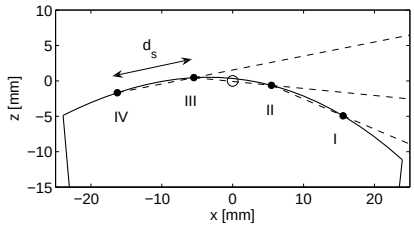

FIG. A1. Calculated positions on the bridge of the four strings in the local reference system of the violin, based on string-crossing angles (dashed lines) and inter-string distance d_s.

For the two inner strings II and III (A and D on the violin) the positions are calculated as

$$p_{II} = R^T(\vartheta_2) \cdot \begin{pmatrix} d_s/2 \\ 0 \\ z_{bs} \end{pmatrix}$$

and

$$p_{III} = R^T(\vartheta_2) \cdot \begin{pmatrix} -d_s/2 \\ 0 \\ z_{bs} \end{pmatrix} ,$$

where ϑ_2 the string-crossing angle between string II and III and z_{bs} the bow-string distance offset associated with ϑ_2 (see Sect. III.E). The positions of the outer strings I and IV (E and G on the violin) are then calculated as

$$p_I = p_{II} + R^T(\vartheta_1) \cdot \begin{pmatrix} d_s \\ 0 \\ 0 \end{pmatrix}$$

and

$$p_{IV} = p_{III} + R^T(\vartheta_3) \cdot \begin{pmatrix} -d_s \\ 0 \\ 0 \end{pmatrix} ,$$

where ϑ_1 and ϑ_3 the string-crossing angles of string combinations I-II and III-IV, respectively.

APPENDIX B: CALIBRATION OF BOW FORCE SENSOR

The coefficients needed for the calibration of bow force are obtained from a force calibration trial (see Sect. IV.B.1) in two steps. In the first step, a second order polynomial is fitted to the curves representing the sensor response s_f (in V) versus the transversal force F_t (in N) measured by the load cell for each of the ten bow positions x_i (see Fig. B1 (a)):

$$s_f = b_2(x_i)F_t^2 + b_1(x_i)F_t . \tag{B1}$$

From theoretical considerations regarding the mechanics of the bow,[28] a quadratic and a linear dependence on bow position is expected for b_2 and b_1, respectively. In the second step, curves are fitted to the coefficients found for the discrete positions x_i, yielding functional expressions for b_2 and b_1 (solid lines in Fig. B1 (b) and (c)). Using the bow position x_B obtained via motion capture, the bow force can then be calculated as

$$F_B(x) = \frac{-b_1(x) + \sqrt{b_1(x)^2 + 4b_2(x)s_f}}{2b_2(x)}\,. \tag{B2}$$

APPENDIX C: BOW FORCE RECONSTRUCTION FROM MOTION CAPTURE DATA

1. Calibration

A calibration is needed to relate bow-string distance (i.e., the distance between the virtual contact point and the line in the x-direction of the frog) to bow force at any bow position. The calibration can be performed using the same calibration trial as for the calibration of the force sensor (see Sect. IV.B.1). The distance between the contact point and the frog line can be calculated in a similar way as for the violin. As the load cell is rather stiff the distance between the contact point and the frog line is determined entirely by the deflection of the bow hair and the bending of the stick.

Similar as in App. B the calibration consists of two steps. In the first step a straight line is fitted to bow-string distance as function of force F_t measured by the load cell for each of the ten bow positions (see Fig. C1 (a))

$$d = b_1 F_t + b_0\,, \tag{C1}$$

This corresponds to Eq. (9), which predicts a linear dependence of d on bow force at fixed bow position. Using Eq. (9), b_1 can be expressed as function of (normalized) bow position γ ($\gamma = x_B/L$; L is the length of the bow hair) as

$$b_1(\gamma) = \frac{\gamma L}{T} + \gamma^2\left(\frac{1}{K_b} - \frac{L}{T}\right)\,, \tag{C2}$$

which means that b_1 is well described by a second-order polynomial (see Fig. C1 (b)). It should be noted that according to Eq. (C2) b_1 becomes zero at the frog, indicating that the measurement of bow force using this method becomes problematic close to the frog.

The constant b_0 represents an offset of the measured bow-string distance, which can be attributed to an offset angle between the x-axes of the frog and the stick segments in the kinematic model of the bow (such an angular offset might originate from changed bow hair tension since the calibration of the kinematic model of the bow). The offset b_0 is linearly dependent on bow position (see Fig. C1 (c)). Even for small angles, in this case 0.3 degrees, the offset can have a significant influence on the reconstructed bow force, and should therefore be taken into account in the calibration.

Given the calibration coefficients the bow force can be calculated as

$$F_B = \frac{d - b_0(\gamma)}{b_1(\gamma)}\,, \tag{C3}$$

ignoring the deflection of the string (see App. C.2 for a discussion of the influence of string deflection).

When the bow is not in contact with the string the calculated bow force becomes negative, which is unphysical. In this case the bow force should be set to zero (i.e., $F_B = 0$ for $d - b_0(\gamma) > 0$).

2. Influence of string deflection in reconstruction of bow force

The string is deflected due to the bow force. Because of the lowering of the string there will be a discrepancy $\delta(F_B)$ between the calculated contact point P (see App. A.1 and Fig. 4) and the actual bow-string contact point. Consequently, the reconstructed bow force obtained by Eq. (C3) will be overestimated, and a correction term should be added to the bow-string distance

$$d = d_{frog} + \delta(F_B)\,.$$

In combination with Eq. (C1) this can be written as

$$d - b_0 = b_1 F_B + \delta(F_B)\,.$$

The correction for string deflection $\delta(F_B)$ is not trivial to determine for a real string as it depends on β as well as the stiffness of the string. For a flexible string, an expression similar to Eq. (8) can be used to describe the string deflection, yielding

$$d - b_0 = b_1 F_B + \frac{\beta(1-\beta)L_s}{T_s} F_B = b_1' F_B\,, \tag{C4}$$

with T_s the string tension and L_s the string length. The corrected coefficient b_1' will be close to b_1 for small β values and increase with increasing bow-bridge distance. The correction will be larger for strings with low tension.

To estimate the influence of string deflection, test measurements were performed, similar to the force calibration procedure described earlier, but replacing the calibration device with a violin. The calibration procedure was performed on each of the four strings and at three bow-bridge distances (10, 30, 50 mm). The reference force was obtained from the bow force sensor, and the calibration coefficient b_1' was calculated as described in App. C.1.

Figure C2 shows the influence of string deflection on the gain factor $1/b_1'$ (for conversion from mm to N) for the G and the E string at three bow-bridge distances. The relative influence was largest close to the frog and tended to disappear when approaching the tip. This can be explained as follows. The absolute deviation caused

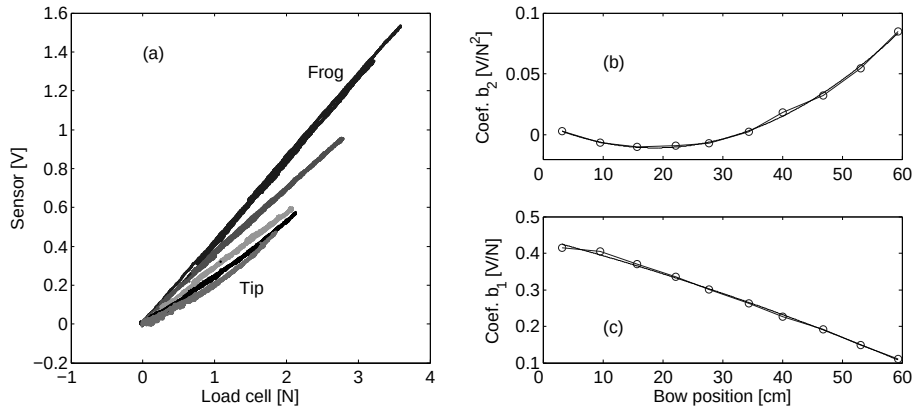

FIG. B1. The sensor is calibrated by pressing the bow hair on a load cell at ten equally spaced positions of the bow from the frog to the tip, and modulating the force periodically. (a) Resulting sensor signal s_f plotted versus reference force F_t measured by the load cell for different bow positions. (b) Quadratic and (c) linear coefficients obtained from second order polynomial fits for each bow position. The dependence of the coefficients on bow position can in its turn be described by second order polynomials (solid lines), yielding functional expressions for b_2 and b_1, used for calculation of bow force in Eq. B2.

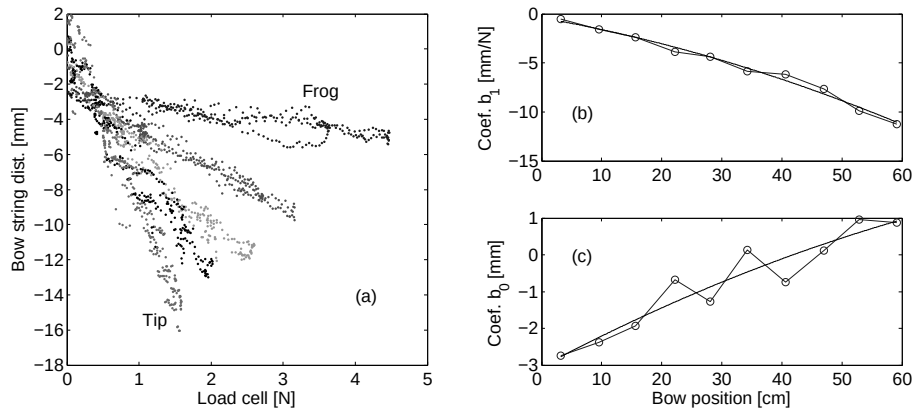

FIG. C1. The motion capture data on the bow-string distance can be used for determining the bow force. (a) Bow-string distance versus bow force measured by the load cell for different bow positions. (b) Linear and (c) constant coefficients obtained from linear fits for each bow position. The dependence of the coefficients on bow position can be described by a second order polynomial, yielding functional expressions for b_1 and b_0, used for calculation of bow force in Eq. C3.

by string deflection is only dependent on bow force. However, the *relative* influence becomes larger for small values of bow position (close to the frog) where the compliance of the bow is small. At the frog the effect on the reconstructed force can therefore be considerable. When using the calibration coefficients obtained from calibration with the load cell the reconstructed force at the frog will be overestimated. As an example, in this test the overestimation was about a factor two on the G string at a bow position of 5 cm and a bow-bridge distance of 53 mm.

An increase of b_1' with bow-bridge distance predicted by Eq. (C4) can also be observed. This results in flatter gain curves for larger bow-bridge distances. Furthermore, the curves are closer to each other for the E string than for the G string, indicating that string deflection is larger for the G string. This is in agreement with expectations based on the properties of the string: the tension of the lowest strings is generally lower than for the high strings (around 40 N for the G string versus 75 N for the E string, according to Pickering[48]).

Even though the effect of string deflection could be observed in the motion capture data, the effect was rather small and overshadowed by noise. It is therefore diffi-

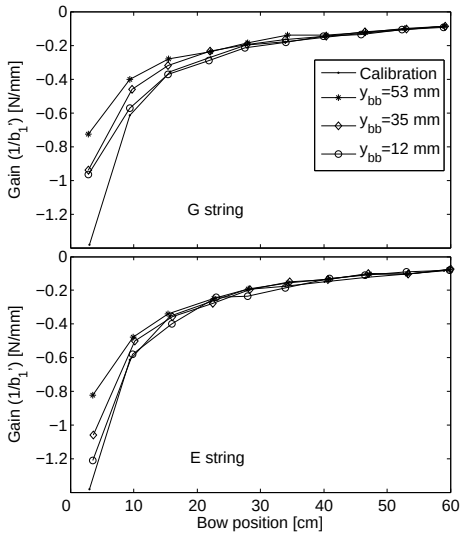

FIG. C2. Influence of bow-bridge distance on the gain factor $1/b_1'$ on (top) the G string and (bottom) the E string.

cult to take these effects into account in a calibration. In general, it can be concluded that the motion-capture method for reconstruction of bow force is less reliable in the lower half of the bow.

[1] W. Goebl and R. Bresin, "Measurement and reproduction accuracy of computer-controlled grand pianos", J. Acoust. Soc. Am. **114**, 2273–2283 (2003).

[2] C. Chafe, *Current directions in computer music research*, chapter Simulating performance on a bowed string instrument., 185–198 (MIT Press, Cambridge) (1989).

[3] D. Trueman, "Reinventing the violin", Ph.D. thesis, Princeton University (1999).

[4] C. Nichols, "The vBow – an expressive musical controller haptic human-computer interface", Ph.D. thesis, Stanford University, San Francisco (2003), URL `http://ccrma.stanford.edu/~cnichols/pdf/vBowDissertation2003.pdf`.

[5] M. S. O'Modhrain, "Playing by feel: Incorporating haptic feedback into computer-based musical instruments", Ph.D. thesis, Stanford University (2000), URL `http://ccrma-www.stanford.edu/~sile/thesis.html`.

[6] S. Serafin, "The sound of friction: real-time models, playability and musical applications", Ph.D. thesis, Stanford University (2004), URL `http://www.imi.aau.dk/~sts/serafinthesis.pdf`.

[7] A. Askenfelt, "Measurement of bow motion and bow force in violin playing", J. Acoust. Soc. Am. **80**, 1007–1015 (1986).

[8] A. Askenfelt, "Measurement of the bowing parameters in violin playing. II: Bow-bridge distance, dynamic range, and limits of bow force", J. Acoust. Soc. Am. **86**, 503–516 (1989).

[9] P. Hodgson, *Motion study and violin bowing* (American String Teachers Association) (1958).

[10] T. Machover, "Hyperinstruments – a progress report 1987-1991", Technical Report, MIT Media Laboratory (1992).

[11] D. Young, "The Hyperbow controller: real-time dynamics measurement of violin performance", in *Proceedings of the NIME-02 Conference on New Instruments for Musical Expression* (2002).

[12] N. Rasamimanana, E. Fléty, and F. Bevilacqua, *Gesture in Human-Computer Interaction and Simulation: 6th International Gesture Workshop, Revised Selected Papers*, chapter Gesture analysis of violin bow strokes, 145–155 (Springer Berlin / Heidelberg) (2006).

[13] J. A. Paradiso and N. Gershenfeld, "Musical applications of electric field sensing", Computer Music Journal **21**, 69–89 (1997).

[14] D. Young, "A system for understanding violin bowing technique through measurement of physical dynamics (abstract)", J. Acoust. Soc. Am. **119**, 3441 (2006).

[15] N. Rasamimanana, D. Bernardin, M. Wanderley, and F. Bevilacqua, "String bowing gestures at varying bow stroke frequencies: A case study (abstract)", in *Proceedings of Gesture Workshop 2007* (Lisbon, Portugal) (2007).

[16] D. Young, P. Nunn, and A. Vassiliev, "Composing for Hyperbow: a collaboration between MIT and the Royal Academy of Music", in *Proceedings of the 2006 International Conference on New Interfaces for Musical Expression (NIME06)* (2006).

[17] A. P. Baader, O. Kazennikov, and M. Wiesendanger, "Coordination of bowing and fingering in violin playing", Cognitive Brain Research **23**, 436–443 (2005).

[18] H. Winold, E. Thelen, and B. D. Ulrich, "Coordination and control in the bow arm movements of highly skilled cellists", Ecological Psychology **6**, 1–31 (1994).

[19] G. Shan and P. Visentin, "A quantitative three-dimensional analysis of arm kinematics in violin performance", Medical problems of performing artists **18**, 3–10 (2003).

[20] P. Visentin and G. Shan, "The kinetic characteristics of the bow arm during violin performance: an examination of internal loads as a function of tempo", Medical problems of performing artists **18**, 91–97 (2003).

[21] L. Turner-Stoker and K. Reid, "Three-dimensional motion analysis of upper limb movement in the bowing arm of string-playing musicians", Clinical Biomechanics **14**, 426–433 (1999).

[22] E. Maestre, J. Bonada, M. Blaauw, A. Pérez, and E. Guaus, "Acquisition of violin instrumental gestures using a commercial EMF tracking device", in *Proceedings of the 2007 International Computer Music Conference (ICMC07)*, volume I, 386–393 (The International Computer Music Association) (2007).

[23] E. Schoonderwaldt, S. Sinclair, and M. Wanderley, "Why do we need 5-DOF force feedback? An analysis of violin bowing.", in *Proceedings of ENACTIVE07* (2007).

[24] URL `http://www.vicon.com`.

[25] The bow and the violin could be tracked with a better resolution if the cameras were closer to the subject. However, the used setup allows for full body motion capture of the player as well, the achieved resolution still being acceptable.

[26] Alternatively, digital probing techniques could be used, e.g., as described in Ref.22.

[27] M. Demoucron, A. Askenfelt, and R. Caussé, "Mesure de la "pression d'archet" des instruments à cordes frottées, Application à la synthèse sonore [Measuring bow force in bowed-string instruments, Application to sound synthesis]", in *8e Congrès Français d'Acoustique* (Tours) (2006).

[28] M. Demoucron, A. Askenfelt, and R. Caussé, "A sensor for

measuring bow force in violin performance", Manuscript in preparation.
[29] F. E. Veldpaus, H. J. Woltring, and L. J. M. G. Dortmans, "A least-squares algorithm for the equiform transformation from spatial marker co-ordinates", Journal of Biomechanics **21**, 45–54 (1988).
[30] A. Askenfelt, "Observations on the violin bow and the interaction with the string", in *Proceedings of the International Symposium on Musical Acoustics*, 197–212 (1995).
[31] N. Pickering, "Physical properties of violin bows", J. Violin Society of America **8**, 41–57 (1987).
[32] URL `http://www.mathworks.com`.
[33] For an extensive overview of conversions between different representation of orientation see Ref.34.
[34] J. Diebel, "Representing attitude: Euler angles, unit quaternions, and rotation vectors", Technical Report, Stanford University, Stanford, California 94301-9010 (2006), URL `http://ai.stanford.edu/~diebel/attitude/attitude.pdf`.
[35] To obtain the acoustically more relevant *relative* bow-bridge distance β, y_{bb} should be divided by the effective length of the string. This requires knowledge of the position where the string is stopped by the player, which could be obtained, e.g., by pitch analysis of the audio recording.
[36] To avoid possible confusion around this subject it should be noted that the bow angles as defined here do *not* exactly equal the Tait-Bryan (or Euler) angles of the relative orientation of the bow and the violin, as suggested in Ref.23.
[37] Euler angles associated with rotation sequence (1,2,3) as described in Ref.34 (also referred to as Tait-Bryan angles).
[38] E. Schoonderwaldt, N. Rasamimanana, and F. Bevilacqua, "Combining accelerometer and video camera: Reconstruction of bow velocity profiles", in *Proceedings of the 6th International Conference on New Interfaces for Musical Expression (NIME06)* (Paris, France) (2006).
[39] URL `http://www.polhemus.com/`.
[40] K. Ng, O. Larkin, T. Koerselmans, B. Ong, D. Schwartz, and F. Bevilacqua, "The 3D augmented mirror: motion analysis for string practice training", in *Proceedings of the 2007 International Computer Music Conference (ICMC07)*, volume II, 53–56 (The International Computer Music Association) (2007).
[41] F. Rabbath and H. Sturm, "Art of the bow with Francois Rabbath", Website, URL `http://www.artofthebow.com/`.
[42] E. Schoonderwaldt, "Visualization of bowing gestures for feedback: The Hodgson plot", in *Proceedings of the 3rd International Conference on Automated Production of Cross Media Content for Multi-channel Distribution (AXMEDIS07)*, volume II, 65–70 (2007).
[43] T. K. Ho, "A computer-assisted approach to the teaching of violin tone production", ACM SIGCUE Outlook **21**, 73–83 (1991).
[44] M. Demoucron and R. Caussé, "Sound synthesis of bowed string instruments using a gesture based control of a physical model", in *Proceedings of International Symposium on Musical Acoustics (ISMA07)* (2007).
[45] A. Perez, J. Bonada, E. Maestre, E. Guaus, and M. Blaauw, "Combining performance action with spectral models for violin sound transformation", in *Proceedings of 19th International Congress on Acoustics (ICA07)* (Madrid, Spain) (2007).
[46] D. Young and S. Serafin, "Investigation the performance of a violin physical model: recent real player studies", in *Proceedings of the 2007 International Computer Music Conference (ICMC07)*, volume I, 394–397 (The International Computer Music Association) (2007).
[47] Arguably, tilt has a certain influence on the spectrum as shown in Ref.49, but the effect is small compared to that of, e.g., bow force.
[48] N. C. Pickering, "Physical properties of violin strings", J. Catgut Acoust. Soc. **44**, 6–8 (1985).
[49] E. Schoonderwaldt, K. Guettler, and A. Askenfelt, "Effect of the width of the bow hair on the violin string spectrum", in *Proceedings of the Stockholm Music Acoustics Conference*, 91–94 (Stockholm) (2003).

Chapter 5

Description, modelling and parametrization of some typical bowing patterns

In the two first parts of this thesis (Chapt. 2, 3 and 4), we have developed tools in order to (a) simulate the motion of the bowed string and synthesise violin sounds, and (b) measure the effective bowing parameters used by the player in real performance. Together, these tools are sufficient to obtain a realistic and gesture-based control of the sound synthesis. The measured bowing parameters can be used directly to control the bowed-string model with adequate mechanical parameters. However, this approach only allows a reproduction of what has been played, which is of limited interest from an user's point of view. A musically motivated challenge consists in creating new control patterns inspired by measurements of violinists' bowing patterns. That would allow a more intuitive control of the notes, obtained through, for example, high-level parameters which automatically generate the time evolution of the control parameters, or by modifying the measurements according to specific musical intentions. This goal can only be achieved by analysing measurements on professional violinists, extracting typical characteristics of the bowing patterns, and formulating rules describing the players' bowing.

In the two following chapters, measurements of the bowing parameters in real violin performance will be presented and described. We will focus on the time evolution of the bow force and the bow velocity in some of the standard bowing patterns, including *martelé*, *sautillé*, and *détaché*. These descriptions will aim at extracting the characteristics of the control parameters, in order to propose adequate models of a wide variety of bowing patterns.

In this chapter, we will first clarify the purpose and discuss the procedure that will be used (Sect. 5.1). Then, we will examine three bowing patterns corresponding to three separate classes of bow strokes. Sect. 5.2 will focus on the class of bouncing bowing patterns for which the *sautillé* provides a representative illustration. In Sect.

5.3, we will examine an accented bowing type called *short martelé* (whose modelling can be applied to a certain extent in the description of *staccato*). Finally, in Sect. 5.4, quickly repeated bowing patterns such as *tremolo* and *fast détaché* will be described. The terminology used in the descriptions and classifications of bowing patterns is taken from the classical reference by Galamian[1] [28].

5.1 Introduction

On the two classes of bow strokes

The present chapter will treat three types of short bow strokes with rapidly varying control parameters, *martelé*, *sautillé* and *tremolo*. The next chapter will focus on sustained notes and difficulties associated with this class of bow strokes, such as bow changes. The reason for this division could seem somewhat arbitrary, but it is justified by considering the way the control is executed.

The basic way of playing the violin consists in drawing the bow steadily across the string. Each bow stroke can be used to produce only one note, like in the détaché, or several notes, like in legato playing. This basic way of playing constitutes a first class of bow strokes that is characterized by a continuous string vibration, during which the player mainly concentrates on maintaining a Helmholtz motion at the required dynamic level and with the desired tone color. The control of the string vibration derives from a (more or less conscious) playing strategy, taking into account musical, mechanical and human control constraints. For instance, the finite length of the bow and the duration of the note will determine the evolution of the bow velocity during the stroke. This way of playing is characterized by the immediate feedback that the player receives from the instrument. This feedback makes a continuous control of the performance possible.

A second class of bowing patterns consists of short or quick bow strokes such as *martelé, spiccato*, *sautillé*, and *tremolo*. The practicing of these bowing patterns aims at 1) refining the combination of bowing parameters in order to get the target sound, 2) being able to use different gestures according to the musical context, and 3) acquiring the technical skills and "feeling" that enable the player to produce almost identical bowing gestures.

These bow strokes are short (and quick, in the case of the tremolo), and it can be assumed that the performance is mainly based on reproduction of well-practiced motor behaviour more than on conscious control in real time. Once the gesture has been initiated, it is often too late for adapting the control to the resulting sound. At best, the gesture will be adapted for the next bow stroke. To some extent, these bow strokes could be considered as ballistic movements [49].

Because a proper performance of these bow strokes requires extensive practicing under a long period of time, they exhibit characteristic and reproducible bowing pa-

[1] Ivan Alexander Galamian (1903-1981) was the head of the violin department at the Juilliard School of Music, New York, from 1946 to 1981 and is the most influential violin teacher of the 20th century.

rameter patterns. This fact makes them particularly well suited for characterisation and modelling of the control parameters. The separation between the two classes of strokes will also reflect the different levels of difficulty of the task. Whereas strokes with large dynamic variations in the bowing parameters like sautillé could be relatively easily modelled, it will be more difficult to extract some characteristics of a continuously controlled gesture such as in détaché.

This characterization does not imply that there is no specific control gesture involved when playing sustained notes like détaché. The previous discussion about long-term practicing in order to impress a particular motoric skill applies to some key points in the control of sustained notes as well, for example the change of bowing direction ("bow change"). Making the transition between two notes in détaché playing as smooth as possible by a proper control of the bow change requires the same kind of well-established, and in some cases unconscious, control as in short, rapid strokes like sautillé. These aspects will be described in the next chapter when studying sustained notes.

Modelling bow strokes

Measurements combining motion capture technique with sensors on the bow (described in Chapt. 4) give the time evolution of the bowing parameters needed for describing the performance: bow force, bow velocity and bow-bridge distance. The measurements could be used directly as control parameters of the model and synthesize different types of bow strokes. However, when possible, it is more rewarding to model the time evolution of the bowing parameters in order to get a parametric description of the bow strokes. The aim of such a modelling is to summarize a given class of bowing patterns in a few parameter profiles that are relevant from the player's point of view.

Then, the first task consists in finding an appropriate way of formalising the time evolution of the control parameters. In the following we will mainly use some simple mathematical functions, sometimes by dividing the bow stroke into different parts, each of them being represented by one function. By grouping measurements of "identical" bow strokes together, characteristic features can be observed which can be used to define the control pattern. This step aims at determining what is important to reproduce in the bowing patterns, what should be left aside, and above all, what we would like to control, and how. The bowing patterns will sometimes exhibit some features that are not really essential to our perception of the stroke. For instance, measurements may show some differences when a specific bowing pattern is played at different positions on the bow (e.g. at the frog or at the tip). However, if a player or an expert listener is not able to discriminate between the same bowing pattern played at different bow positions, the observed differences will not be considered essential. In such cases a compromise in the description of the stroke will be made.

Another important point refers to the complexity of the models and their extrapolation capacities. The simpler a model is, the less we will be able to manipulate

it. On the other hand, a sophisticated model could be difficult to use, but may offer the possibility of going beyond the simple reproduction of a given bow stroke by extrapolating new strokes and introducing variations. For instance, some strokes could be perceptually well reproduced by using a simple sine curve for a certain bowing parameter. As such a model is controlled by only two parameters (amplitude and duration of the stroke), it is very convenient to use. But we often prefer a model with two successive parts of sine curves, allowing an independent setting of two durations, the first one corresponding to the "attack" of the note, and the second one to the "release", for instance. Here again, a compromise has to be found between an acceptable reproduction of the strokes, the extrapolation capacity, and an acceptable usability.

The last point concerns the parametrization of the model. Once an appropriate model has been found, the parameters are determined for a given set of "standard" situations by fitting real data to the model. The three standard conditions were normally three dynamic levels, pianissimo (*pp*), mezzo forte (*mf*) and fortissimo (*ff*), in order to obtain some "presets" of the models. The models and their parametrization were validated by comparing three synthesized versions of a given bow stroke sequence. The first version used the real acquisition data for controlling the simulation. The second version was controlled by a sequence of fitted bowing pattern models, and the last one was created from the preset values of the model, adjusted within the variation range of the model parameters. In all cases presented hereafter, no differences could be heard between the three simulations.

On the influence of the player and the instrument

The measurements presented in the following were made with the combination of motion capture methods and sensors on the bow described in the previous chapter. Most measurements were made with one professional violinist, playing the note G4 = 392 Hz on the D string. The results obviously give a somewhat narrow overview of the bowing technique in violin playing. A more extensive study should include the entire range of the violin, from the G string to the E string, different fingerings (playing the same note near the nut or closer to the bridge on a lower string), different dynamic levels, and different bow positions, among other things. Further, it would have been interesting to compare the bowing techniques of different subjects. However, the purpose of our work, modelling and parametrization of different types of bowing patterns, could be attained with only one player and one note, let alone that the differences in bowing between strings and the diversity in bowing technique among professionals was not reflected in the results.

Concerning the influence of the player, a certain variability from one player to another one could be expected. There are certainly different ways of performing a specific musical idea by modifications of the bowing pattern, as well as there are different interpretations of a given bow stroke, and different techniques for controlling the stroke. The models presented in the following should therefore only be considered as prototypes of bowing patterns, and we cannot claim them to be

general and representative of all players. However, especially for short bow strokes, we can assume that the differences between players are rather small and mainly concern the control gesture itself and not the resulting evolution of the bowing parameters. For instance, Galamian [28] pointed out that each player should try to find the most convenient way of playing rapid staccato. However, whatever the technique used for achieving this bowing pattern, a well-performed staccato will sound like a staccato, and no drastic differences in the bowing parameters should be expected. It is then important to distinguish between, on one hand, the bowing parameters, which are the objective values of the parameters we are interested in for describing the control of the sound (bow force, bow velocity and bow-bridge distance as functions of time), and on the other hand the gesture (the hand and arm movements) used for obtaining the observed evolution of the bowing parameters.

The differences between players will be more critical in the next chapter, dealing with sustained notes. Different bowing techniques are clearly identifiable for these bowing patterns, mainly concerning the balance between bow force and bow velocity, and the attack of the notes.

Finally, concerning the influence of the string and note played, it seems reasonable to assume that there is no drastic influence, at least over the range of a given instrument. Obviously, similar bowing patterns will not be played exactly the same way on a violin and on a cello. For example, the attack requires more time on lower strings, and a higher bow force is needed for maintaining the Helmholtz motion. However, it seems reasonable to assume that the bow velocity profile associated with a certain bowing pattern remains approximately the same across the pitch range of the violin, and that the player adapts the bowing gesture to the string mainly by correcting the ranges of bow force and bow-bridge distance.

In the following, we will cover three types of bow strokes, sautillé, short martelé and tremolo. In each case, measurements of the bowing parameters will first be presented and described, focusing on bow velocity and bow force, which can be assumed to be the most dynamic parameters during short bowing patterns. Then, models will be formulated in order to imitate the time evolution of the bowing parameters. The models are described by a few parameters whose typical values will be determined for exemplary situations.

5.2 Bouncing bow strokes

Bouncing bow strokes are started from the hair and finish off the string. The string is excited during a rather short contact time, set by the rebound of the bow. Because the bow leaves the string, the string is then free to vibrate with a decaying oscillation. This principle of driving the string is shared by several bowing patterns that differ essentially in the technique that is used for controlling the rebound, according to Galamian [28].

In short, the rebound of the bow is used in two main bowing patterns:

- In *spiccato*, "the bow is thrown down on the string for every single note and (at least for the longer strokes) lifted up again."

- The *sautillé* uses the natural rebound of the bow for performing several notes with the same impulse, and the bow comes off the string because of the elasticity of the bow.

As seen in the previous description, the two bowing patterns differ in the control of the rebound. In spiccato playing, the bow is actively thrown down and then lifted, assisted by the mass-compliance system of the bow stick and hair which tends to release the bow from the string. In contrast, sautillé is produced by some less active control of the bow. The player relies on the resonant behaviour of the bow for controlling the "take-off" from the string. For that reason, playing sautillé requires a good knowledge of the dynamics of the bow in order to perform notes at the intended rate and duration.

Two consequences should be highlighted. First, different spiccato can be obtained by controlling the duration of the contact, whereas in sautillé, the force evolution of the contact is essentially set by the bow position and the player has little direct control. This essential difference will later be used for simulating the two kinds of strokes. Secondly, the spiccato cannot be as quick as the sautillé, because it necessitates an active control of the fingers on the bow stick for every note.

Finally, some other bouncing bow strokes could be mentioned here. For example, the *ricochet* and *flying spiccato* are obtained by performing several rebounds during the same bow stroke, i.e. several rebounds during down-bow or up-bow. Because these bow strokes are very close to the two main bouncing bowing patterns above (they differ only in the control of bow velocity), they will be considered as variations of spiccato and sautillé. Once a good description of these main patterns will be obtained, there should be no difficulty in considering several rebounds performed in the same stroke.

All variations of bouncing bowing patterns share the same feature, which is the rebound of the bow from the string. The time evolution of the bow force during the rebound can therefore be considered as the most prominent feature for the perception of the rebound. Consequently, we will first describe and model the evolution of the force during string contact. Then a specific case will be studied with the examination of the sautillé. For this case study, a description and modelling of the bow velocity will first be required, before typical values of the model parameters will be determined. Finally, we will discuss the effect of the model parameters and how they can be empirically changed in order to go beyond the simple imitation and produce various bow strokes.

Bow force patterns during the contact: Characterization and modelling

In the modelling of bouncing bow strokes, the main task is to find a general model for reproducing the time evolution of the force during the rebounds. Fig. 5.1 shows two examples of bow force patterns during sautillé performed at different tempi (90 and 150 bpm) at the same dynamic level (*mf*). Roughly, the force exhibits a bell-like shape characterized by the maximal force that is reached (0.74 and 1.4 N) and the contact time between the bow and string (around 70 ms in both cases). When increasing the bouncing frequency (Fig.5.1, right), some additional ripples appear due to the excitation of two modes of the bow, as pointed out by Askenfelt [5].

In a first approach it seems reasonable not to take the ripples into account as there is presently no clear evidence of their influence on the perceived sound. For this reason we will focus on the reproduction of the global bell-like force profile only.

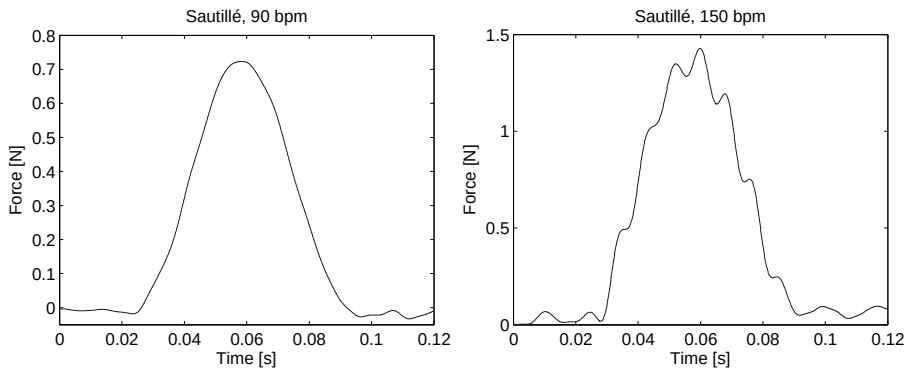

Figure 5.1: Bow force patterns measured by the bow force sensor during the rebound of the bow in bouncing bowing patterns. The figures show patterns during sautillé performed at two tempi: 90 bpm (left) and 150 bpm (right), corresponding to a note rate of 6 and 10 Hz, respectively. At 10 Hz, the pattern exhibits some ripples around 120 Hz, due to excitation of some modes of the bow stick.

A parabola could be used to fit the upper part of the force profile well, but the broader lower part would not be accurately described. When tried, the resulting sound was somehow more percussive than the original. Moreover, the rather steep slope of the force at the beginning may give troubles during the attack. A shifted cosine model as used by Guettler [38] seemed to be more adequate, but the force pattern showed an asymmetry around the maximal value that could not be reproduced: the increasing part of the force profile was slightly shorter than the

decreasing part. The difference was very small, but it could, however, be interesting to include the possibility of changing this parameter. For example, a percussive attack of the bow followed by a longer sustain could be simulated.

The model finally used is described in Fig. 5.2, left. Two successive cosine functions are used, before and after the force maximum. Each function is defined by three parameters (frequencies f_1 and f_2, amplitudes A_1 and A_2, offset O_1 and O_2).

$$F(t) = \begin{cases} A_1(cos(2\pi f_1(t - T_{max})) + O_1) & \text{for} \quad -\frac{\arccos(-O_1)}{2\pi f_1} < t - T_{max} < 0 \\ A_2(cos(2\pi f_2(t - T_{max})) + O_2) & \text{for} \quad 0 < t - T_{max} < \frac{\arccos(-O_2)}{2\pi f_2} \end{cases} \tag{5.1}$$

These parameters are not easy to deal with. For example, the duration of each part of the force profile (and hence the total duration of the contact) depends both on the frequency and the offset of the cosines. Similarly, the maximum force that is reached during the rebound depends on a combination of amplitudes and offsets.

Instead, it would be preferable to use some more "intuitive" and relevant parameters such as the force maximum during the stroke F_{max}, the duration T, the asymmetry of the shape A (defined as the ratio between the increasing time of the profile and the total duration), and the slope at the beginning and the end (a_1 and a_2). As the correspondence between these two sets of parameters is not straightforward and cannot be obtained analytically, we define some main parameters (F_{max}, T and A), directly adjustable by the user, keeping the offset as a small correction of the shape. This gives a more practical correspondence between the "relevant" parameters and the cosine parameters

$$\begin{cases} A_1 = \frac{F_{max}}{1+O_1} & f_1 = \frac{1}{2\pi AT} \arccos(-O_1) \\ A_2 = \frac{F_{max}}{1+O_2} & f_2 = \frac{1}{2\pi(1-A)T} \arccos(-O_2) \end{cases} \tag{5.2}$$

The slopes are then considered as secondary parameters and can be computed (but not adjusted) as

$$\begin{cases} a_1 = & 2\pi f_1 A_1 sin(2\pi f_1 AT) \\ a_2 = & -2\pi f_2 A_2 sin(2\pi f_2(1-A)T) \end{cases} \tag{5.3}$$

Fig. 5.2, right, shows the application of the model on a succession of rebounds. No difference can be seen between the real measurements and the fitted data, and we can conclude that the model succeeds very well in imitating the time evolution of the bow force during string contact. This example shows a sautillé, which is the special case on which we will focus in the following. The model parameters that were used will be described later, when dealing with the parametrization of the models, but before that, a description of the bow velocity in sautillé is required.

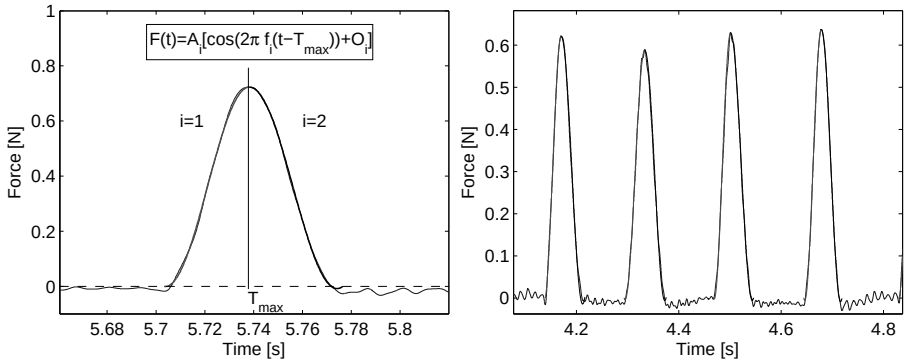

Figure 5.2: Left: Double cosine model used for fitting the bow force during the rebound in sautillé. Right: Example of fitting of the model to measurements. No difference can be seen between measured and fitted data.

The sautillé: Modelling bow velocity

In sautillé playing, the bow bounces on the string while performing a short to-and-fro movement. As mentioned before, the bow bounces only once per bow stroke producing one note, and the rebound is due to the mass and compliance of the bow. A good synchronisation in the bow control is necessary for obtaining the right timing between the horizontal motion of the bow and the rebounds. Guettler [38] showed that a crisp sautillé requires the rebound to first damp the sounding note before starting the next. Strokes were found to be "perfect" when the phase between bow velocity and force was around 53°.

The phase conditions can be observed in Fig. 5.3, showing the bow force, bow velocity and bow-bridge distance for two series of sautillé played at the same dynamic level, but in two tempi. When the bow and the string are in contact, the velocity is plotted in full lines, the dotted lines indicating the motion of the bow off the string. At a moderate tempo (90 bpm, Fig. 5.3, left), the rebounds start after the change in bowing direction and before reaching the velocity maximum. In contrast, for a rapid performance (150 bpm, Fig. 5.3, right), the bow lands on the string just before the bow direction changes and stays in contact with the string during a long part of the note.

The simplest representation of the to-and-fro motion of the bow in sautillé consists in using a half period of a sine curve per bow stroke for the bow velocity. Fig. 5.4, left, shows such a model, with real data in grey and a fitted sine in black. The duration T_{bs} of the stroke is determined by the positions where the velocity crosses zero. The amplitude of the sine must be fitted to data.

In Fig. 5.4, right, the velocity was first segmented into successive bow strokes by determining the positions of the zero crossings in velocity. Then, a non-linear regression algorithm was used to determine the parameters (amplitude V_{max} and

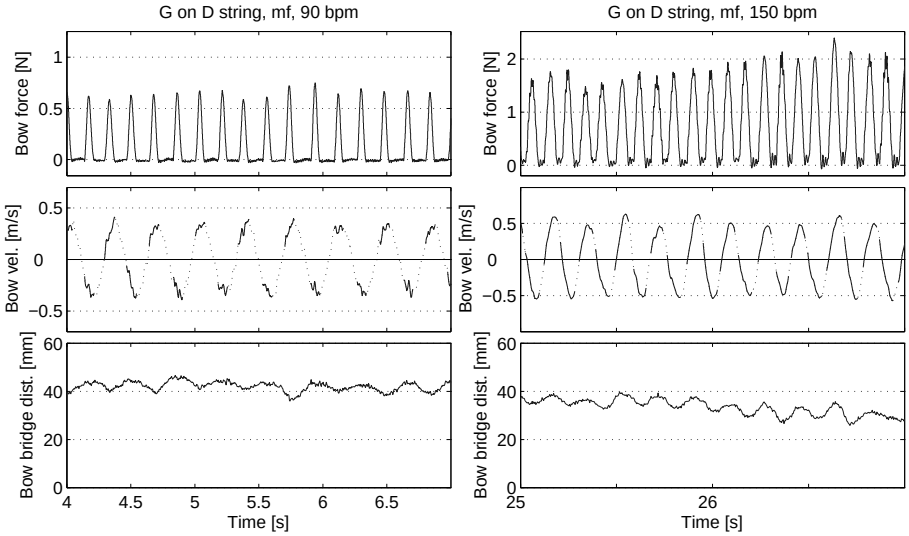

Figure 5.3: Illustration of the bowing parameters measured during sautillé, for two tempos: 90 bpm (left) and 150 bpm (right). From top: Bow force, bow velocity and bow-bridge distance. The bow velocity is displayed in solid line when the bow and the string are in contact. It can be noticed that the synchronisation between the rebounds and the velocity changes with the bow stroke frequency.

frequency $1/2T_{bs}$) for each sine function. From the comparison between measurements and simulated velocity patterns observed in Fig. 5.4, right, we can conclude that this simple model is sufficient for representing the bow velocity in sautillé.

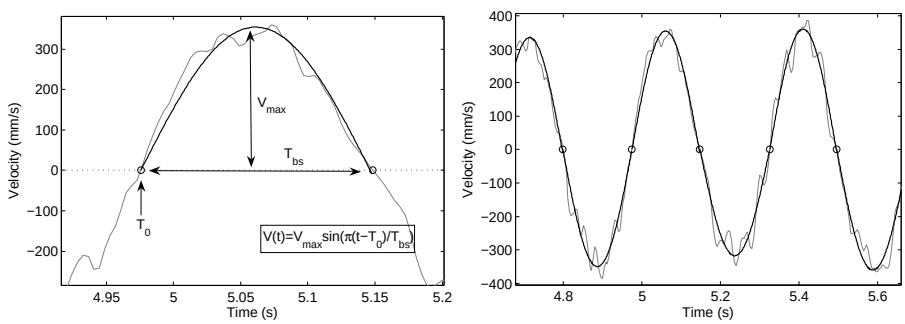

Figure 5.4: Left: Simple sine model used for fitting the bow velocity in sautillé. Right: Example of fitting the model to measurements.

The sautillé: Fitting model parameters to measurements

The parameters permitting to fit the bow velocity and the bow force patterns were determined for three dynamic levels (*p*, *mf*, *f*) and two tempos (90 and 150 bpm). Each series of sautillé was composed of 32 strokes at 90 bpm and 64 strokes at 150 bpm. For the velocity, the measurements were first segmented into successive bow strokes at the zero crossings in velocity, then the sine model was fitted to the pattern for each bow stroke. Results for the velocity amplitude are presented in Fig. 5.5, left. As expected, the amplitude of the velocity is found to increase with increasing dynamic level, from 8 cm/s for piano to 78 cm/s for forte, both at 90 bpm. When the bow stroke frequency was higher (150 bpm), the increase in amplitude was less significant, which could be due to the difficulty in controlling the bow for such rapid movements.

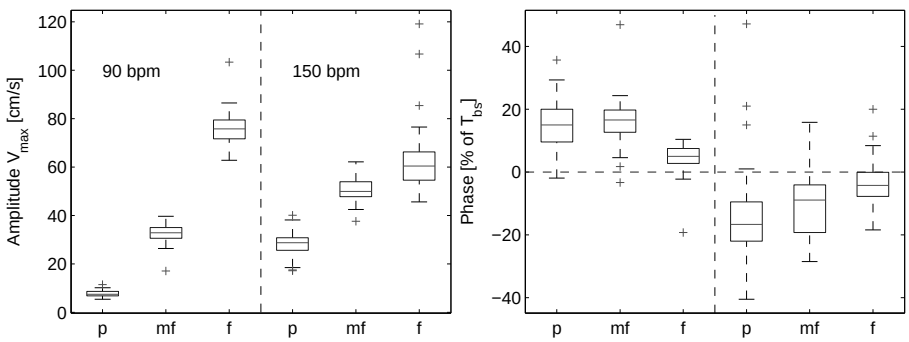

Figure 5.5: Fitting of the velocity model to the measurements during sautillé playing. In each figure, three dynamic levels (*p*, *mf*, *f*) are presented for a moderate and a rapid tempo (90 and 150 bpm). Left: Amplitude of the sine function representing the bow velocity. Right: Phase defined as the time (in percent of the half sine duration) between the beginning of the sine and the beginning of the rebound.

The time between the beginning of the stroke and the beginning of the rebound is used to compute the phase, defined as the ratio between this time and the total duration of the stroke T_{bs}. In Fig. 5.5 (right), the phase is shown for the six conditions. As previously observed, the phase becomes negative for rapid sautillé, which means that the bow lands on the string before the change of bow for the next stroke takes place.

If the phase α is computed with the position of the force maximum as reference, following [38] (see Fig. 5.6), it is interesting to notice that all measurements are found between the two extreme cases presented by Guettler ($\alpha = 0°$ and $\alpha = 107°$). More precisely, the main part of the phases lies between 40° and 80°, independently of the tempo. The phases are distributed around the optimal value reported by Guettler (53°).

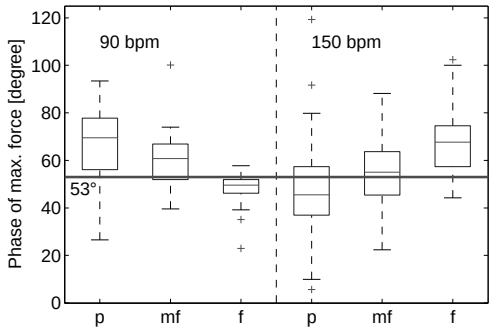

Figure 5.6: Position of the force maximum during sautillé strokes. These phases are in line with Guettler's observation that the optimal phase for the force maximum should be around 53°. All measurements lie between the two extreme cases reported by Guettler ($\alpha = 0°$ and $\alpha = 107°$).

Bow force patterns during the rebounds are fitted by forcing the model to pass through the maximal force in order to obtain a continuity in the two cosine functions at this point. The resulting parameters are presented in Fig. 5.7. The force maximum is found to increase with increasing dynamic level. It is interesting to compare the resulting trends with the velocity amplitude presented above (see Fig. 5.5, left). At 150 bpm it was found that the increase in velocity amplitude was not as clear as for the slower tempo. In contrast, we can notice that the increase in force is very clear for rapid sautillé. The values range from around 0.5 N in piano to more than 3 N in forte. An explanation could be that rapid motions of the bow constrain the gesture of the player in such a way that he cannot control the velocity as freely as when the motion is slower. In order to compensate for this constraint and obtain different dynamic levels, the player is obliged to use bow force and/or bow-bridge distance as main control parameters. This explanation is supported by the observed bow-bridge distances. The mean value of the bow-bridge distance (not shown in the figures) varied with the dynamic level. At 90 bpm, the mean values were 58, 40 and 29 mm for *p*, *mf* and *f*, and at 150 bpm, they were 53, 30 and 30 mm.

The other parameters give an indication of the value to be used for each condition, but no obvious trends can be deduced. However, the two tempi should be kept separated. At 150 bpm, the three dynamic levels do not lead to visible differences in contact time, asymmetry, and offset. In all three cases, the fits give about the same values: around 80 ms for the contact time, a bit less than 50 % for the asymmetry, and not far from 1 for the offset. The relative constancy of these values can probably be explained by the difficulty in performing such fast bowing patterns. The player is more concentrated on obtaining the right timing between the motion of the bow and the rebounds than on an optimal attack of each stroke.

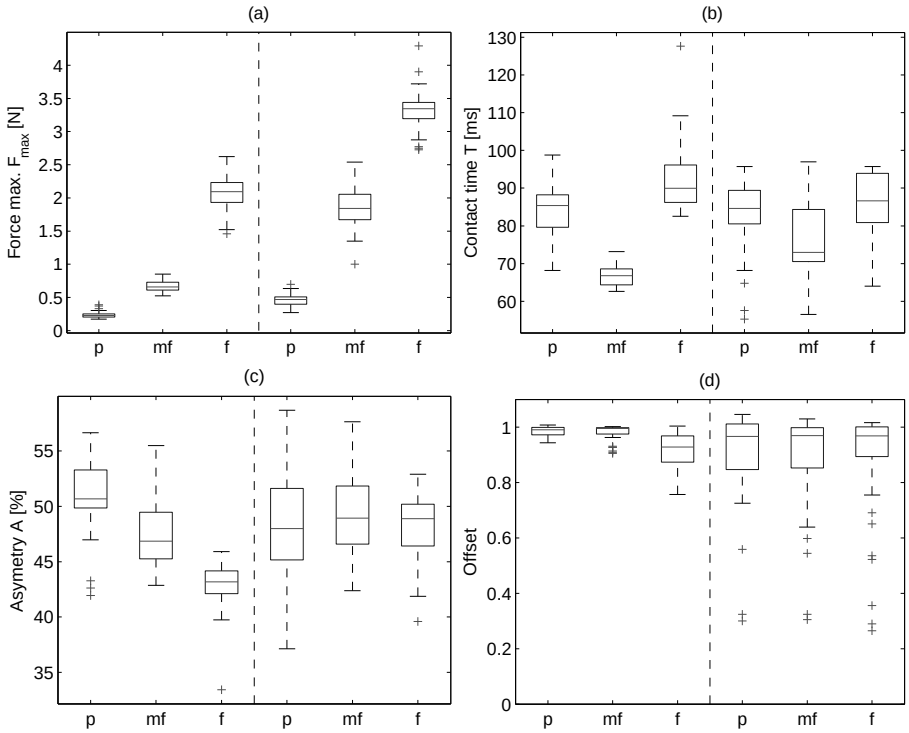

Figure 5.7: Parameters obtained when fitting the force model to measurements in sautillé. In each figure, three dynamic levels (*p*, *mf*, *f*) are presented for a moderate (90 bpm, left half of panels) and a rapid tempo (150 bpm, right part of panels). Each statistical representation shows the result of a fit to a sequence of 32 successive bow strokes at 90 bpm and 64 strokes at 150 bpm: (a) Force maximum, (b) contact time, (c) asymmetry of the force pattern, and (d) offset of the cosine model.

This difficulty in achieving the right timing can be heard in the performance. Many rebounds gave rise to noisy attacks.

At 90 bpm, some differences appear in the contact time and the asymmetry between dynamic levels, which may indicate a more precise control of the rebound by the player. For example, the variations in asymmetry could be interpreted as an attempt of controlling the rebound. At piano level, the player may truncate the landing of the bow in order to avoid a too high bow force, which leads to asymmetries above 50 %. In contrast, in forte playing an additional action of the finger may be necessary, resulting in longer contact time after the force maximum than before and hence to an asymmetry below 45 %.

The parametrization of gesture models leads to typical values for different musical situations. Some of the parameters are very intuitive, such as the maximal

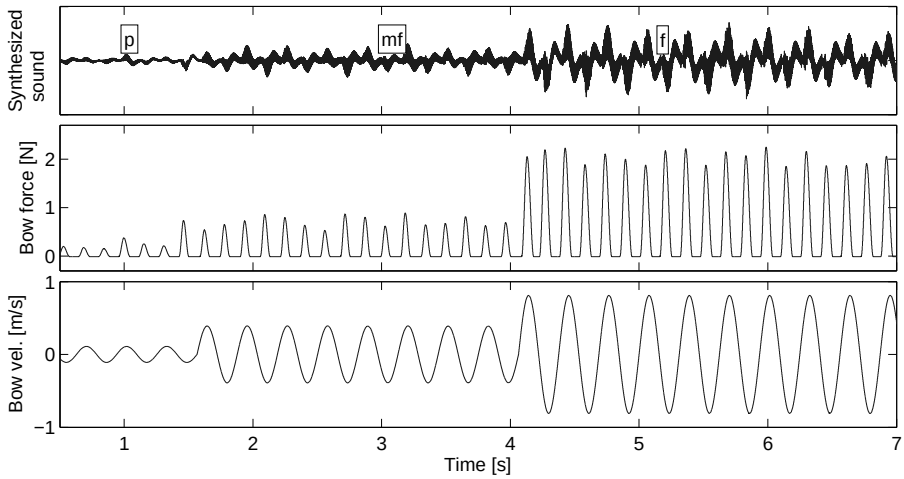

Figure 5.8: Sound synthesis of a series of sautillé notes with increasing dynamic level (p - mf - f). The bowed-string model is controlled with a gesture model describing the bow force during string contact and the bow velocity. Parameters are determined from previous fitting of the model to measurements at the three dynamic levels.

bow force, the amplitude of the velocity and the contact time, and can be easily interpreted in terms of the desired sound level. Other parameters (the asymmetry and the offset) do not really have a gestural significance. They are difficult to interpret and can be considered as indirectly controlled parameters. However, determination of their values was necessary for feeding the velocity and force models with complete sets of data, and for obtaining typical values in order to control the bowed string model.

As an illustration, Fig. 5.8 shows sound synthesis of sautillé performed at 90 bpm at the three dynamic levels. The simulation is performed using the sautillé model described above with adequate values of the parameters. The force maximum, contact time, and velocity amplitude were permitted to vary slightly around their mean values, which can be observed in particular in the force maximum.

However, a simple imitation of the measurements is not the main purpose of the modelling. If that was the case, a straightforward use of measurements to control the bowed-string model would be sufficient. The modelling offers the possibility of playing around with the model parameters, and of going beyond the simple imitation in order to create new strokes. We will close this section by discussing the effect of some of the model parameters, and how they can be changed in order to obtain a variety of different bow strokes.

Extending the model

The gesture model is described by a few parameters that can be changed in order to obtain different time evolutions of the bowing parameters. The force maximum and the velocity amplitude are the basic parameters for obtaining different dynamic levels, as seen in the measurements above. Variation of the phase between the rebound and the velocity profile produces different qualities of the sautillé.

The contact time between the bow and the string may be used in order to reproduce rebounds at different positions on the bow, because the bouncing frequency increases with increasing bow position. Sautillé is usually played around the middle of the bow. Close to the tip, very short rebounds can be obtained, but are very difficult to control. In contrast, in the lower part of the bow (near the frog), the weight prevents the bow from bouncing, and rebounds can hardly be obtained without an active control of the arm.

It is interesting to examine the perceptual effect of the bow force pattern when the contact time is changed. In Fig. 5.7, measurements gave a mean value around 80 ms, with variations from 60 ms to 100 ms. Running the model with very short contact times, around and below 20 ms, the string is hardly driven by friction and the resulting sound is an impact very similar to the striking of the bow stick on the string (*col legno* playing). When the contact time was increased above the mean value, the rebound sounded less and less "natural", as if the bow was thrown down and lifted up quickly through the action of the arm. For example, with $F_{max} = 0.74$ N and $V_{max} = 39$ cm/s, the rebound seemed to be controlled above 140 ms and stopped to sound like a rebound above 200 ms.

The observation that above a given contact time, the generated sound gave the impression that the bow was "thrown down and lifted up again" reminds us of Galamian's description of the *spiccato*. The sautillé model can consequently be extrapolated in order to produce spiccato bowing parameters. The contact time and the maximal force can be set to obtain more or less broad *spiccato*, as described by Galamian. The asymmetry can be used as well to change the balance between the landing and lifting of the bow, producing vowel-like or consonant attacks of the sound, with different durations of the sustained vibration.

Finally, we could foresee that the imitation of other bouncing bowing patterns such as ricochet or flying spiccato presents no specific difficulties. In these two cases, several rebounds are produced during a single bow stroke. The only change required is to modify the velocity profile.

This section aimed at providing a model describing the time evolution of the bow force during the rebound of the bow from the string. Two successive cosine functions were used to allow an accurate reproduction of the force pattern and give the possibility of controlling the intuitive natural features of the contact. Based on measurements during real performance, *sautillé* playing was examined in detail, in order to obtain model parameters that could be used to produce different dynamic levels. Finally, the effects of modifying the contact times were explored, which

indicated a possibility to extend the model to produce variations of bouncing bow strokes such as *spiccato*, *ricochet* and *flying spiccato*.

Leaving the bouncing bowing patterns, we will now examine short bow strokes performed with an initial pressure of the bow on the string.

5.3 Fast martelé

The *fast martelé* (or short martelé, simple martelé, in contrast to the sustained martelé) is one of the three fundamental types of bow strokes together with détaché and spiccato, according to Menuhin [56]. It is a fast, accented bow stroke that requires a good control of the bow for obtaining precise variations of the bow force and keeping the bow parallel to the bridge despite the rapid motion. Galamian emphases the fact that a mastery of this bow stroke is beneficial in general for the bowing technique.

The presentation will follow the same procedure as in the previous section. First, models will be proposed and discussed for the evolution of bow velocity and bow force during the stroke. Then, model parameters will be determined by fitting them to measurements at different dynamic levels. Finally, we will discuss the extrapolation of the modelling to similar bowing patterns such as solid and flying *staccato*.

Description of the bowing pattern

A qualitative description provides some keys to the time evolution of bowing parameters, especially about the bow force:

> "The martelé is decidedly a percussive stroke with consonant type of sharp accent at the beginning of each note and always a rest between strokes. The accent in this stroke requires preparation in the form of a preliminary pressure: the bow has to "pinch" the string before starting to move. This pinching is a pressure stronger than the stroke itself will require, and it has to last just long enough to produce the necessary accentuation at the beginning of the tone. The pressure is then immediately lessened to the degree required. If this preparatory pressure is released too soon, there will not be any accent; if it is released too late, there will be a scratch." (Galamian [28])

This description is illustrated in Fig. 5.9, which shows measurements of bow force and bow velocity during the performance of three fast martelé strokes. During the stroke, the bow force is rapidly decreased from about 1.5 N to less than 0.5 N. During the intermediate periods of rest, the force is increased to the high initial value in preparation of the next stroke.

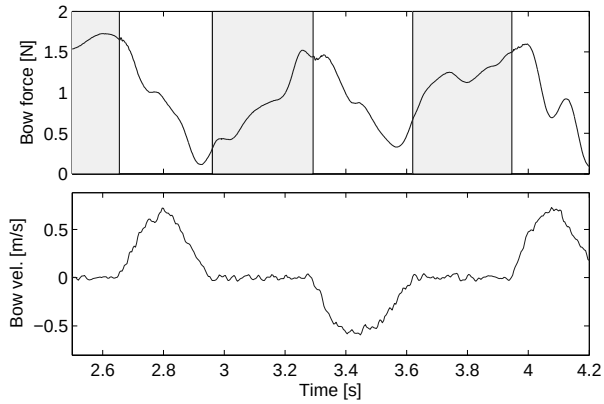

Figure 5.9: Illustration of fast martelé. Top: Bow force. The periods when the bow is at rest are shown shaded. Bottom: Bow velocity. The direction of the bow strokes was down-up-down.

In addition to controlling the timing of the drop in bow force at the beginning of the stroke, the player must take care at the termination of the note, as the duration is short:

> "When most of the pressure is not released at the termination of the stroke, the quality of the martelé suffers. (...) The scratchy sound produced by too much pressure at the instant of stopping or by application of pressure too early before the next stroke should always be avoided." (Galamian [28])

The fast martelé consequently requires an accurate control of the bowing parameters, and the previous description allows to identify the key features of the stroke: As it is a short stroke, the bow velocity will be composed of an acceleration immediately followed by a deceleration, with no sustained part on the vibration. The bow force will be characterized by an almost immediate and constant decrease. The two following sections will provide a quantitative description of these features.

Modelling bow velocity

Fig. 5.10 (left) shows the bow velocity of a series of fast martelé strokes (down bows) performed at forte level during one recording session. It highlights the high reproducibility of this class of bow strokes. During the first part of the stroke, the bow accelerates constantly until a velocity of about 1.1 m/s is reached. Then, the bow immediately slows down (no constant velocity) until it stops. It can be noticed that the decreasing part of the velocity pattern is less similar between successive

bow strokes than the accelerating part. The total duration of the bow stroke varies between 300 ms and 350 ms.

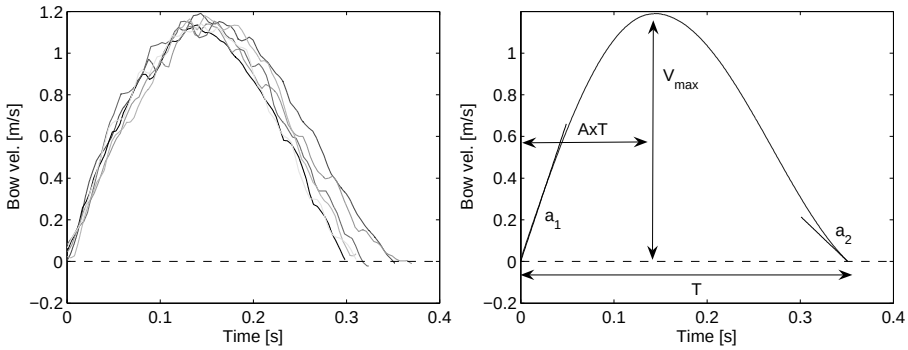

Figure 5.10: Model used for fitting the bow velocity patterns of fast martelé. Left: Successive strokes performed during the same recording session are isolated and plotted together. The velocity shows an approximate bell-shape profile, with a high reproducibility. Right: The cos-cos model described for the sautillé is used for reproducing the time evolution of the velocity.

As these patterns are rather similar to the bow force evolution that was observed during rebounds of the bow, the same model will be used (cos-cos model). If T_{max} denotes the time position of the velocity maximum, T_1 the increasing velocity period of the pattern and T_2 the decreasing velocity period, the velocity is expressed as

$$V(t) = \begin{cases} A_1(cos(2\pi f_1(t - T_{max})) + O_1) & -T_1 < t - T_{max} < 0 \\ A_2(cos(2\pi f_2(t - T_{max})) + O_2) & 0 < t - T_{max} < T_2 \end{cases} \tag{5.4}$$

where

$$T_1 = \frac{\arccos(-O_1)}{2\pi f_1} \quad \text{and} \quad T_2 = \frac{\arccos(-O_2)}{2\pi f_2} \tag{5.5}$$

Following the modelling of the bow force during rebound, we will prefer to control some more intuitive parameters such as the velocity maximum V_{max}, the duration of the bow stroke T, and the asymmetry of the profile T_1/T. The amplitudes and the frequencies of the cosine functions are then deduced from

$$\begin{cases} A_1 = \frac{V_{max}}{1+O_1} & f_1 = \frac{1}{2\pi AT} \arccos(-O_1) \\ A_2 = \frac{V_{max}}{1+O_2} & f_2 = \frac{1}{2\pi(1-A)T} \arccos(-O_2) \end{cases} \tag{5.6}$$

The resulting pattern and the parametrization are illustrated in Fig. 5.10, right. In addition we could be interested in using the acceleration at the beginning and end

of the stroke as parameters instead of the offsets O_1 and O_2. These accelerations can be expressed as

$$\begin{cases} a_1 = & 2\pi f_1 A_1 sin(2\pi f_1 T_1) \\ a_2 = & -2\pi f_2 A_2 sin(2\pi f_2 T_2) \end{cases} \tag{5.7}$$

By setting suitable values for O_1 and O_2 it is therefore possible to choose values for a_1 and a_2 in the intervals $[0\ 1.59V_{max}/AT]$ and $[-1.59V_{max}/(1-A)T\ 0]$, respectively.

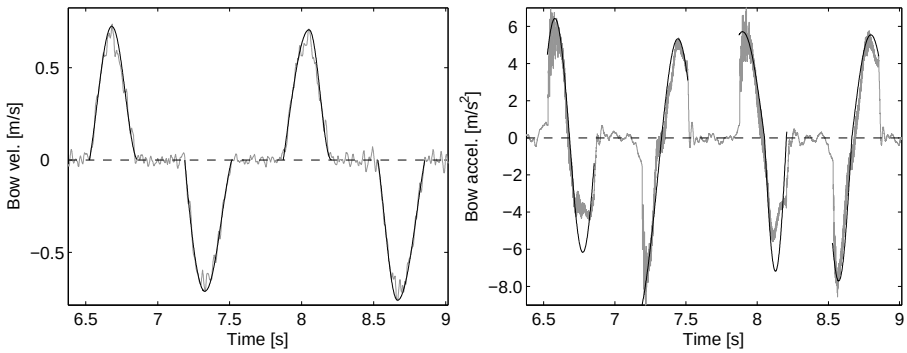

Figure 5.11: Fit of the bow motion for fast martelé using the cos-cos model. Left: Bow velocity computed from motion capture data and comparison with fitted data. Right: Bow acceleration measured by the sensors on the bow and comparison with the derivative of the velocity model in the left panel. Measured data are shown in grey lines. Fitted data using a non-linear regression algorithm for determining the parameters are shown in black lines. In this example, mean parameter values were $V_{max} = 0.7$ m/s, $T = 330$ ms, $A = 0.45$, $a_1 = 6.4$ m/s^2 and $a_2 = 2$ m/s^2.

Measurements were used to determine adequate parameter values. A more complete illustration of this determination will be given later. For the moment, an example will be given in order to illustrate the agreement between modelling and measurements. In Fig. 5.11, left, a non-linear regression algorithm has been used to fit the velocity model to data measured during performance using motion capture. The figure shows a good correspondence between measured data and the cos-cos model. However, the quality of the velocity measurement can be questioned on two points. First, the velocity deduced from the motion capture system was a bit noisy due to the time differentiation of the bow position signal. Secondly, the sampling frequency (250 Hz) may be too low for describing the details of such a short bow stroke well (for 300 ms, there is less than 100 points for each stroke). The bow velocity from the motion capture measurements was checked against more precise data from accelerometers on the bow. Fig. 5.11, right, shows the acceleration signal together with the time derivative of the fitted velocity patterns in Fig. 5.11, left.

We can still observe a good correspondence between the data and the fitted model. In the details we observe two small differences: During down-bows, the second sine corresponding to the deceleration of the bow seems a bit truncated at the peak compared to the model, and during up-bows, the deceleration does not follow the acceleration part directly, and a very short part with constant acceleration around zero can be observed. As these observations relate to different bowing directions, involving different gestures, they are probably related to some habits of the player, more than to a conscious control. Further, it is questionable if such small fluctuations influence the vibration of the string to such an extent that they are perceived in the sound. Simulations using real and fitted data did not sound particularly different.

Modelling bow force

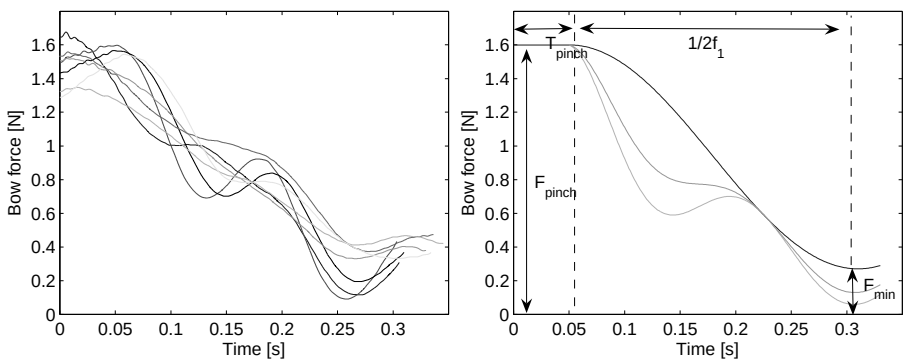

Figure 5.12: Modelling of the decrease in bow force during fast martelé strokes. Left: Bow force of successive strokes from the same acquisition are isolated and plotted together. Right: A short constant part followed by a simple sine is used for simulating the bow force decrease (dark line). A second sine with higher frequency is used to reproduce the damped oscillations of the bow due to the sudden relaxation of the bow force at the beginning of the stroke.

When the bow begins to move in fast martelé, the bow force must be "immediately lessened to the degree required" according to Galamian, which is illustrated in Fig. 5.12, left. The time evolutions of bow force of successive strokes are plotted together, showing a similar overall pattern for the force decrease. Roughly, the force decreases from more than 1.5 to about 0.3 N in 0.2 s (from 0.05 to 0.25 s). Some more or less pronounced oscillations around a frequency of 13 Hz can be observed as well.

The observed decrease in force can be modelled by a sinusoidal decrease. To enable a control of the time during which the string is "pinched", we add a constant part at the beginning. The bow force profile will then be given by

$$F_g(t) = \begin{cases} F_{pinch} & t \leq T_{pinch} \\ \frac{F_{pinch}-F_{min}}{2}(1+\cos 2\pi f_1(t-T_{pinch})) + F_{min} & T_{pinch} < t < T \end{cases} \quad (5.8)$$

The force profile and definition of the parameters are show in Fig. 5.12, right. F_{pinch} represents the bow force at the beginning of the stroke (i.e. the "pinching" of the string), F_{min} the minimum force at the end of the stroke, and f_1 the frequency of the cosine controlling the decrease (the time between the maximum and the minimum of the force is $1/2f_1$).

This modelling provides a good description of the overall shape of the bow force. In a second step, it would be desirable to take the observed ripples at a frequency around 13 Hz into account. These ripples are probably due to the response of the bow when the finger force on the stick is suddenly decreased at the start of the motion. The control of these oscillations may differ substantially between an expert player and a less advanced[2]. Fig. 5.13 shows bow force patterns in fast martelé performed by an advanced but non-professional player. It is surprising to observe the magnitude of the oscillations compared to Fig. 5.12 (left) showing a professional player producing much smoother force patterns.

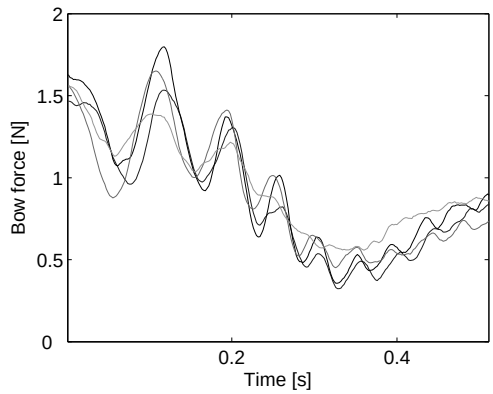

Figure 5.13: Illustration of the bow force during fast martelé strokes performed by an advanced but non-professional violinist. The force shows very strong oscillations due to lack of control of the vibrations of the bow during the decrease in force.

In order to be able to model different performance skills, the ripple component needs to be included. The ripples were modelled with a second damped sinusoid (relaxation time τ) with a higher frequency f_{osc}. The bow force is then given by

[2]Note that the properties of the bow may obviousy also facilitate the performance of the stroke.

$$F(t) = \begin{cases} F_{pinch} & t \leq T_{pinch} \\ F_g(t) + \delta F_{osc}[\cos(2\pi f_{osc}(t - T_{pinch}) + \phi) & \\ \qquad - \cos\phi] \exp -\frac{t - T_{pinch}}{\tau} & T_{pinch} < t < T \end{cases} \tag{5.9}$$

The amplitude of the force ripples is controlled with δF_{osc} and the relaxation time τ. The phase ϕ is used as an additional parameter allowing the production of different types of ripples. For example, for reproducing the ripples observed in Fig. 5.12, left, the phase must be zero. On the other hand, the ripples observed in Fig. 5.13 are better reproduced with $\phi = -\pi/2$, leading to a more abrupt decrease in force at the beginning and oscillations greater than the initial force F_{pinch}.

In the two last sections, we have presented models describing the time evolution of the bow force and the bow velocity during short martelé strokes. As for the bouncing strokes, we tried to model them with "intuitive" parameters that are easily understandable by the user, such as the velocity maximum, the duration of the stroke, and the "pinching" force at the beginning of the stroke. In the next sections, we will first determine the values of the model parameters for typical cases including different dynamic levels, and then we will discuss the extension of the models for producing related bowing patterns.

Fitting model parameters with measurements

A complete parametrization of the martelé model would require extensive studies including numerous playing situations. For example, the fast martelé can be played using different lengths of the bow and at different bow positions.

In the recording sessions reported here, the player was asked to perform martelé strokes at different dynamic levels (*mf-p-f*). Consequently, the player was free to set the parameters of his gestures at his convenience. For example, he was not asked to play martelé strokes using half of the bow length at all three dynamic levels. Naturally, the violinist played the louder dynamic levels with longer bow strokes, and soft levels were played farther from the frog in order to control the bow force easier. We will first examine the model parameters for bow velocity, then for the bow force.

Model parameters for bow velocity

The cos-cos velocity model described before was fitted to measurements of sequences of 16 bow strokes at each dynamic level using a non-linear regression algorithm. Fig. 5.14 shows the value of the five model parameters: velocity maximum, duration of the stroke, asymmetry of the velocity profile, and acceleration at the beginning and end of the stroke. The figures illustrate typical values of the parameters for the three dynamic levels.

From a sound synthesis point of view these values are sufficient, and can be used to control the simulation by producing realistic velocity patterns of the fast martelé at the different dynamic levels. However, some comments can be made concerning the parameter values and their trends versus dynamic level. Empirically, we expect the velocity maximum to be the main parameter varying with the level. The other parameters can be expected to be kept rather constant, or show no systematic variation. For example, the duration of the stroke should not interfere with the dynamic level, as they are two independent musical elements. The musician should be able to play a very short martelé as well as broader versions at all dynamic levels.

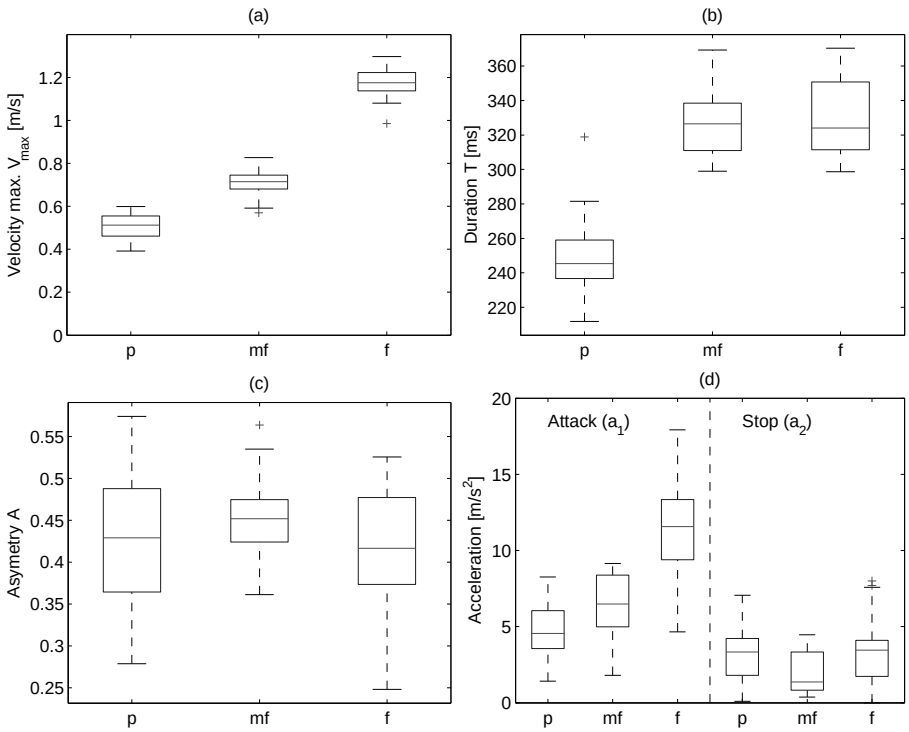

Figure 5.14: Parameters obtained when fitting the cos-cos model to the velocity data in fast martelé strokes. Figures show the parameters obtained from fits of a sequence of 16 bow strokes at each dynamic (*p*, *mf*, *f*): (a) velocity maximum, (b) duration of the stroke, (c) asymmetry of the velocity profile, and (d) accelerations at the attack and when stopping the bow.

As expected, the velocity maximum increased with increasing dynamic level, ranging between about 0.5 m/s (piano) and 1.2 m/s (forte) with rather small spread around the mean values (less than 0.1 m/s). The duration of the bow stroke (see

Fig. 5.14b), was a bit shorter at piano level compared to the other levels (250 ms and 330 ms). It should be noted that this result does not simply reflect the task of successively playing an example at three dynamic levels. During the acquisition the violinist first played *mf*, then *p*, and then *f*, and not *p*-*mf*-*f*, which could have explained a progressive lengthening of the bow strokes. Instead, the lower bow velocity in piano playing allowed for shorter strokes. The martelé is normally played as short as possible, and it is more difficult to stop the bow properly after having reached a high velocity. This could be an explanation to the observed differences in bow stroke duration.

The asymmetry of the velocity profiles (defined as the ratio between the increasing time of the velocity and the total duration of the stroke) was rather constant with mean values between 0.40 and 0.45 (see Fig. 5.14c). This means that the first part with increasing velocity was generally shorter than the second part. Note that decreasing this parameter would give a shorter and more "percussive" attack. When the bow stroke duration is increased at the same time in order to get a constant time for the velocity increase, the stroke can be made a bit broader with a longer velocity decrease while keeping the same attack.

In Fig. 5.14d, left, we can observe a strong correlation between the initial acceleration and the dynamic level, and consequently, also with the maximum bow velocity. The acceleration varies between 5 m/s^2 at piano and 12 m/s^2 at forte level, qualitatively in the same way as the maximum velocity (Fig. 5.14c). As a confirmation, the ratio between the acceleration and the velocity shows the same values independent of the dynamic level. The mean value was around 10 at all three levels, with similar spreads from 2 to 16. As the duration of the velocity increase remained approximately the same in the three cases (between 100 ms and 150 ms), this is to be expected.

Model parameters for bow force

The bow force patterns in fast martelé were more difficult to model than the previous cases for several reasons. First, the bow force during martelé shows a larger variety of patterns. The models proposed before can only give an approximate imitation of these patterns, allowing a reproduction of the main features (decaying trend, oscillations with different amplitudes). Further, the model developed is controlled by a greater number of parameters than, for instance, the velocity pattern (7 compared to 3), which makes the convergence of the iterative algorithm more problematic.

An attempt of fitting the data to the model defined by Eqs. 5.8 and 5.9 is shown in Fig. 5.15. To obtain a convergence of the algorithm, the fit procedure had to be divided into two steps. First, each force pattern is fitted with the cosine model $F_g(t)$ describing the force decrease (Eq. 5.8). This first fit is shown in Fig. 5.15, top. Then the difference between the data and $F_g(t)$ is fitted to a damped oscillation $F(t) - F_g(t)$, where $F(t)$ is defined in Eq. 5.9. This method gives an easier convergence of the algorithm and a better fit to the data. However, the

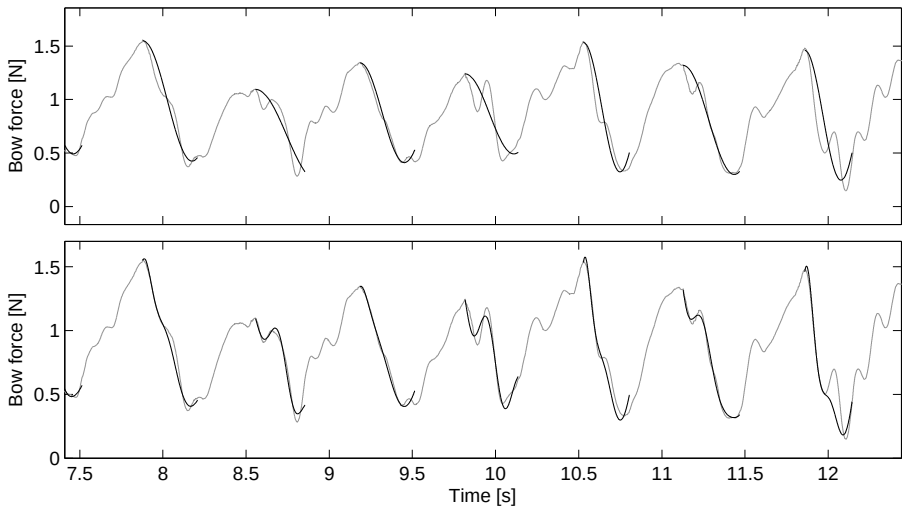

Figure 5.15: Fit of the bow force model to measured data in fast martelé. The fitting is divided into two steps. Top: The parameters of the simple cosine decrease $F_g(t)$ are fitted to the data. This gives a first approximation of the force patterns. Bottom: The difference between the data and $F_g(t)$ is then fitted to the damped oscillations in Eq. 5.9, giving a better description of the measurements.

resulting force profile does not describe the data in a completely satisfying way, as shown in Fig. 5.15, bottom.

Instead of using the approximative parameters obtained from such a fit, some characteristic features describing the data from a more general point of view would be preferable. The parameters of $F_g(t)$ seem to provide a good description of the decrease, and may show less variability between players. The "correction" given by the damped oscillations $F(t) - F_g(t)$ on the other hand, depends on the player and his bowing ability, as shown in Fig. 5.12 and Fig. 5.13. Besides adding sometimes strong oscillations to the decrease, the second term (damped oscillations) has a very small influence on the resulting sound.

Consequently, for our purpose, a simple description may be sufficient, based on the force maximum and its position at the beginning of the stroke (duration of the "pinching"), the force minimum, and the time between the maximum and minimum force (decrease time). These features describe the controlled part of the pattern and can be used to set the parameters of $F_g(t)$. The martelé parameters are shown in Fig. 5.16 for the three dynamic levels. The initial force represented by the force maximum increased with increasing dynamic level, as expected. The mean value varied from about 0.8 N for piano to 2.7 N for forte. The minimum bow force is always very low (less than 0.5 N), but a similar increase with dynamic level can be observed.

It is interesting to notice that the time during which the string is "pinched" also increased with dynamic level. For piano, the mean value was zero, which means that the bow force immediately decreases, or that the force is already decreasing, when the bow starts to move. For mezzo-forte and forte, the force maximum occurred after the beginning of the bow stroke, which means that the player keeps the pressure on the string for a very short time (less than 0.1 s) while the bow is already moving. The duration of the decrease was approximatively the same for the three dynamic levels, which is remarkable because the amplitude of the force variation is very different for the three cases (from 0.8 to 2.4 N).

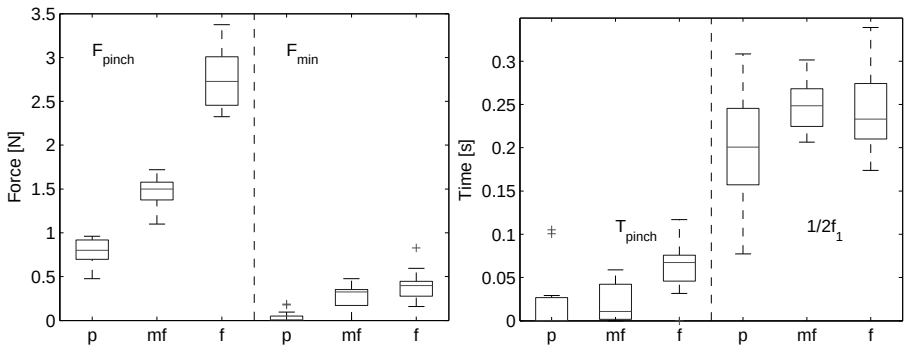

Figure 5.16: Parameters obtained by a two-step fit of bow force to measured data in fast martelé. Left: Maximum and minimum bow force giving a rough description of the force decrease. The maximum is located near the beginning of the stroke, while the minimum is normally reached some time before the end. Right: Parameters for the timing of the stroke. T_{pinch} is the time between the attack of the stroke and the maximum bow force, $1/2f_1$ represents the decrease time (the time between the maximum and minimum bow force).

In this section, the gesture parameters defined before have been used to describe measured bow force and velocity patterns of fast martelé strokes played at three dynamic levels. From this fit, adequate ranges for the values of the model parameters were obtained, which can be used to control our bowed-string model for a variety of fast martelé strokes. In the following section, we will see how we can move away from these standard cases in order to produce related bow strokes.

Extending the model

As in the case of bouncing bowing patterns, the fast martelé model can be used to imitate other bow strokes which share the principal characteristics, i.e. short bow strokes beginning from the string. This includes the *solid staccato*, consisting of successive quick martelé strokes performed in the same bowing direction, as well

as bowing patterns where the bow leaves the string at the end of the stroke (*flying staccato* and *collé*). This section illustrates these bowing patterns and describe how the velocity and force models can be used to imitate their characteristic features.

Solid *staccato*

Galamian [28] describes the *solid staccato* as a

> "succession of short, clearly separated, and consonant-articulated strokes in one bow, performed while the hair of the bow remains in permanent contact with the string. It is practiced most of the time as a series of small, successive *martelé* strokes that follow one another in the same direction of the bow, either up or down. The bow is set firmly for each stroke, and the pressure is released after the accent has sounded on each note."

This is illustrated in Fig. 5.17, showing the time evolution of the bow velocity, the bow acceleration and the bow force during a succession of short strokes played staccato. All notes are performed in the same bowing direction (the bow velocity is always positive), and each time the bow moves, the bow force decreases, showing a time evolution similar to the fast martelé.

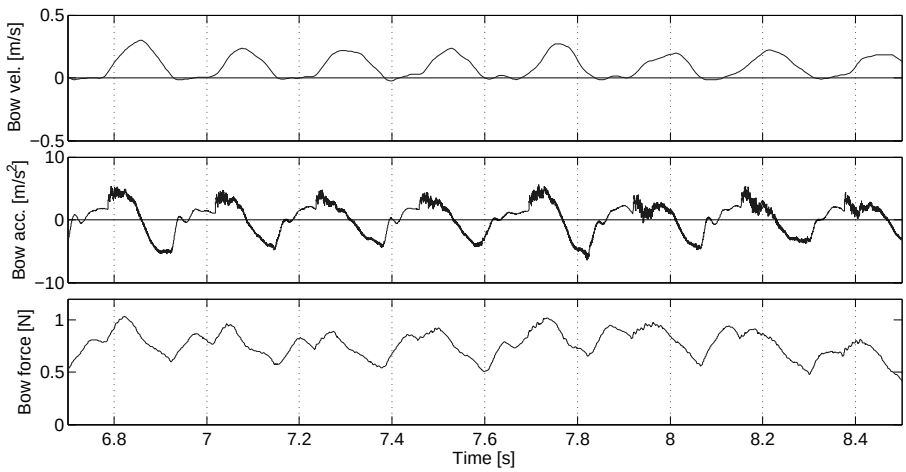

Figure 5.17: Example of *solid staccato*. Successive, very short martelé strokes are performed in the same bow stroke. Top: Bow velocity. Middle: Bow acceleration. Bottom: Bow force. Note that the decrease in bow force is less than for the martelé strokes shown in Fig. 5.15 (from 1 to 0.6 N, approximately).

The imitation of such a time evolution presents no difficulty. It would only consist in repeating the gesture model for fast martelé with slightly modified model parameters.

Flying staccato

The *flying staccato* is very similar to the solid staccato, and consequently also to the short martelé. The only difference lies in the ending of the stroke. The flying staccato "is performed with the same motion as the solid staccato, except that the pressure is lightened and the bow is permitted and encouraged to leave the string after each note" (Galamian [28]). This bowing pattern is illustrated in Fig. 5.18, showing an excerpt of a musical example by Kreisler using flying staccato (indicated by rectangles). Note that in this example, the flying staccato tends to develop into something close to the flying spiccato. In the second sequence, the three first notes are started from the string while the three last notes seem to bounce on the string like in spiccato.

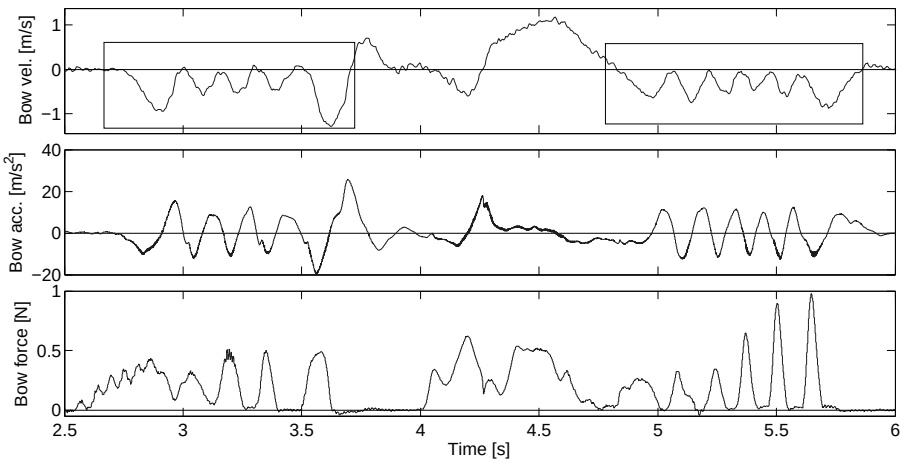

Figure 5.18: Musical example showing the use of the *flying* st*accato*. Top: Bow velocity. Middle: Bow acceleration. Bottom: Bow force. Within the rectangles, several successive short strokes are performed in the same bowing direction. The bow force is maximum at the beginning of the each short stroke and decreases to zero at the end of the strokes.

In order to simulate the flying staccato, the model for the martelé stroke is used, with a force decreasing below zero in order to imitate the release of the bow from the string. However, the bow force must become positive again and damp the free oscillation of the string before the start of the next stroke, else it would sound like a simple spiccato.

Note that a variation of this stroke can be found in the *collé*, which is a bowing pattern starting from the air, but very similar to the martelé: "The bow is placed on the strings from the air and at the moment of the contact the string is lightly but sharply pinched. Simultaneously with the pinch, the note is attacked, and after the instantaneous sounding of the note the bow is immediately slightly lifted off the string in preparation for the next stroke. The pinch is very similar to the martelé attack except for the fact that the time of preparation is reduced to a minimum" (Galamian [28]).

The differences between the bowing patterns described in this section are very subtle and often the difference is made explicit by the musical context. For example, comparing single prototypes of short martelé and solid staccato, no significant differences in the time evolution of bowing parameters can be observed. However, the solid staccato has a character which makes it fit in a sequence of similar notes, whereas the martelé has an individual character and stands out in a sequence of notes. In the same way, the difference between individual strokes of flying staccato and collé lies more in the preparatory gesture than in actual differences in the bowing parameters during the stroke.

5.4 Tremolo and fast détaché

Finally, we will briefly examine some rapid bowing patterns such as *tremolo* and *fast détaché*. They both consist of very rapid bow strokes with the bow on the string from the beginning. In tremolo, the stroke is normally performed as quickly as possible, whereas the fast détaché is performed at a given tempo. In both cases, the main control parameter is the bow velocity. The range of the bow force can be controlled by the player, but the rapid motion does not allow him to control the force variations in detail, and it can be supposed that these variations are mainly induced by the motion of the bow. The player's role consists in applying an overall force control through the bow grip in order to control the natural response of the bow, a kind of passive control.

In this section, we will first illustrate the tremolo and fast detaché. Following, we will make some observations on the time evolution of the bow force at different bowing positions (close to the frog, the middle and the tip), and propose a simple modelling of the bowing parameters. Finally, we will discuss the accentuation of one stroke in a series of bow strokes.

Examples of tremolo and fast detaché

Fig. 5.19 shows two examples of *tremolo* (Fig. 5.19a) and *fast détaché* (Fig. 5.19b). The frequency of the strokes was 8.5 Hz for détaché and 12.8 Hz for tremolo, both played at the tip at mezzo forte level.

As expected, the bow velocity exhibits an almost sinusoidal pattern describing the fast to and fro motion of the bow. In both cases, the amplitude of the velocity

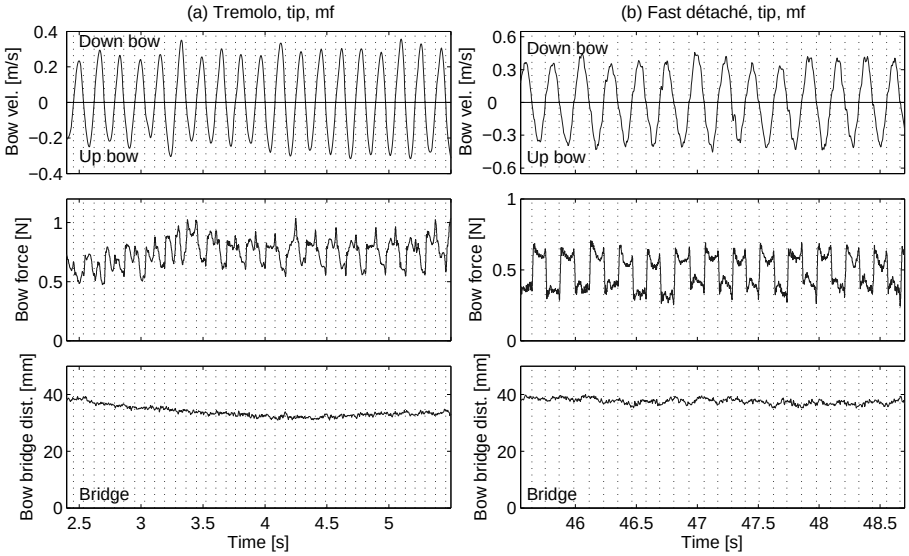

Figure 5.19: Examples of (a) *tremolo* and *(b) fast détaché* performed by the same player at about the same bow position (tip) and dynamic level (*mf*). From top: Bow velocity, bow force and bow-bridge distance. Bow changes are indicated with dashed lines. The fast détaché was played as 32th notes at about 64 bpm (8.5 Hz) and the frequency of tremolo was 12.8 Hz.

was around 0.3 m/s. In the fast detaché (Fig. 5.19b) the bow force shows some interesting patterns with alternating levels around 0.5 N. It can be seen that the lower level (around 0.4 N) corresponds to down-bows and the higher (0.6 N) to up-bows. It seems reasonable to assume that the player does not control this pattern consciously. Because of the asymmetry between down-bows and up-bows we can assume that the changes in bow force are induced by the bowing gesture for obtaining a quick motion of the bow. For example, the alternating motion of the arm when playing the strokes at the tip may induce a force on the forefinger pressing on the bow stick which varies with the direction of the bow. Such an effect could explain the resulting step-wise pattern.

This particular pattern could also be observed in tremolo (see Fig. 5.19a). In that case, the successive steps in force are less clear, probably due to the increase in frequency that makes the gesture less precise. It can be seen that the bow force curve is rather flat, but slightly higher during up-bows. Small peaks can be observed at the bow changes, positive for changes up-bow to down-bow and vice versa.

Another observation can be made, concerning the evolution of the pattern. The measurement in Fig. 5.19a shows the beginning of a long sequence of *tremolo*. The bowing pattern is rather stable between 3.5 and 5.5 s at the end of the series.

However, at the beginning, it can be seen that the bow force pattern evolves and takes some time to become stable, probably reflecting a transitory phase in the response of the bow and an initial adjustment phase during which the player tries out a suitable combination of bow force and bow-bridge distance for producing the tremolo at the requested rate and dynamic level.

As mentioned above, it is unrealistic that the player exerts an active control of the bow force during these rapid bow strokes, with the forefinger pressing on the stick for each note. The variations in bow force are induced by the bow motion rather than being actively controlled, which explains why the changes occur at bow changes. In short, the action of the index finger on the bow stick consists mainly in (a) setting a global value of the bow force (here, around 0.5 N), and (b) damping the oscillations of the bow in order to keep the contact with the string.

Observations on bow force

The previous examples of tremolo and fast detaché played at the tip have shown very specific patterns for bow force. The patterns showed stepwise changes in force with higher values during up-bows. This is, however, not a general feature of rapid bow motions. Actually, a variety of force patterns can be found, depending on bow position, dynamic level and, probably, also on players.

In Fig. 5.20, the dependence of bow force on bow position is illustrated. The same fast détaché is in turn performed at the middle, tip, and frog. The resulting bow force shows three different, but regular, patterns. At the frog (Fig. 5.20c), the force oscillates with a high amplitude (from 0.4 to 1.2 N with a mean value around 0.8 N). The pattern is almost sine-shaped with the lowest force just after the bow change, and the highest force almost coinciding with the maximum in bow velocity. The smooth variations of the force could be explained as follows. At the frog, the player cannot let the full weight of the bow rest on the string, because the resulting force would be too high. When playing at this bow position, he needs to balance the gravity component with the bow grip, which gives poor control possibilities for damping the oscillations of the bow with the index finger. The bow has a first mode of vibration ("bouncing mode") around 15 Hz when supported close to the frog. If some periodical excitations occur in rapid bowing, the resulting bow force will remind of forced oscillations.

As the bow position is shifted towards the middle and tip, the oscillations in bow force tend to disappear. At the middle of the bow (Fig. 5.20a), the bow force is lower and less smooth, showing discontinuities and ripples at the bow changes. In contrast to what was observed at the frog, local force maxima are now found at the bow changes, or just after. During each stroke, the bow force decreases with a damped oscillation.

Finally, at the tip (Fig. 5.20b, described in the previous section), the force variations resemble a switching between two states, on which an influence of the oscillating bow velocity seems to be superposed.

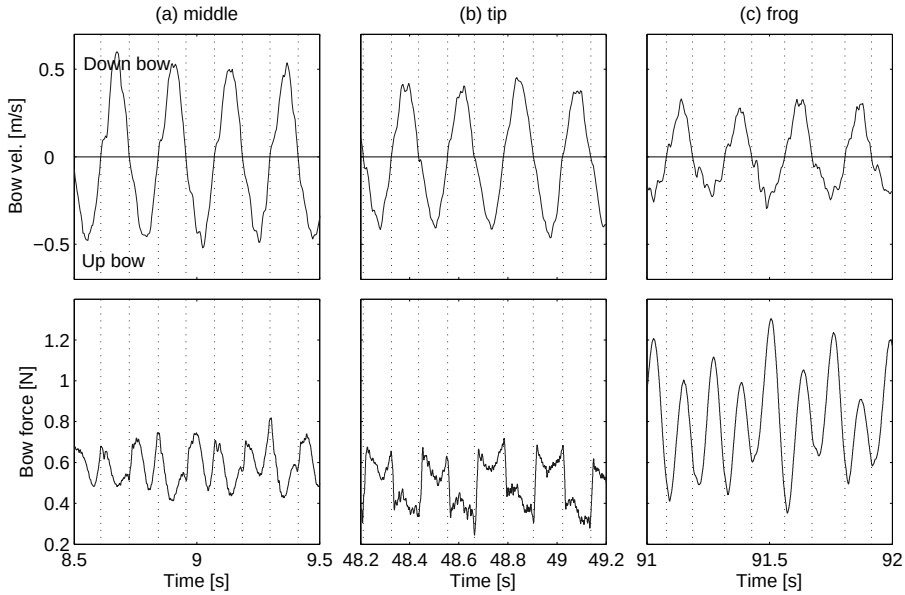

Figure 5.20: Bow velocity and bow force during *fast détaché* performed at different bow positions: (a) Middle of bow, (b) tip, and (c) frog. Bow changes are indicated with dashed lines. The time evolution of the bow force during the strokes is greatly dependent on bow position, resulting in very different patterns.

It should be noticed that despite this great variety in force patterns during the strokes, no significant differences could be heard in the resulting sound. Even for an advanced player, it would be very difficult to guess if a given sound example was played at the frog, tip or middle of the bow.

Fig. 5.21 illustrates the influence of dynamic level on the bow force patterns. A tremolo at the tip is played *mf*, *ff*, and then *pp*. It can be noticed that the force maxima are located at the beginning of the down-bows for *pp* and *mf*. In contrast, during the tremolo performed *ff*, the situation is inverted and the force maxima are found at the beginning of the up-bows.

Modelling bowing patterns

The basic modelling of the tremolo and fast detaché is straightforward. It seems reasonable to model the bow velocity with a sine function whose amplitude will increase with increasing dynamic level. A first approach for the force would be a constant (or slowly varying) bow force corresponding to the mean value of the measured patterns. However, as the details of the bow force patterns vary rather much

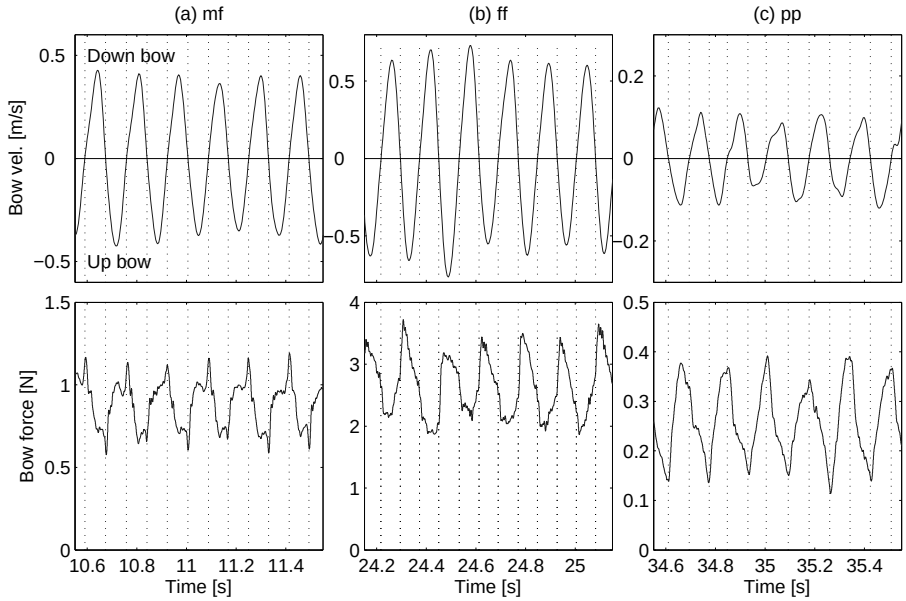

Figure 5.21: Bow velocity and bow force during *tremolo* performed at the tip at different dynamic levels: (a) *mf*, (b) *ff* and (c) *pp*. Bow changes are indicated with dashed lines.

with dynamic level and the bow position, and probably also among players, such a simplification may be too crude and possibly lead to very monotone simulations.

Instead of modelling each case in detail it is more interesting to find a way of offering an intuitive control of the action on the bow in rapid strokes. The measured bow force in Fig. 5.20c, showing a fast détaché performed at the frog, gives an idea for a solution. The bow force has a very clear sine shape and, as mentioned, it seems reasonable to consider the bow as a filter between the player's action (through the fingers) and the bow force at the contact point with the string.

The mechanical system composed of the bow stick and bow hair can be represented by a single oscillator with a fundamental frequency f_{bow}, a damping coefficient r_{bow}, and a mass m_{bow}. The "finger" acts on the mass m_{bow} and the resulting bow force F_b is given by

$$F_b = -Ky \quad \text{with} \quad \ddot{y} + \frac{r_{bow}}{m_{bow}}\dot{y} + \omega_{bow}^2 y = \frac{1}{m_{bow}} F_{finger} \tag{5.10}$$

The mechanical properties representing the bow vary with the bow position. For example, the effective mass of the bow m_{bow} decreases from the frog to the tip, and the spring constant of the deflected bow hair has its lowest value at the middle. Considering the bow stick as a rigid body supporting a single bow hair with tension

T_{bow}, ω_{bow} vary as

$$\omega_{bow} = \sqrt{\frac{T_{bow}}{m_{bow}(\alpha)} \frac{1}{\alpha(1-\alpha)L_{bow}}}$$

where L_{bow} is the length of the bow hair, and α the relative bow position x_b/L_{bow} from the frog. A more accurate relation taking into account the pivoting of the bow around an axis at the frog and the moment of inertia has been given by Askenfelt [5].

The damping coefficient r_{bow} can be assumed to include the damping action of the player's fingers. Instead of considering a component aiming at controlling the mechanical reaction of the bow in the force F_{finger}, the action of the finger is divided into two parts: F_{finger} represents the only active control applied by the player and r_{bow} represents the damping of the bow as well as the damping controlled by the player.

Consequently, the problem of the bow force modelling is transformed into the problem of determining an empirical control of the fingers on the bow, which provides a more intuitive way of controlling the stroke. As discussed before, it seems reasonable to assume a strong correlation between the "active" control of the fingers and the motion of the bow. Under this assumption, we can draw two conclusions. First, the control force F_{finger} should be nearly periodic at the frequency of the bow velocity (i.e. it is correlated with the to-and-fro motion of the bow). Secondly, F_{finger} should be different for different bowing positions because the holding of the bow, and even the bowing gesture, are obviously not the same when playing at the frog or at the tip. For instance, at the frog, the weight of the bow is entirely supported by the hand and the motion is obtained by a combined movement of the wrist and the forearm. In contrast, at the tip the bow can rest on the string and an additional pressure applied by the index finger on the bow stick is required. The action of the wrist is almost negligible compared to the movement of the forearm. The different patterns observed in Fig. 5.20 could therefore be due to the changes in the action of the finger with bowing position, combined with corresponding variations of the dynamic response of the bow. Both effects can be described by the parameters of the simple oscillator.

Precise measurements would be required in order to determine the action of the player's fingers on the bow stick and validate these assumptions. However, empirical considerations will be sufficient for our purpose. In Fig. 5.22 a simulation including impulses by the player's finger on the bow just after each bow change is shown. During one period of the tremolo, the "finger force" consequently shows two successive steps, the highest at the beginning of the stroke. Some variations in the mean value of each step are included. The bow force is shown together with the corresponding F_{finger}. In Fig. 5.22a, the mean value of the initial force impulse is 1.2 N and the following lower step is around 0.8 N. The frequency f_{bow} is set to 13 Hz, the mass m_{bow} is 10 g, and the damping coefficient is set to a rather high value $r_{bow} = 20$. The resulting bow force exhibits a time evolution very similar to the fast détaché at the frog (Fig. 5.20c). The simulated sound, when controlled

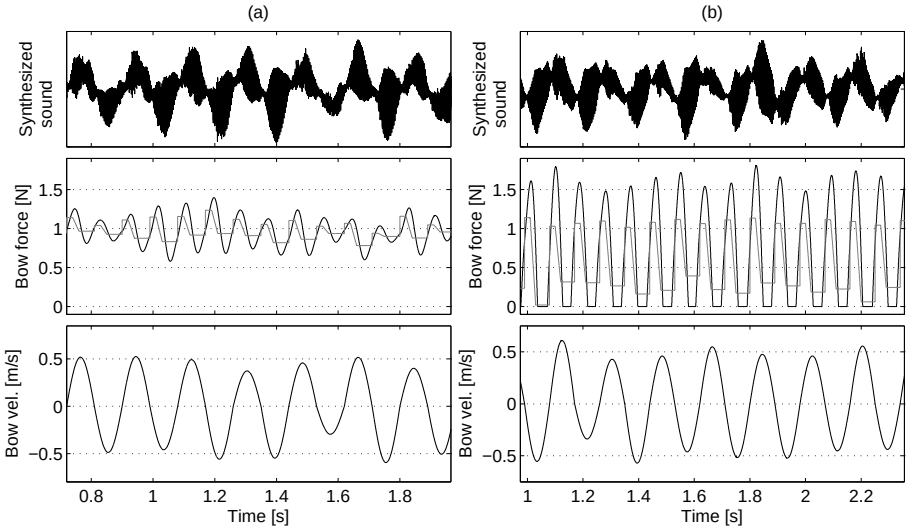

Figure 5.22: Simulations of tremolo using a slightly varying sine shape for the bow velocity and the controlled oscillator for the bow force. Synthesized sound (top), bow force with the original "finger force" in grey (middle), and bow velocity (bottom). The bow-bridge distance was kept constant at $\beta = 0.11$. (a) Normal tremolo obtained by considering a step-wise control of the "bow" with a force impulse after each bow change. (b) Badly controlled tremolo with a too strong difference between the two steps in force and a lower damping coefficient of the bow, producing bouncing of the bow on the string.

with this combination of input parameters, is very convincing, and includes natural irregularities that would not have been obtained with a constant bow force.

The main interest of the proposed model lies in the intuitive correspondence between the model parameters and the empirical experience of violin playing. As an illustration, an uncontrolled (or badly controlled) tremolo was simulated. Starting from the previous example, the approach is rather straightforward. If the player gives a too strong impulse after each bow change, and if the mechanical response of the bow is not well damped, the bow will tend to leave the string and an unwanted bouncing will be obtained. In Fig. 5.22b, the initial impulse is kept unchanged, but the following step is very low (around 0.3 N). Further, the damping coefficient r_{bow} was decreased to 5. The resulting bow force reaches zero during each stroke and shows some patterns similar to the force patterns during rebounds (Chapt. 5.2). It is interesting to notice that the resulting synthesis is a .... *sautillé*. Note that this transition from a fast détaché or a tremolo to a sautillé is an usual exercise practiced by violin players.

Observations on accented notes

We will close this section dealing with fast détaché by describing how quick dynamic changes such as accentuations are performed by players and can be produced with the bowed-string model. The previous measurements were concerned with rapid bow strokes played without dynamic variations from one stroke to another. However, the player can highlight some notes using accents. For instance, in a group of sixteenth notes, the first note is often accentuated in order to mark the beat. In a similar way, accents are sometimes placed on appropriate notes in order to make a specific rhythm appear in an otherwise monotonous succession of fast notes.

The performance of accents is illustrated in three examples at different dynamic levels. The level is controlled by all three bowing parameters, but fast changes in level cannot easily be achieved through variations in bow-bridge distance. Bow velocity and bow force can be expected to be the main parameters controlling accented strokes. This is illustrated in Fig. 5.23. Fast détaché was played at the middle, tip and frog as in Fig. 5.20, with accentuations on every eighth note.

The bow velocity is still kept sine-shaped but the amplitude was increased on each accented note. Whereas the maximum velocity was always between 0.3 and 0.4 m/s during unaccented, "normal" strokes, it reached more than 0.5 m/s in the accented notes. The variations in bow force were even more obvious. On each accented note, a peak in bow force was clearly visible. When played at the middle of the bow, these peaks reached 1.5 N compared to an average value around 0.5 N during non-accented strokes. Moreover, the force maxima coincided with the velocity maxima, which indicates a fundamental difference compared to other dynamical bow strokes such as fast martelé. In the martelé, the maximum force was concentrated to the very beginning of the stroke to obtain an initial "consonant". In the case of accentuations, the variations in bow force and velocity are strongly correlated in order to obtain strong variations in sound level, and no particular articulation or noise between the strokes. In that sense, the accentuation in fast détaché is very close to a sforzando as described by Askenfelt [4].

It should also be noticed that the local variations in bow force are not exactly concentrated to the accents, they affect at least the stroke before and the stroke after. This is particularly obvious when comparing the fast détaché at the tip in Fig. 5.20b and the accented version in Fig. 5.23b. In the normal case, the steps in bow force are always flat, slightly varying around a mean value, whereas in the accentuated case, the last stroke before the accentuation shows a strong increase at the very end of the note, and a decrease during the two following notes. The same behaviour in force could also be observed at the middle of the bow (Fig. 5.23a), and at the frog (Fig. 5.23c). In all three cases, the patterns observed in fast détaché without accents (Fig. 5.20) are still recognizable (for instance, at the tip, it is interesting to observe the same discontinuities at the bow changes), but the time evolution seems to follow a rather broad envelope including the adjacent notes.

This last observation leads to a straightforward way of simulating accentuations,

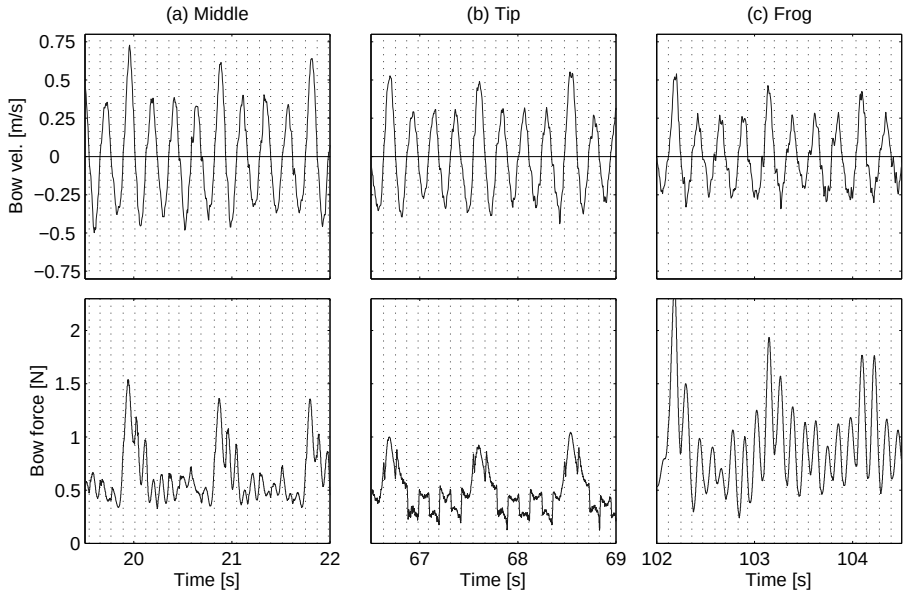

Figure 5.23: Measurements of bow velocity (top) and bow force (bottom) during tremolo performed at the same bow positions as in Fig. 5.20. The first note in each group of eight is accented showing local variations in bow velocity and bow force. The notes are played at (a) the middle, (b) tip, and (c) frog. Bow changes are indicated with dashed lines.

illustrated in Fig. 5.24. The original bow force is simply added to a sine-shaped envelope, whose maximum is located at the middle of the stroke (grey line in Fig. 5.24, right). The resulting bow force pattern is very similar to the time evolution of the force observed in Fig. 5.23b. The bow velocity should be modified as well during the accented note. In Fig. 5.25, the described modification of bow force is applied around the accented note, and the velocity of the accented stroke is multiplied by 1.8.

This section has dealt with rapid repetitive bowing patterns played with the bow in permanent contact with the string such as tremolo and fast détaché. Measurements have been presented and analyzed, illustrating different performance conditions (sound level and bow position). As expected, the bow velocity exhibited a regular sine-shaped pattern describing the to-and-fro motion of the bow. Interestingly, the bow force was found to have different time evolutions depending on the bow position and the dynamic level, but nearly periodical patterns could be observed in all cases. It was assumed that the details in the bow force cannot be controlled by the player for each note, which led to a modelling including three components: (1) the dynamic properties of the bow, represented by a simple os-

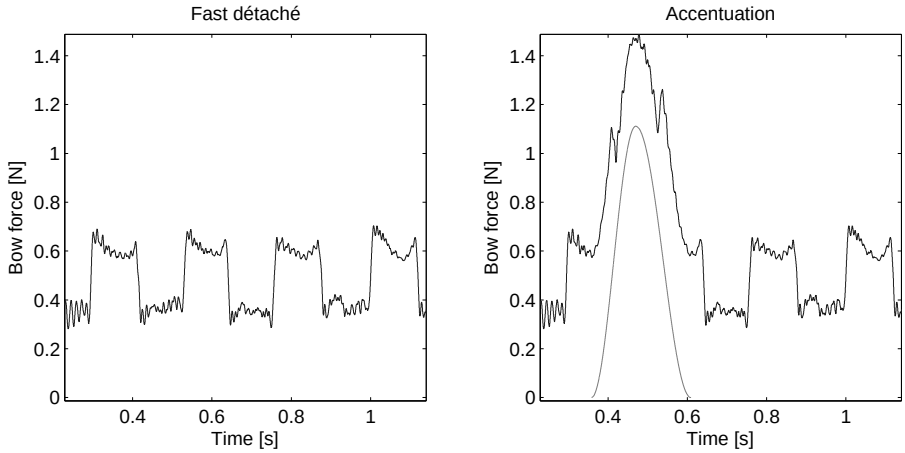

Figure 5.24: Accentuation applied to measurements by adding a sine-shaped envelope to the bow force. Left: Original bow force during fast détaché played at the tip. Right: The same data when modified by adding the envelope (in grey).

cillator with frequency f_{bow}, (2) the "active control" exerted by the player on the bow, and (3) a control of the bouncing resonances of the bow, represented by a damping coefficient in the oscillator model. This empirical modelling provides the means for producing different time evolution of the bow force, giving realistic simulations of the rapid bow strokes in tremolo and fast detaché. In the last section, the performance of accentuations of one note in a rapid sequence was analyzed, and a simple rule for producing accented notes, based on a local modification of the bow force and the bow velocity patterns, was presented.

5.5 Conclusion

We have examined a number of important bowing patterns in this chapter, dealing with the bouncing bow strokes *sautillé* and *spiccato*, followed by *fast martelé,* and *fast détaché*, which are played with the bow in continuous contact with the string. These bowing patterns provide representative illustrations of the violin technique. After including the sustained bowing patterns like *détaché*, which will be tackled in the next chapter, every standard bowing pattern can be reduced to one of these classes, with very small deviations. For instance, the modelling proposed for the sautillé can be used to produce adequate control parameters representing bouncing bow strokes such as spiccato and ricochet. The short martelé shows no principal control differences compared to a solid staccato, and appropriate model parameters can give a flying staccato as well.

For each of the classes described above, we have presented representative bow-

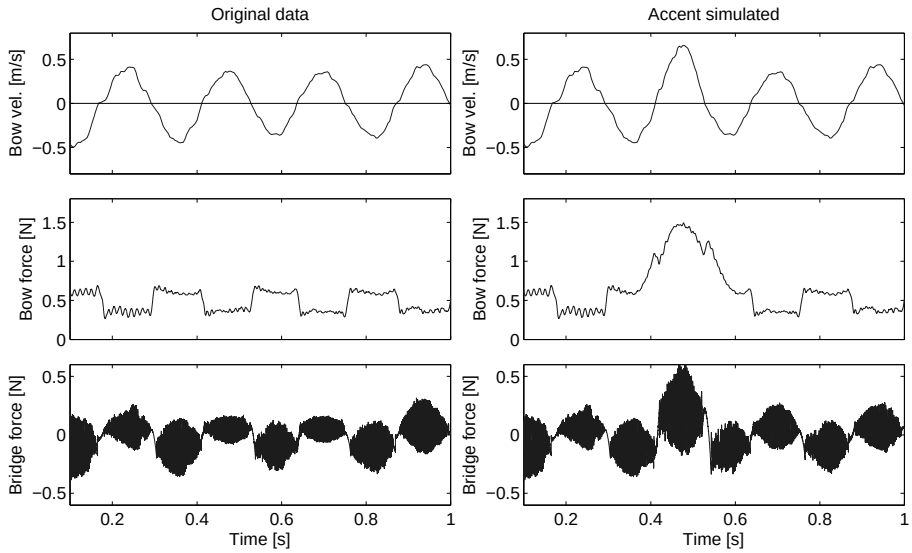

Figure 5.25: Modification of a fast détaché in order to obtain an accentuation on one of the notes. From top: Bow velocity, bow force and the resulting bridge force. Left: Original data from measurements (without accents). Right: Simulated accentuation obtained by adding a sine-shaped envelop to the bow force (amplitude 0.55 N) and multiplying the bow velocity by 1.8.

ing parameters, measured during real performance. From analyses of the measurements, we have empirically deduced simple models that reproduce the time evolution of the bowing parameters well. Following, model parameters have been deduced for typical performance situations by fitting the measurements to the models. We have also discussed the extrapolation of the models in order to obtain other bowing patterns.

With the adequate parametrization, the gesture models produce very satisfying sound synthesis, when used to control the bowed-string model. Special care was taken to obtain an intuitive parametrization of the models. We wanted the model parameters to be relevant and as understandable as possible from a string player's point of view. For instance, bow force patterns during the rebounds were parametrized by the contact time between the string and bow, and the maximal force. For tremolo, bow force was deduced from the finger action by the player on the bow, which is much easier to describe qualitatively than the contact force between the string and the bow. In the design of the models, choices were made in order to permit extrapolation to related types of bow strokes by simply modifying relevant parameters.

The three classes of bowing patterns described in this chapter show subtle dif-

ferences in the control of the bow force which requires different types of modelling. For bouncing bow strokes, the force is essentially dependent on the dynamic properties of the bow, and the player has only limited control. The player can choose the relevant bouncing position on the bow in order to obtain the desired bouncing frequency, or he can give an impulse to throw the bow down on the string and lift it up again, as discussed in Sect. 5.2. However, under these conditions, he has no control on the specific force pattern obtained during the short moment of the rebound and consequently, on the effective contact with the string. Concerning the martelé, the specific shape of the bow force results from an active and constant control of the bow during the stroke, combined with the dynamic response of the bow. The action of the player consists in making the desired overall decrease of the force and in mastering the damping of the oscillations of the bow. The model was consequently composed of an active part describing the global shape of the force, combined with damped oscillations describing unwanted, more or less controlled vibrations. Finally, the tremolo illustrated another sort of uncontrolled patterns. In that case, the motion of the bow is very quick and the player cannot control the bow-string contact in detail. The force control aims at keeping an average level of the bow force, and the characteristic patterns observed in Sect. 5.4 are mainly due to an interaction between the arm movement and the holding of the bow. This interaction influences the action of the fingers on the bow, which works in combination with the bow resonances to modulate the bow force. For that case, we preferred a pseudo-mechanical modelling to describe the bow-string interaction.

We should underline that this mechanical modelling of the bow could have been used in all three cases. Actually, at the end of Sect. 5.4, we have seen that an adequate control of the "finger force" could produce a sautillé with the same force model as for the tremolo. In a similar way, the time evolution of the bow force during martelé strokes could have been produced by considering a specific shape of the "finger force", such as a constant force followed by a sudden decrease. However, for each bowing pattern, we have chosen the modelling method that seemed most natural and easy to work with. For example, the parameters of the tremolo model are not easy to set in order to obtain the sautillé. Obtaining another contact time, for example, is not straightforward when changing the tremolo parameters. In contrast, with the modelling of the bouncing bowing patterns, such changes of the sautillé are straightforward.

The models described in this chapter can be considered as basic bricks of a musical discourse. The model parameters for each bow stroke provide a faithful description of isolated strokes, and could be used to analyse a musical performance. So far, they are the only patterns that the bowed-string model has learnt to perform, as if it was practicing scales. The choice of the parameters to be used for each note during a musical performance, i.e. the time evolution of the model parameters, will create the relation between individual strokes and the musical context, making the music appear.

Chapter 6

Observations on sustained bowing patterns

This last chapter presents measurements and observations on sustained bowing patterns, in particular *détaché*. This large class of bow strokes presents a specific difficulty for our purpose of controlling the bowed-string model with simple high-level parameters. Whereas the time evolution of bowing parameters during short bow strokes can be efficiently modelled as seen in the previous chapter, the same approach applied to sustained bowing patterns would lead to very stereotypic and non-expressive performances. The continuous control of the sound allows continuous variations in expressivity and musical intention, and consequently almost infinite possible variations of the control parameters. Any type of control which not interact in real time with the model will consequently restrict the expressive capabilities.

The difficulties in controlling sustained notes have resulted in that the purpose of this chapter will be more modest. The chapter aims at providing a global description of the use of bowing parameters in sustained bowing patterns and some features that are typical of basic musical tasks, such as scales and repeated notes.

As a first approximation, a détaché can be viewed as a bow stroke with constant, or slowly varying, bowing parameters. Such a basic control leads to very artificial sounds that hardly can be recognized as violin tones. In contrast, when real measurements are used for controlling the bowed-string model, it sounds like a violin. From this simple observation, we can conclude that the characteristics of the details of the bowing gesture are of primary concern in the identification of the stroke and for the judgement of the realism of the sound. This view applies even if all low-level variations in the bowing parameters cannot be attributed to conscious actions by the player, but originate from the mechanical properties of the bow and string in combination with some unstableness in the player's bow control.

All bowing gestures are dependent on the limitations of the human motor control in the interaction with the instrument. For instance, in order to keep a constant

bow force the player has to progressively vary the pressure of the fingers on the bow stick as the bow moves, which produces inevitable, small variations in the bow force. A first step in the modelling of sustained bow strokes should consequently provide a description of such features.

In the first section we will present measurements of the bowing parameters in basic détaché strokes. In the following sections, these measurements will be used as a database of realistic input parameters for controlling the bowed-string model. The reference strokes in the database can be modified, or interpolated, in order to adapt the bowing parameters to various conditions, such as a different durations or dynamic levels. The change of bowing direction ("bow change") constitutes a playing gesture of particular importance, and requires a separate study, presented in the last section.

Two kinds of applications of the results can be expected. Combined with studies of performance expressivity and rule-based performance systems, they could provide some keys for the development of automatic generation of control parameters for violin synthesis, based on the score information. However, this would require a more complete study than the basic observations that are reported here. In particular, it should include analysis of bowing parameters and high-level descriptors such as the dynamics and tonal quality in a chosen set of musical examples. An application closer to our field of research could be foreseen where the current results could be used for incorporating violin-like control features in a system for continuous control of the bowed-string model. For example, the two basic control systems mentioned before (midi wind controller and graphical tablet) allow real-time, continuous control of the three main bowing parameters. However, a bowing gesture like a bow change will be difficult to imitate in detail and the interfaces will not be able to reproduce important features of the gesture. Consequently, when an event is recognized as a bow change by the control interface, it could be interesting to include some informed small variations in the bowing parameters on top of the modelled gesture for a bow change. In this way a more realistic control of the bow change is obtained, including low-level variations in the bowing parameters which change from time to time, at the same time as the global characteristics of the control gesture are preserved.

6.1 Playing détaché

Drawing the bow in a continuous stroke across the string is the most basic way of playing bowed string instruments. The player will face a variety of situations during the performance where such strokes need to be mastered. Depending on the musical context, sustained notes of different duration should be combined or interleaved with accented notes and bouncing bowing patterns. For instance, one of the most arduous challenges consists in alterning fast and slow bow strokes while keeping the same sound quality. Consequently, a basic training of advanced players consists in playing scales with increasing bow velocities at the same dynamic level,

which is achieved by increasing the tempo while using the same length of the bow (the whole bow, or one third, for instance).

In most cases, a large variety of bowing patterns are possible for performing the notes and musical intentions given in the score. The choice is dependent on the level of the player's bowing technique, among other things. In this section we will focus on some standard situations of particular importance. First, we present measurements of a technical exercise consisting in playing détaché strokes with the whole bow and increasing bow velocity. Following, the problem of obtaining different dynamic levels will be analyzed, and, finally, we will discuss the use of measured bowing parameters for controlling synthesis of sustained notes with the bowed-string model.

Playing with different bow velocities

In a first experiment, a violinist was asked to play simple détaché strokes with the whole bow (from the frog to the tip) for different note durations (whole notes, half notes, quarter notes and eighth notes). There was no special instruction about the dynamic level or the bow force. The violinist should feel comfortable when playing, and was consequently let free to perform them in the most appropriate way according to his own preferences. The resulting acquisitions permit us to have a closer look on standard détaché strokes at different bow velocities.

The bowing parameters (bow velocity, bow position, bow force and bow-bridge distance) are presented together with the recorded sound in Fig. 6.1 and Fig. 6.2 for the different durations. Note that, in Fig. 6.1a, the bow is used very close to the tip where the bow force sensor is not very sensitive. The strong variations observed at the tip could consequently be an artefact of the measurement method.

Overall description of the bowing parameters

Because the player uses about the same length of the bow in the four cases, the mean value of the bow velocity increases with decreasing note duration. For the whole notes, the bow moves rather slowly (about 12 cm/s), while much higher bow velocities are reached for eighth notes (mean value 65 cm/s, highest values around 100 cm/s). For intermediate durations, the bow velocity is around 22 cm/s (half notes) and 54 cm/s (quarter notes). The bow force increased much less, from 0.4 N for whole notes to 0.8 N for eighth notes, with intermediate values of 0.5 N (half notes) and 0.6 N (quarter notes). Concerning bow-bridge distance, no clear tendency could be observed. The mean values were between 25 and 40 mm, with a very slight increase from whole notes to quarter notes. It is interesting to notice that the bow-bridge distance tends to increase at the bow changes, which produce local peaks in bow-bridge distance (amplitude between 6 and 10 mm). This feature is especially prominent for whole notes and half notes (Fig. 6.1), whereas for eighth notes, the bow-bridge distance is much more stable (Fig. 6.2b).

As mentioned before, no special instruction was given concerning the dynamic level, and consequently a variation in the amplitude of the sound with duration could be observed. The amplitude was low for the whole notes and increased significantly for quarter notes and eighth notes, following the increase in bow velocity. The resulting variation of the sound level reached 11 dB. These measurements have a special interest for our purpose. They can be considered as the most natural way of performing detaché strokes at a given bow velocity, giving a reference for the sound level and typical variations of the bowing parameters. Starting from these data, it should be possible to extrapolate the bowing parameters and obtain other levels and sound qualities.

On the bow force

In Fig. 6.1 and Fig. 6.2, rather strong variations in the bow force around their mean values can be observed. The bow force is far from being constant and, in particular, an overall increase during each down-up bow cycle could be noted, sometimes with a small gap at bow changes near the tip (see for instance Fig. 6.1b or Fig. 6.2a). The bow force increases during up-bows when the bow position approaches the frog, and drops suddenly before starting the next stroke.

Oscillations with a rather large amplitude (peak to peak value around 0.3 N) can be observed when bowing near the frog, and especially just after the bow change. Note that these oscillations increase with the bow velocity. They are very small for whole notes (Fig. 6.1a) and clearly visible for eighth notes (Fig. 6.2b). The oscillations are most probably due to the resonances of the bow, which are more easily excited when the motion is faster, and the acceleration higher at the bow changes. The bow resonances are damped by the player's grip of the bow, with the index finger resting on the stick. In this case the durations of the notes are so long that the player has time to adjust the damping for each note, but a less efficient control of the damping is expected when the motion is faster. The observed force oscillations can be viewed as footprints of the bow, which adds a ripple to the slowly varying control component of the bow force set by the player.

Consequently, a constant or slowly varying approximation of the bow force in the modelling of detaché strokes seems a little too coarse. The force exhibits some characteristic variations that are clearly identifiable and should be reproduced to imitate typical features of the bow force control.

On the bow velocity

The major change in bow velocity with decreasing note duration has been mentioned above: the mean value increased with decreasing duration, as expected from the "constant-length-of-bow" instruction. However, the bow velocity was not constant during each stroke but accelerated gradually, which is especially visible for quarter notes and eighth notes (Fig. 6.2). This acceleration is slightly larger during down-bows. For quarter notes (Fig. 6.2a) the mean value of the maximal velocity during

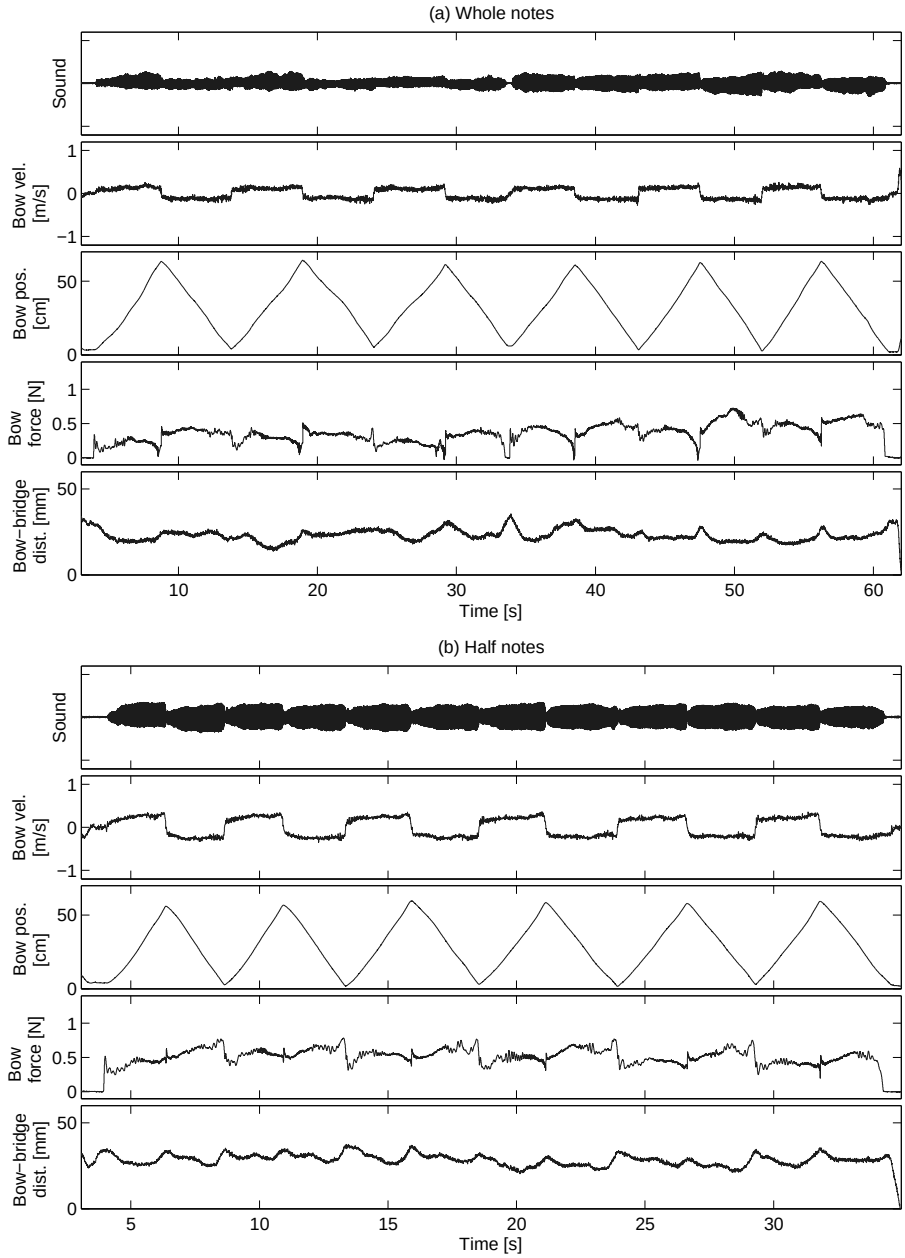

Figure 6.1: Recorded sound and measured bowing parameters (from top: bow velocity, bow position, bow force and bow-bridge distance) for detaché strokes: (a) whole notes, and (b) half notes played with the whole bow.

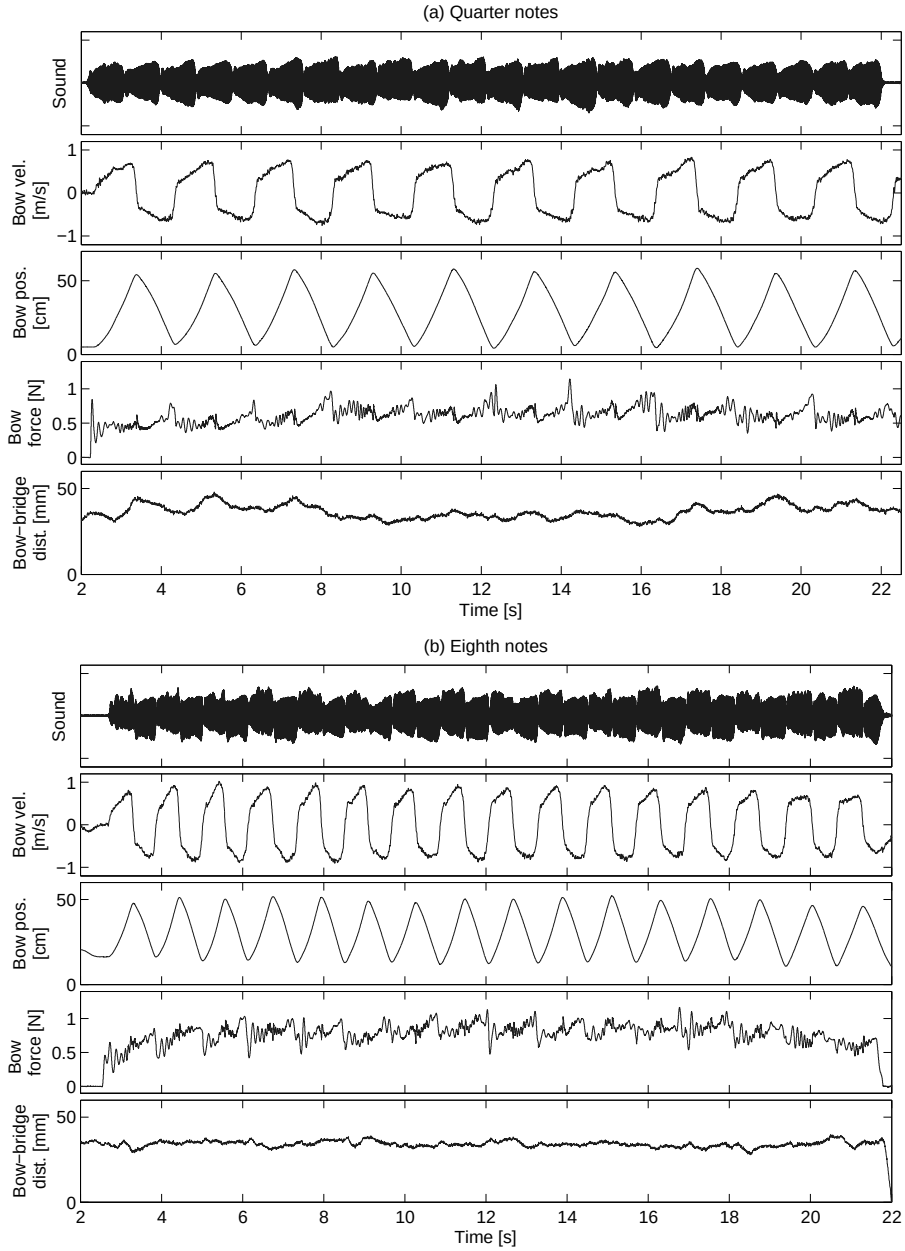

Figure 6.2: Recorded sound and measured bowing parameters (from top: bow velocity, bow position, bow force and bow-bridge distance) for detaché strokes: (a) quarter notes and (b) eighth notes played with the whole bow.

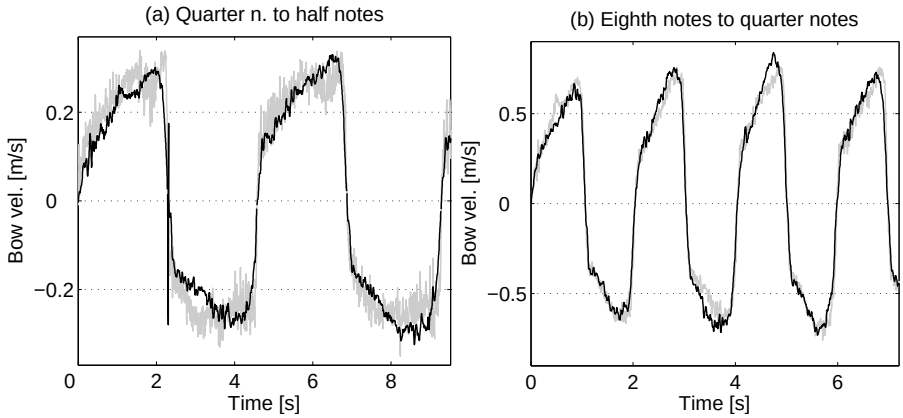

Figure 6.3: Illustration of the similarity between velocity patterns for notes with different durations. Velocity patterns are stretched in order to get the target duration and then multiplied by a factor corresponding to the ratio between the two mean velocities. (a) Quarter note modified to get a half note. (b) Eighth note modified to get a quarter note. Measurements of the target duration are shown in grey and the modified patterns in black. The two curves are very similar and the interpolation possibility will be used later for creating bow strokes with any duration from the reference patterns.

each stroke was 77 cm/s for down-bows and 68 cm/s for up-bows. The maximal values were reached at 84 % of the stroke duration for down-bows and at 72 % for up-bows. Consequently, the patterns during up-bows are generally more rounded than the patterns during down-bows.

The bow velocity patterns share another property that can be seen in the measurements. The acceleration of the bow during the sustained part of the stroke increases with the mean value of the velocity. For half notes, the variation in velocity during the strokes is about 15 cm/s for a mean value of 22 cm/s, whereas for eighth notes, the variation is about 40-50 cm/s around a mean value of 65 cm/s. This observation will make the interpolation of velocities between notes with different durations easier. For instance, the velocity pattern of eighth notes can be stretched to the duration of a quarter note, and then modified in amplitude in order to get the desired mean value (by multiplying it with a factor 54/65 in this case). The obtained velocity patterns are very similar to the patterns of measured quarter notes, as seen in Fig. 6.3b. Consequently, this property will be very useful when interpolating between notes for the synthesis.

Playing various dynamic levels

In Chapt. 3.4, we have illustrated the influence of bowing parameters on the vibration level. The bowed-string model was controlled with constant parameters, and the vibration was analyzed and plotted in Schelleng diagrams. These results show how much the dynamic level can be changed, but many combinations of bowing parameters can produce the same sound level, and a multitude of paths in the parameter space could be imagined in order to change the dynamics. The next step consequently requires a description of what the player really does when changing the dynamic level. The following experiments will illustrate some possible strategies. We will first examine how different dynamic levels for similar bow strokes are obtained, then the case of continuous changes in level during *crescendo* and *diminuendo* will be analyzed.

Détaché at different dynamic levels

Whole notes (duration 4 s) were played detaché at three dynamic levels (*pp*, *mf* and *ff*) with the whole bow (see Figs. 6.4 and 6.5). The bow velocity was very similar in all cases, around 13 cm/s, and the different dynamic levels were obtained almost entirely by varying the bow-bridge distance. Changes in dynamic level are usually obtained by changing the bow velocity as well. But changes in velocity are often limited by musical constraints such as the necessity to "save bow" for long notes, and the difficulty in playing with very high bow velocities, or too low. In earlier measurements [4] in which the player was free to vary all three bowing parameters, no marked change in bow velocity with dynamic level was observed. In the present experiment, it was consequently decided to force the player to use the same bow velocity in order to focus on the variation of the two other bowing parameters.

On average, the sound level increased by 6.1 dB from *mf* (Fig. 6.4b) to *ff* (Fig. 6.4a) and decreased by 6.9 dB from *mf* to *pp* (Fig. 6.5). In order to study the corresponding variation of bowing parameters, the bow-bridge distance and the bow force were averaged across the duration of the measurements (5 s to 25 s in Fig. 6.4 and Fig. 6.5). The average bow-bridge distance was reduced from 52 mm for *pp* to 25 and 19 mm for *mf* and *ff* ($\beta = 0.16$, 0.07 and 0.04). Simultaneously, the average bow force was increased from 0.17 to 0.47 and 1.15 N. Perceptually, an increase in bow force is an efficient tool for raising the dynamic level, as the relative proportion of strong higher partials is increased. This effect, reflected in the value of the spectral centroid, contributes significantly to the impression of "brilliance" which is characteristic of loud dynamic levels in all musical instruments. Besides this effect, an increase in bow force is required for maintaining stable Helmholtz motion as the bow velocity is increased and the bow-bridge distance decreased for increasing the dynamic level. This requirement will be discussed below.

As the three acquisitions were performed with approximately the same bow velocity (13 cm/s on average), it can be interesting to visualize the measurements in a corresponding Schelleng diagram. In Chapt. 3, the string vibrations were

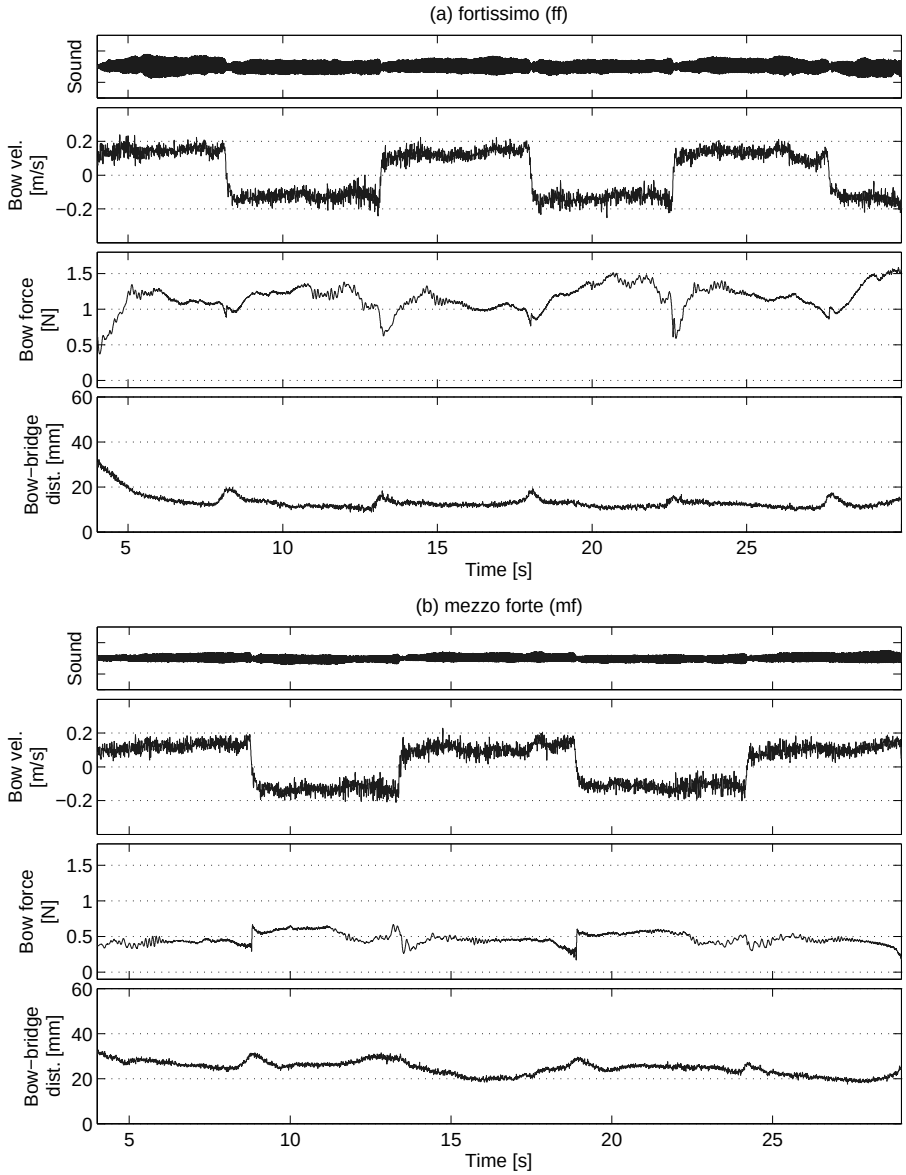

Figure 6.4: Measurement of bowing parameters for whole notes played with the whole bow at different dynamic levels. From top: sound, bow velocity, bow force and bow-bridge distance. (a) *fortissimo*. (b) *mezzo-forte*.

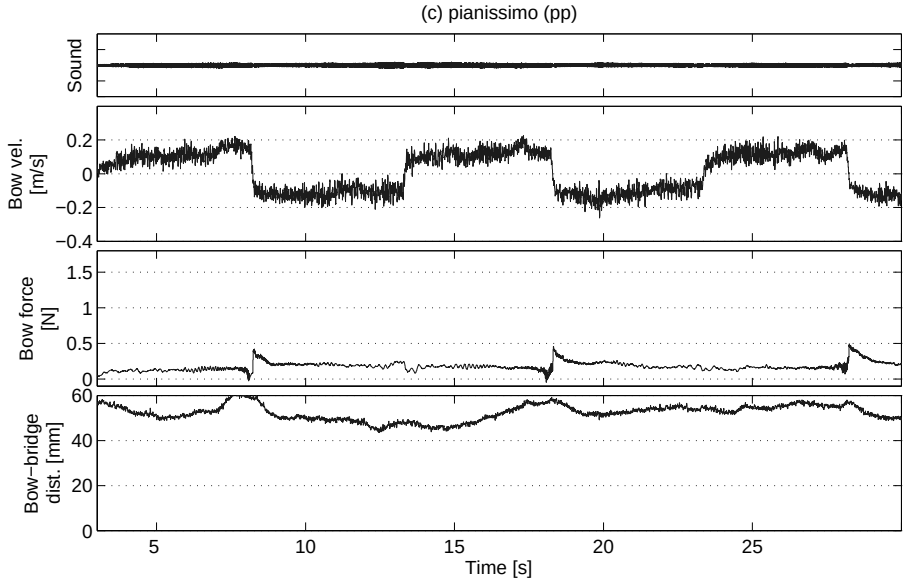

Figure 6.5: Measurement of bowing parameters for whole notes played with the whole bow at different dynamic levels (continued). *Pianissimo*

simulated for various bow-bridge distances and bow forces, and the vibration level was computed and plotted in Schelleng diagrams. For comparison, Fig. 6.6 shows the current measurements at the three dynamic levels plotted on top of a Schelleng diagram representing simulated vibration levels for a bow velocity of 10 cm/s, approximately corresponding to the velocity during measurements.

Three separated regions, used to perform the three dynamic levels, are clearly identified. Their average positions seem to lie on a straight line, indicating a linear variation of the force with bow position on a logarithmic scale. In Fig. 6.6, the best fit for a line passing through the three regions is given by[1]

$$\log F_b = -1.34 \log \beta - 4.215 \tag{6.1}$$

or

$$F_b = 0.0148 \beta^{-1.34} \tag{6.2}$$

The corresponding regression line is included in Fig. 6.6. The slope of the fitted line on a logarithmic scale is -1.34, which should be compared with the slopes of the maximum and minimum bow force, which according to Schelleng are -1

[1] In the following log means the natural logarithm.

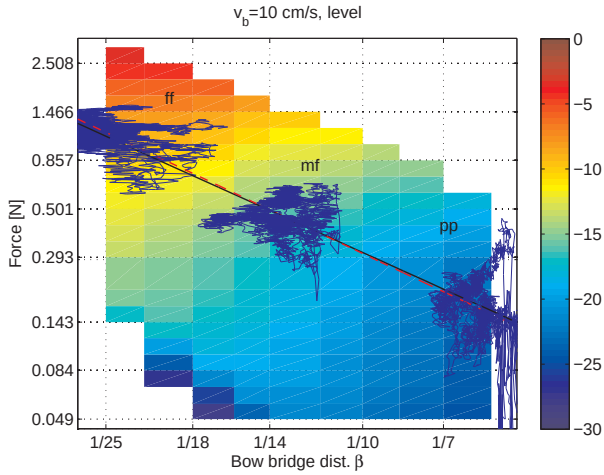

Figure 6.6: Visualization of the combinations of bow-bridge distance and bow force measured for detaché strokes played at three dynamic levels (*pp*, *mf* and *ff*) in a Schelleng diagram. The diagram shows the vibration level in simulations (in color) as a function of bow-bridge distance and bow force for a bow velocity (10 cm/s), which is close to the average velocity in the measurements (13 cm/s). The regions defined by the different dynamics lie on a straight line with a slope of -1.23 (black line). If the line is forced to go through the origin of Schelleng diagam the slope is -1.29 (red dashed line).

and -2, respectively. With Eq. 6.1 we can obtain intermediate dynamic levels by interpolating between the measured levels.

The interpolation depends on the bow velocity, and it would be interesting to find an empirical way of changing the dynamic level for any value of bow velocity. The most straightforward solution consists in expressing the bow force relative to the reference force described in Chapt. 3, given by the force at the intersection between the minimal force and the maximal force ($F_{ref} = 8Rv_b/(\mu_s - \mu_d)$). By observing that the interpolation line found above goes very close to this reference value ($\log F_{ref} = 4.76$ and Eq. 6.1 gives $\log F_b = 4.54$ for $\beta_{ref} = Z/4R$), we can find a similar interpolation line passing through the reference force

$$\log F_b = -1.39 \log \beta - 4.35 \tag{6.3}$$

The slope is now -1.39 and the corresponding line (shown in Fig. 6.6) is very close to the originally fitted line. Note that, if only the bow-bridge distance was changed while keeping the bow force constant, the variations could endanger the Helmholtz motion. For instance, the average value of the bow force for *pp* is very close to the minimum bow force corresponding to the bow-bridge distance used for

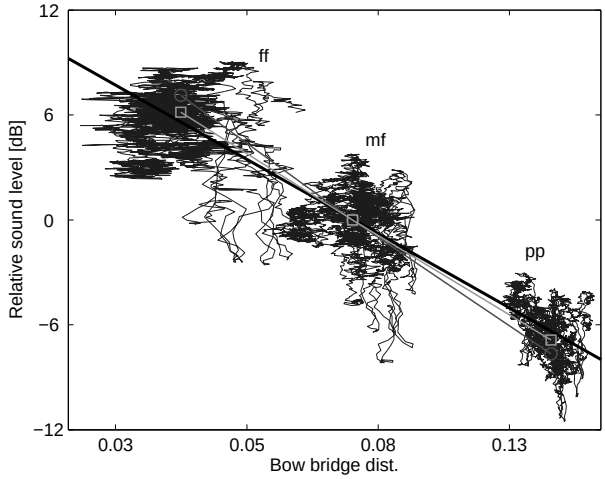

Figure 6.7: Relative sound level of the measured detaché strokes plotted as function of the bow-bridge distance. The reference level (0 dB) is the average level at *mf* . The regions corresponding to the three dynamics (*pp*, *mf* and *ff*) lie on a straight line (full black line). Vibration levels interpolated in Schelleng diagrams obtained with simulations (see Chapt. 3) show a very good aggrement with the measurements. Line with circles: Interpolation in the Schelleng diagram for 10 cm/s. Line with squares: Interpolation for 20 cm/s.

ff. In a similar way, the bow force used for *ff* is above the maximal bow force for the bow-bridge distance used in *pp*. The interpolations obtained with Eq. 6.3 will always be in the middle range of the Schelleng diagram, and this result will be used later for safely changing the sound level of a given bowing pattern.

The relation between the sound level and the bowing parameters is still lacking in the preceding description. Fig. 6.7 shows the variation of the sound level as function of the bow-bridge distance (in log scale). Again, the three regions corresponding to the three dynamic levels are separated and located on a straight line. The fitted line through the three regions, shown in Fig. 6.7, gives the approximate change in the sound level L_{db} with bow-bridge distance β

$$L_{db} \propto -8.5 \log \beta \tag{6.4}$$

It is surprising to observe how close the level variations obtained with simulations are to the measured variations. For instance, if the average bow-bridge distance and the average bow force for the three measured dynamic levels are used to interpolate levels in simulated Schelleng diagrams for a velocity of 10 cm/s, the resulting variations compared to *mf* are +7.1 dB for *ff* and -7.7 dB for *pp*. These values are plotted in Fig. 6.7 for the corresponding bow-bridge distances (line with

circles). The deviation compared to the fitted line (black) is very small but the average bow velocity is somewhat higher than 10 cm/s, which could explain the deviation. As a comparison, if the same interpolation is done for the corresponding diagram at 20 cm/s, the level differences are now +6.1 for *ff* and -6.9 for *pp*, (line with squares in Fig. 6.7) which is even closer to the measured levels.

Crescendo and diminuendo

In the previous experiment, we focused on the variation of the bow position and the bow force for changing the dynamic level of sustained notes, and the bow velocity was assumed to be constant. However, during notes with continuous variations in dynamics (*crescendo* or *diminuendo*), players usually change the bow velocity during the duration of the stroke in combination with changes in bow-bridge distance in order to attain a wider range in dynamic level. This adds a third parameter to the strategies for obtaining a desired sound level, and the examination of level variations with bowing parameters in real performance becomes less straightforward.

In this experiment the player performed two versions of repeated crescendo-diminuendo. In the two cases, the crescendo was played down-bow and the following diminuendo, up-bow. In a first version, the duration of the notes was rather long (around 5 s), and in a second version, shorter notes were used (around 3 s). Due to the necessity of saving bow for long bow strokes, the variations in bow velocity were significantly lower in the first version than in the second. This difference allowed an analysis of two ways of changing the sound level, with and without predominating variations in bow velocity. The first version will be denoted "without velocity" in the following, and the second version "with velocity".

Bowing parameters measured during the experiments are shown in Fig. 6.8. As expected, the experiment "without velocity" (Fig. 6.8a) shows small variations in the bow velocity, compared to the experiment with shorter notes (Fig. 6.8b). In the first case, the velocity varies from 10 cm/s at the beginning of the crescendo to 20 cm/s at the end, whereas in the second case, the velocity varies from 10 to 50 cm/s. It can also be seen that the dynamic span is slightly lower in the first case (27 dB compared to 31 dB), mainly because the maximal level is higher in the experiment with higher velocities. In Fig. 6.8a, the sound level hardly reaches -20 dB, while in Fig. 6.8b, the level goes higher, with a maximum around -15 dB.

In both cases, the bow-bridge distance was decreased with increasing velocity, and the bow force was increased at the same time. In "without velocity", the bow was slightly closer to the bridge (14 mm) at the maximal level than in "with velocity" (18 mm). In contrast, the variations in bow force were clearly smaller in Fig. 6.8a than in Fig. 6.8b. In the second case "with velocity", the force reached more than 2 N and sometimes 2.5 N, whereas in the first case "without velocity" it hardly reached 1.8 N.

Because of the variations in bow velocity, it is not possible to examine the relative variations of the bow-bridge distance and bow force in Schelleng diagrams, as in the previous section. However, we can use the relative force ($F_b/F_{ref}(v_b)$) plot-

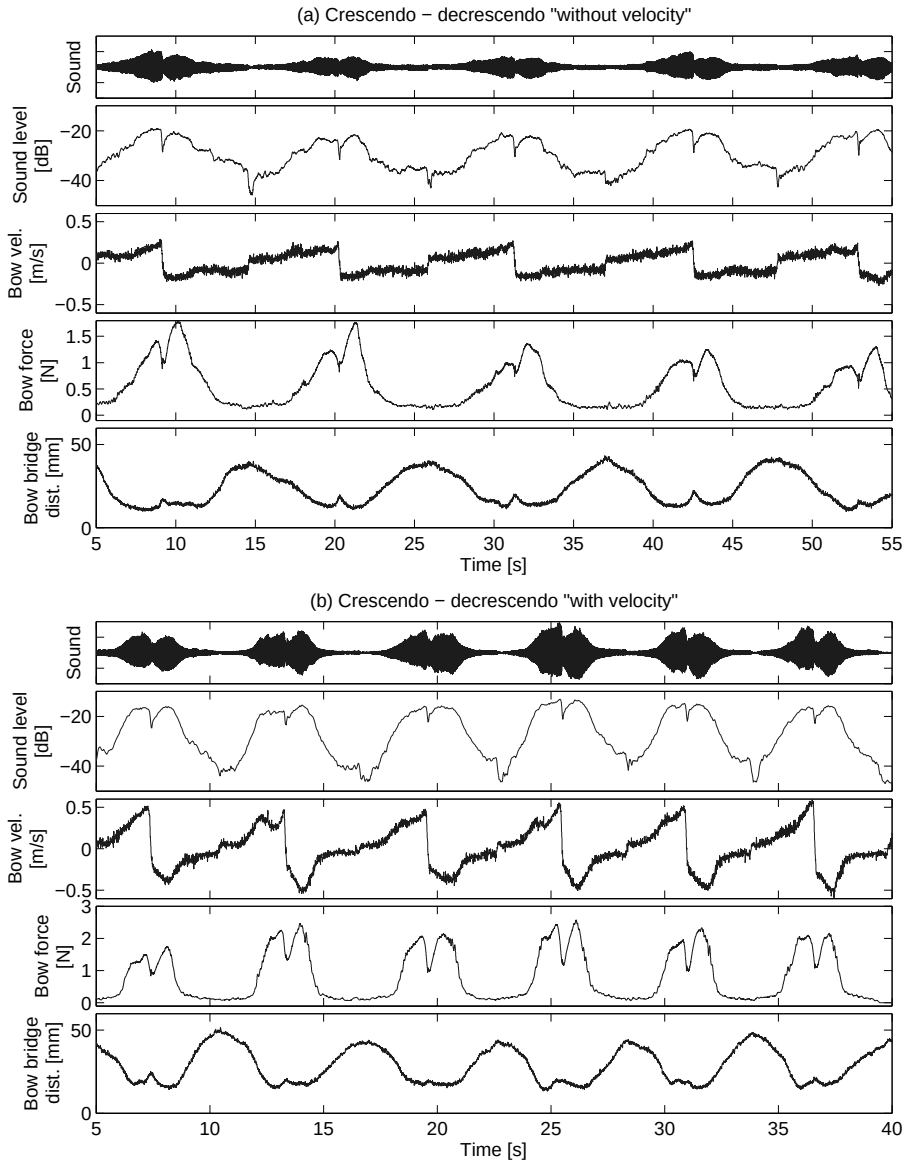

Figure 6.8: Sound and measured bowing parameters for two versions of crescendo - diminuendo played down-bow - up-bow. From top: Sound, sound level, bow velocity, bow force and bow-bridge distance. (a) Dynamic variations for notes with long duration (5 s), showing very small variations in bow velocity. (b) Dynamic variations for shorter notes (3 s) showing larger variations in bow velocity.

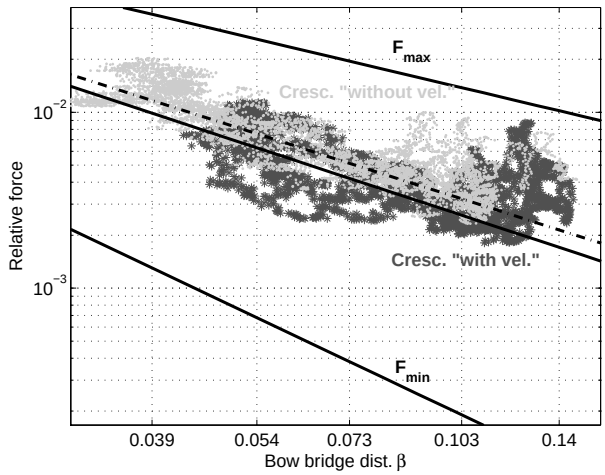

Figure 6.9: Overall variation of bowing parameters during the crescendo - diminuendo in a relative Schelleng diagram, allowing a representation of bow force and bow-bridge distance in the same diagram for any bow velocity (see text). Minimum and maximum force limits are represented with straight lines. The trajectory of the measurements are plotted with dots for the version with long notes ("without velocity") and with stars for the short notes ("with velocity"). The full black line is the fit for sustained sounds at different dynamics (see previous Section), and the dashed line is a better fit with a slightly different slope (-1.32 instead of -1.39).

ted in the relative Schelleng diagram defined in Chapt. 3. In this representation, the maximum and the minimum bow force do not depend on bow velocity, and the trajectories can be made independant of the bow velocity[2]. This is illustrated in Fig. 6.9, in which the minimum and maximum bow force limits are represented with straight lines, and the bowing parameters (relative bow force and bow position) measured during crescendo and diminuendo are plotted. This representation allows a check of that the bowing parameters remain in the Helmholtz region, at a safe distance from both the minimum and maximum bow force. Moreover, it is interesting to notice that, in this representation, the bow force and the bow-bridge distance follow the same path, which would not be the case in a normal Schelleng diagram. A deviation between the two would be observed if the bow-bridge distance decreased due to the increase in bow velocity.

This result should be compared with the variations that were obtained for sustained notes at different dynamic levels in the previous section. In that case, we found a straight line passing through the three regions (*ff, mf* and *pp*) and the force

[2]Note that the bow-bridge distance also could be normalized with β_{ref} in order to obtain a diagram whose limits do not depend on the string properties. In the following, only the force is normalized as we focus on only one note.

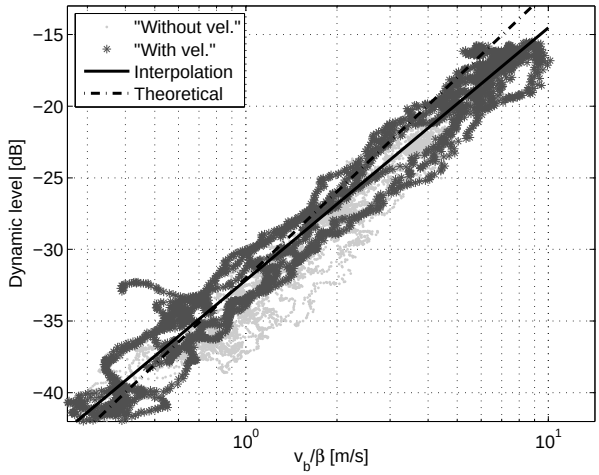

Figure 6.10: Representation of the variations of the sound level versus v_b/β during the crescendo - diminuendo for the two experiments ("with velocity", stars, and "without velocity", dots). A good fit is obtained with $L \propto 7.7 \log(v_b/\beta)$ (black line). The theoretical variation $L \propto 8.7 \log(v_b/\beta)$ is shown in dashed line.

reference ($\log(F_b/F_{ref}) = -1.39 \log(\beta/\beta_{ref})$). This interpolation is shown in Fig. 6.9, black line. We can notice that this interpolation is in good agreement with the bowing parameters measured during the crescendo and diminuendo, even if a better fit could be found (dashed black line). Sustained notes and crescendo - diminuendo are rather different tasks, but this agreement seems to reflect a consistency in the player's choice of bowing parameters at different dynamic levels. The Schelleng limits suggest a "natural" way to follow in the determination of the bow-bridge distance when a given variation in dynamic level is required within a given span of bow velocity.

The previous description provides a way of determining the bow force from the bow-bridge distance and the bow velocity. A next step would consist in describing the variation of the sound level as function of the bowing parameters. The main parameters which set the dynamic level are the bow velocity and bow-bridge distance, the evolution of the vibration level being theoretically proportional to v_b/β, as described in Chapt. 3. Consequently, the most straightforward way of analysing the measurements consists in plotting the sound level against this ratio. This is illustrated in Fig. 6.10 which shows the data measured during the two experiments. In the first case, the predominating variable in the ratio is the bow-bridge distance, whereas in the second case, both the velocity and the bow-bridge distance participate to the variation of v_b/β. As seen in Fig. 6.10, the variation of the level with this ratio is rather linear, defining a diagonal region with a width of about 5 dB.

In simulations, a contribution of about 1.8 dB per log force unit was found, which, combined with the overall range of the force (2 log units) is in agreement with the observed variation range. A good fit of the variation is obtained with a line whose slope is 7.6 dB per log unit.

This result can be compared with the theoretical variation of the vibration level in the Helmholtz description (i.e. no influence of the bow force). With $L \propto v_b/\beta$, we obtain $L_{dB} \propto 20\log(v_b/\beta)/\log 10 = 8.7\log(v_b/\beta)$. The theoretical slope is then greater than the observed one, but the deviation is not very strong on the range we are interested in, compared to the dispersion of the data (see dashed line in Fig. 6.10).

The previous observations suggest a practical way of visualizing the effect of bowing parameters on the sound level, as well as the trajectory of the stroke in the parameter space. The ratio v_b/β is the most relevant variable describing the variation in the sound level. The bow force gives a small contribution, but is mainly used for staying in the Helmholtz region of Schelleng diagrams. Consequently, we can build a "level diagram" depending on the ratio v_b/β and the bow force F_b, in which the variation in level is continuous, whatever the bow velocity. In the background of Fig. 6.11a and Fig. 6.12a, the variation in level obtained in simulations at the same four bow velocities v_b as in Chapt. 3 (5, 10, 20 and 50 cm/s) are plotted versus the variable v_b/β instead of the bow-bridge distance β. The vibration level is shown in colors, and can be seen to vary continuously except at the borders of the playable region. In this representation, the minimum bow force changes with the parameter set in the simulations (one set per velocity), in contrast to the line describing the maximal bow force which is the same for the four sets. This is due to the dependency of F_{min} on v_b/β^2 whereas F_{max} varies as v_b/β.

The crescendo - diminuendo measurements can be plotted on top of these diagrams and compared with the level variations obtained in the simulations. The crescendo - diminuendo performed "with velocity" is shown in Fig. 6.11b, and superimposed on the simulated level diagram in Fig. 6.11a. In order to allow a comparison of the two spans in level variations, the level of the measurements is shifted using the average levels of the simulation and measurement at a mean force of 0.5 N.

The figures show a remarkable overall agreement between the variations in level in the simulations and measurements. The color code for the levels is seen to correspond within an error of about 5 dB compared to a total variation of 30 dB. This is a somewhat surprising fact when considering all possible sources of errors and approximations (including measurement errors in bowing parameters and levels), the crude calculation of the sound level, and the simplicity of the bowed-string model used for the simulations. It is satisfying to see (Fig. 6.12) that also the version with long notes in the crescendo - diminuendo ("without velocity") gives a similar agreement between simulations and measurements.

Previously we have observed a consistency in the trajectories of the measured bowing parameters in the variable space (β,$F_b/F_{ref}(v_b)$) of a normalized Schel-

leng diagram. In the level diagram, however, the corresponding trajectories are expressed as $\log F_b \propto \log(v_b/\beta^{1.39})$, and the consistency between the trajectories whatever the value of the bow velocity is lost, which explains the deviations between the trajectories in Fig. 6.11 and Fig. 6.12.

Application: Modifications of measurements for controlling the model

The modelling of sustained bowing patterns and the description of the time evolution of the bowing parameters with a limited number of parameters is not as straightforward as for the bouncing, dynamic bow strokes in the previous chapter. As illustrated by the measurements on sustained notes above, there is a large variation in the bowing parameters during a stroke, which is not straightforward to imitate. However, our measurements provide a significant quantity of examples describing the time evolution of bowing parameters in various playing situations. A more realistic control of the model could therefore be obtained by using measurements from this "database" directly as input parameters.

Despite a significant amount of collected exemplary bowing patterns, the measurements do not cover all playing possibilities. For instance, intermediate durations are required, as well as intermediate dynamic levels. In order to increase the synthesis capabilities of the model, measurements can be modified according to simple rules that are deduced from the previous observations. In this section, we will illustrate such possible modifications of the dynamic level and the durations.

Modifying dynamic levels

The prototypes of sustained notes provided by the measurements are performed at a given dynamic level. A transformation to other levels based on empirical observations requires a systematic approach, but the pitfalls are numerous.

The empirical effect of bowing parameters on the sound level is well known. For instance, we can think of increasing the bow velocity or decreasing the bow-bridge distance for playing louder. However, empirical modifications quickly become a tedious work when trying to find the right profile of a given bowing parameter for producing a desired variation in sound level, and at the same time, trying to make corrections of the other parameters for maintaining a stable Helmholtz motion, or keeping the same sound quality. For instance, increasing the bow velocity alone decreases the spectral centroid and does not lead to a convincing increase in loudness.

This section aims at proposing a systematic procedure for changing the level of a sustained note. We must consider two constraints in order to perform the change. First, a given change in sound level is wanted, possibly varying in time for performing dynamical variations such as crescendo. Secondly, we must consider a constraint on the bowing gesture. Typically, variations in bow velocity are limited by the length of bow available and the duration of the note. If the time evolution

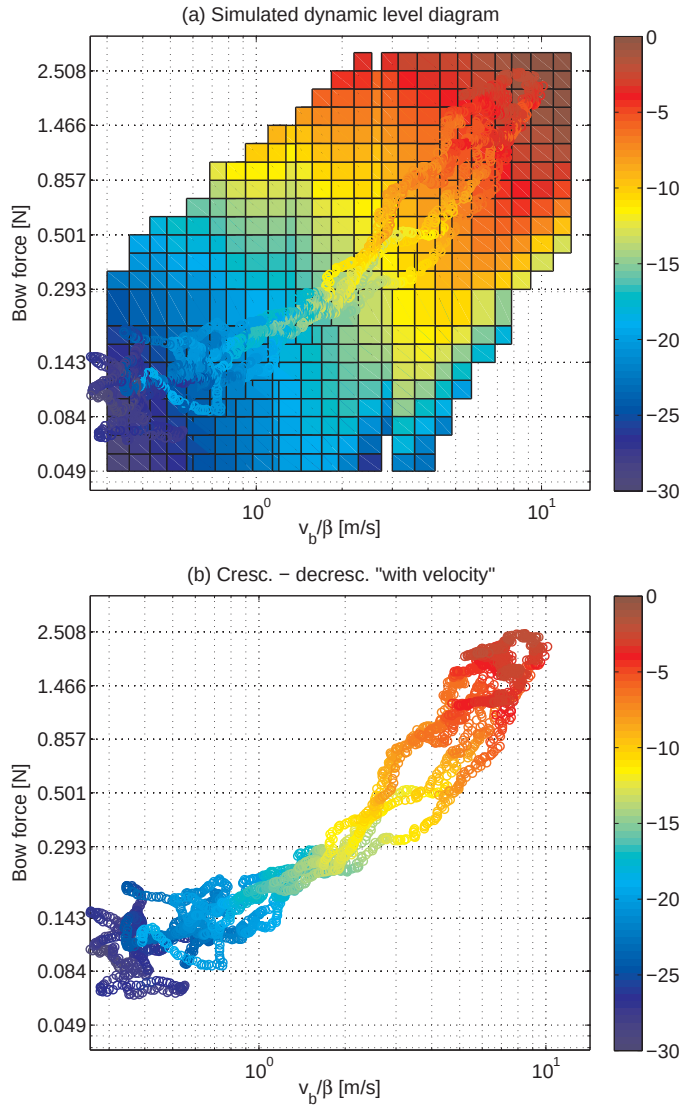

Figure 6.11: Visualization of the crescendo - diminuendo measurements for short notes in the variable space of a level diagram. The sound level (in color) is plotted as a function of the ratio v_b/β and the bow force F_b. (a) The simulations of vibration levels in Schelleng diagrams at four bow velocities (Chapt. 3) are combined in a level diagram (background). Data from the crescendo "with velocity" are superimposed for checking the agreement between simulations and measurements. (b) Visualization of the crescendo - diminuendo measurements without the background.

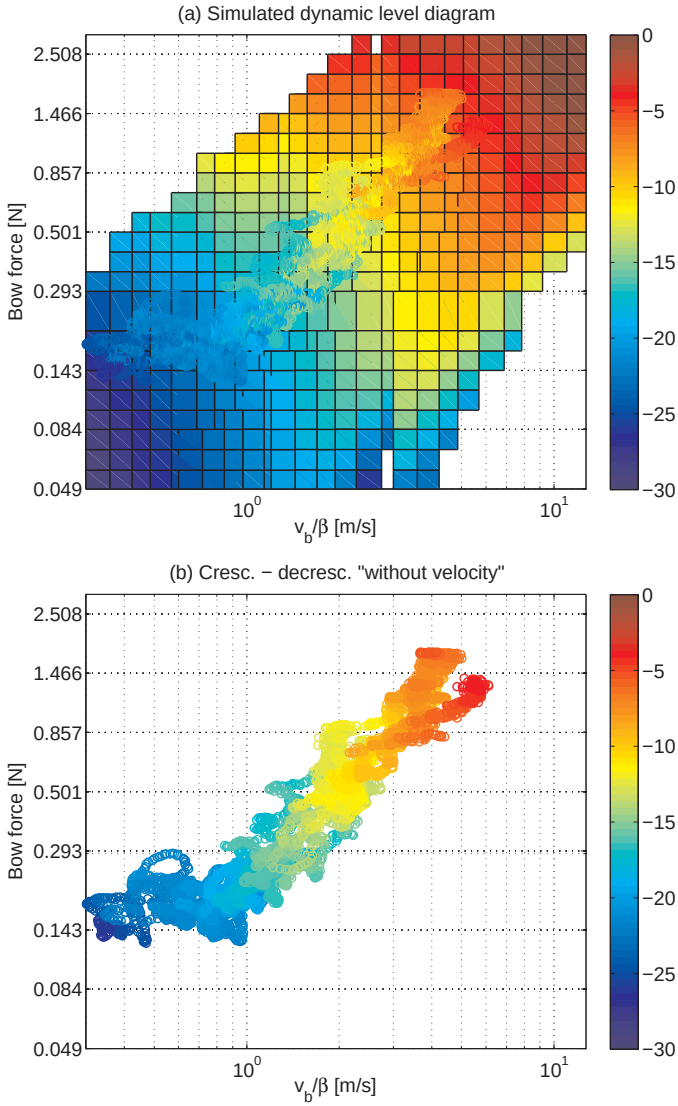

Figure 6.12: Visualization of the crescendo - diminuendo measurements for long notes in the variable space of a level diagram. The sound level (in color) is plotted as a function of the ratio v_b/β and the bow force F_b. (a) The simulations of vibration levels in Schelleng diagrams at four bow velocities (Chapt. 3) are combined in a level diagram (background). Data from the crescendo "without velocity" are superimposed for checking the agreement between simulations and measurements. (b) Visualization of the crescendo - diminuendo measurements without the background.

of the three bowing parameters can be deduced from these two constraints alone, the complexity of the problem will have been significantly reduced. The previous observations on how the variations in dynamic level are achieved in real performance provide the keys to the following procedure.

In a first step, the variation of bow-bridge distance has to be found, according to the change in level and the velocity profile. For that purpose, the theoretical evolution of the vibration level with bow velocity and bow-bridge distance can be efficiently used, as seen in the previous section. If we consider a change ΔS in the level, starting from the original values of the bow velocity v_b^0 and the bow-bridge distance β^0 provided by the measurements, we can write

$$\Delta S = \alpha(\log \frac{v_b}{\beta} - \log \frac{v_b^0}{\beta^0}) \tag{6.5}$$

where v_b and β are the new values of the bow velocity and the bow-bridge distance which give a change ΔS in level compared to the initial values v_b^0 and β^0. The coefficient α was determined previously from real performances and is theoretically 8.7. Consequently, the new value of the bow-bridge distance can be deduced from

$$\beta = \frac{v_b}{v_b^0} e^{-\Delta S/\alpha} \beta^0 \tag{6.6}$$

In a second step, we must determine the bow force in order to stay in the Helmholtz region of the Schelleng diagram. This could theoretically be done in a number of different ways. However, we have seen before that the player tends to follow a straight line in the relative Schelleng diagram, in the direction of the corner of the Helmholtz region. For simplicity, and with a good approximation, we assume that the line goes exactly through this origin. This has the advantage of ensuring that we will stay in the Helmholtz region, provided that the initial parameter combination (β^0,F_b^0/F_{ref}^0) lies between the minimum and the maximum bow force. The slope of this line is given by

$$\gamma = \frac{\log(F_b^0/F_{ref}^0)}{\log(\beta^0/\beta_{ref})} \tag{6.7}$$

Finally, the new value of the bow force is determined by

$$F_b = \left(\frac{\beta}{\beta_{ref}}\right)^{\gamma} F_{ref}(v_b) \tag{6.8}$$

The procedure is illustrated in the following example, with two successive half notes from the measurements described at the beginning of this section. A linear variation from 0 to +6 dB in level is desired during the second note in order to produce a crescendo. For simplicity, we consider no variation in the bow velocity, so the level variation will result from a variation in bow-bridge distance only, combined with an adaptation of the bow force.

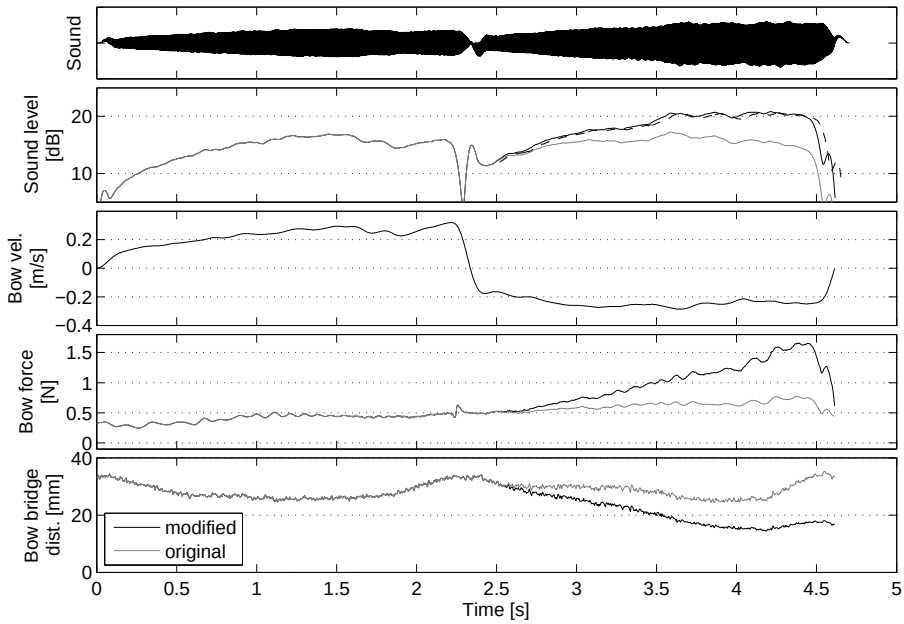

Figure 6.13: Modification of measured bowing parameters for obtaining a crescendo on the second note in two detaché strokes by variation of the sound level (see text). The original data are shown in grey and the modifications in black. From top: Sound of the modified simulation, sound levels, bow velocity, bow force and bow-bridge distance. A linear increase of the difference in dynamic level between the original modified simulations was the target, without changing the bow velocity. As a result, the bow-bridge distance was decreased compared to original data, and the bow force increased significantly. The change in sound level is in agreement with the expected variation, shown by the dashed line.

The input parameters and the resulting simulation are shown in Fig. 6.13. First, the new bow-bridge distance is computed with Eq. 6.6. In this case, $v_b = v_b^0$ (no modification of the bow velocity), and the relation simply becomes $\beta = \exp(-\Delta S/\alpha)\beta^0$, with $\Delta S = 6t/T_{stroke}$ (linear variation of the level up to 6 dB during the duration T_{stroke} of the note). In this example, α was set to its theoretical value ($\alpha = 8.7$ dB/ log unit of v_b/β). As seen in Fig. 6.13 the modified bow-bridge distance deviates more and more from the original values with increasing time. While the original bow-bridge distance always is more than 25 mm, the modified distance decreases to 15 mm. The maximal deviation between original and modified bow-bridge distance is as large as 20 mm.

The bow force is computed by combining Eq. 6.8 and Eq. 6.7 in order to obtain an acceptable trajectory in the relative Schelleng diagram. In Fig. 6.14

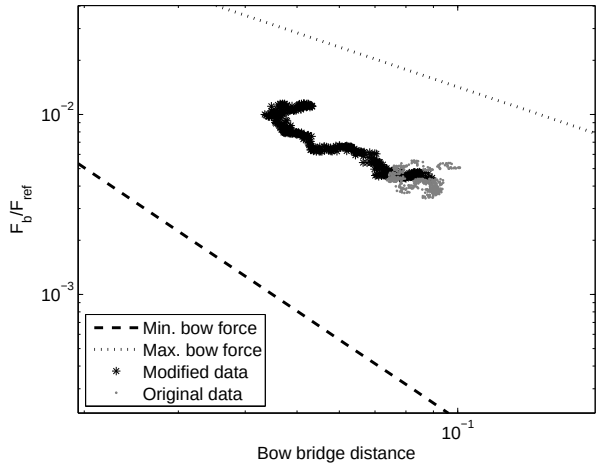

Figure 6.14: Relative Schelleng diagram showing the original data (in grey) and the modified values (in black) for obtaining the changes in sound level in Fig. 6.13. The procedure described in text permits to calculate the required variation of the bowing parameters. While the original data for the detaché notes are confined to a limited region, the modified parameters describing a crescendo follow a straight trajectory in direction of the corner of the Helmholtz region, as observed in real measurements.

the trajectory of the modified parameter combination (β,F_b/F_{ref}) is illustrated together with the original parameter data. As expected, the modification follows a linear trend towards the corner of the Helmholtz region. The resulting bow force is shown in Fig. 6.13 and is significantly enhanced, with an increasing deviation compared to the original data up to 1 N.

The levels of the simulated sounds are compared in Fig. 6.13. The difference between the modified simulation and the original increases with time. It is satisfying to observe that the level of the modified simulation shows a very good agreement with the expected level variation (shown with dashed line in the figure). Note that, because of a significant incertainty in the value of α for the model, such an agreement could not be taken for granted.

Modification of the duration of bow strokes

At the beginning of this chapter, it has been shown that détaché strokes with different durations have a very similar time evolution when they are normalized to the same duration and amplitude. This observation provides a simple rule for obtaining various durations from a limited set of bowing prototypes. The principle of the modifications consists in modifying only the duration of the sustained part of the

stroke by stretching or compression, while keeping the transitory part unchanged in order to keep an acceptable quality of the bow change.

A database containing isolated détaché strokes from the measurements was built, with basic descriptors such as the duration or the dynamic level. Each prototype was segmented into three intervals corresponding to the attack of the note (i.e. the second part of the bow change), the sustained part, and the first part of the bow change (i.e. the segment where the velocity decreases to zero, without the attack of the next note). When a note with a certain duration is required, the bowing patterns with the closest durations are inspected. A prototype is chosen and the sustained part stretched or compressed in order to obtain the desired duration. Then, the velocity and force ranges are scaled by interpolating between the two sets of prototypes with the closest durations. Finally, the new sustained part is appended to the scaled attack and end for completing the stroke.

This procedure provides a possibility of building any rythmic sequence from a limited number of examples as illustrated in Fig. 6.15. Velocity profiles with realistic shapes are obtained and the variations in bow force during the stroke are reproduced. Note that the oscillations of the force at the frog will have a different frequency, but if the database contains examples sufficiently close in duration (like for example the measurements presented in Fig. 6.1 and Fig. 6.2), the frequency of the oscillations will not be multiplied by more than 1.5 and less than 0.75, which can be considered acceptable.

The continuity of the bowing parameters between successive notes must be paid particular attention. The velocity shapes will be adequately connected because each pattern begins at zero velocity (attack from the string) and finishes with a zero velocity (change of bowing direction). Discontinuities or unrealistic bow acceleration patterns can be neglected in a first step. The continuity of the bow force patterns is more problematic because each stroke begins and finishes with a different force value. If the resulting force discontinuities at the junction between the notes are not too strong, they can be kept as they are in a first approximation. In the next part of this chapter (Sect. 6.2), we will make some observations on bow changes, which could provide some rules for solving the problem of force discontinuity. For instance, a rapid sinus-shaped transition in force at the bow change could be considered in order to connect the notes.

The present section has dealt with the sustained part of détaché bowing patterns. We have made some observations on the time evolution of the bowing parameters, and on the player's control strategy for changing the dynamic level. Further, we have deduced some simple rules in order to control the bowed-string model to obtain notes with different dynamic levels, variation in sound level during the note, and with different durations from prototypes. The transition between notes causes a specific problem because the proposed modifications do not take the behaviour of the string when the bowing direction is changed into account. In some cases, the regular Helmholtz motion may be threatened by the parameter changes, and some "playing" skills are required in order to make proper bow changes.

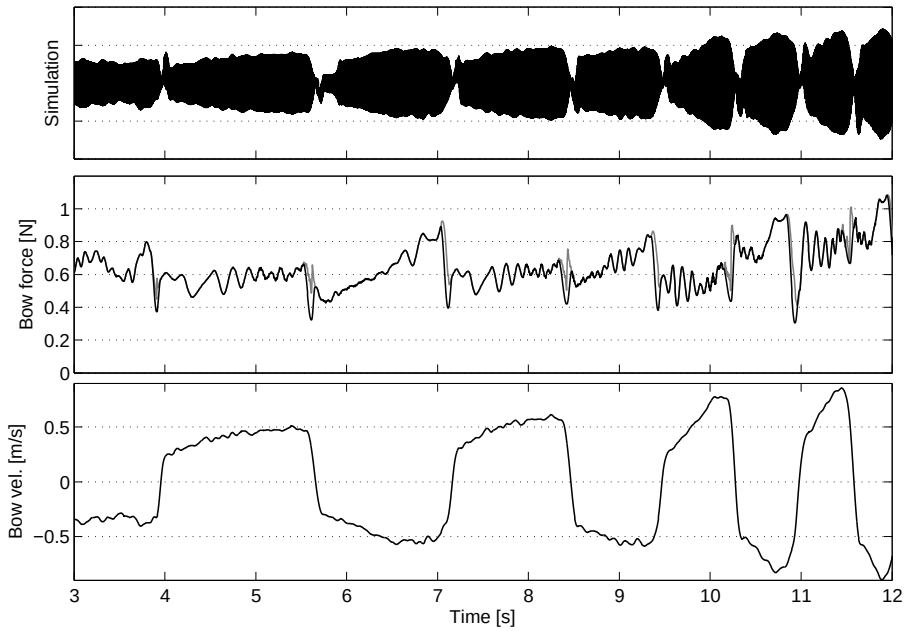

Figure 6.15: Modification of measured bowing parameters for obtaining various durations of the bowing patterns. A database of exemplary bowing patterns representing standard durations is used for interpolating new durations of the strokes. The sustained part of the bowing parameters is stretched or compressed in order to obtain the desired duration, and the bow force and velocity are scaled to the appropriate ranges. For the bow force at the change, a rapid sinus-shaped transition (in black) is used to bridge the discontinuity (in grey).

6.2 Bow direction changes

Players of bowed instruments commonly separate notes by changing the direction of the bow motion ("bow changes") and the separation can be made more or less pronounced (*detaché* - *portato* - *martellato*). Acceptable bow changes require accurate control and coordination of a set of bowing parameters, in particular bow speed, bow force and bow-bridge distance. Long practice is required before optimal control is achieved.

This section aims at giving some detailed descriptions of the bowing gesture during bow changes. We will first introduce the problem by illustrating different types of bow changes and the arm motion during the change. Then, measurements will be presented and analysed in order to extract some characteristics of the time evolution of the bowing parameters. Finally, using the data for controlling the

synthesis algorithm, we will discuss how modifications of the parameters influence the bow-string interaction and resulting string vibrations during bow changes.

Introduction

Illustration of bow changes

Bow changes can be performed in various ways according to the musical context and the desired separation between the notes. For instance, during a long legato phrase, long notes requiring more than a full bow stroke are played by making the bow changes as inaudible as possible in order to not interrupt the sound. In contrast, the articulation (separation) between notes is of primary importance in music from the baroque period and accentuation can be used for highlighting some notes, or giving a very powerful sound.

Fig. 6.16 illustrates different performances of a bow change. In Fig. 6.16a some basic bow changes during simple détaché are shown. Basically, the example consists in playing separate notes with no particular expression and without trying to make the bow changes as smooth as possible. The bowing parameters patterns are very similar to the shapes observed in Sect. 6.1. The bow velocity increases slightly during the sustained part, and the bow changes are very short, giving rather sharp triangular patterns for bow position. As noticed before, the bow-bridge distance is slightly increased at the change, showing peaks, which could make a good attack after the change easier. However, it could also be an artefact of the gesture, and we can have doubts about the intentional aspect of this feature[3]. Finally, the bow force shows very strong peaks (around 1 N) during bow changes at the frog (from up-bow to down-bow) while its mean value during the main part of the stroke is around 0.5 N.

In Fig. 6.16b articulated détaché is shown. The slope of the velocity during the change is lower, giving rounded corners of the triangular patterns for bow position. As a consequence, the bow force must be strongly decreased at the change for avoiding scratchy sounds, resulting in deep gaps in bow force.

Finally, accentuated détaché is illustrated in Fig. 6.16c. The bow is strongly accelerated at the beginning of each note (more than 10 m/s^2 and a maximal velocity around 0.7 m/s) and the bow velocity decreases during the remaining part of the stroke, gradually reaching very low values close to zero. The bow force follows a similar pattern with a sudden increase at the change, up to about 1.8 N. Note that these patterns corresponds to a variety of very strong and exaggerated accents.

In the following part of this section, we will focus only on "natural" bow changes during détaché, i.e. a simple transition between two opposite directions of the bow motion.

[3]These peaks could be produced by some changes in the trajectory of the bow. If the bow is not parallel to the bridge at the change, which is often the case when playing near the tip, such peaks in bow-bridge distance should be observed.

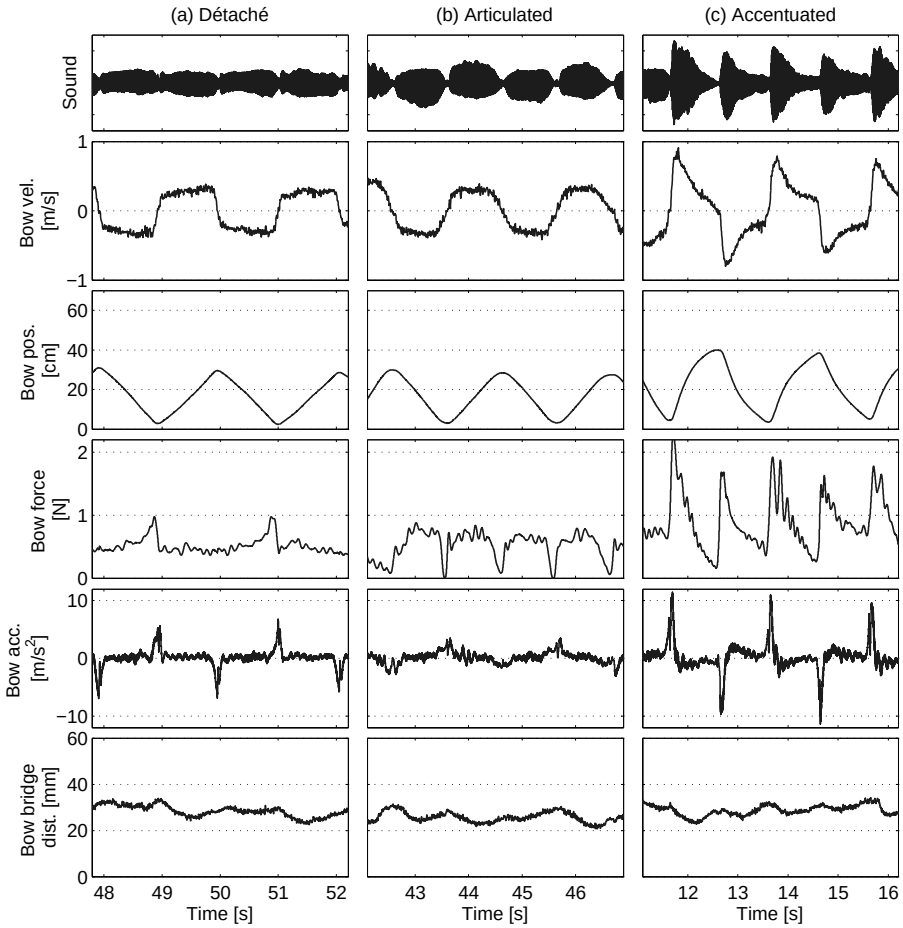

Figure 6.16: Illustration of different types of bow changes. (a) Simple détaché with no particular expression. (b) Articulated détaché in which the notes are clearly separated. (c) Accented détaché with a strong dynamic variation at the beginning of each note (accents). From top: sound, bow velocity, bow position, bow force, acceleration in the bowing direction, and bow-bridge distance.

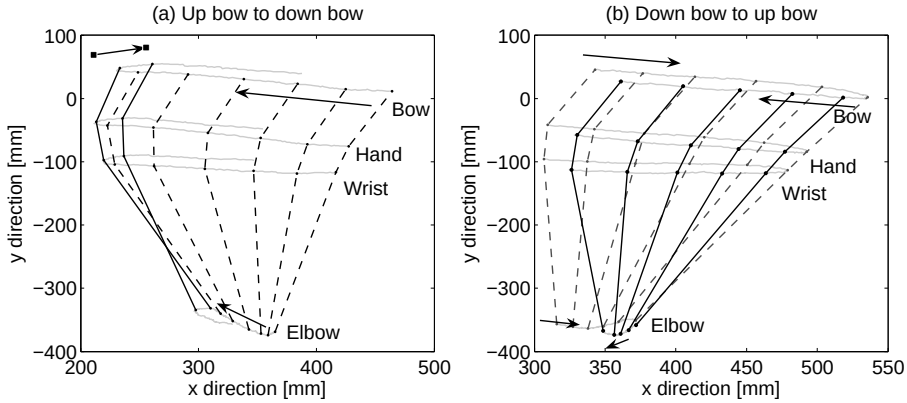

Figure 6.17: Trajectory of the different parts of the arm during the bow change (elbow, wrist, hand and bow). (a) Bow change from up-bow to down-bow. (b) Bow change from down-bow to up-bow.

Arm motion

In his reference work on violin teaching [28], Galamian pointed out that "drawing a straight line with the arm is not natural". All the elements of the arm, from the shoulder to the fingers, have to be well synchronized in order to obtain the intended motion and trajectory of the bow. In particular, during bow changes several techniques can be used depending on the role of the fingers and the wrist, or the rounding of the trajectory [86]. The motion of the arm may influence the shape of the bow velocity during the change and it is therefore necessary to examine it more closely.

In Fig. 6.17, the trajectory of the arm is shown for changes from up-bow to down-bow (Fig. 6.17a) and for down-bow to up-bow (Fig. 6.17b). The data were obtained using the motion capture system described in Chapt. 4 with additional markers at several positions of the arm, shown in the figure (elbow, wrist and hand). The string direction is along the y-axis and the bow is consequently moved in the x-direction.

Two observations can be made concerning the bow change gestures. First we can notice that the motion of the arm is not symmetrical, i.e. the relative trajectory of the arm elements is not the same after and before the bow change. In particular, the motion of the elbow is much shorter after the change, which results in a more pronounced action of the forearm. For instance, when changing from down-bow to up-bow (Fig. 6.17b), the elbow and wrist angles are sharper after the change. This observation suggests that the acceleration of the bow after the change in bowing direction is mainly led by the forearm and the hand. Secondly, it can be noted that the trajectory is rounded at the change, which often is the case for avoiding a complete stop of the bow and getting a smoother movement.

Observations on bow changes

General description

A comparison between different players allows us to observe shared features of the changes. In Fig. 6.18, the bowing parameters measured during détaché for two players are presented. Differences can be observed, such as a shorter bow-bridge distance for player 2 (Fig. 6.18b), and a slightly different velocity shape or small ripples at the change from down-bow to up-bow for player 1 (Fig. 6.18a). However, the similarities of their gestures are clearly visible as well and dominate the comparison.

First, we can note that a peak in bow force at the frog is present in both cases. Apart from this peak, an overall decrease in bow force at the changes can be observed. For both players, the bow force is lower at the beginning of the notes. This feature is clearer for player 2 (Fig. 6.18b): the force suddenly decreases just before the change and progressively regains its mean value after the change.

Secondly, for both players the bow acceleration patterns during the change consist of two successive peaks. A zoom on two of these peaks is shown in Fig. 6.19. In both cases, a large peak is followed by a smaller one[4]. This discontinuity in the acceleration shape is somehow surprising because a well-performed bow change is generally claimed to be achieved with a very smooth motion.

A first explanation of the pattern could come from the bow-string interaction during the bow change. The friction between the string and the bow hair could shortly act against the change and produce the discontinuity. However, the double peak pattern is observed even when a bow change is made by playing on a smooth, unrosined support. The interpretation that the double peak is an artefact of the bow-string interaction consequently must be discarded. Instead the phenomenon seems to be a characteristic of the player's gesture.

An interpretation of the two peaks from that approach will be illustrated in the next section. However, a first indication can be found by comparing Fig. 6.18 with the accentuated détaché shown before (Fig. 6.16c). In the case of simple détaché, the final velocity of the previous stroke is higher than the initial velocity of the next stroke, and the second acceleration peak is smaller than the first one. In contrast, for accentuated détaché strokes (Fig. 6.16c), the final velocity before the change is very small and the bow must be strongly accelerated for reaching the maximal velocity during the initial accent. The acceleration patterns is still composed of two peaks, but the second one is much higher than the first. Consequently, it can be concluded that the two peaks correspond to the two phases of the motion: the deceleration of the bow before the change and the following acceleration after the change.

[4]Note that it could also be seen as a global sine shape, corresponding to the pendulum motion expected during the change (according to Galamian [28]), with a gap during the bow change.

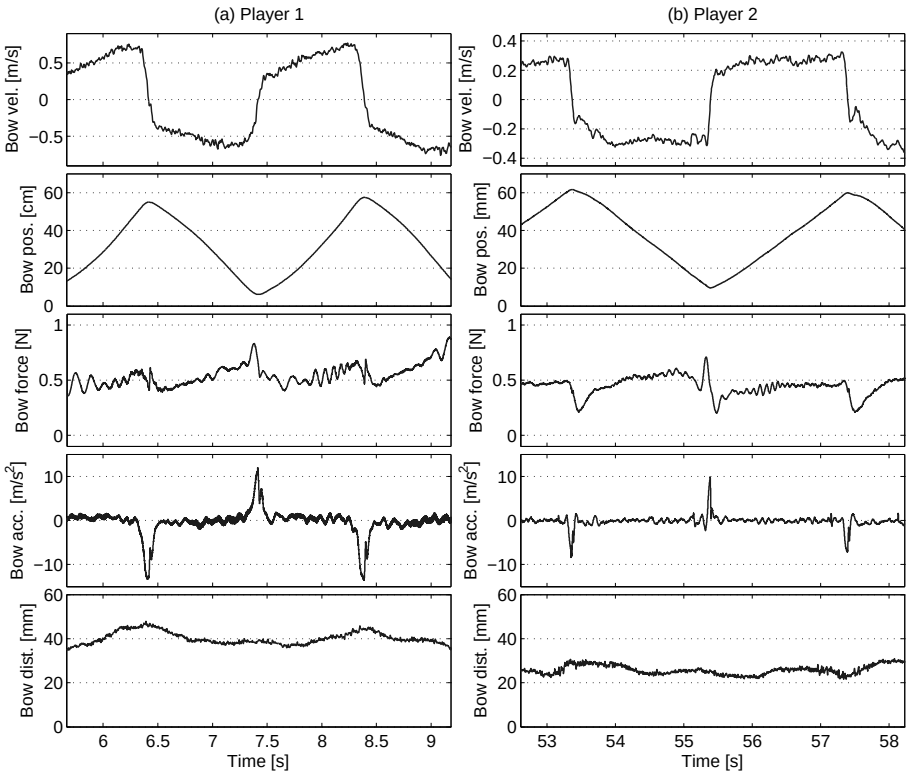

Figure 6.18: Examples of bowing parameters during détaché for two players illustrating differences and similarities during bow changes. From top: Bow velocity, bow position, bow force, acceleration in the bowing direction, and bow-bridge distance. A comparison between the two players shows shared features of the bow changes: An overall decrease in bow force and a characteristic pattern in the acceleration, composed of two successive peaks.

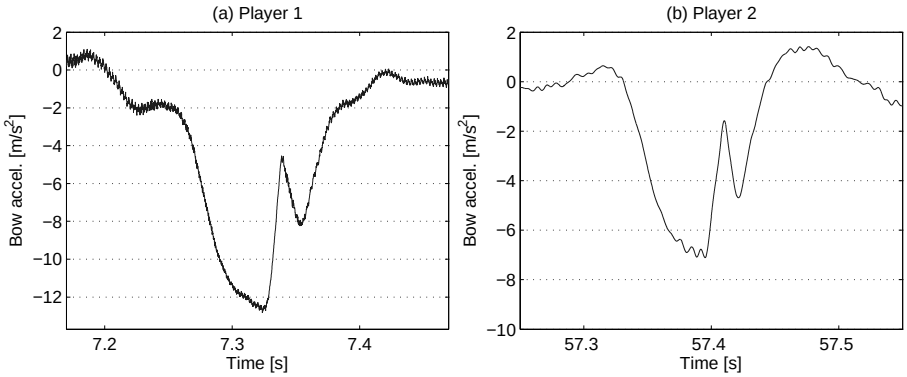

Figure 6.19: Illustration of the similarity between acceleration patterns in the bowing direction during bow changes for two players.

Synchronization between bowing parameters

The interpretation of the measurements during bow changes is not straightforward when looking at the time evolution of the bowing parameters. For instance, we have seen that the bow acceleration is composed of two peaks, but we still don't have a full explanation of this feature. Similarly, a lowering of the bow force at the change was observed.

The time evolution does not give an appropriate representation of the change. In particular, as the change in direction is not immediate, the time when the velocity crosses zero gives rather poor information about the moment of the bow change. The bow can stay almost immovable during a few milliseconds before and/or after the change, which is not accurately visible in the time representation. Such a short time of rest could drastically change the observation and interpretation of the bowing parameters. Moreover, it can be considered that the player does not think in terms of time when performing the change, but in terms of movement. This means that the chronology of actions during the change (like reducing bow force and then pressing again) is not fixed on an absolute time line.

This suggests a representation based on the motion of the bow rather than time. In Fig. 6.20, corresponding to a change at the frog (from up-bow to down-bow), the bowing parameters are first plotted versus time (Fig. 6.20a), then as a function of bow position (Fig. 6.20b), providing an interesting comparison. The evolution of the bowing parameters before the bow change (defined as the zero crossing in velocity) is plotted in grey, and the evolution after the change in black. In Fig. 6.20a, we can see that the change takes place during the decrease in bow force, around the middle. However, the representation versus bow position (Fig. 6.20b) leads to another conclusion. The decrease in bow force is vertical, which means that the bow does not move during the drop in force. The bow is then pressed down again

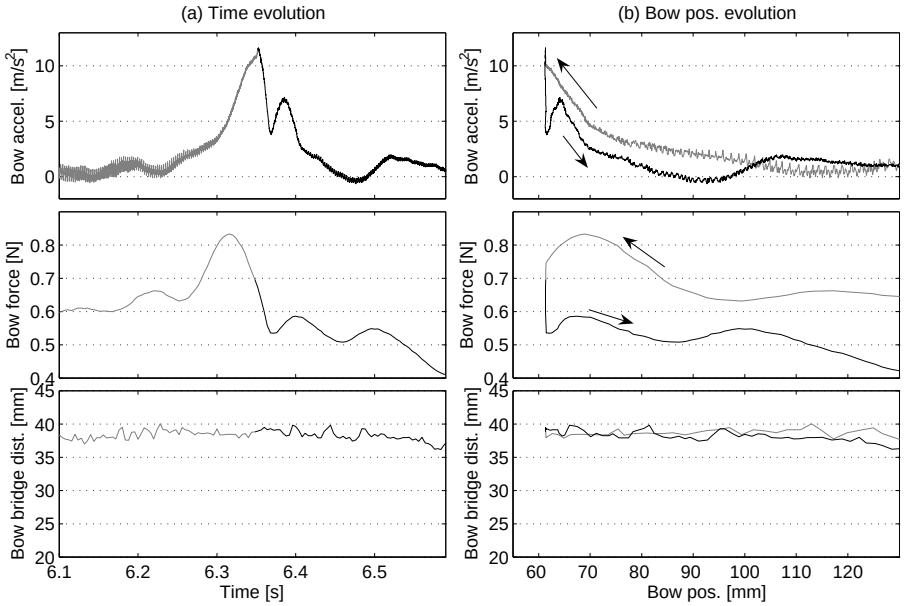

Figure 6.20: Illustration of the synchronization between bowing parameters for a bow change performed at the frog (up-bow to down-bow). From top: Acceleration in the bowing direction, bow force, and bow-bridge distance. (a) Time evolution of the bowing parameters. (b) Evolution of the parameters versus bow position, highlightening the two successive phases of the change (deceleration followed by acceleration). The parameters before and after the change are plotted in grey and black, respectively.

as the bow starts to move (increasing bow position), exactly at the beginning of the next stroke. We can therefore obtain a more accurate idea of the synchronization of the bowing parameters during the change with this representation.

The interpretation of the acceleration pattern observed before is straightforward when looking at the representation using bow position (Fig. 6.20b). The two successive peaks are clearly related to the initial deceleration of the bow before the change, and to the following acceleration at the beginning of the next stroke, respectively. The sudden decrease between the two peaks is vertical when plotted versus bow position, and corresponds exactly to the moment when the bow is at complete rest.

Concerning the bow-bridge distance, no specific variation is expected during the bow change. In Fig. 6.20, it can be seen that the bow-bridge distance is almost constant. However, at bow changes at the tip (down-bow to up-bow) as shown in Fig. 6.21, the distance is increased and then decreased noticeably around the

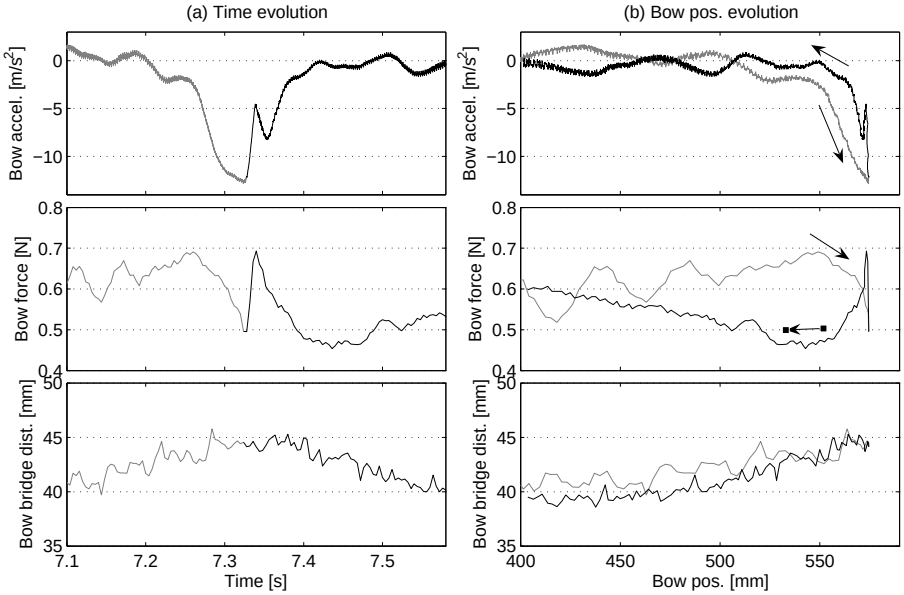

Figure 6.21: Illustration of the synchronization between bowing parameters for a bow change performed at the tip (down-bow to up-bow). From top: Acceleration in the bowing direction, bow force, and bow-bridge distance. (a) Time evolution of the bowing parameters. (b) Evolution of the parameters versus bow position, highlightening the two successive phases of the change (deceleration followed by acceleration). The parameters before and after the change are plotted in grey and black, respectively.

change, resulting in the small peaks that were observed before. The maximum bow-bridge distance coincide with the change in bowing direction, which is more pronounced in the representation using bow position. In Fig. 6.21, a small ripple in bow force can also be observed during the bow change. It is surprising to observe the perfect synchronisation with the moment when the bow is at rest, and with the gap in bow acceleration. The ability of the player in obtaining such a quick variation in force, lasting only around 15 ms, could be questioned, but no satisfying alternative interpretation has been found. Interestingly, these ripples during bow changes from down-bow to up-bow were only observed with one player (of about ten subjects) and could therefore be an artefact of this player's bowing technique.

Properties of the acceleration patterns

Bow changes are a technical gesture requiring years of training in order to obtain an acceptable quality, i.e. an optimal connection between two notes without scratching

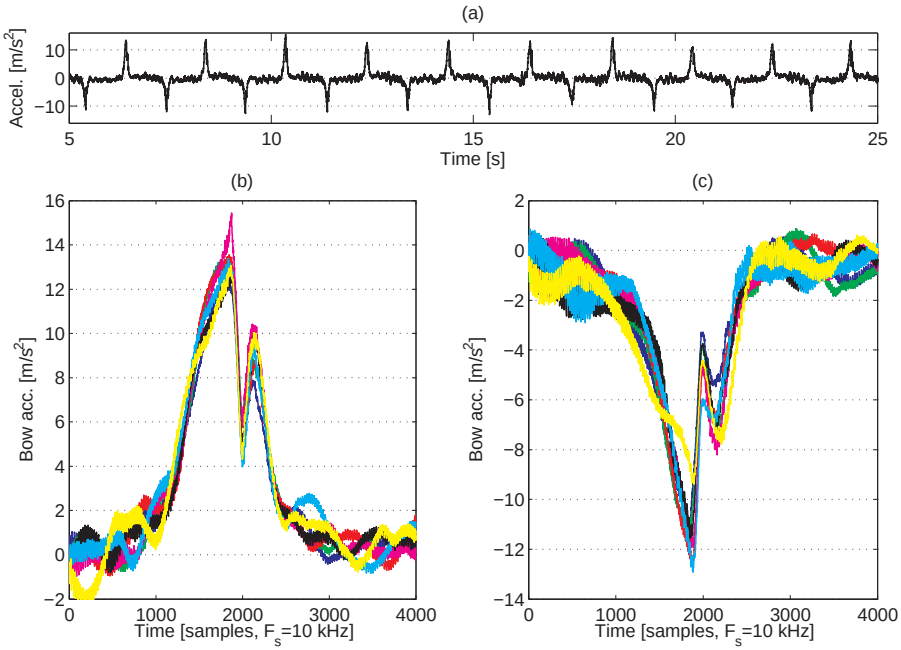

Figure 6.22: Illustration of the high reproducibility of the acceleration patterns at bow changes. When plotted together the acceleration patterns of repeated bow changes during the same acquisition exhibit a high reproducibility in time and amplitude. (a) Acceleration during the acquisition. (b) Bow changes from up-bow to down-bow. (c) Bow changes from down-bow to up-bow.

noises. The bow motions for similar bow changes performed by an experienced player could therefore be expected to show strong similarities. In order to examine these similarities, it is more rewarding to focus on the bow acceleration, which provides a more accurate description of the details of the bow motion than the velocity.

We have seen that the acceleration pattern at the bow change is composed of two successive peaks, corresponding to two phases of the motion. It is interesting to notice the constancy of this pattern and the high reproducibility. In Fig. 6.22, a long acquisition of repeated détaché strokes was performed in order to obtain a long series of successive bow changes for the same class of strokes. Acceleration patterns were isolated and plotted together, showing a very good reproducibility in time and amplitude for the two cases of changes (down-bow to up-bow, Fig. 6.22c, and up-bow to down-bow, Fig. 6.22b).

In Fig. 6.22b, showing all bow changes plotted together, the values of the first peak fall between 12 and 15 m/s^2, and between 7.7 and 10 m/s^2 for the second

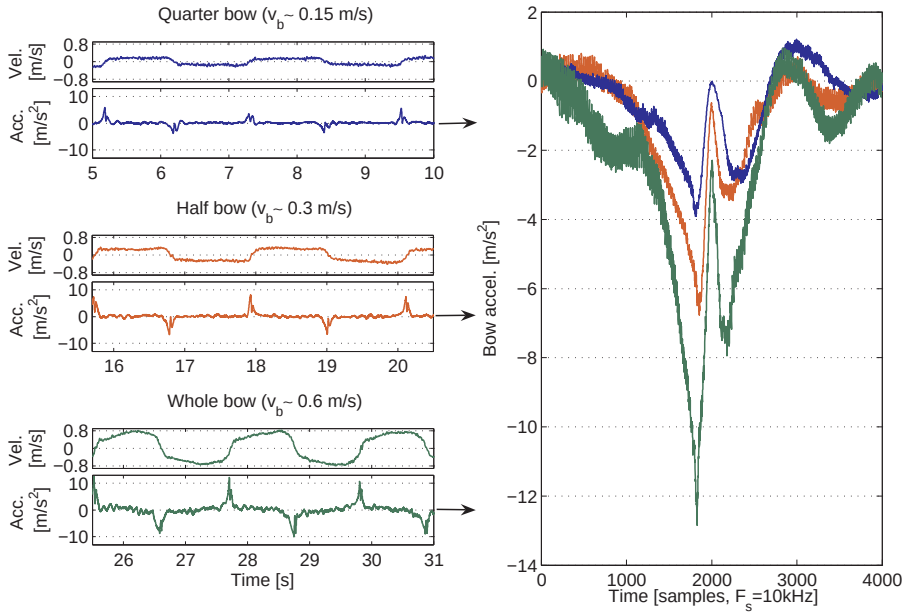

Figure 6.23: Similarity between acceleration patterns at bow changes during détaché performed with different bow velocities (left panels; from top: v_b= 0.15, 0.3 and 0.6 m/s). The global shape of the acceleration during the bow change remains the same for increasing bow velocity (right panel), and the total duration of the pattern is the same, lasting about 150 ms.

peak, the dip in the gap in between variying from 4.2 to 6.4 m/s^2. The timing of the patterns is very precise and on a short time scale. The duration from the first peak to the minimum in the gap, and the duration from the minimum to the second peak, are both very short, lasting 15 and 13 ms, respectively, with a small variation of ±1 ms. It is difficult to determine the exact beginning and end of the changes, but, if we consider the time when the absolute value of the acceleration begins to increase significantly without decreasing before the maximum, the durations of the two phases of motion are between 60 and 120 ms for the deceleration, and between 30 and 50 ms for the acceleration.

The measurements above were performed for fast détaché strokes with an average bow velocity around 50 cm/s during the sustained part. The transitions could change drastically for other velocities. For example, it would be easier, and probably faster, to change the bow direction with a lower bow velocity both before and after the bow change. However, observation of acceleration patterns for such cases shows an unexpected behaviour: the total time of the transition seems to remain the same, independent of the initial and final bow velocities.

This is illustrated in Fig. 6.23, which shows exemplary acceleration patterns for three bow velocities (v_b=60, 30 and 15 cm/s). The shapes of the acceleration are very similar in the three cases, including the double peaks and the gap in between. As mentioned before, it is difficult to determine the beginning and the end of the transitions accurately, but nevertheless, no significant differences in the timing of the patterns can be observed. For all three cases, the strong variations in the acceleration are concentrated to a time interval lasting around 150 ms. Because of this time constancy, the amplitude of the variations increases with increasing bow velocity.

Representation of measurements in Guettler diagrams

The performance of bow changes requires not only a good synchronization between the variation of bowing parameters, but it must also respect some proportions between them. For instance, the amplitude of the decrease in bow force is dependent on the velocity variation after the change. If the bow has to be strongly accelerated at the beginning of the next stroke, a higher bow force is required for avoiding a whistling attack of the note. We can consequently expect a coordinated relation between the values of the bowing parameters at the bow change.

If the vibration of the string is sufficiently damped during the deceleration, the following acceleration can be seen as a simple attack in which case, according to Guettler, the acceleration and the bow force are the relevant parameters. However, in real playing, these parameters vary continuously, which is a rather different situation compared to Guettler's analysis based on constant parameters during the attack. Further, Guettler diagrams are dependent on bow-bridge distance and, in playing, this distance also varies slightly from one bow change to the next during one acquisition. The variations are naturally larger between different classes of détaché. As a consequence, measurements including different bow-bridge distances cannot be compared by plotting them in the same diagram. A solution was reached by plotting all bow changes in the same acceleration - bow force diagram à la Guettler, and indicating the bow-bridge distance with different colors, in order to allow a visualization of all relevant parameters.

The problem of the non-constancy of parameters during the change was handled by considering their values at the very beginning of the stroke. As seen above, the beginning of the next stroke after the change corresponds to the minimum in the gap in acceleration. In the following, we will consequently consider the values of the bow acceleration, the bow-bridge distance and the bow force at this time.

In order to describe the overall range in bow acceleration, the measurements presented in Sect. 6.1 were analysed. Increasing bow velocities during the stroke resulted in increasing accelerations at the change. The measurements include acceleration values between 0 and 12 m/s^2, and even up to 40 m/s^2 for sixteenth notes played with the whole bow.

The results are shown in Fig. 6.24. Letting aside the extreme case of sixteenth notes played with the whole bow, all bow forces are found between 0.2 and 1.1 N,

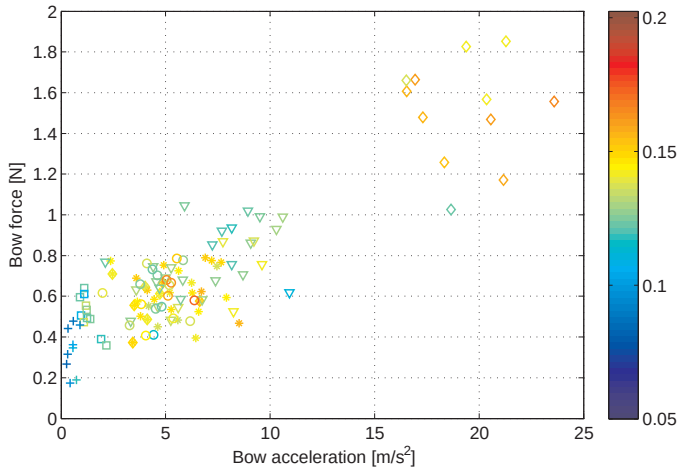

Figure 6.24: Initial acceleration and bow force at bow changes in detaché strokes plotted in a Guettler diagram. The data are obtained from the measurements described in Sect. 6.1 (détaché performed with the whole bow and decreasing durations). The data points represent whole notes (+), half notes (□), quarter notes (o), eighth notes (▽), sixteenth notes with the whole bow (◇), and with one third of the bow (*). The relative bow-bridge distance β is shown in color (range 0.05 - 0.2)

and the range of acceleration goes from 0.3 to 12 m/s^2. The data are clustered along a line with slope 0.06 N/(m/s^2), and form a well-defined region for the performance of bow changes. No clear tendency with bow-bridge distance can be observed. The data seems to be rather well mixed whatever the bow-bridge distance. However, a trend in acceleration can be discerned: Whole notes with low accelerations at the change are played closer to the bridge than, for example, sixteenth notes with higher acceleration.

Some observations related to the performance of bow changes have been made in this section. We have observed a decrease in bow force around the actual moment of the change in bowing direction, and a synchronization between the bowing parameters at the change. The synchronization was made visible by introducing a representation of the bowing parameters versus bow position instead of time. Focusing on the acceleration patterns, a detailed examination of the bow motion was made possible. The acceleration patterns, which were composed of two successive peaks corresponding to the deceleration and acceleration at the bow change, showed a very high reproducibility in a large set of examples. Interestingly, the duration of the changes was found to be very similar for different types of détaché.

Simulations and modifications of bow changes

In this section, measurements are used for controlling the bowed-string model and simulating bow changes. Bowing parameters at the bow change are modified and the influence of these modifications on the vibration of the string are examined. From the previous observations of the parameters, we can extract two interesting features to modify. First, we will examine the significance of the reduction in bow force for the performance of the change. Secondly, the duration of the bow changes will be modified in order to observe the influence on the resulting string motion and the perception of the change.

Modification of bow force

Fig. 6.25a shows a simulation of an exemplary bow change extracted from a succession of détaché strokes. The bow velocity and force were used with a constant bow-bridge distance ($\beta = 0.12$) to control the model. A simulated bow change is obtained, showing a very good transition between the two notes. The periodic triggering of the slip phases is maintained until the very end of the first note and builds up quickly during the attack of the following note, except for three additional slips around time 1.05 s. The duration of the bow change, from the last slip triggering of the first note to the first triggering of the second note, is around 28 ms.

In order to evaluate the quality of bow changes, three features can be examined: the duration of the bow change (between the last and first slip triggering before and after the change, respectively), the existence of prolonged periods, and the time before a periodic triggering of the second note is reached after the change. Prolonged periods will produce scratchy, "choked" sounds, whereas the existence of additional slips after the change will characterize a "loose" attack with multiple slips. In both cases the perceptual prominence depends on the duration before nominal periodic triggering is reached [37]. The duration of the "silent" phase of the change without slips reflects the separation between notes and the swiftness of the change. Modifications will be examinated under the light of these three criteria.

In a first modification, the force reduction was exaggerated and the minimal value in the gap was reduced to 0.1 N instead of 0.6 N. The bowing parameters and the resulting simulation are shown in Fig. 6.25b. The quality of the transition seemed to be improved: the additional slips after the change have disappeared and the duration of the bow change (from last-slip to first-slip) was significantly reduced to 16 ms. Consequently, the player could probably obtain a better bow direction change by lowering the force more at the change. However, we can question the ability of the player in performing such a quick and precise variation of the force. We can also note the importance of a rapid increase in bow force after the change. If such a low bow force (0.1 N) was kept constant during the attack, a Helmholtz motion would not be obtained for the second note.

When the bow force is kept constant (Fig. 6.25c), we can see a single prolonged period before the change (an isolated slip triggering) and some aperiodic vibrations

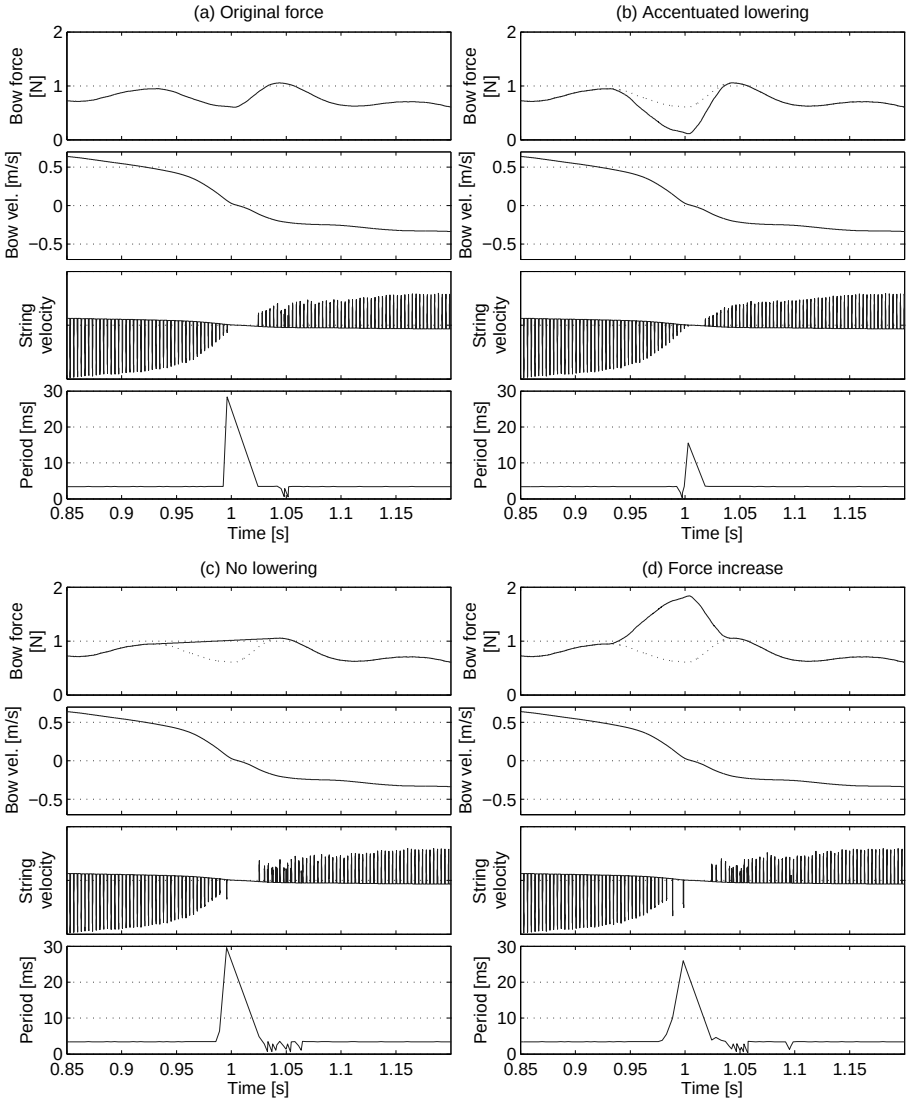

Figure 6.25: Modification of the bow force during bow changes. Bow changes are simulated with similar bowing parameters as in measurements, except for the bow force which is modified in order to examine the influence of a force reduction during the bow change. From top: Bow force, bow velocity, string velocity under the bow, and period time between successive slip triggerings. (a) Original bowing parameters including a slight reduction in the bow force during the bow change. (b) Exaggerated reduction in bow force. (c) No reduction in bow force. (d) The reduction is replaced by an increase in bow force.

during the attack of the second note. The same features can be seen when the bow is pressed harder on the string during the change instead of reducing the bow force (Fig. 6.25d). These effects are very short, lasting less than 40 ms, and may not be important perceptually. However, we must remember that in both cases, the bow force is returned to a reasonable value shortly after the modification. Consequently, when the string velocity and the duration of the bow change are compared with the bow force shape, it can be seen that the string vibration is drastically changed during the entire modified interval, and that a periodic vibration is not reached until the end of the modification when the bow force is returned to its original value.

In conclusion, the simulated modifications of bow force allowed a striking illustration of several effects of the observed force reduction during the bow change. Before the change, the force reduction helps the string to remain in Helmholtz motion, avoiding prolonged periods due to a too low bow velocity compared to the bow force. By decreasing the maximum static friction force, it also allows the vibration to begin quicker after the change and consequently, it reduces the transition time between the two directions of the string vibration. However, in order to avoid a "loose" multiple-slip attack, the bow force must be quickly increased again after the bow change.

A last point should be underlined concerning the reduction in bow force. By decreasing the friction force between the bow and the string, it may reduce the force that acts against the bow motion and therefore help the player in performing the action.

Stretching / compressing the bow changes

A rather constant transition time for the bow change has been observed before, whatever the bow velocity during the sustained part of the notes. In order to study the effect of different durations of the bow change, the time evolution of the bowing parameters was stretched and compressed by simulations. Such a modification not only changes the duration of the bow change, but also the bow acceleration and the variation in bow force. These changes may have a drastic effect on maintaining the Helmholtz motion to the very end of the first note, and quickly establish a periodic motion during the attack of the second note, as seen in the previous section. For instance, when the bow change is stretched to twice the initial duration, the acceleration is divided by two, and it will not be a surprise if the quality of the transition is influenced, in this case by the appearance of prolonged periods. However, in the two simulations presented hereafter, it will be seen that the alteration of this quality remains reasonable.

The same exemplary bow-change pattern as in the previous section was modified (see Fig. 6.25a). The limits of the modified interval was determined by the peaks in the bow force before and after the change, which correspond well to the beginning and end of the acceleration pattern. In Fig. 6.26a, the interval is compressed to half the initial duration, and in Fig. 6.26b, it is stretched to twice the initial duration.

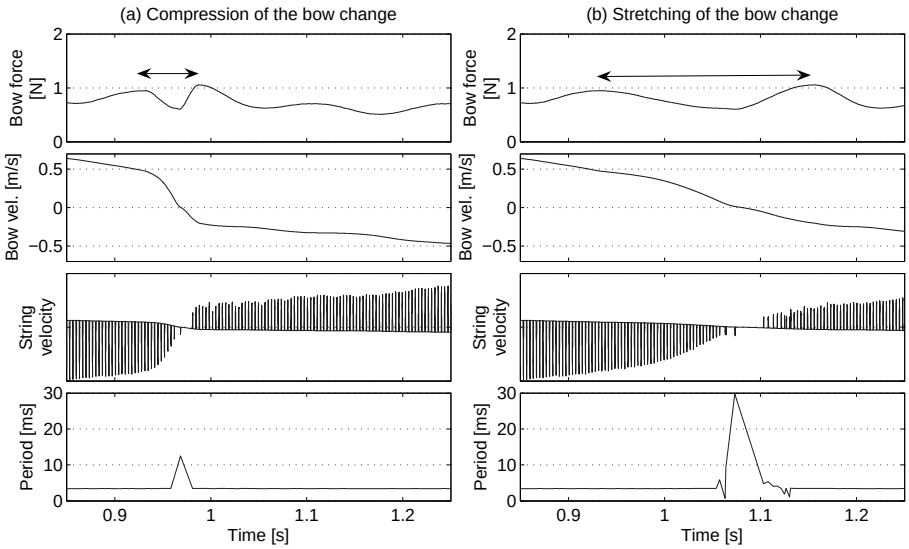

Figure 6.26: Modification of the duration of the transition between the two notes. The time evolution of the bowing parameters is stretched or compressed for obtaining various durations of the change indicated by the double arrow. (a) The transition is compressed to half its initial duration (showed in Fig. 6.25a). (b) The transition is stretched to twice its initial duration.

The compression reduces the time interval between the end and the beginning of the two strokes from 28 to 12 ms without adding extra slips or prolonged periods, as seen in Fig. 6.26a. Moreover, the amplitude of the string velocity during the decrease and the attack around the bow change were significantly increased compared to Fig. 6.25a, as expected from the higher deceleration/acceleration during the bow change. This produces a very clear and swift transition between the two notes, and the bow change can be described as "perfect". However, such a quick transition is not very realistic in performance and does not sound natural. Note that the increase of the acceleration during the attack of the second note could give rise to additional slips and alter the quality of the attack. When the duration of the bow change was shortened to 1/5 of the original value, additional slips were produced. The aperiodic part of the attack lasted more than 80 ms. Such poor attacks can be avoided by reducing the lowering of the force accordingly.

When the duration of the bow change is stretched by a factor two, some irregular slips before and after the change can be seen in Fig. 6.26b, due to a lower acceleration with unchanged bow force, but the quality of the transition was still acceptable. The main difference of the change is the slow decrease and attack of the two notes, resulting from the lower deceleration and the following acceleration. This produces a short diminuendo followed by a short crescendo and the separation

between the notes is clearer than during a normal bow change.

The simulations with modified durations of the transition showed that the bow change can be compressed or stretched to a certain extent without changing the string motion drastically, i.e. by still maintaining a periodical triggering of Helmholtz motion. However, even when the periodic triggering is preserved, the modified bow changes can sound unnatural if they are too quick or too slow. Consequently, when modifying bow changes for synthesis with the bowed-string model, it is important to mimic the basic timing features of a real bow-change gesture.

6.3 Conclusions

With this chapter, we have completed our overview of the different bowing patterns used in violin playing. It has treated sustained, continuously controlled bow strokes such as *détaché* and the specific difficulties related to this class of bow strokes for a gesture-inspired control with the bowed-string model. The performance of such bowing patterns is dependent on a large set of parameters including the player's gestural habits and constraints, the mastering of the bow, the musical context, and the feedback of the sound of the violin. The global shape of the bowing parameters showed typical variations, probably related to performance habits, when playing technical exercises, which could be modelled by parameterized profiles as in the previous chapter on dynamic bow strokes. However, the parameters of such models for sustained notes would not be easy to deal with, and in particular, the small, partly uncontrolled, variations observed during the sustained strokes would not be reproduced, whereas they are important features for the realism of the control. A contour characterization of the bowing parameters could be used, as proposed by Maestre [50]. Another approach using performance constraints optimization [58, 69] seems very promising, but could not be studied within the present work. Instead, as a temporary step, we decided to use our measurements on sustained notes as a database of typical bowing patterns in detaché. This approach requires a performance-based description (duration, dynamic level, etc) and some simple rules, based on real performance strategies, for modifying the original bowing parameters. By using such a systematic procedure, it is possible to build musical phrases of notes with different durations and dynamics, compiled from modified reference strokes in the database.

In this chapter, we have presented and commented measurements with several performance constraints related to the length of bow used for the stroke, the duration of the notes, and the dynamics. In particular, the bow velocity patterns for different durations have shown strong similarities when normalized to the same duration and the same amplitude. This observation led to an elementary procedure in order to produce various bow stroke durations from a limited set of exemplary bow strokes, based on stretching/compression and amplitude rescaling of the sustained part, but with unchanged transitions. In order to examine strategies for changing dynamic level, we introduced the relative Schelleng diagram, which allows a

representation of the playable Helmholtz region in one diagram whatever the bow velocity. The relative Schelleng diagram was supplemented by a level diagram representing the sound level as function of the bow force and the ratio between the bow velocity and bow-bridge distance. Simulations obtained for different velocities in Chapt. 3 showed continuous level variations in this diagram, except for values close to the minimum bow force, and the agreement between measured level variations and simulated level was found to be very good. From the observation of the player's performance strategy in these diagrams, it was possible to develop a systematic procedure for modification of the dynamics of exemplary measurements. The procedure determined the variations in bow-bridge distance and bow force from a desired change in sound level under given velocity constraints.

Finally, in the last section, we studied the performance of bow changes between long sustained notes. Empirically expected variations of the bowing parameters were observed and quantified using the measurements. A representation showing the patterns of bowing parameters as function of bow position instead of time was introduced, in order to allow a more intuitive visualisation of the bow changes. Using this representation, two successive phases (deceleration and acceleration) of the bow change were clearly observed, and the synchronization between the bowing parameters during the changes determined. A close examination of the bow acceleration patterns showed strong similarities for various gesture constraints and, in particular, a constant time around 150 ms for the execution of the change in bowing direction, independently of the bow velocities before and after the transition. Finally, modifications of the bowing parameters during the bow changes (force reduction and timing) were simulated in order to examine their influence on the string motion just before and after the bow change.

In conclusion, the measurements, analyses and models contained in this chapter have given a firm base for an adequate control of the synthesis of sustained bow strokes like détaché with our bowed-string model.

Conclusions

In the introduction to this work, we identified three problem areas related to the control of sound synthesis based on physical modelling: playability, relation between the control parameters and the sound properties, and the time evolution of the control parameters in order to obtain a realistic control of violin synthesis, or in other wording "How to play the virtual violin?" The present work aimed at a close examination of (a) the behaviour of the model for different sets of control parameters, and (b) the control of the bowing parameters in real violin playing, with the purpose of proposing some well-founded solutions for the control of virtual bowed-string instruments, based on sound knowledge about the characteristics and constraints in real music performance.

The initial steps were concerned with the development of the necessary research tools, including

- a physical model of the bowed string based on modal formalism, eventually working for real-time implementations.
- a setup for measurement of bowing parameters in real performance. For that purpose, an original design of a sensor for bow force was developed and combined with an optical motion capture system.

The playability of the model and the relation between the control parameters and the sound properties were first investigated by performing a large set of simulations with varying bow forces, bow-bridge distances and bow velocities. The playability, i.e. the control parameter space in which Helmholtz motion is obtained, was found to be in good agreement with theoretical expectations. Concerning the sustained parts of the notes, the simulations showed a regular slip triggering between the theoretical maximum and minimum bow force limits at given bow velocities and bow-bridge distances. During attacks, optimal regions for obtaining regular triggerings could be identified in the bow acceleration - bow force space at a given bow-bridge distance. Also in this case the theoretical limits were in good agreement with the simulations, but one of the limits had to be slightly adapted for fitting the playable region well.

The fact that a splendid agreement could be found between simulations and theoretical results was a good sign, as our purpose was to improve the control of the

physical model using "natural" parameters in playing. In particular, the playable regions could be described by analytical relations depending on the mechanical properties of the system, without necessitating a systematic evaluation through numerous simulations. By representing the measurements in a relative Schelleng diagram, it was also possible to illustrate trajectories of bowing parameters in the playable region. It was shown in Chapter 6, that exemplary sustained notes were played in the region defined by the two theoretical force limits, far above the minimum bow force and well below the maximum force.

The same approach with systematic simulations was also used to examine the relation between the vibration properties and the control parameters inside the playable region. In particular, we examined the variations of the vibration level and the spectral centroid, which reflect two main characteristics of the sound in music performance: the dynamic level and the brilliance. A description in analytical terms of the relations between these characteristics of the sound and the bowing parameters was not found, but a visualization in Schelleng diagrams allowed making some general observations.

The spectral centroid was found to depend mainly on the location of the bowing parameters in the relative Schelleng diagram. On a logarithmic scale, the spectral centroid varied linearly from minimum to maximum bow force. In this representation, the influence of bow velocity was negligible. In addition, it could be observed that the maximum value of the spectral centroid, which was obtained close to the maximum bow force limit, increased with decreasing bow-bridge distance. Interestingly, with constant bow force and bow velocity, the spectral centroid was slightly decreasing with decreasing bow-bridge distance, which is in contradiction to player's usual assumptions.

The vibration level showed the expected variation in the parameter space: the level increased with decreasing bow-bridge distance, and higher levels were reached by increasing the bow velocity. An influence of the bow force could be observed as well. In a diagram of bow force versus the ratio between bow velocity and bow-bridge distance, the simulations showed a continuity in the level variations at the four bow velocities that were considered (from 5 to 50 cm/s).

The simulations gave valuable insights into the behaviour of the model by examining two of the problems listed above (playability and relation between sound properties and control parameters). The third problem area related to a realistic time evolution of the control parameters for violin synthesis. That task required examination of the actual bowing parameters used by violinists during the performance. For that purpose, a large number of measurements were analyzed in order to find the most appropriate way of controlling the model. This led us to separate our analysis into two classes of bow strokes according to the principle of bow control. The first class was composed of typical bowing patterns with rather short, dynamic or bouncing bow strokes (*sautillé*, *fast martelé*, *tremolo*), which to a large extent rely on the dynamic properties of the bow. The reproducibility between strokes was high, due to the predictable mechanical response of the bow, well-defined gesture habits, and long practicing.

The second class of bow strokes was composed of sustained bowing patterns such as *détaché* and *legato*, during which the player continuously controls the bowing parameters, according to musical intentions. These strokes were more difficult to model due to a more active control and feedback by the player during the notes.

For the first class of bow strokes, we deduced simple models describing the time evolution of the bowing parameters during the stroke by analytical functions. These models were controlled by a limited set of parameters that were made as intuitive as possible. The model parameters were fitted to measurements for typical cases of playing conditions (different dynamic levels and tempi).

For the second class of bow strokes with sustained strokes, we preferred to base the control of the bowed-string model on real measurements. The reason was that the characteristic small fluctuations in the bowing parameters could not be easily modelled. In that case, simple rules had to be defined in order to offer a possibility of extrapolating new bow strokes from the exemplary strokes. From observations on bow velocity profiles for notes with different durations, a straightforward procedure was deduced for obtaining strokes with different durations. The method consisted in a stretching/compressing and rescaling of the sustained part of the stroke, keeping the transitions unchanged.

An examination of the playing strategies for obtaining different dynamic levels led to a procedure that enabled a systematic deduction of the bow force and the bow-bridge distance when changing the sound level. From a desired level variation and some constraints on the velocity variation (for example a linear variation in velocity with the level), the procedure determines a "correct" combination of bowing parameters in order to follow a realistic path in the Schelleng space, ensuring that the bow force stays within the playable range. The problem of bow changes between long sustained notes was also tackled, in order to observe some key features of the detailed variations in the bowing parameters during the changes, and their influence on the resulting string motion.

Throughout this work, we have described possible applications as they appeared. The bowed-string model can be controlled in real time, using an appropriate interface, or off line, by defining envelopes of the control parameters, for example by a score-based generation. For these two main applications, the examination of bowing parameters actually used in real performance provides improved solutions.

For score-based synthesis, the implementation is immediate: Notes are described by key characteristics such as the bowing pattern, the duration, and the dynamic level, which permits to select the adequate bow-stroke model and set the right parameters. In the case of real-time control, the bow-stroke models can be used for creating realistic bowing patterns from a simple interface. An obvious example is violin synthesis controlled with a midi keyboard, which is certainly not suitable for the control of instruments producing sustained sounds. In that case, mappings can be defined between midi messages (e.g. key velocity) and parameters for the bowing pattern models. In contrast, midi wind controllers provide a better interface for controlling the sustained part of the sound, but the interface is not adequate for

gestures requiring a specific motoric skill such as bow changes. Features observed in Chapter 6 can be used to implement bow-change models based on realistic gestures and triggered by interface events. Other interfaces can be adequate but limited in the measurements of bowing parameters. For example, the Augmented Violin developed at Ircam only provides information about the acceleration of the bow and the bow force. By using gesture recognition combined with an adequate mapping between the performance measurements and bowing pattern models, it could be possible to obtain a satisfying hybrid control of the synthesis.

In short, the best interface for a realistic control of the bowed-string model would be the violin itself. However, this interface necessitates gesture skills developed through long periods of practicing. An implementation of realistic and expert-controlled features in the model will have two main purposes: (a) to improve the control exerted by a non-expert user, and (b) to improve the realism of the control through an inadequate interface.

In this thesis, we have explored one way of approaching the problem of the control of sound synthesis by physical modelling. This approach was based on the assumption that the behaviour of the physical model is similar to the behaviour of the real instrument, i.e. that the model parameters are realistic. Under this assumption, the examination of bowing parameters used in real performance provides some insights into a realistic control of the model. However, the present work has some limitations, which offer alternative perspectives on future work on control of models for bowed string instruments in particular, and on the control of virtual instruments in general.

First, we have based our analyses on only one player. We gave a justification in Chapter 5 under the light of our objectives: the main idea was to find prototypes for controlling the model and, at least in a first step, we were not interested in studying differences or similarities between players. A comparison between players could be used to assess the properties of the control parameters that were deduced in this work, or supplement them by offering alternative control strategies. However, it is not sure that such a comparison would show major differences between players on the time scale we were interested in, i.e. the bow stroke. More interesting results could be expected to show up on a larger time scale including sequences of notes that builds a musical phrase. A considerable improvement regarding the usability of models for sound synthesis would lie in a "style-based" control on phrase level, i.e. a mapping between control models like those described in this work, and the time evolution of the notes and typical musical intentions.

A deficiency of the present work lies in the lack of perceptual validation through systematic and objective listening tests with professional violinists. Besides assessing the correctness and musical significance of the models and rules deduced in this work such validations could be used to tune the models, by setting values of thresholds for the model parameters and acceptance limits. Further, verbal descriptions of the sounds obtained with a given set of model parameters could help in building musically-based presets for the control of the synthesis.

Finally, other ways could be considered in order to control the model and supple-

ment the previous examination. For instance, gesture optimization is a promising way of automatically generating control parameters with a given set of gesture constraints. Systematic real-time analyses of the simulated vibration could also be interesting for optimizing the control, and introducing feedback in the interaction between a "virtual player" and the virtual instrument. For example, by defining rules describing the action of the player at a certain moment depending on the musical purposes (target) and the actual string motion (sounding result), it should be possible to implement a realistic feedback depending on the actual state of the simulation, instead of the invariant patterns proposed in the present work.

A "virtual player" should include a lot of features that were not within reach in the present work, in order to perform in a musically meaningful manner. Such features could include biomechanical constraints from the modelling of the arm, which could be used to deduce the time evolution of bowing parameters for different players with, for example, various gesture capabilities or different temperaments. An automatic exploration of the virtual model could also be considered, reproducing the practicing phase of the player. In this way, the "right" regions in the control parameter spaces could be found depending on the playing skills of the virtual player. Suitable parameter envelopes for a given sound target could also be proposed. Such an approach would be particularly interesting in order to control models not mimicking real musical instruments, for which no references can be found in the real world.

With these perspectives I close the thesis. I hope that the work has given a better understanding of the problems and possibilities in the control of physical models of musical instruments, even though not all aspects have been possible to take into account. It is left to future work to fully explore this fascinating area of music performance.

Bibliography

[1] J. M. Adrien. *Etude de structures complexes vibrantes, applications à la synthèse par modèle physique*. PhD thesis, Université Paris 6, 1988.

[2] J. Antunes, M. G. Tafasca, and L. L. Henrique. Simulation of the bowed-string dynamics: part 1 - a nonlinear modal approach. In *Congrès Français d'Acoustique*, Lausanne, Suisse, 2000.

[3] A. Askenfelt. Measurement of bow motion and bow force in violin playing. *Journal of the Acoustical Society of America*, 80(4):1007–1015, 1986.

[4] A. Askenfelt. Measurement of bowing parameters in violin playing. II: Bow-bridge distance, dynamic range and limits of bow force. *Journal of the Acoustical Society of America*, 86:503–516, 1989.

[5] A. Askenfelt and K. Guettler. The bouncing bow: An experimental study. *Catgut Ac. Soc. J.*, 3(6):3–8, November 1998.

[6] A. Askenfelt and E. V. Jansson. On vibration sensation and finger touch in stringed instrument playing. *Music Perception*, 9(3):311–350, 1992.

[7] R. Badeau, G. Richard, and B. David. Fast adaptative esprit algorithm. In *IEEE workshop on Statistical Signal Processing SSP'05*, Bordeaux, France, 2005.

[8] E. Bavu, J. Smith, and J. Wolfe. Torsional waves in a bowed string. *Acta Acustica*, 91:241–246, 2005.

[9] J. Bensa, S. Bilbao, R. Kronland-Martinet, and J. O. Smith. The simulation of piano string vibration: from physical model to finite differences schemes and digital waveguides. *Journal of the Acoustical Society of America*, 114:1095–1107, 2003.

[10] J. Bensa, S. Bilbao, R. Kronland-Martinet, J. O. Smith, and T. Voinier. Computational modeling of stiff piano strings using digital waveguides and finite differences. *Acta Acustica*, 91:289–298, 2005.

[11] J. Bensoam. *Représentation intégrale appliquée à la synthèse sonore par modélisation physique : méthode des éléments finis*. PhD thesis, Université du Maine, 2003.

[12] X. Boutillon. Model for piano hammers: Experimental determination and digital simulations. *Journal of the Acoustical Society of America*, 83:746–754, 1988.

[13] X. Boutillon. Analytical investigation of the flattening effect: the reactive power balance rule. *Journal of the Acoustical Society of America*, 90(2):754–763, August 1991.

[14] A. Caclin, S. McAdams, Smith B. K., and S. Winsberg. Acoustic correlates of timbre space dimensions: A confirmatory study using synthetic tones. *Journal of the Acoustical Society of America*, 118(1):471–482, 2005.

[15] C. Chafe. *Current directions in computer music*, chapter Simulating performance on a bowed instrument. MIT Press, Cambridge, 1989.

[16] C. Chafe. Pulsed noise in self-sustained oscillations of musical instruments. In *IEEE Int. Conf. on Acoustics, Speech and Signal Processing*, Albuquerque, April 1990.

[17] A. Chaigne and A. Askenfelt. Numerical simulations of piano strings. I: A physical model for a struck string using finite difference methods. *Journal of the Acoustical Society of America*, 95(2):1112–1118, 1994.

[18] A. Chaigne and A. Askenfelt. Numerical simulations of piano strings. II: Comparisons with measurements and systematic exploration of some hammer-string parameters. *Journal of the Acoustical Society of America*, 95:1631–1640, 1994.

[19] L. Cremer. *The physics of violin*. The MIT Press, 1984.

[20] V. Debut. *Deux études d'un instrument de musique de type clarinette: Analyse des fréquences propres du résonateur et calcul des auto-oscillations par décomposition modale*. PhD thesis, Université Aix-Marseille II, 2004.

[21] M. Demoucron, A. Askenfelt, and R. Caussé. Mesure de la pression d'archet des instruments à cordes frottées, application à la synthèse sonore. In *8ème Congrés Français d'acoustique*, Tours, France, 2006.

[22] K. v. d. Doel. *Sound Synthesis for Virtual Reality and Computer Games*. PhD thesis, University of British Columbia, 1998.

[23] C.-A. Faure and X. Boutillon. Détermination et étude expérimentale de la fréquence d'oscillation d'une corde frottée. *C. R. Acad. Sci. Paris*, 317(2):1377–1382, 1993.

[24] N. H. Fletcher and T. D. Rossing. *The physics of musical instruments*. Springer, 1997.

[25] E. Fléty, N. Leroy, J.-C. Ravarini, and F. Bevilacqua. Versatile sensor acquisition system utilizing network technology. In *Proceedings of the International Conference on New Interfaces for Musical Expression (NIME)*, 2004.

[26] F. G. Friedlander. On the oscillations of the bowed string. In *Proceedings of the Cambridge Philosophy Society*, volume 49, pages 516–530, 1953.

[27] C. Fritz, I. Cross, B. C. J. Moore, and J. Woodhouse. Perceptual thresholds for detecting modifications applied to the acoustical properties of a violin. *Journal of the Acoustical Society of America*, 122(6):3640–3650, December 2007.

[28] I. Galamian. *Principles of violin playing and teaching*. Prentice-Hall, 1962.

[29] P. M. Galuzzo. *On the playability of stringed instruments*. PhD thesis, Trinity College, University of Cambridge, October 2003.

[30] C. E. Gough. Real-time simulation of violin sounds by electronic violin and measured impulse responses. In *International Symposium on Musical Acoustics*, Barcelona, Spain, 2007.

[31] J. M. Grey and J. W. Gordon. Perceptual effects of spectral modifications on musical timbres. *Journal of the Acoustical Society of America*, 63(5):1493–1500, 1978.

[32] K. Guettler. Wave analysis of a string bowed to anomalous low frequencies. *Catgut Acoust. Soc. J.*, 2(6):8–14, November 1994.

[33] K. Guettler. *The bowed string -On the development of Helmholtz motion and on the creation of anomalous low frequencies*. PhD thesis, Royal Institute of Technology (KTH), Stockholm, Sweden, 2002.

[34] K. Guettler. On the creation of the helmholtz motion in bowed strings. *Journal of the Acoustical Society of America*, 88(6):970–985, 2002.

[35] K. Guettler. A closer look at the string player's bowing gestures. *Catgut Acoust. Soc. J.*, 4(7), May 2003.

[36] K. Guettler. Looking at starting transients and tone coloring of the bowed string. *Journal of the ITC-SRA*, 18, 2004.

[37] K. Guettler and A. Askenfelt. Acceptance limits for the duration of pre-helmholtz transients in bowed string attacks. *Journal of the Acoustical Society of America*, 101(5):2903–2913, May 1997.

[38] K. Guettler and A. Askenfelt. On the kinematics of spiccato and ricochet bowing. *Catgut Ac. Soc. J.*, 3(6):9–15, November 1998.

[39] K. Guettler, E. Schoonderwaldt, and A. Askenfelt. Bow speed or bowing position - which one influences the spectrum the most ? In *Proceedings of the Stockholm Music Acoustics Conference (SMAC '03)*, volume 1, pages 67–70, 2003.

[40] H. von Helmholtz. *Lehre von den Tonempfindungen.* Braunschweig, 1862.

[41] L. Hiller and P. Ruiz. Synthesizing musical sounds by solving the wave equation for vibrating objects: Part I. *Journal of Audio Engineering Society*, 19(7):542–551, July 1971.

[42] D. A. Jaffe and J. O. Smith. Performance expression in commuted waveguides synthesis of bowed strings. In *Proceedings of the International Computer Music Conference*, 1995.

[43] K. C. Kar, N. K. Datta, and S. K. Ghosh. Investigations on the bowed string with an electrically driven bow. *Ind. J. Theor. Phys.*, 1951.

[44] J. B. Keller. Bowing of violin strings. In *Comm. Pure Applied Math.*, volume 6, pages 483–495, 1953.

[45] J. Kergomard, V. Debut, and D. Matignon. Resonance modes in a one-dimensional medium with two purely resistive boundaries: Calculations methods, orthogonality and completeness. *Journal of the Acoustical Society of America*, 119(3):1356–1367, March 2006.

[46] M. Kimura. How to produce subharmonics on the violin. *Journal of New Music Research*, 28(2):178–184, 1999.

[47] A. Langhoff, A. Farina, and L. Tronchin. Comparison of violin impulse responses by listening to convoluted signals. In *International Symposium on Musical Acoustics*, Paris, France, 1995.

[48] H. Lazarus. *Die Behandlung der selbsterregten Kippschwingungen der gestrichenen Saite mit Hilfe der endlichen Laplacetransformation.* PhD thesis, Technischen Universität Berlin, 1972.

[49] D. J. Levitin, S. McAdams, and R. L. Adams. Control parameters for musical instruments: a foundation for new mappings of gesture to sound. *Organised Sound*, 7(2):171–189, 2002.

[50] E. Maestre. Coding instrumental gestures. Master's thesis, Universitat Pompeu Fabra, Barcelona, Spain, 2006.

[51] E. Maestre, J. Bonada, M. Blaauw, A. Pérez, and E. Guaus. Acquisition of violin instrumental gestures using a commercial emf tracking device. In *Proceedings of the 2007 International Computer Music Conference (ICMC07)*, volume I, pages 386–393, 2007.

[52] M. E. McIntyre, R. T. Schumacher, and J. Woodhouse. Aperiodicity in bowed-string motion. *Acustica*, 49:13–32, 1981.

[53] M. E. McIntyre, R. T. Schumacher, and J. Woodhouse. On the oscillations of musical instruments. *Journal of the Acoustical Society of America*, 74(5):1325–1345, 1983.

[54] M. E. McIntyre and J. Woodhouse. On the fundamentals of bowed string dynamics. *Acustica*, 43(3):93–108, 1979.

[55] M. E. McIntyre and J. Woodhouse. A parametric study of the bowed string: the violinist's menagerie. *CAS J.*, 42, November 1984.

[56] Y. Menuhin. *Violin and viola.* Kahn and Averill Pub., 1998.

[57] J. Meyer. The sound of the orchestra. *Journal of Audio Engineering Society*, 41(4):203–213, April 1993.

[58] W. L. Nelson. Physical principles for economies of skilled movements. *Journal Biological Cybernetics*, 46(2):135–147, 1983.

[59] M. Palumbi and L. Seno. Metal string. In *Proc. International Computer Music Conference*, Beijing, China, 1999.

[60] A. Perez. Gesture based synthesis of bowed string instruments. Master's thesis, Universitat Pompeu Fabra, 2006.

[61] N. C. Pickering. Physical properties of violin strings. *Catgut Acoust. Soc. J.*, 44, 1985.

[62] N. C. Pickering. *The bowed string.* Amereon, LTD., 1991.

[63] R. Pitteroff. *Contact mechanics of the bowed string.* PhD thesis, Cambridge University, 1995.

[64] R. Pitteroff and J. Woodhouse. Mechanics of the contact area between a violin bow and a string. part II: simulating the bowe string. *Acustica*, 84:744–757, 1998.

[65] C. V. Raman. On the mechanical theory of vibrations of bowed strings. *Indian Assoc. Cult. Sci. Bull.*, 15:1–158, 1918.

[66] C. V. Raman. Experiments with mechanically-played violins. In *Proc. Indian Assoc. Cultivation Sci.*, volume 6, pages 19–36, 1920-1921.

[67] N. Rasamimanana. Gesture analysis of bow strokes using an augmented violin. Master's thesis, Université Paris 6, 2004.

[68] N. Rasamimanana. *Geste instrumental du violoniste en situation de jeu : analyse et modélisation.* PhD thesis, Université Pierre et Marie Curie, 2008.

[69] N. Rasamimanana and F. Bevilacqua. Effort-based analysis of bowing movements: evidence of anticipation effects. *Journal of New Music Research. In print.*

[70] P. Schaeffer. *Traité des objets musicaux.* Éditions du Seuil Saint-Amand, impr. Bussière, 1966.

[71] J. C. Schelleng. The bowed string and the player. *Journal of the Acoustical Society of America*, 53(1):26–41, 1973.

[72] E. Schoonderwaldt, K. Guettler, and A. Askenfelt. An empirical investigation of bow-force limits in the schelleng diagram. *Acta Acustica united with Acustica*, 94:604–622, 2008.

[73] E. Schoonderwaldt, N. Rasamimanana, and F. Bevilacqua. Combining accelerometer and video camera: Reconstruction of bow velocity profiles. In *Proceedings of the International Conference on New Interfaces for Musical Expression (NIME)*, pages 200–203, 2006.

[74] R. T. Schumacher. Self-sustained oscillations of the bowed string. *Acustica*, 43(2):243–254, 1979.

[75] R. T. Schumacher. Measurements of some parameters of bowing. *Journal of the Acoustical Society of America*, 96(4):1985–1998, October 1994.

[76] S. Serafin. *The sound of friction.* PhD thesis, Stanford University, 2004.

[77] S. Serafin, M. Burtner, S. O'Modhrain, and C. Nichols. Expressive controllers for bowed string physical models. In *Proc. DAFX 2001*, Limerick, Ireland, december 2001.

[78] S. Serafin, R. Dudas, M. Wanderley, and X. Rodet. Gestural control of a real-time physical model of a bowed string instrument. In *Proc. ICMC 99: International Computer Music Conference 1999*, Beijing, China, October 1999.

[79] S. Serafin, J. O. Smith, and J. Woodhouse. An investigation of the impact of torsion waves and friction characteristic on the playability of virtual bowed strings. In *IEEE workshop on Applications of Signal processing to audio and acoustics*, pages 87–90, 1999.

[80] S. Serafin and D. Young. Bowed string physical model validation through use of a bow controller and examination of bow strokes. In *Proc. SMAC 2003*, Stockholm, Sweden, August 2003.

[81] J. H. Smith and J. Woodhouse. The tribology of rosin. *J. Mech. Phys. Solids*, 48:1633–1681, 2000.

[82] J. O. Smith. *Techniques for digital filtr design and system identification with application to the violin.* PhD thesis, Stanford University, 1983.

[83] T. Tolonen, V. Välimäki, and M. Karjalainen. *Evaluation of Modern Sound Synthesis Methods*. Helsinki University of Technology, Laboratory of Acoustics and Audio Signal Processing, Espoo, Finland, 1998.

[84] C. Valette. *Mécanique de la corde vibrante*. Hermes, 1993.

[85] M. M. Wanderley and P. Depalle. Gestural control of sound synthesis. *Proceeding of the IEEE*, 92(4):632–644, April 2004.

[86] C. E. Williams. *Violin bowing skill analysis: the mechanics and acoustics of the change in direction*. PhD thesis, University of Melbourne, 1986.

[87] J. Woodhouse. On the playability of violins. part I: reflection functions. *Acustica*, 78:125–136, 1993.

[88] J. Woodhouse. On the playability of violins. part II: Minimum bow force and transients. *Acustica*, 78:137–153, 1993.

[89] J. Woodhouse. Bowed string simulation using a thermal friction model. *Acta Acustica*, 89:355–368, 2003.

[90] J. Woodhouse. On the "bridge hill" of the violin. *Acta Acustica United With Acustica*, 91:155–165, 2005.

[91] J. Woodhouse and P. M Galluzzo. The bowed string as we know it today. *Acta Acustica*, 90:579–589, 2004.

[92] D. Young. *A methodology for investigation of bowed string performance through measurement of violin bowing technique*. PhD thesis, Massachussetts Institute of Technology, 2007.

[93] D. Young and S. Serafin. Playability evaluation of a bowed string physical model. In *Proc. NIME 2003*, Montreal, Canada, May 2003.